工學博士 學位論文

굽힘 효과를 고려한 다점계류 된 심해용 FPSO의 계류삭 피로평가

Fatigue Assessment for Mooring Chain Link of Spread-Moored FPSO in Deepwater Considering Bending Phenomenon

指導敎授 崔 慶 植

2012年 8月

韓國海洋大學校 大學院

海洋工學科

黃 外 柱

本 論文을 黃外柱의 工學博士 學位論文으로 認准함.

위원장 공학박사 이 주 성 (인)

위 원 공학박사 서 영 교 (인)

위 원 공학박사 이 승 재 (인)

위 원 공학박사 정 준 모 (인)

위 원 공학박사 최 경 식 (인)

2012년 8월 일

한국해양대학교 대학원

CONTENTS

LIST OF TABLES

LIST OF FIGURES

ACRONYMS

ABS	American Bureau of Shipping
ALS	Accidental Limit State
API	American Petroleum Institute
ASTM	American Society for Testing and Materials
BV	Bureau Veritas
CALM	Catenary Anchor Leg Mooring
CAPEX	Capital Expenditure
COG	Center of Gravity
DFF	Design Fatigue Factor
DNV	Det Norske Veritas
DOF	Degree Of Freedom
FEA	Finite Element Analysis
FLS	Fatigue Limit State
FMS	Fatigue Methodology Specification
FPU	Floating Production Unit
FPSO	Floating, Production, Storage & Offloading
IPB	In-Plane Bending
IRM	Inspection, Repair and Maintenance
IWRC	Independent Wire Rope Core
JIP	Joint Industry Project
LF	Low Frequency
MBL	Minimum Breaking Load

NT	Nominal Tension
OD	Outer Diameter
OOL	Oil Offloading Line
OPB	Out-of-Plane Bending
OPEX	Operating Expenditure
OS	Offshore Standard
QTF	Quadratic Transfer Function
RAO	Response Amplitude Operation
RP	Recommended Practice
SALM	Single Anchor Leg Mooring
SCF	Stress Concentration Factor
SN	Stress-Number of cycles
SPM	Single Point Mooring
SURF	Subsea Umbilical, Riser and Flowline
TAP	Theoretical Anchor Position
TN	Tension-Number of cycles
TT	Tension-Tension
ULS	Ultimate Limit State
WF	Wave Frequency

NOMENCLATURE

A	Section area of catenary line
A_{chain}	Section area of chain
A_k	Horizontal distance to anchor from fairlead
A_X, A_Y	Screen areas for wind or current in longi. and trans. direction
a	Horizontal distance from fairlead to line segment or anchor
a_D	Intercept parameter of SN curve
$\boldsymbol{C}$	Frequency-dependent potential damping matrix
C_X, C_Y	Drag coefficients for longi. and trans. direction due to wind and current
C_Z	Drag coefficient for moment
D	Nominal diameter of chain
D_i	Fatigue damage in sea state i
D_h	Horizontal distance to anchor from fairlead
$\boldsymbol{D_1}$	Linear damping matrix
$\boldsymbol{D_2}$	Quadratic damping matrix
d	Depth from fairlead to anchor
d_{cs}	Fatigue damage based on combined spectrum
d_{NB}	Fatigue damage based on narrow-banded spectrum
d_m	Mean position due to current or wind sea states
E	Young's modulus
$E(.)$	Expected value in statistics
F_{Dj}	Drag force at j-th lumped mass

F_M	Horizontal force considering mooring loads
F_{Sj}	Soil reaction force at j-th lumped mass
F_{Wj}	Buoyancy weight at j-th lumped mass
F_X, F_Y	Drag forces in longi. and trans. direction due to wind and current
F_h	Horizontal force from taut mooring line
F_v	Vertical force from taut mooring line
f	frequency (Hz)
f_p	Peak frequency of wave
g	Gravity acceleration
$\boldsymbol{H}$	Response Amplitude Operator (RAO) matrix
H_s	Significant wave height
I	Moment of chain interlink of OPB mode
I_{zz}	Moment of inertia in yaw at COG of FPSO
$I_{\psi\psi}$	Moment of inertia in yaw for added mass of FPSO
i,j,k	Indices of chain node, radial and time in calculating stress on chain
K	Fatigue coefficient
$\boldsymbol{K}$	Position-dependent stiffness matrix
k	Constant in calculating OPB stress for locking mode
$\boldsymbol{k_{ojj}}$	Diagonal terms in mooring stiffness matrix of FPSO
L	Length of a chain
L_{PP}	Length of FPSO from forward perpendicular to after perpendicular
$\boldsymbol{M}$	Mass matrix of vessel including added mass
M_{IPB}	Bending moment due to IPB mode
M_M	Horizontal moment considering mooring loads

M_{OPB}	Bending moment due to OPB mode
M_{Rot}	Reaction moment at loading point for OPB or IPB mode
M_Z	Moment due to drag force from wind and current
M_{axx}	Added mass for surge
M_{ayy}	Added mass for sway
$M_{ay\psi}$	Added mass for sway/yaw
$M_{a\psi\psi}$	Added mass for yaw
$\boldsymbol{M_j}$	Mass matrix of j-th lumped mass
M_s	Station keeping moment introduced by a mooring line
m	Inverse slope parameter of SN or TN curve
$\boldsymbol{m_j}$	Added mass matrix of j-th lumped mass
$\boldsymbol{m_{jj}}$	Diagonal terms in asymptotic added mass
m_n	Spectral moment of n-th order
N	Number of cycles to failure in TN or SN curve
n	Hardening exponent of material
n_j	Number of cycles experienced by chain link within j-th tension or stress range
p_i	Probability for fraction of stress or tension in sea state *i*
q_{CU}	Current drag force
q_{WI}	Wind drag force
q_{WA}	Wave excitation force in 1st or 2nd order
q_{OTH}	Other forces including force from mooring system
R_i	Offset position due to current or wind sea state *i*
r_i	Half of chain diameter
r_o	Half of distance between inner sides of chain

SCF_{IPB}	SCF on chain surface for IPB mode
SCF_{OPB}	SCF on chain surface for OPB mode
SCF_{TT}	SCF on chain surface for tension
S_σ	Response spectrum
S_η	Wave spectrum, i.e. spectral density of wave elevation
S_v	Wind spectrum, i.e. spectral density of wind speed fluctuation
s	Length of mooring line
T	Tension force
T_i	Time duration of sea state i
T_d	Design service life
T_k	Tentative segment tension force at k-th iteration in time domain analysis
V	Wind or current velocity
V_{eq}	Equivalent current velocity
V_{1hr}	Wind velocity based on one (1) hour average
X_{AEast}	Anchor position in East direction
X_{ANorth}	Anchor position in North direction
X_G	Distance of COG from FPSO coordinate system
X_{East}	Vessel position in East direction
X_{North}	Vessel position in North direction
χ	Non-dimensional frequency in Kaimal wind spectrum
ψ	Vessel orientation from North
ψ_j	Segment length error of j-th lumped mass
ΔR	Ratio of tension variation to MBL
ΔS	Stress variation

ΔT	Tension variation
$\boldsymbol{\Delta\psi}$	Length error derivation matrix
α	Yield offset in Ramberg-Osgood Law, Interlink angle for OPB
α_o	Angle between normal vector at chain contact surface and chain centerline
β	Interlink angle for IPB
ε_{ln}^{p}	Logarithmic plastic strain
ε_n	Nominal strain
θ	Described angle in FEA for chain links
λ	Peakness parameter in Ochi-Hubble spectrum
$\lambda_{LF,}\lambda_{WF}$	Normalized variance of low frequency and wave frequency
μ	Friction coefficient, mass per unit length of mooring line
ν_o	Mean zero-up crossing rate
ν_y	Mean zero-up crossing ratio in combined spectrum
ρ	Correction factor in combined spectrum, air density
σ_{IPB}	Bending stress purely generated from IPB mode
$\sigma_{LF,}\sigma_{WF}$	Standard deviation of low frequency and wave frequency
σ_{NT}	Stress generated due to nominal tension
σ_{OPB}	Bending stress purely generated from OPB mode
σ_{PIPB}	Max principal stress of chain link for IPB mode
σ_{POPB}	Max principal stress of chain link for OPB mode
σ_{PTT}	Max principal stress of chain link for tension
σ_{Proof}	Stress generated due to proof load
σ_S	Standard deviation of stress
σ_{Total}	Total stress calculated from FEA in specified stage

σ_Y	Standard deviation in combined spectrum
σ_n	Nominal stress
σ_{true}	True stress
σ_y	Yield stress
σ_v	Standard deviation of fluctuating wind velocity
ω	Angular frequency (= $2\pi f$)

굽힘 효과를 고려한 다점계류 된 심해용 FPSO의 계류삭 피로평가

황 외 주

Department of Ocean Engineering
Graduate School of
Korea Maritime University

요 약

Oil 및 Gas 자원과 관련된 해양에너지 개발에서는 지속적으로 새로운 최첨단의 기술과 높은 생산성 등이 요구되고 있다. 특히, 심해 및 초극심해에서 가동되는 부유식 해양설비의 경우 변화무쌍한 해양환경에 대하여 제 위치를 유지(Station-keeping)하는데 있어서 중요한 역할을 하는 계류시스템에 대한 강도 및 피로평가와 관련한 요구조건 역시 점차 강화되고 있다.

본 연구는 계류시스템의 구성요소 중의 하나인 계류삭(Mooring Chain)에 대한 피로평가를 다루고 있다. 일반적인 계류삭의 피로평가는 계류계를 구성하는 계류삭 간의 굽힘강성을 무시하고 단순히 인장변화에 따른 영향만을 고려하고 있다. 하지만, 해양설비의 가동 수심이 깊어짐에 따라 부유체의 수평거동을 최소화하고 경비를 절감하기 위하여 선인장력(Pre-tension)을 최대한 가하여 주는 타우트(Taut) 혹은 세미타우트(Semi-taut)형식의 계류방식이 많이 사용되고 있다. 이러한 방식의 경우 계류삭 상호간의 마찰력 증대로 부유체의 운동에 따른 계류선의 각 변화에 따라 계류삭에 면내외(In-plane or Out-of-plane) 굽힘 응력이 발생하여, 이에 따른 IPB (In-Plane Bending) 및 OPB (Out-of-Plane Bending) 피로손상

을 유발시킨다.

본 연구의 목적은 이러한 굽힘 효과가 고려된 계류삭의 피로손상을 평가하는 것으로, 비선형 유한요소해석(Non-linear FE Analysis)을 통한 인장력과 각변화에 따른 계류삭 간의 굽힘강성 및 계류삭 면에서의 응력집중계수 등을 계산하는 방법과 굽힘 효과를 고려한 계류삭의 피로수명 계산 절차를 제안하는 것이다. 그리고 이러한 결과물들을 다점계류 된 심해용 FPSO의 계류계에 적용하여, 인장효과만을 고려한 일반적인 경우와 굽힘 거동을 함께 고려한 경우에 있어서의 피로수명을 계산하고 비교 분석하여, 이를 통하여 심해용 계류시스템 피로설계의 기술적 지식을 정립하는 것이다.

계류삭의 굽힘 하중에 대한 기계적 거동 검토는 비선형유한요소 프로그램인 ABAQUS를 사용하여 선인장력(Pre-tension)과 마찰계수에 따른 계류삭 간의 굽힘강성(Bending Stiffness) 및 응력집중계수(Stress Concentration Factor)를 계산하였다. 해석 결과로부터 선인장력이 클수록 큰 굽힘강성과 응력을 나타내었다. 기본적으로, 계류삭 간의 마찰계수는 OPB JIP (Joint Industry Project)의 제안에 따라 0.7을 사용하였고, 마찰계수에 따른 응력의 변화를 확인하기 위하여 다양한 값을 사용하여 그 결과를 비교 분석하였다. 본 해석에 대한 자세한 사항은 본문의 6장에 기술하였다.

본문의 7장에서는 계류삭의 굽힘 효과를 고려한 계류삭의 피로수명 계산 절차를 제공하고 있으며, 이를 세미타우트(Semi-taut) 형식으로 다점계류된 심해용 FPSO에 적용하여 피로수명을 계산하였다. FPSO의 유체역학적 특성인 진폭응답함수(Response Amplitude Operator) 및 이차전달함수(Quadratic Transfer Function)는 DNV (Det Norske Veritas) 선급의 WADAM을 사용하여 계산되었다. 계류된 FPSO의 거동 계산은 준동적해석(Quasi-dynamic Analysis) 기준의 BV (Bureau Veritas) ARIANE7을 사용하였으며, 이 방법을 사용하면 해양의 수많은 가동조건에 대하여 계류시스템을 고려한 부유체의 거동을 시간이력 대별로 정확하고 빠르게 구할 수 있다. 이렇게 구해진 FPSO의 6자유도 거동은 계류선의 선동적해석(Line Dynamic Analysis)에 사용되었으며, Rainflow Counting 방법으로 계류삭 간의 각변화폭과 인장력 변화폭을 계산하고 피로수명을 계산하였다. 여기서, 비선형 유한요소해석(Non-linear Finite Element Analysis)을 통해 계산된 굽힘강성 등이 계류

선의 동적 거동 계산을 위한 모델링에 사용되었다. 적용된 해양환경은 서부아프리카 해역을 대상으로 하고 있으며, 해당 해역에서의 파랑, 바람 및 조류에 대한 자료가 사용되었다. 특히, 서부아프리카 해역의 파랑 특성인 너울과의 중첩 환경을 고려하여 Ochi-Hubble 스펙트럼을 사용하였고, 풍속은 Kaimal 스펙트럼을 사용하였다.

본 연구의 결과, 계류삭의 피로수명 산정 시 일반적으로 적용되는 인장력 변화에 따른 피로수명에 비하여 굽힘 효과를 함께 고려할 경우의 피로수명이 상당히 낮음이 확인되었다. 이는 계류삭의 피로해석 시 선인장력이 큰 심해역 또는 초극심해용 부유체에 있어서 굽힘 효과가 필수적인 요소라는 것을 의미한다. 더욱이, 계류삭의 굽힘 효과를 고려할 때, 정적 인장력이 큰 계류계에서 더 큰 피로손상이 계산되었으며, 면내굽힘의 영향이 전체 피로수명 계산에 미치는 영향이 작지 않음도 발견할 수 있었다.

끝으로, 본 연구에서는 계류삭 간의 마찰로 유발되는 굽힘 거동에 대한 메커니즘을 이론적, 해석적 바탕에서만 기술하였으나, 향후 추가 연구로써 이에 대한 다양한 실험적 검증과 실제 해상환경에서 계류삭의 피로수명에 영향이 클 것으로 판단되는 부식, 해양생식(Marine Growth) 등이 어떻게 OPB / IPB 피로손상에 영향을 미치는가에 대한 검토 및 분석이 필요할 것이다.

Fatigue Assessment for Mooring Chain Link of Spread-Moored FPSO in Deepwater Considering Bending Phenomenon

Hwang, Oeju

Department of Ocean Engineering
Graduate School of
Korea Maritime University

Abstract

Consistently, the demand for offshore energy development with regards to oil and gas resources has increased, and the field has required state of the art technologies and concepts for better engineering productivity. In particular, the mooring system, which plays a major role in keeping floaters in position in deep and ultra-deep water, also requires more stringent requirements, not only for strength, but also for fatigue.

This paper covers the fatigue assessment of chain links, a component of the mooring system of floaters. In general, the mooring chains are designed only for tension fatigue, with little consideration given to the bending stiffness. However, in cases of increased water depth, the floater is normally installed in a taut or semi-taut mooring configuration so that it can minimize the horizontal offset from the external environmental loads. To make such a taut line configuration, high pretension is generated by pulling up the mooring lines. Unfortunately, an instance of friction-induced bending can be generated between chain links according to the

mooring line's angular change. These types of bending stresses are referred to as OPB (Out-of-Plane Bending) and IPB (In-Plane Bending) stress, which can cause fatigue failures; i.e. OPB/IPB fatigue.

The objective of this study is to propose a proper assessment procedure for fatigue calculation of mooring chains, including the friction-induced bending phenomenon. To that end, using ABAQUS, nonlinear FE analyses were used to determine the mechanical properties (e.g. stress concentration factor (SCF) and bending stiffness) between chain links for the angular behavior and nominal tension. Finally, the fatigue lives of the first chain links were obtained and analyzed by utilizing FEAs results from a spread-moored deepwater FPSO,

As mentioned above, ABAQUS, a conventional tool for nonlinear FE analysis, was utilized to investigate the mechanical behavior of chain links under their angular change. Through these analyses, the effects of factors such as pretension and friction coefficient were examined. Thereafter, bending stiffness and stress concentration factors on the chain were calculated. Based on these calculations, it was determined that a higher pretension generated higher bending stiffness and stress levels. It should be noted that a friction coefficient of 0.7 was applied in the analysis as per the recommendation of OPB JIP (Joint Industry Project). In Chapter 6, this is described in further detail.

Chapter 7 covers the assessment procedure for chain fatigue by taking into account the bending phenomenon of chain links, and, to calculate fatigue life, its application to deepwater FPSOs with a semi-taut mooring configuration. Hydrodynamic properties of the FPSO, i.e. Response Amplitude Operator (RAO) and Quadratic Transfer Function (QTF), were obtained by using DNV WADAM. In addition, by using BV ARIANE7, the six (6) Degrees of Freedom (DOF) of the FPSO (in terms of the mooring legs) were computed based on quasi-dynamic analysis, which made it possible to obtain the time series of the FPSO motions both quickly and accurately. The line dynamic analysis used to compute the dynamic motions of the mooring line was performed by using OrcaFlex in time domain, from which the cycle numbers and ranges of chain interlink angles and tension

were computed using the Rainflow Counting method. In the analysis, the bending stiffness, along with the interlink angle of the chain was applied as input. Thereafter, each mooring chain's fatigue life was calculated. Finally, the effects of friction-induced bending on chain fatigue were compared and analyzed. On-site environments used for this study were the metocean data collected from the West African Offshore. The Ochi-Hubble spectrum and Kaimal spectrum were utilized for wave and wind realization, respectively.

From these studies, it was possible to conclude that friction-induced OPB/IPB fatigue of mooring chains is significant in three ways. First, in the case of semi-taut or taut mooring configurations normally used for deepwater or ultra-deepwater, the bending phenomenon of mooring chains is especially relevant in terms of fatigue strength. Second, higher pretension decreased the fatigue strength of the chains to a much greater extent than was previously known. Finally, In-plane Bending (IPB) was also found to be an essential factor in chain fatigue.

Lastly, this paper covers results only for the FE-based mechanism between chain links to determine the friction-induced bending effects in which the basis was theoretical and analytical. Therefore, in a future project, to reach more definitive conclusions, it will be necessary to a) look into other effects on the chain's OPB/IPB fatigue, such as corrosion and marine growth on mooring chains, and b) to collect various experimental data.

1. Introduction

Consistently, the demand for offshore energy development with regard to oil and gas resources has increased, and the field has required state of the art technologies and concepts for better engineering productivity. In particular, for deep water or ultra deep water (depths greater than 1500m), the sustained drive to improve the harvests from offshore oil exploration, production, and transportation has led to the specific needs of various floating structures like FPSOs and SPARs In addition, most offshore floaters have been required to meet rigorous design requirements in terms of structural strength and fatigue in order to reduce the levels of unknown or potential risks (Brown, et al., 2006; Chakrabarti, 2008; Wyllie, et al., 2006). Lanquetin (2006) suggested in this regard four floaters' integrity managements gained from actual offshore experiences; 1) FEA and mooring model, 2) IRM (Inspection, Repair and Maintenance) plan, 3) data management, and 4) emergency response.

Floating offshore structures, which, like any other vessel, must be able to withstand environmental factors such as current, wind and wave, require station keeping systems to maintain stability. Therefore, mooring systems, which are widely-applied and specifically designed for this purpose, have to provide maximum station-keeping capability and high global performance to ensure allowable excursions against environmental loads (ISO, 2005a). The performance characteristics of mooring systems are typically a function of the following factors: the type and size of the floater in use, the operational water depth, acting environmental loads, sea bed conditions, and, finally, the competence of the mooring lines, anchors, and clump weights.

Unlike general trading ships, offshore floaters remain in a fixed position throughout their lives without regular dry docking for inspections and/or repairs. In addition, since they must remain in place even in the most severe weather conditions, the mooring legs must be designed to withstand the effects of any and

all environmental factors. Even in cases where sea conditions may be mild, the sea wave loads can cause fatigue damage to the mooring legs.

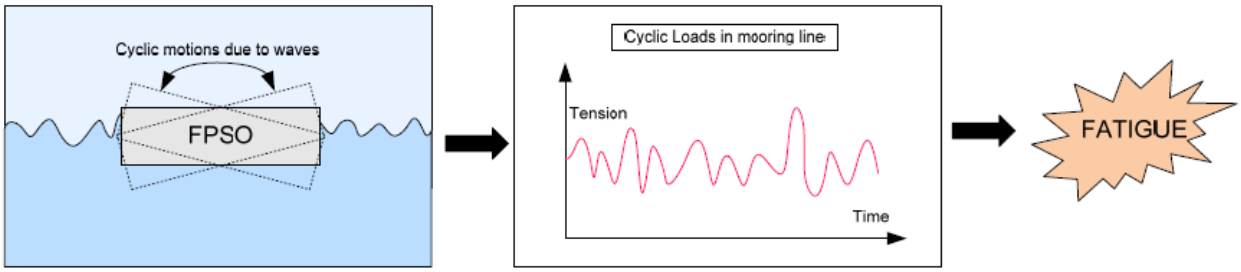

Fig.1-1 Mooring fatigue from floater's cyclic motions due to waves

Generally, mooring legs have been designed with due consideration given to tension fatigue as mooring lines have no bending stiffness. This would be sufficient in the case of catenary mooring legs, which are normally installed for shallow water. However, in the case of deep or ultra-deep water, the mooring legs are generally designed with a taut or semi-taut configuration to save costs. Unfortunately, due to FPSO motions in adverse sea conditions, the high tension involved in this type of configuration produces unexpected friction at the mooring top chains.

Depending on how frequently the chain is exposed to these types of stresses, such friction between chain links can lead to bending, which eventually reduces fatigue endurance. This bending-induced fatigue is called out-of-plane bending (OPB) fatigue or in-plane bending (IPB) fatigue according to the direction of the links. It has been found that frictional forces intensify as tension in the mooring leg increases and many studies (Brown, et al., 2005; Brake, et al., 2007; Denayrolles, 2011; Jean, et al., 2005; Kang, et al., 2010; Lim, et al., 2010; Melis, et al., 2005; Rampi, et al., 2006; Thomas, 2011) have been carried out on this issue. Fig.1-2 shows the phenomenon of friction-induced bending between chain links.

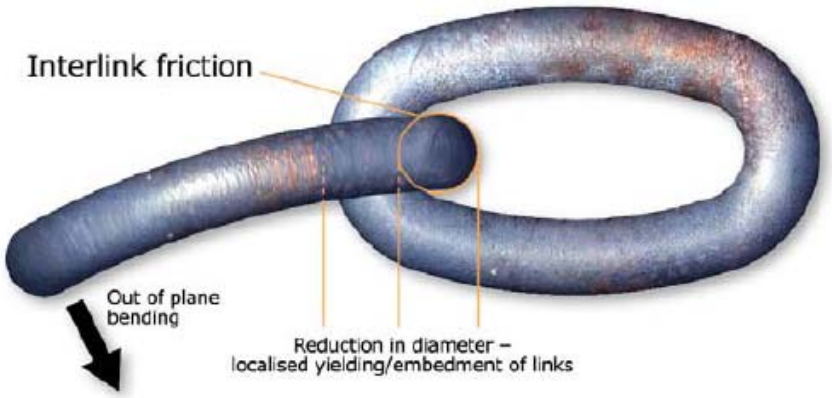

Fig.1-2 Schematic concept of Out-of-plane Bending (OPB)

1.1 Background of Research

The Girassol Loading Buoy was installed in September 2001 on Block 17 of the 'Girassol' oil field situated off the coast of Angola at a depth of 1350m. The purpose of the loading buoy was to offload the refined oil product to the transportation shuttle, which was positioned in proximity to the FPSO. However, after only 235 days of service, an unexpected failure of the chains in the chain hawse of the Girassol Loading Buoy was reported. Fig.1-3 shows the development diagram of the deepwater offshore field of Girassol, and Fig.1-4 shows the offloading buoy of the Girassol as well as the chainhawse of the failed chain link. The ruptures in four mooring legs (Legs B1, B4, B5 and B6) occurred at the exactly same location: the 5th link of the upper chain segment connected to the buoy inside a standard-type curved hawse (TOTAL, 2004; Jean, et al., 2005).

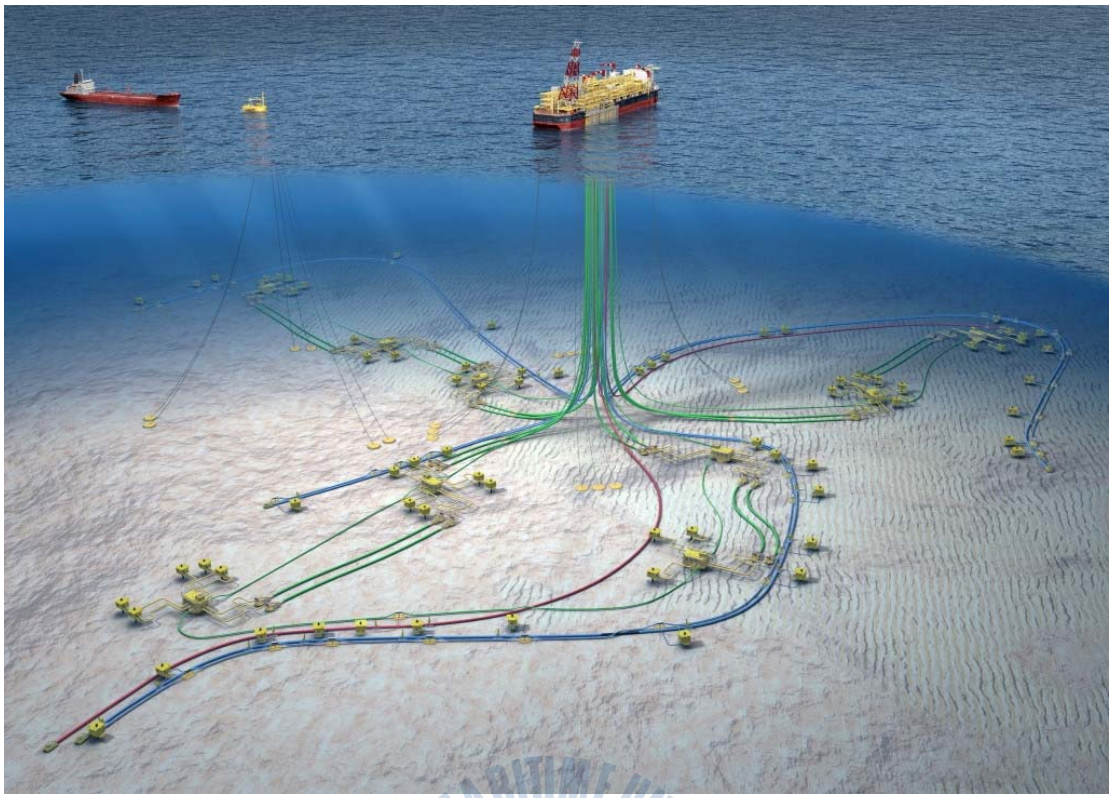

Fig.1-3 Diagram of the deepwater offshore field of Girassol

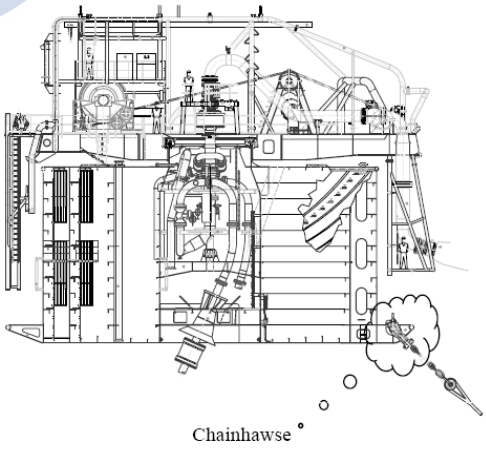

Fig.1-4 Offloading buoy of Girassol field

Through in-depth studies of the root causes of the mooring link's failure, it was found that the chain link ruptures were caused by friction-induced bending as shown here in Fig.1-5.

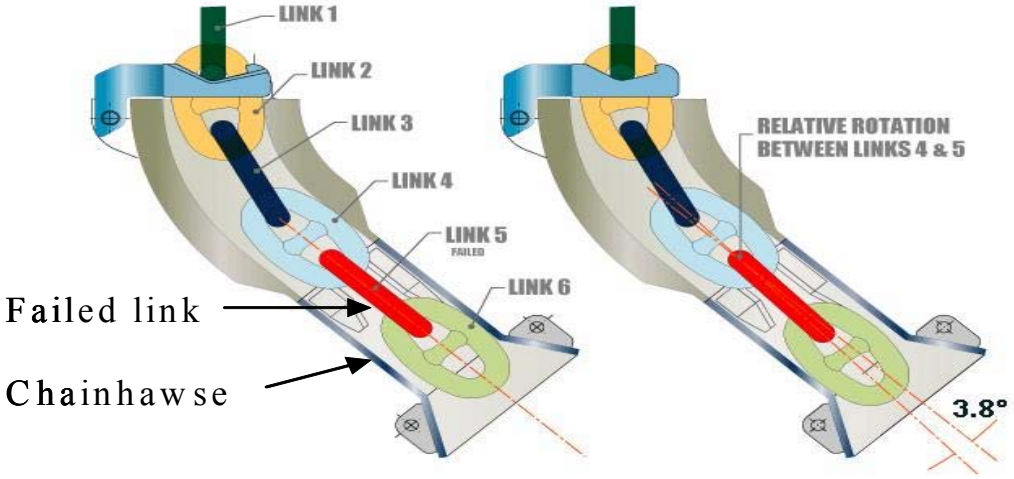

Fig.1-5 Failed chain link of Girrasol offloading buoy

Fig.1-6 Photos of failed chain link of Girassol offloading buoy

As shown in Fig.1-6, the crack was initiated at the location of max stress in its out-of-plane bending. Studies identified the root cause as OPB fatigue stress, combined with tension variations occurring mainly in the 5th link inside the chainhawse.

Until the incident described above, most research on chain fatigue focused almost exclusively on tension and tension-bending in gypsy wheel fairlead, which has been reasonably well documented and incorporated in design practice. Fig.1-7 shows the load mechanism and fatigue testing undertaken by BOMEL JIP (NDE,

2005; HSE, 2006). Study of Vargas et al. (2004) for studless mooring chain links in fairlead was referred to the determination of SCF in Rules.

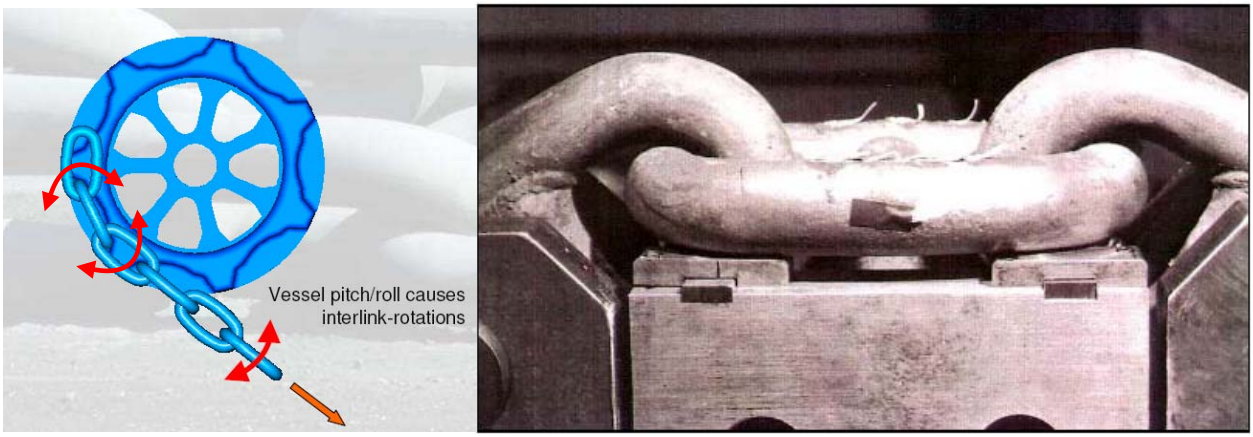

Fig.1-7 Schematic diagram of tension-bending in gypsy wheel fairlead and BOMEL testing

The load mechanism is related to the eccentricity of thrust lines with respect to the bar neutral axis. This effect is enhanced where the change of angle is greater. The imposed hogging moment is balanced by a counter effect at the other end of the link.

Thus, the chain links within the fairlead are subjected to an instance of out-of-plane bending which is proportional to the tension in the mooring line. Tension variations in the mooring line result in a range of stresses due to both the tension and out-of-plane bending in the link. As a vessel pitches and/or rolls, the chain link will experience cyclic loading, which eventually leads to fatigue failure. API (2005) and other relevant codes (ABS, 1999a, 2004; BV, 2004; DNV, 2011) recommend that chain links be exposed to tension bending for a limited period of time in order to ensure mooring integrity and reduce the possibility of tension bending fatigue.

Because the bending stiffness between chain links is generally neglected in the widely-adopted catenary mooring configuration, this bending fatigue has not been documented. However, because higher OPEXs (Operating Expenditures) for the station-keeping design are required as the operational depths of the offshore floaters increases, taut or semi-taut mooring configurations were recommended by

applying initial high pretension in order to enhance the OPEX efficiency for offshore developments. This minimizes the excursion of the floater, but could lead to higher bending stiffness among the interlinks, which, in turn, could lead to OPB cyclic loading of the chain link.

In particular, the mooring systems of deep water floaters (such as FPSOs), require more stringent design requirements due to the tremendous repair costs involved in cases of unexpected failures. In addition, the mooring systems of floaters require much higher fatigue requirements because they remain in the same location for a period of 20 years or longer. Furthermore, these systems cannot be inspected due to the unpredictability of the sea environment. Table 1-1 gives some brief differences between typical and deepwater mooring systems.

Table 1-1 Difference between typical and deepwater mooring systems

Type / Item	Typical Mooring	Deepwater Mooring	Remark
Permanent or Not	Provisional Mooring of Ships	Permanent Mooring of Offshore Floaters	Demand High Fatigue Life
Inspection or Not	Inspectable Mooring Line	Uninspectable Mooring Line	Demand High Fatigue Life
Controllable or Not	Controllable Sea State	Uncontrollable Sea State	Severer Environment
Water depth	Shallow Water	Deep Water	Increase Pretension => Increase Surface Friction => Induce OPB
Mooring Configuration	Catenary Mooring	Taut (or Semi-Taut) Mooring	Increase Pretension => Increase Surface Friction => Induce OPB
Material	Ship Mooring Chain Material	Offshore Mooring Chain Material	High Quality Material => Optimized Size => Stress Increased

1.2 Objectives of Research

To determine an accurate mechanism and applicable solution for the bending-induced fatigue of chain links, various studies, including the joint industry development (JIP), were implemented worldwide. OPB JIP (SBM, 2006), which is

hosted by the French offshore engineering company SBM, is one of them. However, the JIP is still ongoing.

This research was carried out separately from the results from the JIP to determine applicable solutions regarding the chain bending mechanism. The objective of this study is to propose a proper assessment procedure for fatigue calculation of mooring chains (including the bending phenomenon), and, using relevant nonlinear FE analysis methods, to figure out the mechanical properties (e.g. stress concentration factor (SCF) and bending stiffness) between chain links. To that end, the impact of friction-induced bending stresses (like OPB and IPB) on offshore deepwater floaters in terms of chain fatigue strength will also be evaluated. A spread-moored deepwater FPSO with semi-taut mooring configuration was used for the assessment of mooring chain fatigue.

2. Mooring Overview

2.1 Mooring Systems

Most floating facilities are designed to stay at a single location secured to the sea floor. The type of floaters is generally decided depending upon the project's purpose, capital expenditure (CAPEX), operating expenditure (OPEX) and floater's motion, etc (Hall, 2005). In Fig.2-1, the general floater types according to the natural periods of heave motion are given. For instance, the semi-submersible typed floater has a resonance above 20 seconds and therefore, it is known that the motion ability is more beneficial rather than ship-typed drillship.

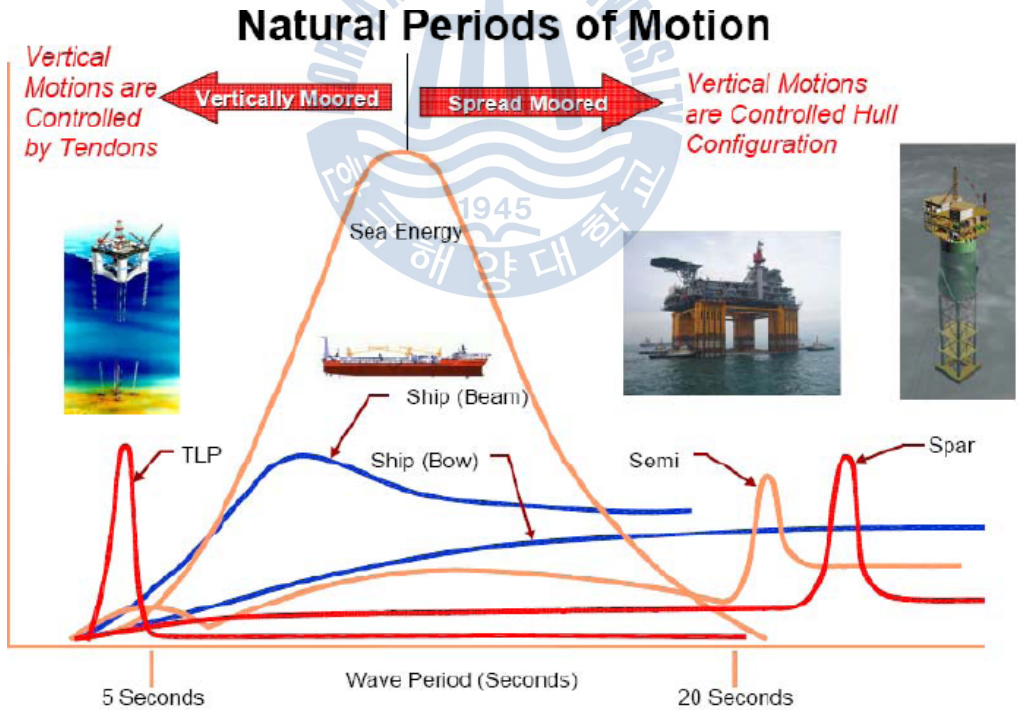

Fig.2-1 General type of floaters according to natural periods of motion

In particular, FPSO, one of main types of floating production facilities, has different design philosophies in designing station-keeping system. Since the FPSO has demerit in terms of roll motion, the mooring system is designed to be able to freely rotate in accordance with the wave orientation on site, which is called as

‘weathervane system’. The weathervane can be achieved with uniquely designed device, e.g. ‘turret’. Typically the turret has two (2) different types of systems for achieving successful weathervane; external turret and internal turret. Both are proven systems permitting the floater to freely weathervane, allowing normal operations in normal sea conditions.

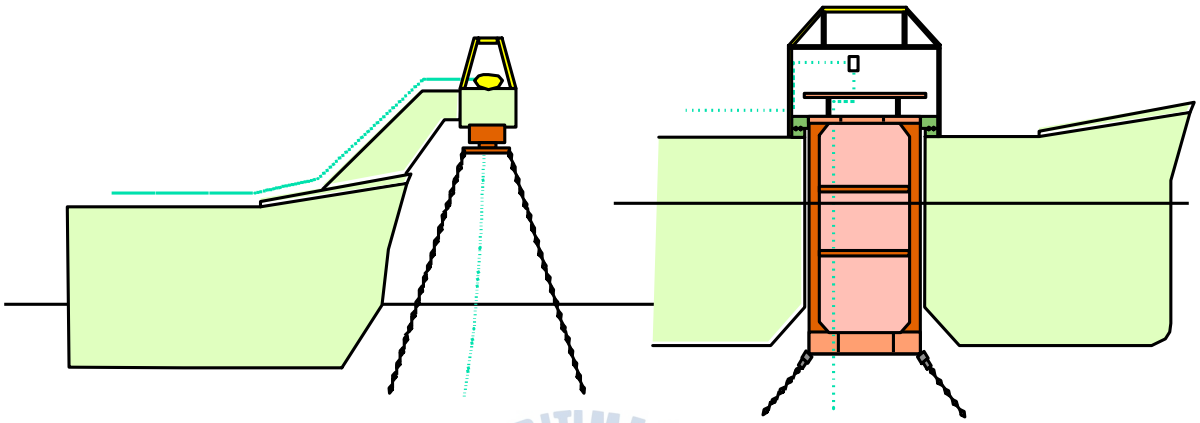

Fig.2-2 External turret and internal turret system

It is known that external turret systems are less expensive than internal turret designs and can be delivered in a shorter period of time. And mooring systems can be mounted at either the bow or stern of converted tankers or new-build vessels. However, the external turret system may be applicable only for small number of risers and in mild to moderate sea conditions. For internal turret systems, it can be extensively applicable in moderate to harsh environments and adopted with large number of risers. As well, permanent and disconnectable system can be applied depending on the offshore development purpose.

The others for keeping the offshore floaters on site are Soft Yoke, CALM (Catenary Anchor Leg Mooring) and SALM (Single Anchor Leg Mooring), which is classified as SPM (Single Point Mooring) system and utilized at shallow waters. Fig.2-3 gives the brief descriptions of these SPM systems.

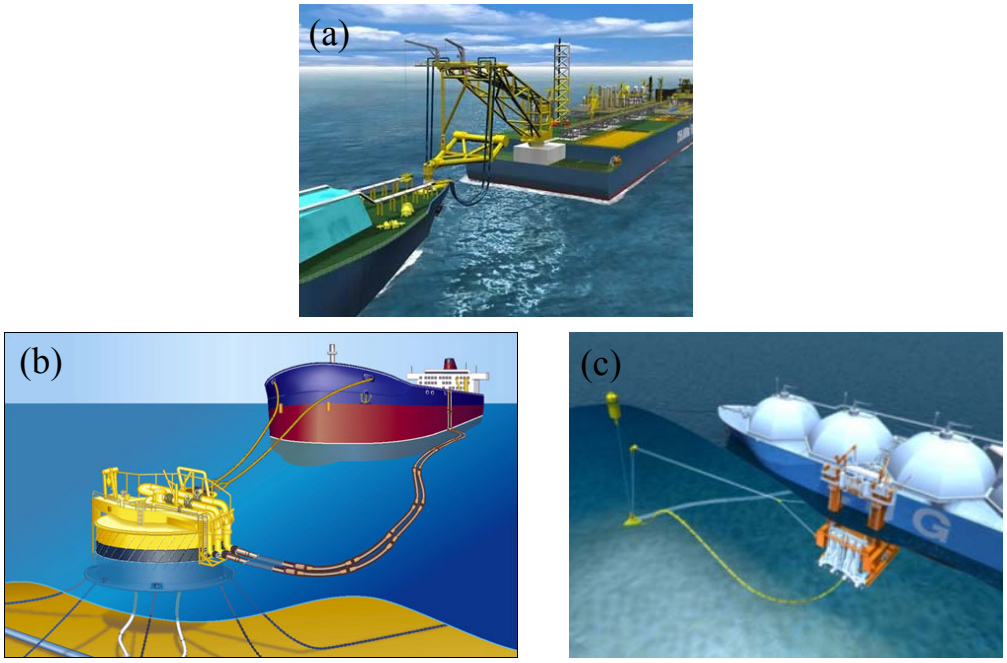

Fig.2-3 General descriptions of Soft Yoke(a), CALM(b) and SALM(c)

Spread-mooring type is another unique station-keeping system of offshore floating facilities. Especially, for the calm sea condition such as African western offshore the type is much more economical solution rather than the turret systems. As reported in many offshore journals, recently the offshore oil fields of African western offshore, e.g. Nigeria, Angola or Gabon, was developed along with spread-mooring typed FPSO since the sea environmental conditions at the site are relatively calm and constant; e.g. primal wave direction from southwest, except for infrequent squalls that are generated over land over the summer months. However, most of the sites have ultra deep water depth above 1000m (Bang, 2002; Maretti, et al., 2009; Hollister, et al., 2004).

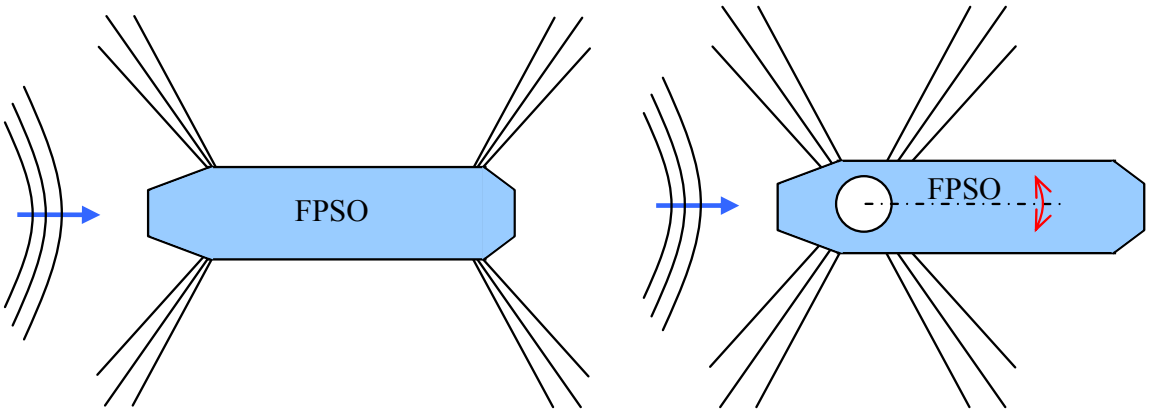

Fig.2-4 Spread-moored FPSO and single point moored FPSO with turret

2.2 Mooring Leg Configuration

The primary purpose of mooring legs is to maintain an offshore floating structure on station within a specified tolerance, typically based on an offset limit determined from the configuration of the risers. Also the mooring system is to provide a restoring force that acts against the surrounding environmental loads such as wind, current and wave. The horizontal components of the mooring legs' tension give such restoring force. The vertical force of mooring legs can be quite considerable in determining payload capacity since it acts as a vertical weight on the floating facility.

As shown in Fig.2-5 below, if the angle is large to the vertical, the restoring force will be increased while the vertical load on the vessel will be reduced. Also, for the in-plane of the sea surface one component of mooring tension will oppose the environmental loading while the lateral component will balance with other mooring legs (HSE, 2006; NDE, 2005).

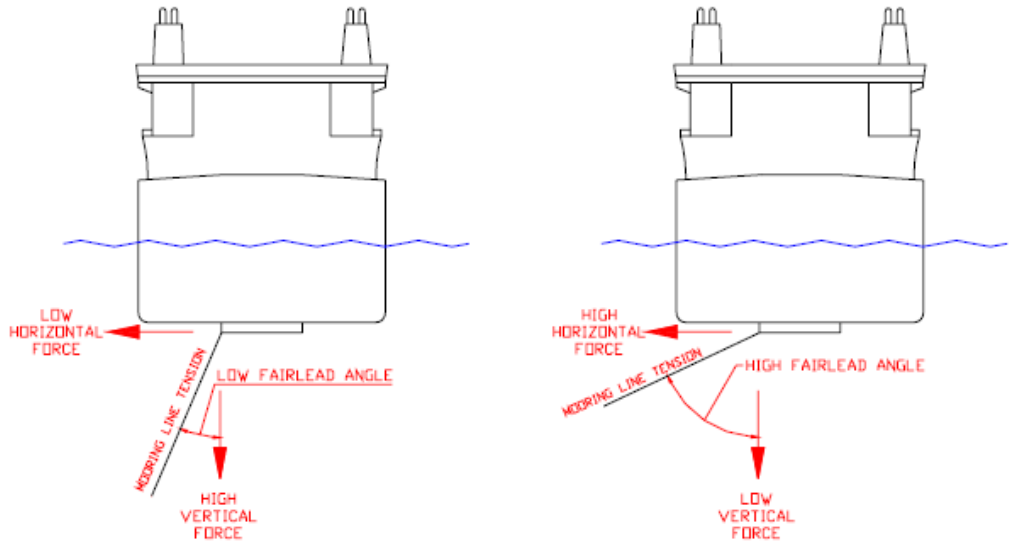

Fig.2-5 Shallow and steep mooring line angle illustration

The primary function of the mooring system is to counteract the horizontal environmental loadings so that the floating structure can remain with specified tolerances. Until the horizontal restoring force by mooring legs balances the environmental loadings, the floater will offset as shown in Fig.2-6. The longer offset the floater is horizontally moved due to the environmental loadings, the higher tension the mooring legs statically needs.

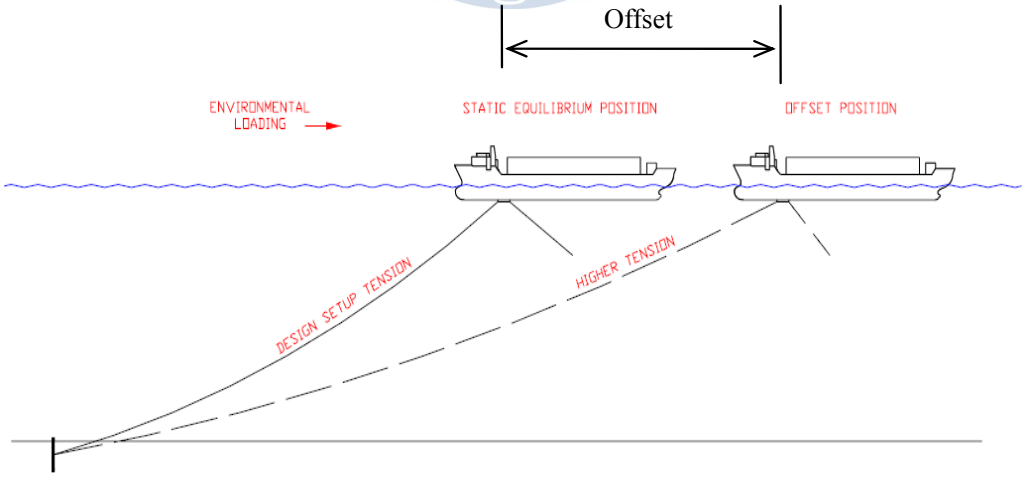

Fig.2-6 Offset position and tension effect

Therefore, it is essential that when determining the mooring leg configurations the engineers estimate the resultant offset under the severest environmental

condition and take into account the cost from the installation to the on-site operation. Normally there are two main types of mooring leg configuration for either spread-moored or SPM; catenary and taut-leg configuration.

Catenary type is the more general mooring configuration, which generates restoring force through the lifting and lowering of the line onto the seabed, plus a limited amount of line stretch. As illustrated in Fig.2-7, in catenary mooring system, the wetted weight of the suspended part of the mooring line balances the station keeping moment, i.e.;

$$M_s = w\, s\, a \tag{2-1}$$

where, M_s is moment introduced from a mooring line and w is the buoyancy-corrected weight per unit length, s is the line length, and a is the horizontal distance from the fairlead to the center of gravity of the suspended line.

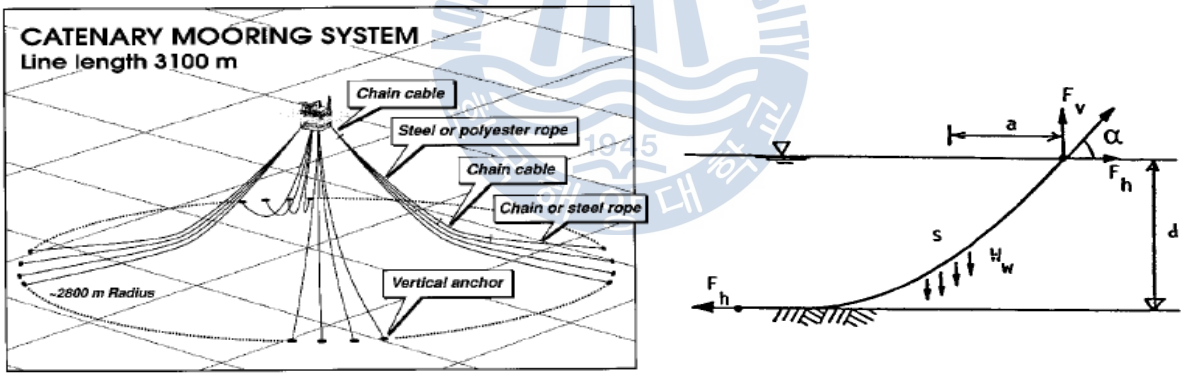

Fig.2-7 Catenary mooring system and force balance

In taut mooring system, the material properties of the mooring lines, e.g. its elasticity is used. The compliance to allow for the sea environment must be provided entirely by the axial elasticity of mooring legs. This mooring configuration is relatively new and typically used in deepwater to limit floater offset. The weight of mooring legs is light compared to the line tension, and the lines will be nearly straight between the fairlead to the anchor. In this case the vertical force is taken up as anchor and vessel reactions directly. The taut mooring system and its force balance are illustrated in Fig.2-8. The vertical force is

determined by Eq.(2-2), and accordingly the vertical force decreases with increasing mooring leg length.

$$M_s = F_h d = F_v a \tag{2-2}$$

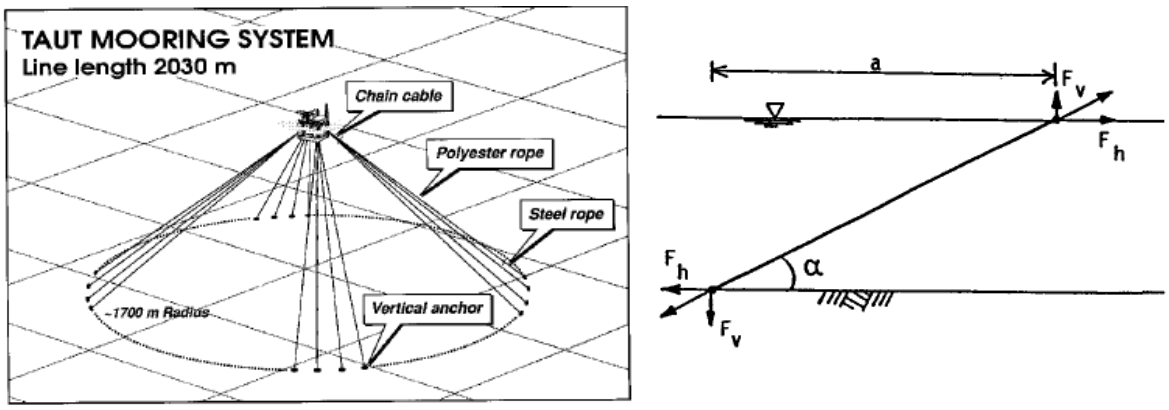

Fig.2-8 Taut mooring system and force balance

Taut mooring system often utilizes synthetic ropes to obtain sufficient elasticity and reduce the weight. Note that the synthetic ropes give rise to important dynamic effects, for example hysteresis, due to its more complex behavior than steel. Besides, the high tension of the mooring legs to keep the tolerable offset under sea environments induces out-of-plane bending behavior of top chain links, i.e. the subject of this research. Sometimes, semi-taut mooring configuration is utilized in deepwater to slightly reduce the high tension by combining with catenary effects.

2.3 Mooring System Elements

In this section, some elements of mooring system to understand this research are briefly described.

● Chain

Chain is the most common element in mooring system, which is a flexible connection through multiple rigid metal links. Chain is available in different chain construction. For offshore mooring lines, in common two constructions are used; stud link chain and studless link chain. Note that the studless link chain is often

used for permanent offshore mooring due to some reasons; better inspection of weld and crown area, elimination of stud locating problems, etc. And Fig.2-10 gives the comparison of the geometry of both links. Basically, mooring chains should be confirmed in terms of the reliability in the offshore operation of floaters (Fernandez, 2008; API, 2001; ABS, 1999; Petruska, 2008; DNV, 2009).

Fig.2-9 Studless chain (left) and stud link chain (right)

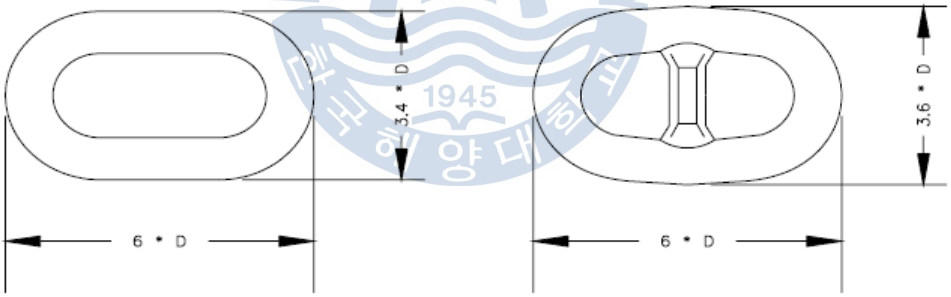

Fig.2-10 Comparison of the geometry of studless (left) and stud link chain (right)

● Wire Rope and Synthetic Rope

Wire rope construction types are widely used for offshore mooring lines (API, 2001; DNV, 2009b). Typically six strand independent wire rope core (IWRC) is utilized due to its lateral flexibility and relative cheapness, which is given in Fig.2-11. Spiral strand wire is generally torque balanced and sheathing protects the wire from corrosion. The typical differences of the main wire rope constructions are indicated as table 2-1.

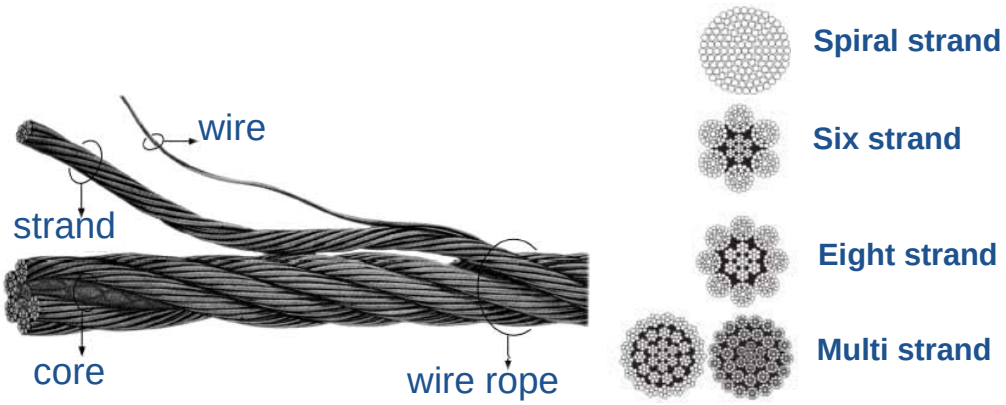

Fig.2-11 Illustration of the make-up of different wire rope types

Table 2-1 Indicative differences between two main wire rope constructions

Spiral strand construction	Six strand (IWRC) construction
Higher strength to weight ratio	Higher elasticity
Higher strength to diameter ratio	Greater flexibility
Torsionally balanced	Lower axial stiffness
Higher resistance to corrosion	Ultimate tensile = 1860MPa
Higher fatigue resistance	
Ultimate tensile = 1570MPa	

On the contrary, the synthetic fiber rope is far lighter than the wire rope but its tensile strength and modulus offer certain advantages for offshore mooring. Synthetic fiber ropes are made of visco-elastic materials, so their axial stiffness varies with the duration of load application, the load magnitude. In general, it is known that the synthetic mooring lines become stiffer after a long time in service and creep over time, and so the creep rupture and fatigue is critically possible failure mode. A recent guideline for the use of synthetic fiber ropes is given by lots Classes (API, 2001; DNV, 2005b; BV, 2004).

● Anchoring System

Anchoring system is a main mooring system in offshore floating facilities. In selecting the proper anchoring system of offshore floaters, not only the water depth but also the conditions of sea bed are the major factors. In particular, for the deep water the common type anchoring system, for instance drag anchors, will not be capable of resisting the tension force from the mooring legs for all the service time of offshore facilities.

Thus, for the deepwater installation of the offshore floating structure like FPSO, the suction anchoring system as shown in Fig.2-12 is mainly utilized (Dahlberg, 2006). Suction anchoring system uses steel pipes, although the diameter of the pipe is much larger than the common steel pile, so that it can endure the suction pressure inside. The principle of the suction anchoring system is that when pressure inside the pipe is lower than outside by suction pumps the steel-piped anchor is sucked into the seabed and the holding capacity of the suction anchor is generated by the friction of the soil along the length of the pipe and the lateral soil resistance. The system is designed to be capable of withstanding both horizontal and vertical loads from the mooring legs (DNV, 2005a; Eltaher, et al., 2003; Sparrevik, 2002). Normally the mooring chain link part directly connected to the suction anchor is called as ‘bottom chain’, whereas the mooring chain connected to fairlead of a floater is ‘top chain’ part.

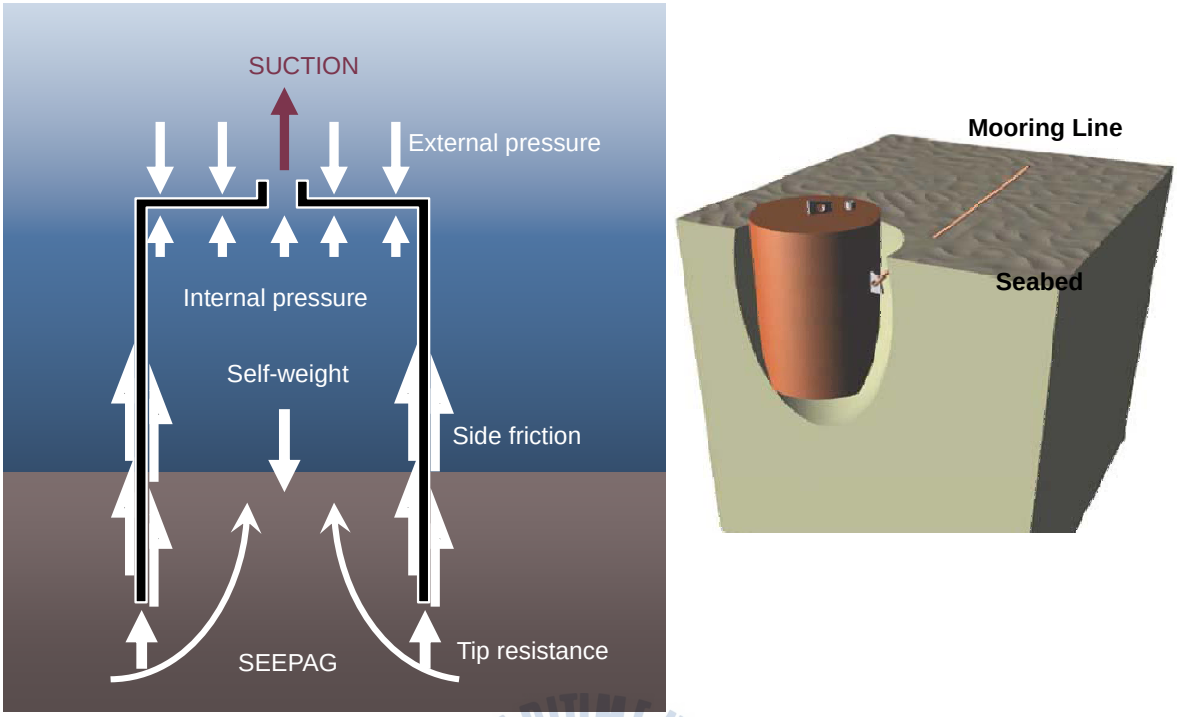

Fig.2-12 Suction anchoring system and its principle

2.4 Manufacture of Mooring Chain

The life of mooring chains, the most important element of mooring system, generally begins with the steel bar cutting and transported to the manufacturing workshop, where they undergo seven operations: pre-heating, bending, welding of links, trimming, shaping, post-heating treatment, and investigation by ultra sonic and proof loading tests. Fig.2-13 describes these manufacturing cycles of mooring chains.

Particularly, the proof load test which is the final stage of the manufacturing process is highly of importance in calculating OPB stress of chain links. At this stage, the proof load of around 70% of minimum breaking load (MBL) is applied for the strength confirmation (Denayrolles, 2011; HSE 2006; NDE, 2001, 2005). During the test, the chain link will have plastic behaviors at the contact surface between the chain links, which generates some residual stress and deformation of the surface with respect to out-of-plane bending friction.

Fig.2-13 General process of chain link manufacture

For the offshore mooring chains, it is normal that three classified materials are utilized; R3, R4 and R5, which are general grade names of offshore chain. DNV (2010a) gives the effective elastic modulus in the mooring analysis for preliminary design as follows, in which '*D*' is chain diameter in mm;

- Stud link chain R3: (12.028 – 0.053D) 10^4MPa
- Stud link chain R4/R5: (8.208-0.029D) 10^4MPa
- Studless link chain R3: (8.37-0.0305D) 10^4MPa
- Studless link chain R4/R5: (7.776-0.01549D) 10^4MPa

From the data of VICINAY (HSE, 2006; NDE, 2005), a mooring chain manufacturer, the stress strain curves for each offshore mooring chain are given as Fig.2-14 below.

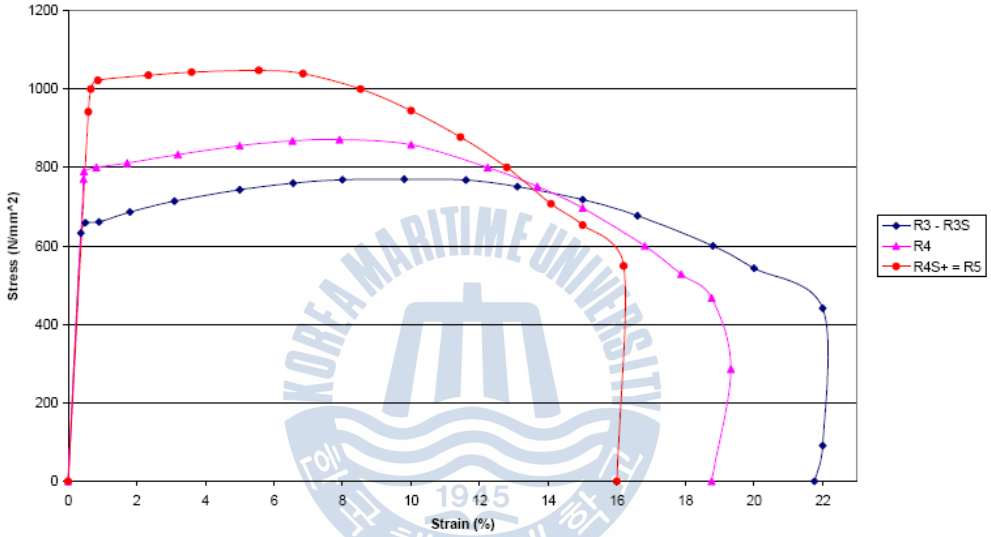

Fig.2-14 Stress strain curves for R3, R4 and R5 offshore mooring chain

2.5 Design of Mooring Lines

In the design of mooring lines of offshore floating facilities, it is necessary to determine the design environmental loadings, e.g. current, wind and wave, from the metocean data surveyed on-site. Based on the surveyed data, mooring analysis is performed to predict extreme responses such as line tensions, and vessel offsets combining to other external loads like riser loads, offloading tandem loads. The mooring system shall be confirmed for the floater under consideration to be capable of keeping it within the required tolerance. Further, the mooring legs have sufficient fatigue endurance for the whole time in place.

Not only API (2005) but also various Classes, e.g. ABS (1999), DNV (2010a), BV (1998, 2004), etc., offer design guidelines for the mooring lines' design. Most of them suggest that the mooring system be analyzed according to design criteria formulated in terms of three limit states:

- ULS (Ultimate Limit State) to ensure that the individual mooring lines have sufficient strength to withstand the extreme loads

- ALS (Accidental Limit State) to ensure that the mooring system has sufficient capacity to withstand the failure of one or more mooring lines.

- FLS (Fatigue Limit State) to ensure that the individual mooring lines have sufficient capacity to withstand cyclic loading.

This research for assessing OPB effects of mooring lines due to high pretension of a deepwater floater was undertaken as the work of FLS to ensure the fatigue strength of mooring lines. Recently the numerical modeling and analysis was getting increasingly important for carrying out the design of mooring lines (Brown, et al., 2005; Connaire, et al., 1999; Hassen, et al., 2009; Heurtier, et al., 2001). Since no physical model test facilities can accommodate all water depths and mooring lines, the numerical approach is a best solution to understand the mooring lines' behavior.

In general, the numerical approach has two types; frequency domain approach and time domain approach (Boom, 1985). However, the frequency domain approach cannot fully deal with the nonlinear effect of mooring lines including OPB phenomenon of chain links. Instead, the time domain approach is widely used to compute the mooring lines' behavior; even though its behavior has nonlinearities (Gao, 2008). Sometimes, a combined time and frequency domain approach is often employed to reduce the complexity and computation effort associated with the full time domain simulation (Brown, et al., 1999; ISO, 2005a).

3. Fatigue Assessment of Mooring Chain

3.1 Tension Fatigue

The largest cause of structural failure of mooring legs, in particular for steel chain links, is fatigue damage. Under repeated cycles of relatively low stress levels a steel metal fails due to the growth of internal cracks that can be initiated from local fabrication defects or at stress concentrated spots. Such metal fatigue failures are quantified from experimental data by the use of SN (Stress-Number of cycles) curves which is normally plotted in logarithmic form (Almar-Naess, 1985).

Tension fatigue analysis is the most common process for assessing the mooring chain fatigue, in which only axial stiffness of mooring lines is considered. Thus, API (2005) and BV (2004) suggest TN (Tension versus number of cycles) curves to calculate accumulated fatigue damage instead of SN curves. TN curves gives the number of cycles to failure for a specific mooring component as a function of constant normalized tension range, based on the results of experiments. TN curves also typically correspond to a lower bound defined as bound of a two sided, 95% interval (i.e. 2.5% probability of fatigue resistance exceedance).

Basically the fatigue damage accumulated from the cyclic loadings can be calculated based on Miner. For an environmental sea state *i*, the cumulative fatigue damage can be achieved as follow;

$$D_i = \sum_{j=1}^{N} \frac{n_{T_j}}{N_j} \tag{3-1}$$

where, j = j-th tension or stress range

N_j = Number of cycles to failure at j-th tension or stress range

n_{T_j} = Number of cycles experienced by the chain link within the j-th tension or

stress range

API (2005) offers proper TN curves based on many reliable test results for calculating the nominal tension fatigue life of mooring chain links.

$$N \Delta R^m = K \tag{3-2}$$

where, N = Number of cycles to failure

ΔR = Ratio of tension range to minimum breaking load (MBL) of chain links;

$$\Delta R = \frac{\Delta T}{MBL}$$

m = Inverse slope parameter of TN fatigue curve

K = Fatigue coefficients

For stud link chain, BV (2004) describes two parameters of TN curve; m = 3.36 and K = 370 but, for studless link chain, K is 170 which is much lower. But API (2005) gives references more in detail regarding these two coefficients as following Table 3-1.

Table 3-1 TN curve parameters specified in API RP-2SK (2005)

Component	m	K
Stud Link	3.0	1,000
Studless Link	3.0	316

While, DNV OS-E301 (2010a) 'POSMOOR' for the fatigue capacity of mooring chain gives SN curves instead of TN curves:

$$N \Delta S^m = a_D \tag{3-3}$$

Above Eq.(3-3) can be linearized by taking logarithms as follows;

$$log(N) = log(a_D) - m\, log(\Delta S) \tag{3-4}$$

where, N = Number of cycles to failure

ΔS = Stress range of chain link (in MPa)

a_D = Intercept parameter of SN curve

m = Inverse slope of SN curve

The parameters of a_D *and* m are given Table 3-2, which is recommended by DNV (2010a).

Table 3-2 SN curve parameters specified in DNV OS-E301 (2010a)

Component	m	a_D
Stud Link	3.0	1.2×10^{11}
Studless Link	3.0	6.0×10^{10}

3.2 Tension Bending Fatigue

As mentioned in Chapter 1, the fatigue assessment of chain links is normally undertaken for tension fatigue due to negligible bending stiffness between chain links in case of slacked mooring configuration. Many design codes from API (2005), DNV (2010a), BV (2004) and ABS (1999) include recommendations on the design for tension bending fatigue of chain at wheel fairleads. However, any codes do not provide detailed practical guidance on analysis and on the interlink friction effects.

Note that tension and bending effects on chain fatigue will coexist. Hence, the calculation of fatigue damage due to chain link's bending is required to consider the tension value; e.g. pretension to meet the tolerable offsets (Huang, 2002). This research was performed to propose more rational approach regarding the tension bending fatigue of chain links, which is more important design factor in terms of chain fatigue rather than just tension fatigue.

From the results from various OPB fatigue studies including OPB JIP, it was recommended that DNV B1 curve (for forged elements) is appropriate in assessing fatigue damage, in which the inverse slop m of SN curve is 3.0 and $log(a_D)$ =

12.436. Besides, in case of use of B1 curve specified in DNV RP-C203 (2011) and NORSOK N-004 (2004a), it is recommended that the design fatigue factor be 10. And for fatigue safety factor, BV (2004) recommends three (3) as a minimum safety factor to top chain segments when taking into consideration OPB fatigue or local actions. API (2005) offers a guideline for minimum fatigue life of three (3) times of service life.

In summary, below the differences between the tension fatigue and bending induced fatigue are briefly given.

● Tension Fatigue
- All segments along a mooring leg are considered; for top/bottom chain and spiral strand wire.
- Fatigue damage is calculated based only on tension variation without friction induced bending.
- Normal descriptive SN or TN curve is adopted to calculate fatigue damage.

● Bending induced fatigue (e.g. OPB/IPB fatigue)
- Top chain of mooring line is subjected to bending (OPB or IPB) due to FPSO motion, especially in deepwater the high pretension worsen the fatigue endurance.
- Predominantly OPB fatigue failure occurs in the first link after a link constrained by chain stopper.
- Fatigue failure can be propagated fast.
- Thus, additional stress from the chain links' bending to be taken into account.

3.3 Fatigue Calculation Methods

In computing fatigue damage of mooring lines, both the vessel motion analysis and the mooring line dynamics are necessary. The dynamic behavior of mooring lines can be split into two modes; wave frequency and low frequency from the response of vessel caused by steady wave, wind and current forces, and wave

frequency (WF) and low frequency (LF) wave loads and LF wind forces (DNV, 1999, 2010a, 2011; Gao, et al., 2007b, 2008). However, some studies mentioned that wave frequency is more significant than low frequency motion in terms of mooring fatigue and, the contribution of environmental forces from current and/or wave directly acting on the mooring lines is relatively small (Huang, 2002; Gao, et al., 2007a, 2007b).

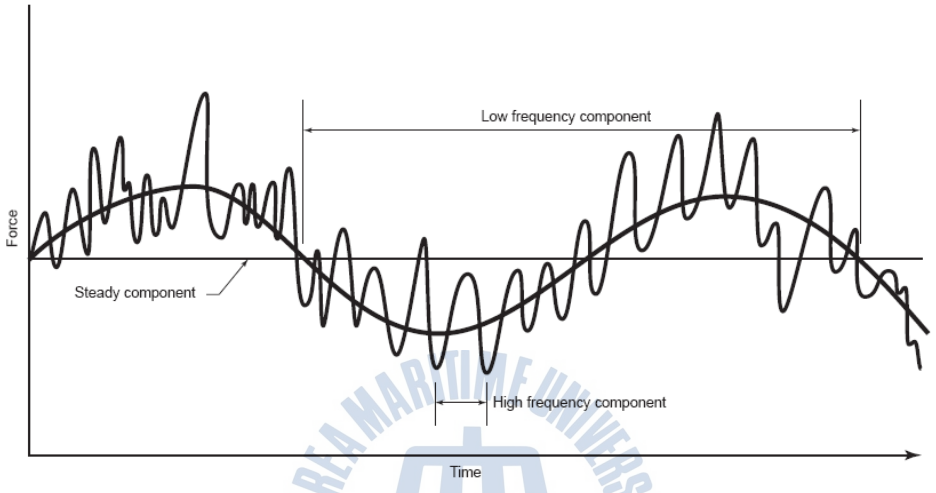

Fig.3-1 Typical wave frequency and low frequency motion

The equation of vessel motions in regular waves may be written as follows;

$$M\ddot{x} + C\dot{x} + D_1\dot{x} + D_2 f(\dot{x}) + K(x)x = q_{WI} + q_{WA}^{(1)} + q_{WA}^{(2)} + q_{CU} + q_{OTH} \qquad (3\text{-}5)$$

where, $\boldsymbol{M}$ = Mass matrix of vessel incl. frequency-dependent added mass ($=m + m_{add}$)

$\boldsymbol{C}$ = Frequency-dependent potential damping matrix

$\boldsymbol{D_1}$ = Linear damping matrix

$\boldsymbol{D_2}$ = Quadratic damping matrix

$\boldsymbol{K(x)}$ = Position-dependent stiffness matrix

$f(\dot{x})$ = Vector function in which each element is given by $\dot{x}_i|\dot{x}_i|$

q_{WI} = Wind drag force

$q_{WA}^{(1)}$ = First order wave excitation force

$q_{WA}^{(2)}$ = Second order wave excitation force

q_{CU} = Current drag force

q_{OTH} = Other forces including force from mooring systems

In Eq.(3-5) above, the motions can be split into wave frequency part and low frequency part; i.e. $x = x_{WF} + x_{LF}$.. And then, the wave frequency motions can be obtained by a linear analysis, in which the quadratic damping is linearized by setting zero (0). The equation of wave frequency of vessel motion can be given as equation (3-6) and this can be solved out based on the frequency domain.

$$M\ddot{x}_{WF} + C\dot{x}_{WF} + D_1\dot{x}_{WF} + Kx_{WF} = q_{WA}^{(1)} \tag{3-6}$$

While, the equation of the low frequency motion can be obtained along with the mooring forces;

$$M\ddot{x}_{LF} + D_1\dot{x}_{LF} + D_2 f(\dot{x}_{LF}) + Kx_{LF} = q_{WI} + q_{WA}^{(2)} + q_{CU} + q_{OTH} \tag{3-7}$$

In Eq.(3-7) above, due to the second order of wave and nonlinear wind and current forces, the low frequency of vessel motion is not Gaussian properties (Gao, 2008). It is known that the motion amplitude is highly dependent on the stiffness of the mooring system and the damping but, it may be difficult to accurately quantify it. Besides, depending upon the water depth, the number of mooring lines and risers, the damping values vary. In DNV OS-E301 (2010a), the damping coefficients for each motion of a ship in 150m water depth along with 12 mooring lines and no risers as below.

- Surge damping coefficient : 5 ~ 10% of critical damping

- Sway damping coefficient : 15~20% of critical damping

Note that BV (1998) recommended that the damping coefficients for surge, sway and yaw are 3%, 3% and 5% of critical damping respectively. However, in this research the results from the actual model tests were utilized.

Some studies described that mooring systems also contribute damping of the LF vessel motion and the damping effect increases with the presence of the WF motion.

3.3.1 Frequency Domain Analysis

Fatigue damage is assessed at a given probability level. The probability level for the fraction of stress (or tension) between range of S and $S+\Delta S$ is given as following Eq.(3-8);

$$p_i = p(S)\,\Delta S \tag{3-8}$$

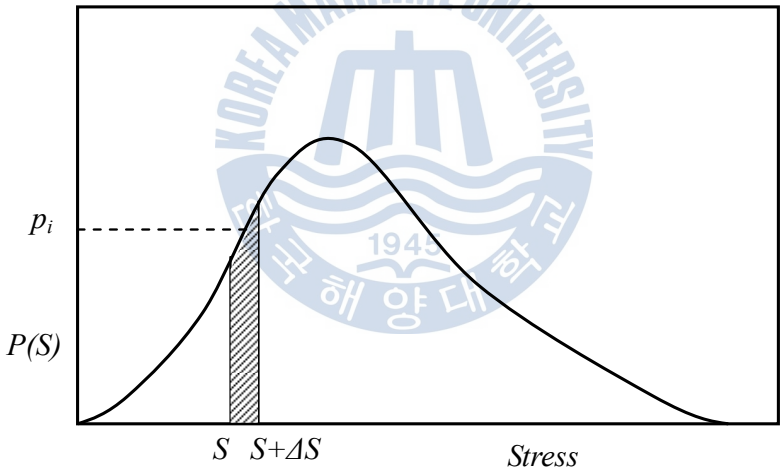

Fig.3-2 Example probability density function of stress

If n is the total number of cycles in the lifetime, the number of cycles at level i is given by Eq.(3-9);

$$n_i = p_i\, n \tag{3-9}$$

Accordingly the fatigue damage based on Miner rule can be defined as Eq.(3-10);

$$D = n\sum \frac{p(S)\Delta S}{N(S)} \tag{3-10}$$

As $\Delta S \to 0$,

$$D = n\int_0^\infty \frac{1}{N(S)} p(S)dS \tag{3-11}$$

Introducing SN curve to the fatigue damage equation Eq.(3-11) above, the damage can be obtained as Eq.(3-12);

$$D = \frac{n}{a_D}\int_0^\infty S^m p(S)dS = \frac{n}{a_D} E(S^m) \tag{3-12}$$

where $E(S^m)$ is the expected value of the stress range to the power m in state i. The response spectrum based on the linear model can be directly given by considering the relation between the transfer function and wave spectrum and, from which the spectral moment can be obtained and introduced to the equation of fatigue damage (Chakrabarti, 1994; DNV, 2010a). Following Eq.(3-13) gives the fatigue damage in sea state i assuming a narrow-band response complying with Gaussian and Rayleigh distribution.

$$d_{NBi} = \frac{v_{0i}T_i}{a_D}(2\sqrt{2}\sigma_{Si})^m \Gamma\left(\frac{m}{2}+1\right) \tag{3-13}$$

where, σ_{Si} is the standard deviation of the stress (or tension) process and $\Gamma(\,)$ is the gamma function. In this case, the number of cycles is computed from the mean zero-up crossing rate v_{0i} and the duration of the sea state $T_i = p_i T_d$, in which T_d is design service life.

The response spectrum based on the linear model in general is calculated by multiplying the transfer function with the wave spectrum from sea environments.

$$S_\sigma(\omega|H_s,T_z,\theta) = |H_\sigma(\omega|\theta)|^2 S_\eta(\omega|H_s,T_z,\theta) \tag{3-14}$$

The spectral moments of order n of the response spectrum for a given heading are calculated as Eq.(3-15);

$$m_n = \int \omega^n S_\sigma(\omega|H_s, T_z, \theta) d\omega \tag{3-15}$$

However, in the tension process of mooring lines the expression for a narrow-banded process is no longer appropriate since the spectral characteristics of the mooring tension has normally a high frequency mode and a low frequency mode. The computation of each process; e.g. wave frequency and low frequency, may underestimate the fatigue damage because the overlapping area in the response spectrum of wave and low frequencies cannot be accurately taken into account (DNV, 2010a; Hwang, et al., 2008; Kang, 2011). Hence, many studies (Ong, et al., 2003; Gao, et al., 2007a, 2007b) on the appropriate computation in the frequency domain analysis were carried out.

DNV (1999, 2010a) recommended using the combined spectrum approach and dual narrow-band approach, which was developed by Jiao et al. (1990) and widely used in design codes. The combined spectrum approach provides a more simple and conservative approach in computing the fatigue damage. The fatigue damage for sea state *i* is denoted by Eq.(3-16);

$$d_{cs_i} = \frac{\nu_{yi} T_i}{a_D} \left(2\sqrt{2}\sigma_{Yi}\right)^m \Gamma\left(\frac{m}{2} + 1\right) \tag{3-16}$$

The standard deviation of the process includes both wave frequency and low frequency components as Eq.(3-17);

$$\sigma_{Yi} = \sqrt{\sigma_{LFi}^2 + \sigma_{WFi}^2} \tag{3-17}$$

And the mean zero-up crossing rate is computed from the moments of the combined spectrum as Eq.(3-18).

$$\nu_{yi} = \sqrt{\lambda_{LFi}\nu_{LFi}^2 + \lambda_{WFi}\nu_{WFi}^2} \tag{3-18}$$

where, the symbol λ represents the normalized variance of the corresponding stress (or tension) component, which are given by equations (3-19);

$$\lambda_{LF} = \frac{\sigma_{LF}^2}{\sigma_{LF}^2 + \sigma_{WF}^2} \qquad \lambda_{WF} = \frac{\sigma_{WF}^2}{\sigma_{LF}^2 + \sigma_{WF}^2} \tag{3-19}$$

Meanwhile, the dual narrow-banded approach takes the results of the combined spectrum approach and multiples it by a correction factor based on the two frequency bands. The correction factor can be described as Eq.(3-21);

$$d_{DNBi} = \rho_i \, d_{CSi} \tag{3-20}$$

$$\rho_i = \frac{v_P}{v_{yi}} \left\{ \lambda_{LFi}^{\frac{m}{2}+2} \left(1 - \sqrt{\frac{\lambda_{WFi}}{\lambda_{LFi}}} \right) + \sqrt{\pi \lambda_{LFi} \lambda_{WFi}} \frac{m\Gamma\left(\frac{1+m}{2}\right)}{\Gamma\left(\frac{2+m}{2}\right)} \right\} + \frac{v_{WFi}}{v_{yi}} \lambda_{WFi}^{\frac{m}{2}} \tag{3-21}$$

where, $v_P = \sqrt{\lambda_{LF}^2 \lambda_{WF}^2 + \lambda_{LF} \lambda_{WF} v_{WF}^2 \delta_W^2}$ with $\delta_w = 0.1$.

3.3.2 Time Domain Analysis

Time domain analysis is more accurate approach than frequency domain analysis in computing fatigue damage of the mooring lines since it uses directly time series of stress or tension along with non-linearity in motion (DNV, 2004; Ormberg, et al., 1998). The counting algorithm is identical for narrow-band or wide-band, stationary or non-stationary, and Gaussian or non-Gaussian processes (Gao, 2008).

ASTM (2005) gives many kinds of the counting algorithm for counting the cycle numbers from the series of the resultant values like stress or tension; e.g. peak counting, range counting, level-crossing and rainflow counting.

The peak counting method identifies all peaks in the time history and uses the peak values above reference level which corresponds to the mean values. This method basically assumes a symmetric property centered at the mean value. However, it is know that the method gives a quite conservative estimate.

The range counting method considers a peak and the following valley as half a cycle of the range as well as a valley and the following peak. This method is

established on the local load cycles and ignores the effect of global large cycles. Therefore, it underestimates the true wide-banded fatigue damage.

The level-crossing counting method uses the cycles of stress range based on the counting of up-crossing above and down-crossing below the mean value at fixed load levels. This also takes into account the interaction between cycles and gives priority to large load cycles.

Proposed by Matsuishi and Endo, the rainflow counting method is also known as the pagoda-roof method. This has proved to be the most accurate method for estimating fatigue damage under random process (Almar-Naess, 1985). The principle of the rainflow counting method can be explained using the stress-strain curve, which is illustrated in Fig.3-3.

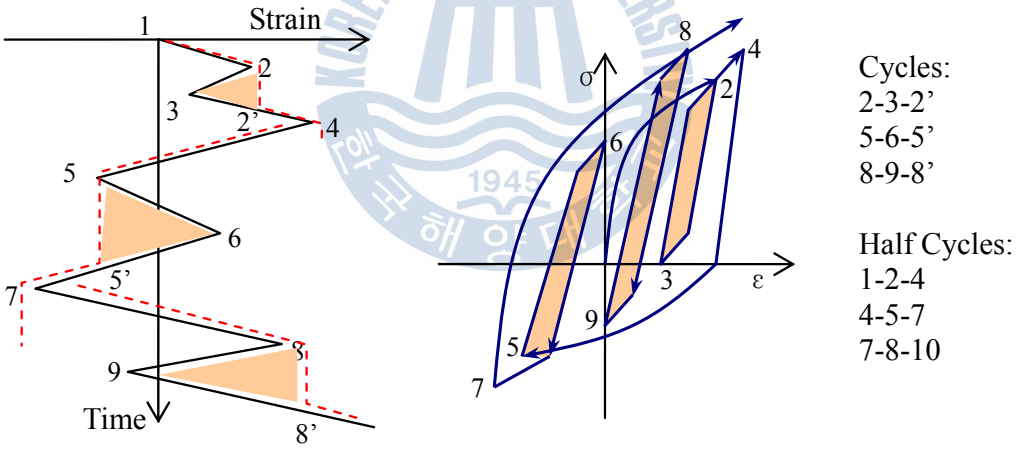

Fig.3-3 Principle of rainflow counting method in strain time history

The rainflow counting has obtained its name from an analogy of rain falling down a pagoda roof. The rules of rainflow counting method are as follows;

- Rain will flow down the roof initiating at the inside of each peak or valley. When it reaches the edge it will drip down.

- The rain is considered to stop, and a cycle is completed, when it meets another flow from above.

- Starting from a peak, the flow also stops when it comes opposite a more positive peak than that from which it started. Starting from a valley, the flow stops when it comes opposite a more negative valley than that from which it started.

For time domain approach, the fatigue damage can be simply calculated based on Miner rule (BV, 2009). In this method, the number of cycles per year in sea state i is denoted as Eq.(3-22);

$$n_i = \frac{p_i(365.25)(24)(60)(60)}{T_{zi}} \tag{3-22}$$

where, T_{zi} = Zero up-crossing period [in sec] in sea state i

p_i = Probability of occurrence in sea state i

4. Chain Interlink Mechanism

Some references shows chain mechanism between interlinks in terms of OPB fatigue failure.

- Rolling Mode

Chain links under low pretension would be freely rotated, but when the pretension in the mooring leg increases it will become more and more difficult to obtain such free rotation between successive links since the friction force will be higher with the increased tension. Eventually, the point of application of the tension would be away from the plane of symmetry of the link, so that small bending stress can be generated. The rolling stresses can be analytically calculated but they are too small to make the fast failure.

- Sliding Mode

It is possible for a chain link to slide on the inside of the adjacent link and this mode is sliding mode of chain link. The stress from this mode is too low to cause the OPB fatigue problem.

- Locking Mode

In the manufacturing process of a chain, a proof load (between 65 ~ 80% of MBL) is applied on all links in order to confirm its strength. From the proof load, the chain surface would be permanently deformed with an elliptical shape. Due to the deformed surface, the chain links cannot roll or sliding anymore. The links are stuck and it is called as ‘locking mode’ of chain links. This locking mode continues till the applied moment exceeds that generated by friction, then sliding occurs. This mode causes mainly OPB stresses that can rupture a chain link.

If a rotation is imposed on one chain link, the complete chain will have to bend just like a rod. Once the friction force overcomes the material resistance, the chain links would slide along the chain surface. Once the link slides on the inside of the adjacent link, the mechanism causes OPB stresses that are low if preceded by the rolling mechanism, but can be high if preceded by the sticking mode. Following Fig.4-1 shows each mode with respect to OPB fatigue of chain interlinks, which is extracted from the empirical results of OPB JIP hosted by SBM (Jean, et al., 2005).

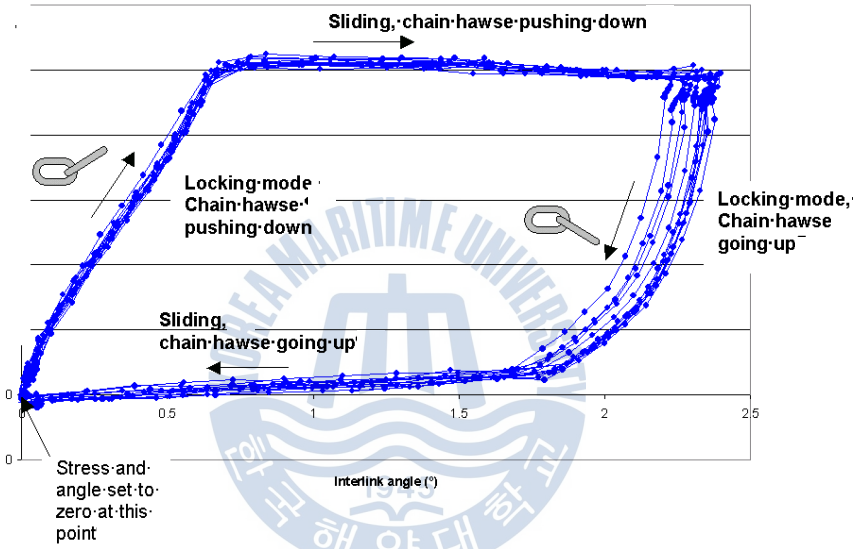

Fig.4-1 Interlink modes of chain with respect to OPB stress

4.1 Analytical OPB Stress

The analytical bending stresses for the three modes, e.g. rolling, sliding and locking mode, of chain interlinks are described (Rampi, et al., 2006). Fig.4-2 identifies the relevant parameters regarding OPB link undergone. Geometrically the bending stress can be achieved based on the static force and moment equilibrium. The general form of OPB stress is denoted by Eq.(4-1);

$$\sigma_{OPB} = M_{OPB} \cdot \frac{r_i}{I} \tag{4-1}$$

where, M_{OPB} = OPB moment

I = Moment of inertia of OPB link

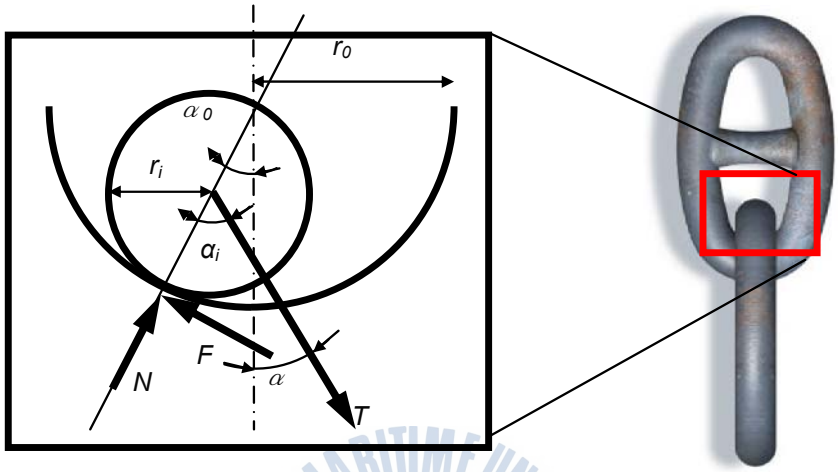

Fig.4-2 Identification of relevant parameters regarding OPB stress

1) Rolling Mode

$$\alpha_0 = \alpha\left(\frac{r_i}{r_0 - r_i}\right) \tag{4-2}$$

$$M_{OPB} = r_i(\cos\alpha \sin\alpha_0 + \cos\alpha_0 \sin\alpha)T \tag{4-3}$$

where, T is tension of mooring chain link

2) Sliding Mode

$$M_{OPB} = r_i \, \mu \, T \tag{4-4}$$

where, μ is interlink friction coefficient

3) Locking Mode

$$\sigma_{OPB} = \frac{k \, T^{0.75}}{2 \, r_i}\alpha \tag{4-5}$$

where, k and constant of 0.75 were obtained from some empirical results and the OPB stress to be in MPa and r_i to be in meter.

From the studies by Jean et al. (2005), the calculation of bending stress of chain link was proposed. In Locking mode, a chain link was assumed a tensioned beam taking into account the effect of large displacement, which is denoted by;

$$EIy''+T\cos(\alpha_T)\big(y(L)-y(s)\big)-T\sin(\alpha_T)(L-s)-M=0 \tag{4-6}$$

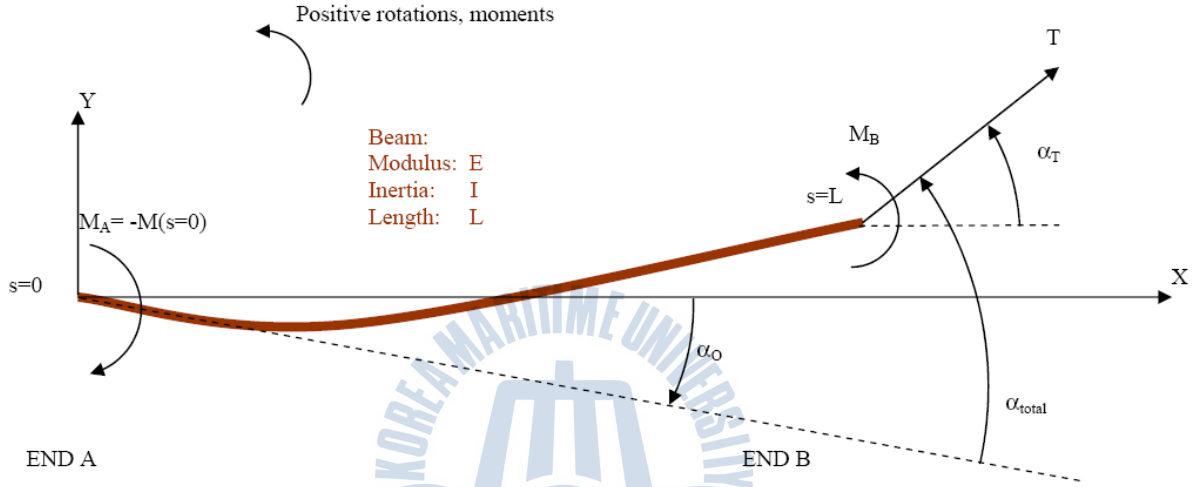

Fig.4-3 Analytical model of chain considering bending under tension

Assuming that both angle of tension a_T and fairlead angle a_0 are relatively small, Eq.(4-6) above can be presented as Eq.(4-7);

$$M(s)=M_B\frac{\cosh(ks)}{\cosh(kL)}+(\alpha_T-\alpha_0)\sqrt{EIT}\,\frac{\sinh\big(k(L-s)\big)}{\cosh(kL)} \tag{4-7}$$

in which, k is $\sqrt{\dfrac{T}{EI}}$

And, Eq.(4-7) can be simplified to Eq.(4-8) if the chain length is longer than the characteristic length *1/k* and no moment is applied to the end B.

$$M_A=-\sqrt{EIT}\,(\alpha_T-\alpha_0)\tanh(kL)\approx-\sqrt{EIT}\,\alpha_{Total} \tag{4-8}$$

4.2 Failure Mechanism of Chain Link

In general, the failure mode of chain link has two different modes; tension and bending crack mode. The tentative fatigue cracks due to only tension cyclic loads are located at the straight section and bend section presenting the geometric changing area as shown in Fig.4-4. On the contrary, the potential cracks due to OPB fatigue loads are placed on the curved surface of chain link, see Fig.4-5.

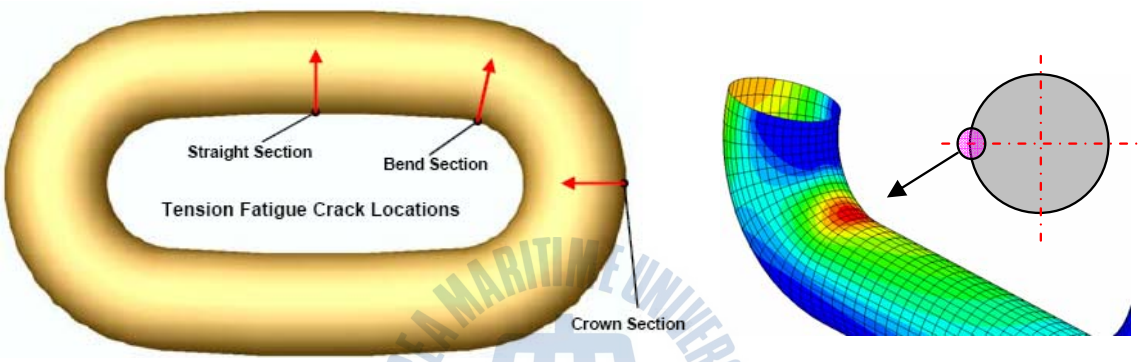

Fig.4-4 Tentative cracks of chain link due to tension fatigue loads

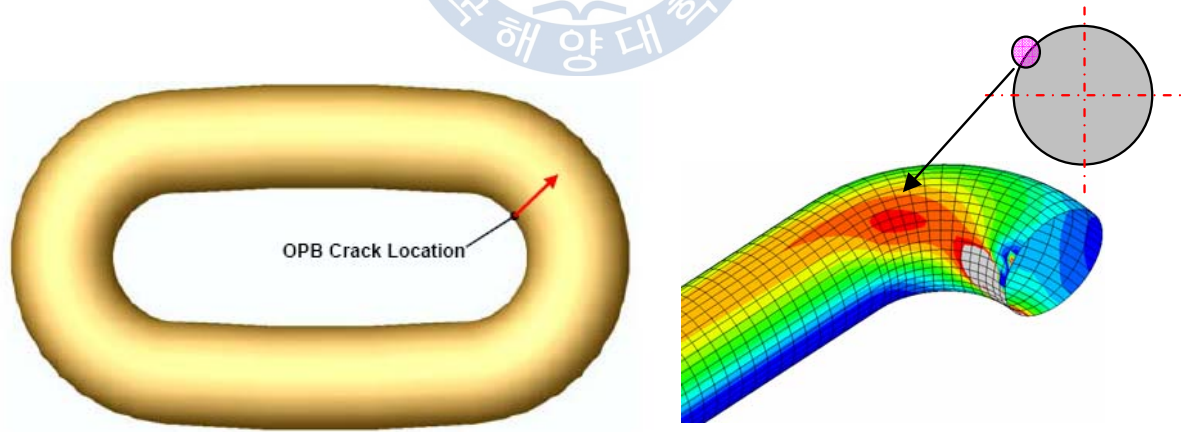

Fig.4-5 Tentative cracks of chain link due to OPB fatigue loads

When a rotation angle α_{total} is imposed on the chain, the bending moment (out-of-plane) is generated in the link and besides, due to the high friction the link cannot roll on each other, which is given in Fig.4-6. Repeated angular motion of FPSO top chain due to sea environments will accumulate fatigue damage, so that

the chain interlink can be rupture by OPB effect. For vertically configuring chain, the chain link is rotated in-plane bending (IPB) in same way (Denayrolles, 2011).

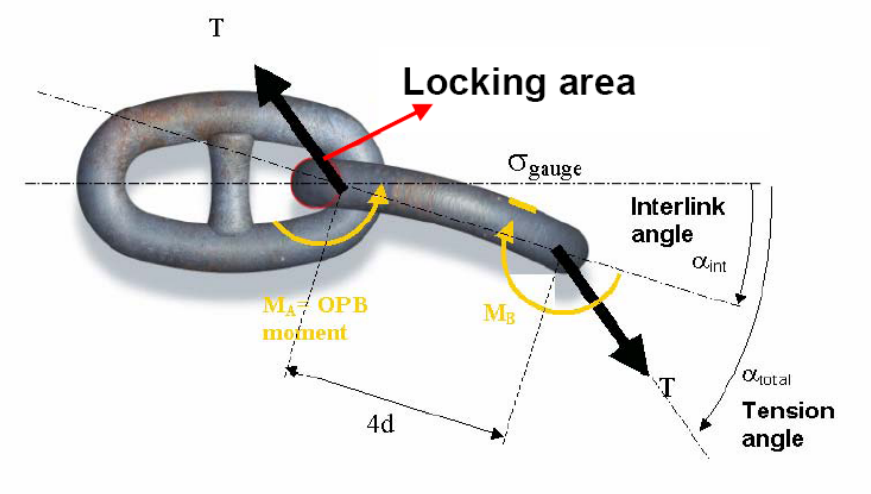

Fig.4-6 Illustration of chain link in bending mode under locked by tension

Also, bending-induced stress of chain links can be generated by two different modes; in-plane bending (IPB) and out-plane-bending (OPB) loading, which is classified by the direction of chain link's axis. In calculating fatigue damage due to chain bending mode under high pretension, these two modes must be taken into account.

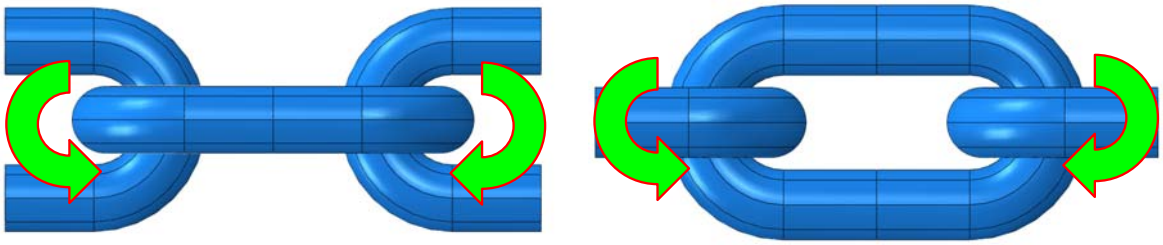

Out-of-plane Bending (OPB)

In-plane Bending (IPB)

Fig.4-7 Out-of-plane bending (OPB) and In-plane bending (IPB) modes

The effects on the torsional moment of mooring chains was studied by Ridge et al. (2006), but, through the numerical studies, it is suitable to neglect the stress on chain links from torsional moment unless the relatively high and potentially

destructive rotation is applied. Therefore, in this research the torque induced from mooring chain links' in-line axial rotation is neglected.

In summary, the major parameters with respect to the bending-induced fatigue of mooring chain links can be summarized; pretension of FPSO, friction coefficient between chain interlinks, proof loads influencing the deformation of their contact surface and direction of bending moments (Kang, et al., 2010; Dahlberg, 2011).

5. Time Simulation of Mooring Lines

5.1 Mooring Static Equilibrium

Prior to the time simulation based on time domain approach, the mooring lines are required to be positioned in the equilibrium under the actions: horizontal tension, line tension and weight. Basically there are some assumptions in solving equilibrium equations; the bending stiffness and elasticity effects of mooring lines are neglected and also, any direct environmental loading and its response on the lines are neglected (Chakrabarti, 2008). Fig.5-1 illustrates the three forces of a portion of a mooring line under consideration.

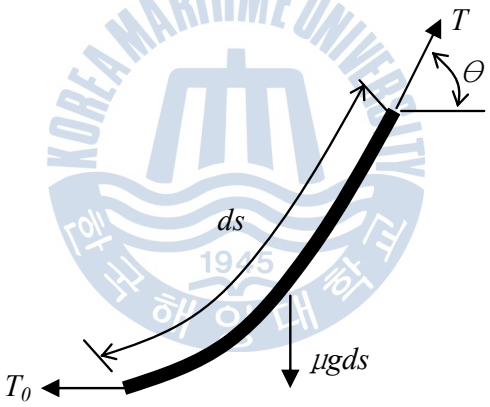

Fig.5-1 Forces of a portion of a mooring line

Considering the static equilibrium, the tension is calculated as Eq.(5-1);

$$T = \sqrt{(\mu g\, ds)^2 + T_0^2} \tag{5-1}$$

in which, μ is the mass per unit length of the mooring line. And introducing a constant having the dimensions of length defined by; $A = \frac{T_0}{\mu g}$, Eq.(5-1) above is denoted as Eq.(5-2);

$$T = \mu g \sqrt{ds^2 + A^2} \tag{5-2}$$

where, the length ds can be obtained by $ds = A\tan(\theta)$.

Meanwhile, with axial elasticity of a mooring line, the equilibrium equation can be indicated as equations (5-3) and (5-4);

$$ds_x = ds\left(1 + \frac{T}{AE}\right)\cos(\theta) \tag{5-3}$$

$$ds_y = ds\left(1 + \frac{T}{AE}\right)\sin(\theta) \tag{5-4}$$

where, ds_x and ds_y are the axial stretch of the line in horizontal and vertical direction respectively and, AE is axial stiffness per unit length of mooring line.

To estimate the line profile in the static equilibrium, the tension, paid-out length of mooring lines and distance between fairlead and anchor are necessary. When two of these three parameters are known, the third can be calculated. ARIANE7, a conventional program of BV for mooring analysis, utilizes Brent algorithm. The theory report of ARIANE7 (BV, 2009) briefly describes the basis of the algorithm. Brent algorithm is a combining method of the bisection method, the secant method and inverse quadratic interpolation to figure out the exact solution, for which Newton's method for nonlinear interpolations is initiated and iterated consecutively. Finally, when the algorithm finds the equilibrium solution, the moored system is ready to run the time simulation.

5.2 Quasi-dynamic Analysis

The fully time domain analysis for the moored system will give the most accurate solutions not only for the vessel motion moored but also for the dynamic behaviors of all individual lines. However, it might take too much time to complete all the computations on every operating sea state for mooring fatigue. Hence, BV proposed more simple approach; i.e, quasi-dynamic analysis.

Quasi-dynamic analysis takes into account not only the wave and low frequency motions of vessel but also displacement at the upper end of the mooring line, i.e. fairlead parts. Also, the weight and the buoyancy of the mooring line components, their axial stiffness and reactions from seabed are considered. However, it does not include only line dynamic analysis of mooring lines (BV, 2009).

The mooring loads of each line between a floater and an anchor on seabed can be calculated for each time step. At each time step of the simulation based on the quasi-dynamic analysis, the horizontal distance and azimuth angle for the k^{th} mooring line are achieved as following Eqs.(5-5) and (5-6) respectively. Fig.5-2 shows the indications for the calculations between a floater and an anchor.

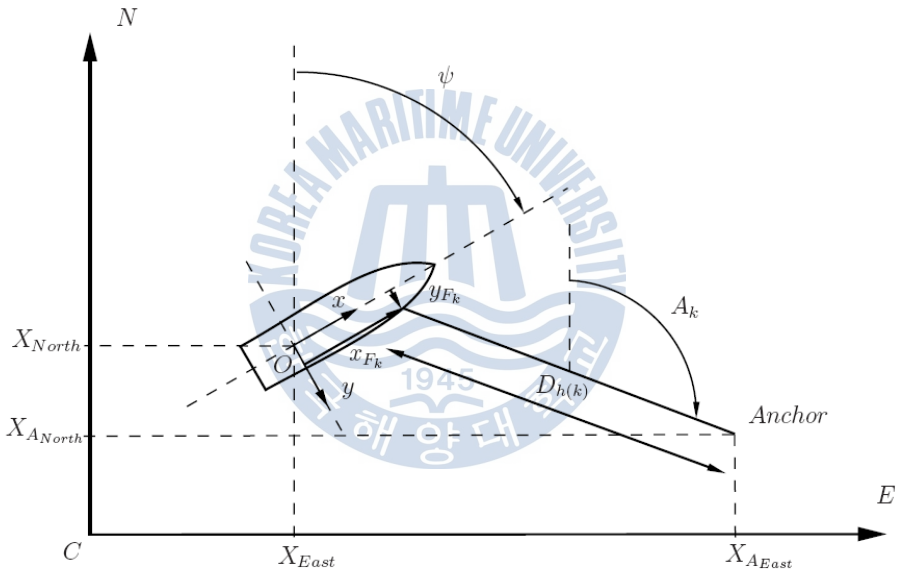

Fig.5-2 Indications between a floater and mooring anchor on seabed

$$D_{h(k)} = \sqrt{(X_{North} - X_{A_{North}} + x_{F_k} cos\psi + y_{F_k} sin\psi)^2 + (X_{East} - X_{A_{East}} + x_{F_k} sin\psi + y_{F_k} cos\psi)^2} \tag{5-5}$$

$$A_k = atan\left(\frac{X_{East} - X_{A_{East}} + x_{F_k} sin\psi + y_{F_k} cos\psi}{X_{North} - X_{A_{North}} + x_{F_k} cos\psi + y_{F_k} sin\psi}\right) \tag{5-6}$$

And, the horizontal components of force on the floater from each mooring line are then calculated based on the floater's axis system as per the equations (5-7), (5-8) and (5-9);

$$F_{Mx} = \sum_{k=1}^{N_{Lines}} T_{Hk} cos(A_k - \psi) \tag{5-7}$$

$$F_{My} = \sum_{k=1}^{N_{Lines}} T_{Hk} sin(A_k - \psi) \tag{5-8}$$

$$M_{Mx} = \sum_{k=1}^{N_{Lines}} \left[x_{F_x} T_{Hk} sin(A_k - \psi) - y_{F_x} T_{Hk} cos(A_k - \psi) \right] \tag{5-9}$$

where, F_{Mx}, F_{My} and M_{Mx} are respectively total horizontal forces in x-direction and y-direction and moment considering mooring loads and T_{HK} is the horizontal tension force of k^{th} mooring line. With ARIANE7, the 6-DOF motions of a floater were computed along with all mooring lines, by which it is possible to obtain much quicker solutions for all the fatigue sea states than fully-coupled analysis and then, the results are simply applicable to the line dynamic analysis hereafter (Heurtier, et al., 2001).

5.3 Line Dynamic Analysis

It is general that the traditional theoretical approach to solve the dynamic behavior of mooring lines is based on non-linear numerical analysis due to the geometric non-linearity of mooring lines (Boom, 1985; Journee, et al., 2001). Note that lumped mass method is more general technique in case of mooring lines considering no bending stiffness between mooring chain interlinks. Many studies (Chen, et al., 2001; Boom, 1985; Martins, et al., 2002; Yang, 2007) regarding the line dynamic response of mooring lines had been carried out.

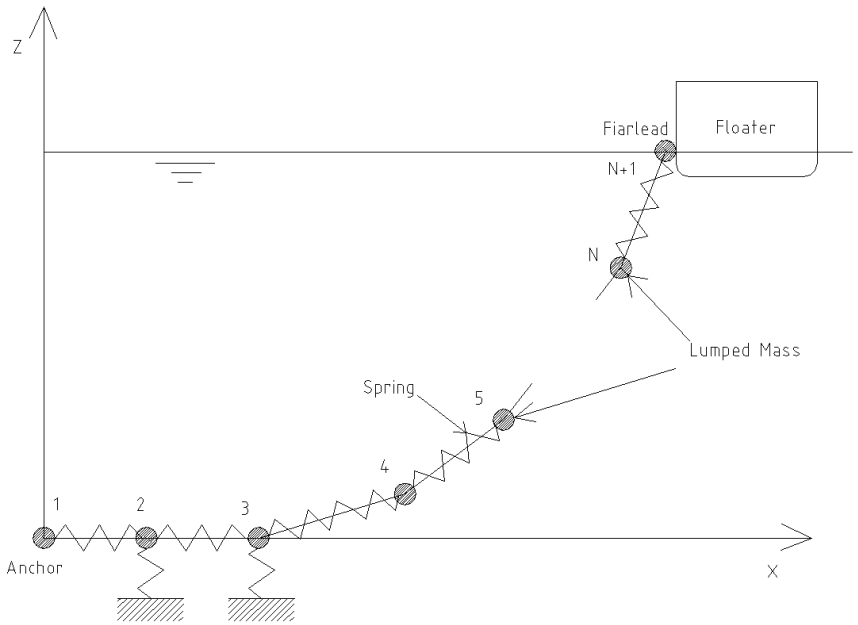

Fig.5-3 Illustration of lumped masses for a mooring line

Based on Fig.5-3 showing the illustration of lumped masses for a mooring line, the governing equation as denoted in Eq.(5-10) can be achieved for the j-th lumped mass in global coordinates.

$$\left(M_j + m_j(t)\right)\ddot{X}_j(t) = F_j(t) \tag{5-10}$$

where, M_j = Mass matrix of j-th lumped mass node

m_j = Added mass matrix of j-th lumped mass node

And, the external force F_j inducing on j-th lumped mass can be written by Eq.(5-11);

$$F_j(t) = T_j(t) - T_{j-1}(t) + F_{Dj}(t) + F_{Wj}(t) + F_{Sj}(t) \tag{5-11}$$

where, T_j and T_{j-1} = Tensions at j-th and (j-1)-th lumped mass node respectively

F_{Dj} = Drag force at j-th lumped mass node

F_{Wj} = Buoyant weight at j-th lumped mass node

F_{Sj} = Soil reaction force at j-th lumped mass node

Introducing the finite difference methods, the tension of a mooring line at the certain instantaneous time can be obtained. Following Eq.(5-12) is proposed by Boom (1985) on the condition of no bending stiffness between chain links.

$$T_{t+\Delta t}^{k+1} = T_{t+\Delta t}^{k} - \frac{1}{\Delta \Psi_t^k}\left[l_j^2 \left(\Delta x_j - (1 + \frac{T_j}{EA_j}) \right)^2 \right]_t^k \tag{5-12}$$

where, Ψ_j = segment length error vector of j-th lumped mass node

T_k = Tentative segment tension vector at the k-th iteration

$\Delta \Psi$ = Length error derivation matrix ($= \frac{\partial \Psi}{\partial T}$)

To calculate fatigue life considering the bending effect of chain links, the line dynamic analysis was undertaken by OrcaFlex, a conventional tool made by Orcina. Note that the validations for OrcaFlex had been performed in the various fields of offshore engineering and fully proven. In particular, it is possible to model the bending stiffness of chain interlinks in utilizing OrcaFlex (Orcina, 1987).

6. FE Analysis for Chain OPB and IPB

As mentioned above, the bending induced fatigue (i.e. both OPB and IPB) of chain links is very locally found and so, it is necessary to find out accurate stress patterns on chain links by the non-linear finite element analysis considering surface contacts, material plasticity, etc. Hence, the software for calculating the hotspot stresses on a chain link was utilized by ABAQUS, a conventional FE program made by SIMULIA (2008).

Note that it maybe impossible to find out the hotspot stress for all kinds of mooring chain links including size, material, etc. Therefore, in this research the chain component with OD147 of top chain link with R3 grade and studless type was taken into account. Gao et al. (2005) studied the corrosion deterioration of mooring chains but, in this analysis the effect on corrosion was not considered.

6.1 FE Modeling of Chain Link

It is typical that the geometries of chain link are nearly identical regardless of the manufacturers. The studless chain link of OD147 applied herein has the geometry shown in Fig.6-1.

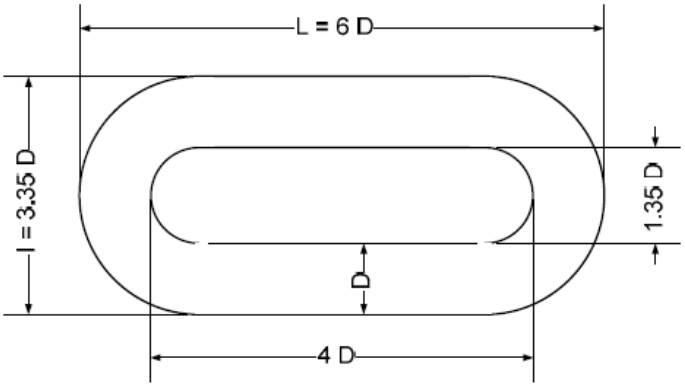

Dimension of Chain links:

D = 147mm

L = 6D = 882mm

I = 3.35D = 492.5mm

Fig.6-1 Standard geometry of studless chain link of OD147

Based on the geometry of the chain link, the FE models for both OPB and IPB were built comprising of one half link plus one intermediate link considering the symmetric configurations as shown in Fig.6-2.

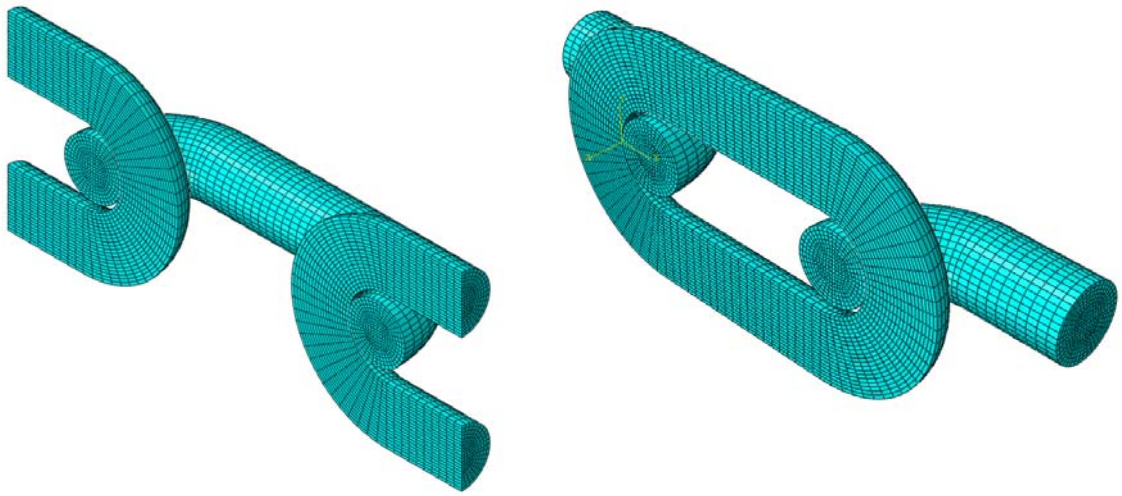

Fig.6-2 FE Models for OPB (left) and IPB (right)

In the FE models, the elements are composed of solid elements (C3D8I) and membrane elements (M3D4) with 1μm thickness on the chain surface to identify the stresses at the chain skin. The element size are kept consistently approx. 10mm so that the chain geometry can be smoothly modeled as shown in Fig.6-3, which was recommended from OPB JIP to save the computation time of the non-linear FE analysis (Denayrolles, 2011).

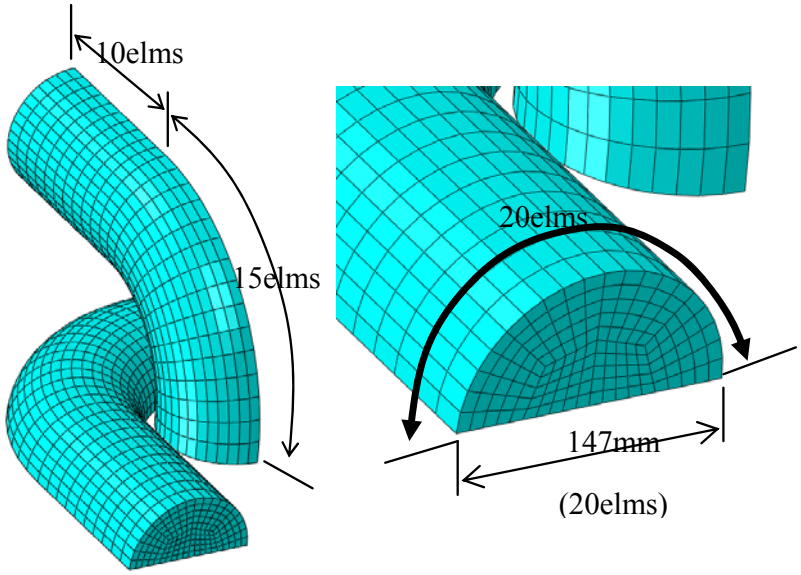

Fig.6-3 Detailed element modeling of chain links

Besides, the contact surface between chain interlinks was defined to transfer the surface tractions each other through the contact boundaries, which is given in Fig.6-4. In the contact model, the friction coefficient of 0.7 was considered, which was determined on the purpose of critical design assessment. In the analysis, the kinetic friction coefficient at the sliding mode was not taken into consideration. Actually, from the results of many experiments undertaken through OPB studies including OPB JIP, the friction coefficient between chain links are around 0.3 in salt water and 0.5 in air dry, without considering the time effects such as corrosion, marine growth, etc (Jean, et al., 2005). However, the JIP recommended that the friction coefficient of 0.7 be applied based on the computation calibrations (Denayrolles, 2011).

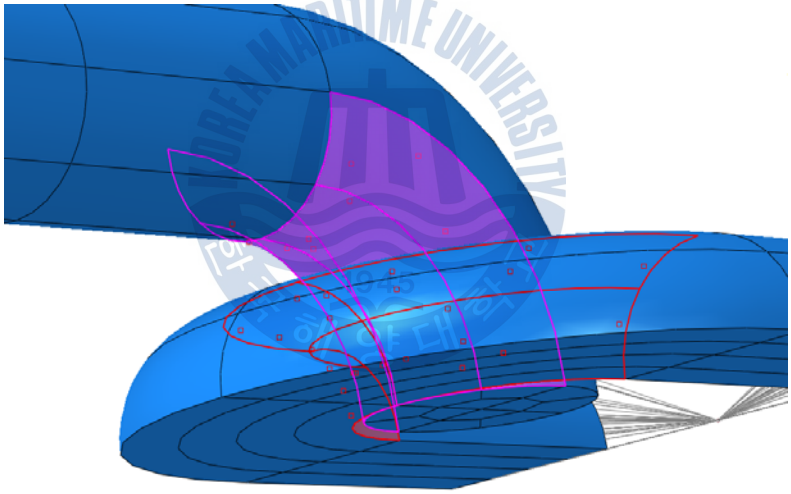

Fig.6-4 Definition of contact surfaces between chain links

6.2 Input of Material Properties

Under the proof loading to the chain link, the adjacent regions of the contact surfaces experience elastoplastic deformation, which may eventually increase the friction during the chain links' rotation (Kang, et al., 2010; Denayrolles, 2011). Therefore, it is importance to accurately input the material properties of chain links prior to FE analysis. As mentioned, the grade R3 has material characteristics of the following Table 6-1, which was supplied by a chain manufacturer RAMNAS.

Table 6-1 Material properties of chain grade R3 applied in FEA

Characteristics	Value
Yield strength	520MPa
Ultimate tensile strength	690MPa
Ultimate tensile strain	18%
Young's modulus	2.09E+05MPa
Poisson ratio	0.3
Min. Breaking Load	15536kN

Noted that the plastic law was modeled as multi-linear and the isotropic hardening for the material was assumed. The material law proposed by Ramberg-Osgood (Ramberg, W. and Osgood, W., 1943) was used for modeling the elastoplastic behavior of the chain material, which is described as Eq.(6-1).

$$\varepsilon_n = \frac{\sigma_n}{E} + \alpha \frac{\sigma_y}{E} \left(\frac{\sigma_n}{\sigma_y} \right)^n \tag{6-1}$$

where, σ_n = Nominal stress

ε_n = Nominal strain

σ_y = Yield stress

a = Yield offset in Ramberg-Osgood law (=0.804)

E = Young's modulus

n = Hardening exponent of material (=15.84)

And, from the manufacturer's data, the necessary input data for modeling the material property of chain links were obtained. In ABAQUS, the stress-stain relation as input data is required to be expressed in true stress (i.e. Cauchy stress), and logarithmic plastic strain (SIMULIA, 2008; Boresi, 1993). So, the nominal stress-strain data was converted as following equations (6-2) and (6-3);

$$\sigma_{true} = \sigma_n (1 + \varepsilon_n) \tag{6-2}$$

$$\varepsilon_{ln}^p = ln(1 + \varepsilon_n) - \frac{\sigma_{true}}{E} \tag{6-3}$$

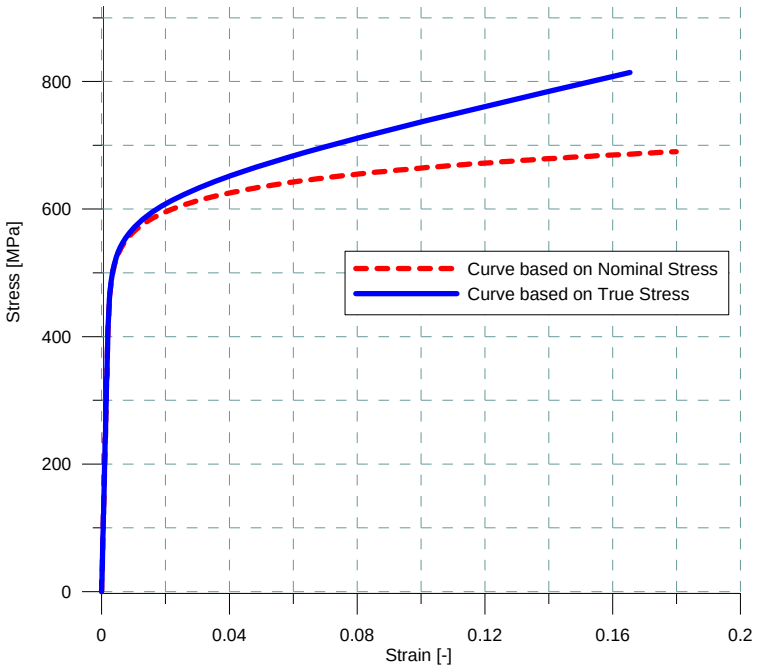

Fig.6-5 Comparison of stress-strain relations based on nominal and true stress

6.3 Boundary Conditions and Applied Loads

For boundary conditions for performing FE analysis of both OPB and IPB modes, the symmetry plane conditions were utilized on the whole FE models. Fig.6-6 gives the boundary conditions applied to OPB and IPB models respectively. At the extremity of the first link, the symmetry conditions are also used and while, the extremity of the opposite link was used as a loading point.

Tension and rotational angle for simulating the chain links' behavior were applied at the opposite extremities as shown in Fig.6-7.

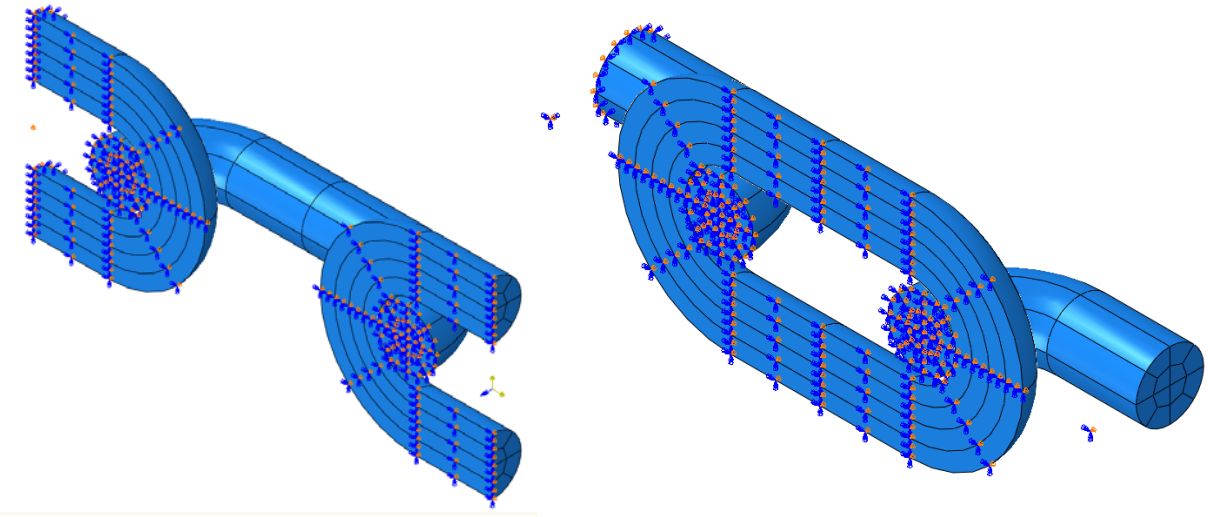

Fig.6-6 Symmetry plane conditions for OPB (left) and IPB (right) models

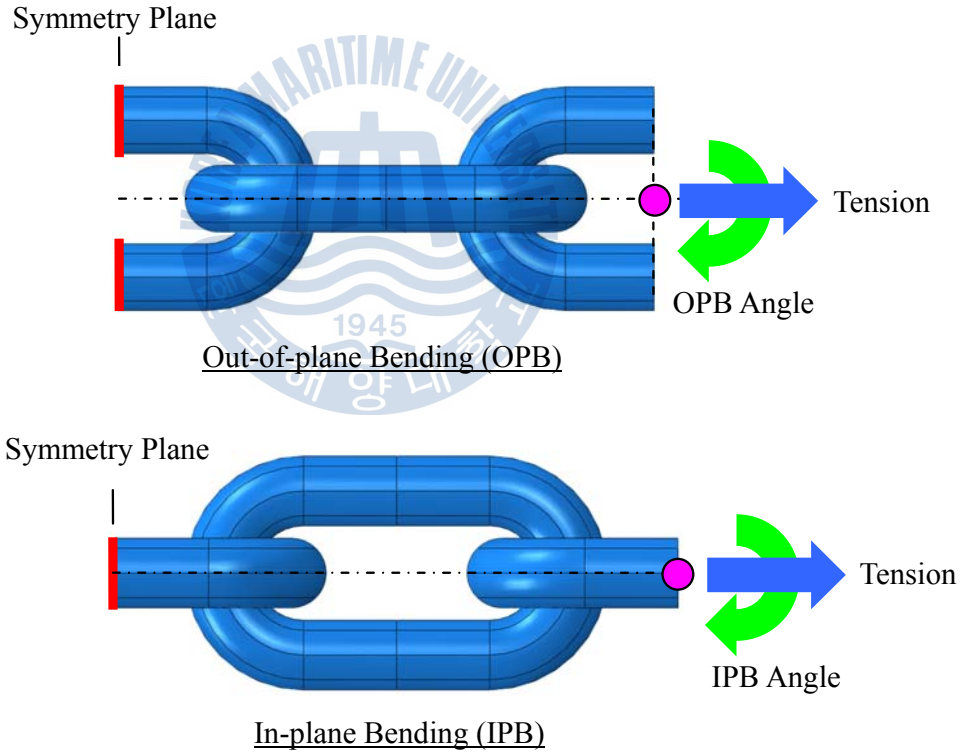

Fig.6-7 Applied loading conditions and angle for OPB and IPB models

In the FE analysis, three loading conditions; e.g. proof load, nominal tension and OPB/IPB rotation were consecutively taken into consideration. Proof tensile load undertaken in the manufacturing stage of chain links was applied, which is an important parameter in terms of bending induced fatigue on the chain links because it increases friction effects between chain links due to its plastic deformed surface.

The proof tensile load of 10875kN, which is 70% of MBL in accordance with the supplier's data, was applied at the first stage. The nominal tensile loads were determined by considering the static line loads from the calculation of quasi-dynamic mooring analysis by ARIANE7. From the results of the mooring analysis, all the tension loads of mooring lines of the FPSO were found abt. 2000kN. Therefore, the nominal tensions of five loads; i.e. 1850kN, 1950kN, 2050kN, 2150kN and 2250kN were considered in the non-linear FE analysis of chain links to cover all the tension ranges. And, finally the OPB/IPB rotation was imposed at the loading point of the chain link model. Fig.6-8 gives the loading steps used in the non-linear FE analysis by ABAQUS.

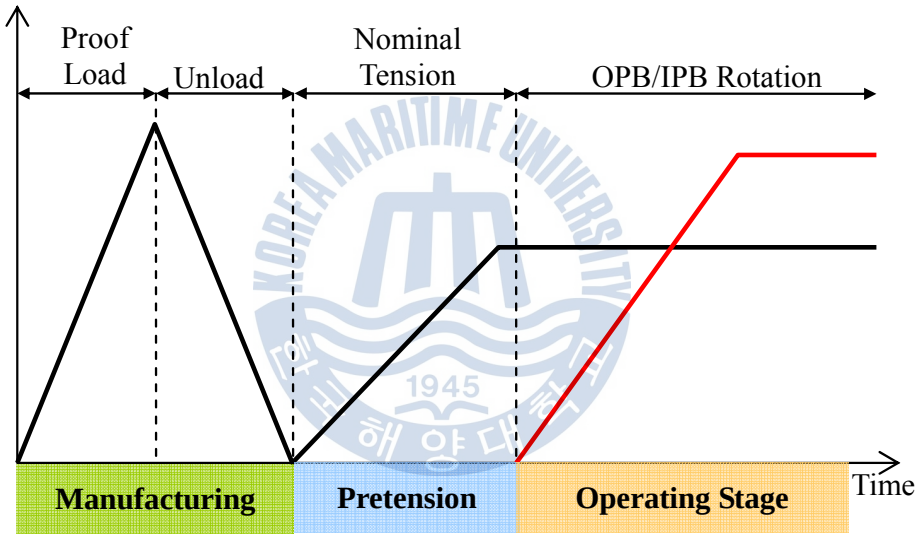

Fig.6-8 Time steps of loadings in non-linear FE analysis

6.4 Interlink Angle and Moment

To find out the dynamic behaviors of mooring lines by the time simulation for the moored FPSO, it is necessary to input the bending stiffness of chain interlinks into the mooring input data. Bending stiffness of chain interlinks can be calculated from the FE analysis of chain links.

The moments can be calculated at the connection between the first link and the central link. In Fig.6-9, the interlink angle for OPB mechanism is defined along with the moment and, the interlink angle for IPB in Fig.6-10.

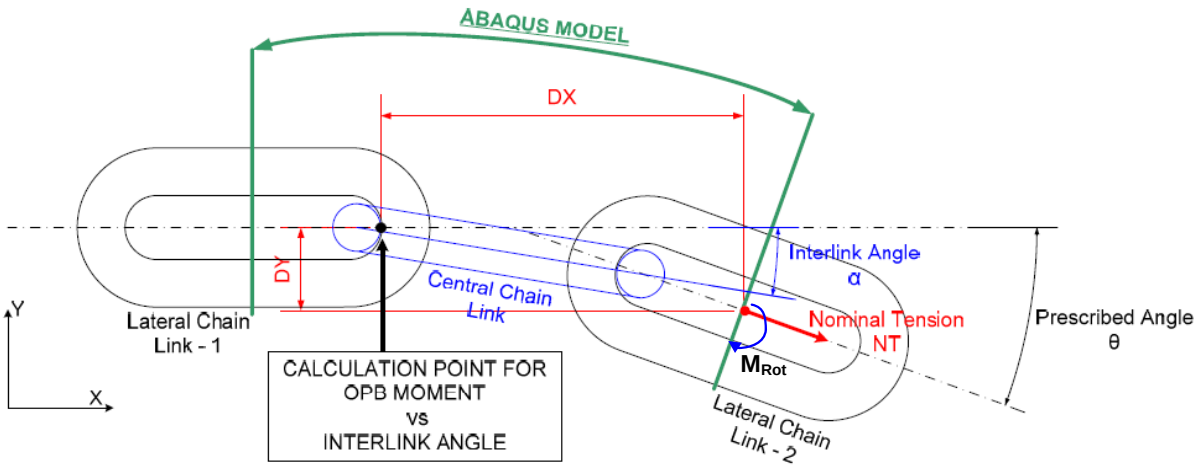

Fig.6-9 Definition of OPB angle and moment

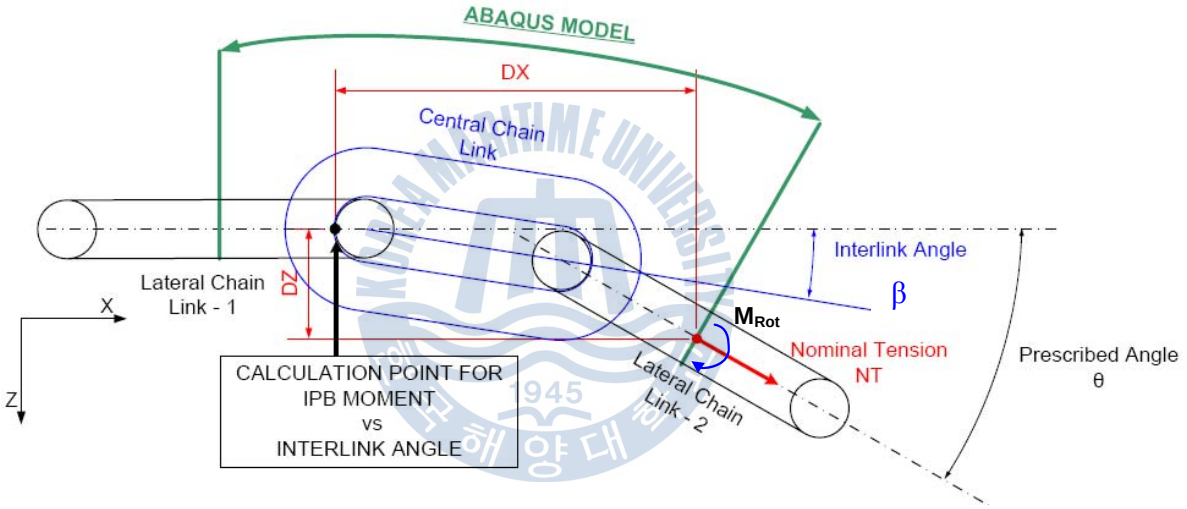

Fig.6-10 Definition of IPB angle and moment

When applying the prescribed angle Θ as shown above, the central chain link would not be rotated as much as the applied angle Θ due to its stiffness and surface frictions along with tension. The angle of the central chain link is defined as 'interlink angle α'. At any position, the links are under static equilibrium and especially, the bending moments at the connection between interlinks will be generated. The moments for each OPB and IPB angle are calculated as equations (6-4) and (6-5);

$$M_{OPB} = M_{Rot} + NT\,(D_X \sin\theta - D_Y \cos\theta) \quad (6\text{-}4)$$

$$M_{IPB} = M_{Rot} + NT\,(D_X \sin\theta - D_Z \cos\theta) \quad (6\text{-}5)$$

where, M_{OPB} = OPB bending moment at the calculation point (Fig.6-9)

M_{IPB} = IPB bending moment at the calculation point (Fig.6-10)

M_{Rot} = Reaction moment at the loading point in applying prescribed angle

α = Interlink angle for OPB

β = Interlink angle for IPB

6.5 Hotspot Stress and Stress Concentration Factor (SCF)

In general, when classifying the stress in terms of fatigue strength, there are three terminologies; nominal stress, hotspot stress and notch stress (DNV, 2011). Nominal stress is a stress value in a component using general theories such as beam theory and hotspot stress is a structural stress on the surface at the hotspot considering the geometric configuration. And finally, the notch stress is a total stress value at the root of a notch taking into account the weld geometries. In terms of OPB/IPB fatigue, the hotspot stress is adequate.

The stress can be extracted from the max principal stresses (non-averaged for conservative purpose) at each node on the surface of chain links. Fig.6-11 shows the nodes on the chain surface for reading hotspot stresses from the FE analysis. Noted that the reading nodes in Fig.6-11 were determined based on the tentative OPB failure modes through the lots experimental results.

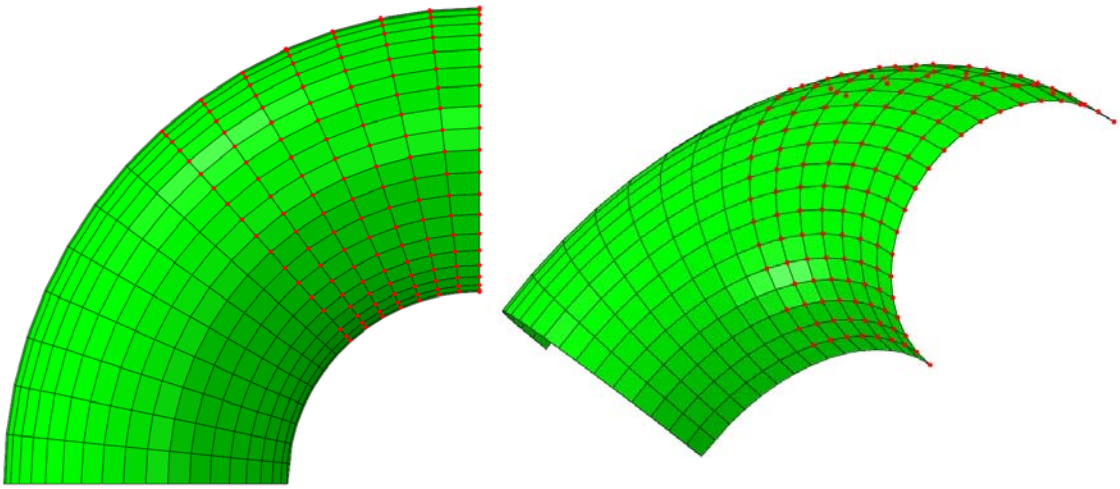

Fig.6-11 Nodes on the chain surface for reading hotspot stresses

From the results of FE analysis for OPB and IPB, the stress concentration factors (SCF) can be achieved based on the following equations (6-6), (6-7) and (6-8).

$$SCF_{TTi} = \frac{\sigma_{PTTi}}{\sigma_n} \tag{6-6}$$

$$SCF_{OPBi} = \frac{\sigma_{POPBi}}{\sigma_n} \tag{6-7}$$

$$SCF_{IPBi} = \frac{\sigma_{PIPBi}}{\sigma_n} \tag{6-8}$$

where, SCF_{TTi} = SCF at node i on the surface of chain link for tension

SCF_{OPBi} = SCF at node i on the surface of chain link for OPB mode

SCF_{IPBi} = SCF at node i on the surface of chain link for IPB mode

σ_{PTTi} = Max principal stress at node i of chain link for tension

σ_{POPBi} = Max principal stress at node i of chain link for OPB mode

σ_{PIPBi} = Max principal stress at node i of chain link for IPB mode

σ_n = Nominal stress of chain link ($= \frac{T}{A_{chain}}$)

A_{chain} = Section area of chain link

6.6 Results of FE Analysis for Chain Links

From the results of the non-linear FE analysis to investigate OPB and IPB mechanism, the max principal stresses as hotspot stress were evaluated at all the concerned nodes on the chain surface. Contact area is subject to complex phenomena and so, in the post-processing from the analysis this area was not addressed. In particular, the OPB JIP highlighted that the friction in the contacting area tends to smooth the micro-fissures which prevents to extent the fissure propagation (Dahlberg, 2011). In Fig.6-12 below, the contact pressure and the deformed shape at the contact area between chain links at the proof load are shown.

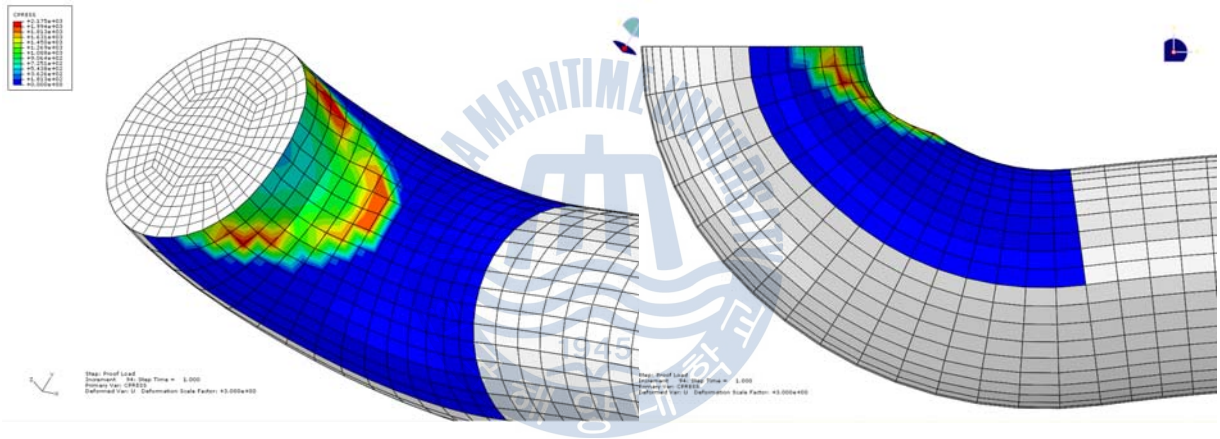

Fig.6-12 Contact pressure on chain link and deformed shape

Due to the physical complexity, the contact area was not included in reading the hotspot stresses from the FE analysis.

The plastic deformed surface at the contact areas under the proof load makes the chain links difficult to rotate along with the friction at the OPB/IPB angle stage. Fig.6-13 shows the contact pressure step-by-step from proof load to the OPB angle.

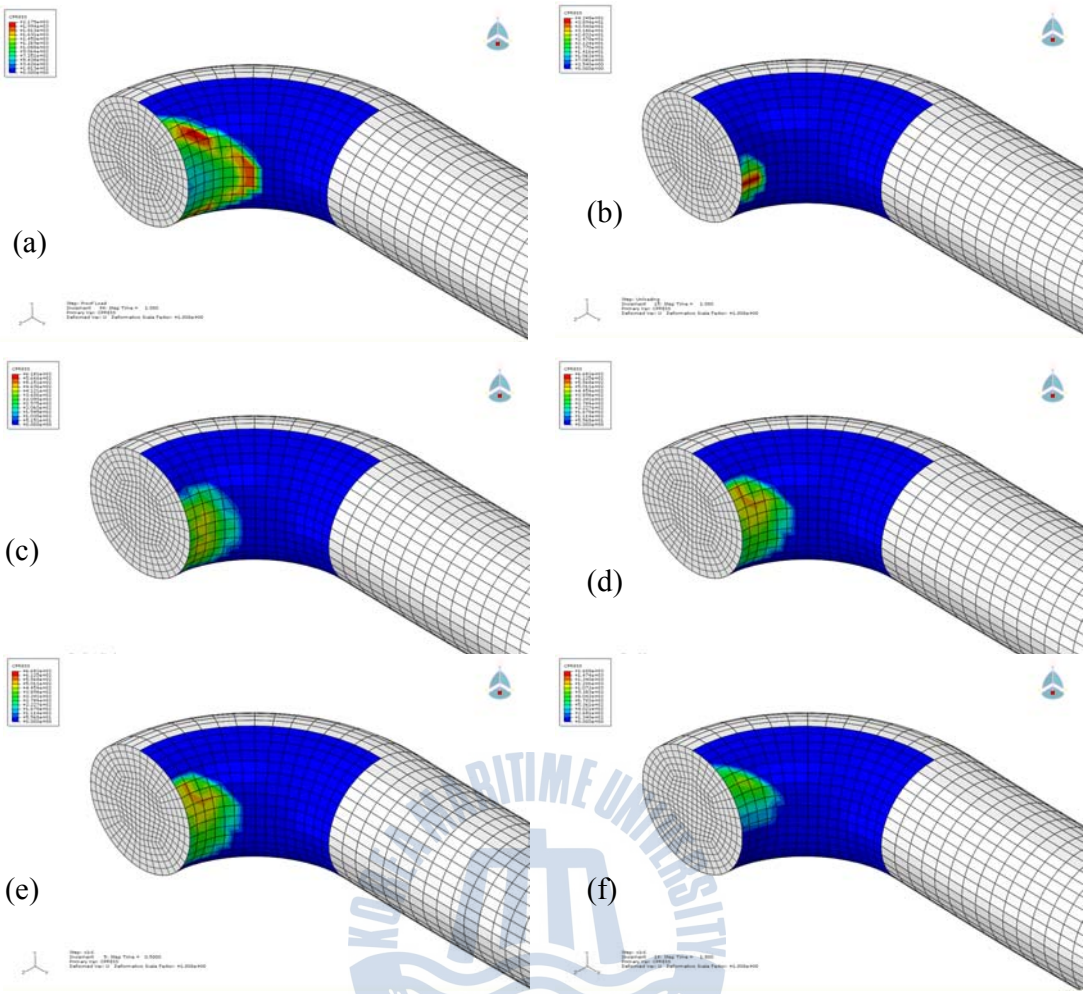

Fig.6-13 Contour of contact pressures according to analyzed step for OPB

The contact pressured area after proof loading was decreased according to the unloading force (b) and at the nominal tension the pressured area was enlarged again (c) and then, when applying OPB rotation the pressure area was relocated to the upper surface (d and e), which may be the ‘locking mode’. Finally, at the breaking point of its friction the contact pressure was suddenly somewhat decreased (f). Likewise, for IPB FE analysis there were same conclusions as shown in Fig.6-14.

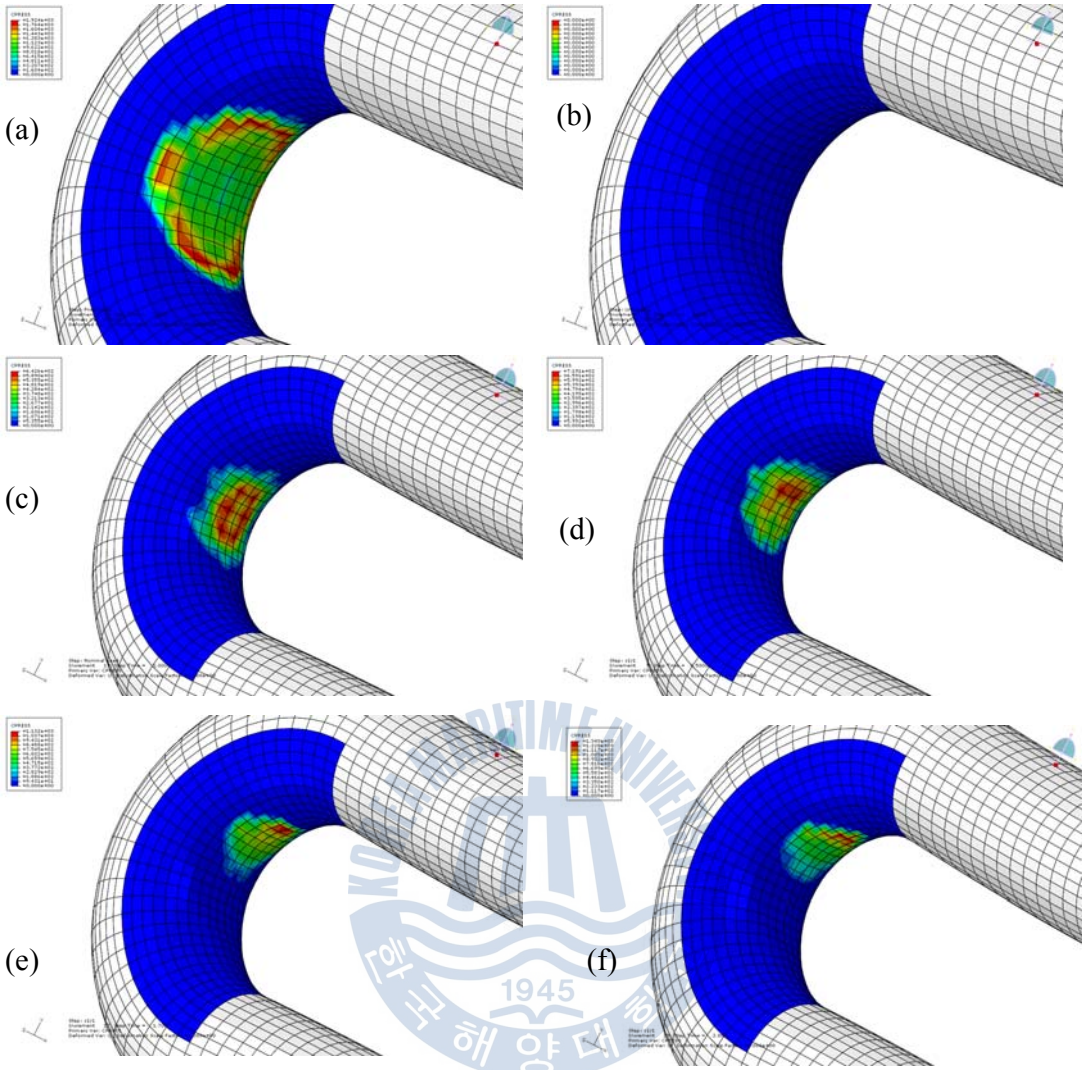

Fig.6-14 Contour of contact pressures according to analyzed step for IPB

And, investigating the contact shear stresses from the FE analysis, they were played a role in generating torque moment onto the chain with increasing OPB/IPB angles, which is presented in Fig.6-15 below; i.e. (a)→(b)→(c)→(d).

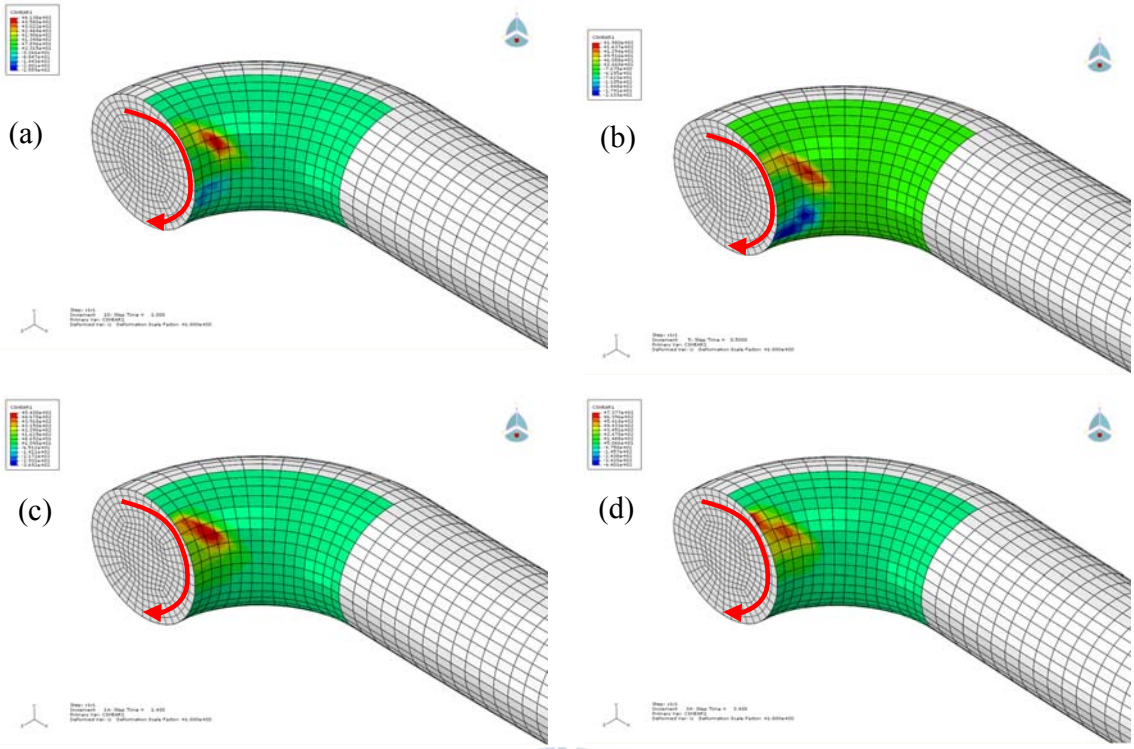

Fig.6-15 Contact shear stress generating torque moment to chain link for OPB

The contact shear stresses of IPB model showed different patterns. With increasing IPB angles, the contact shear generated tractions along the chain's surface as illustrated in Fig.6-16, from which the IPB stresses were made.

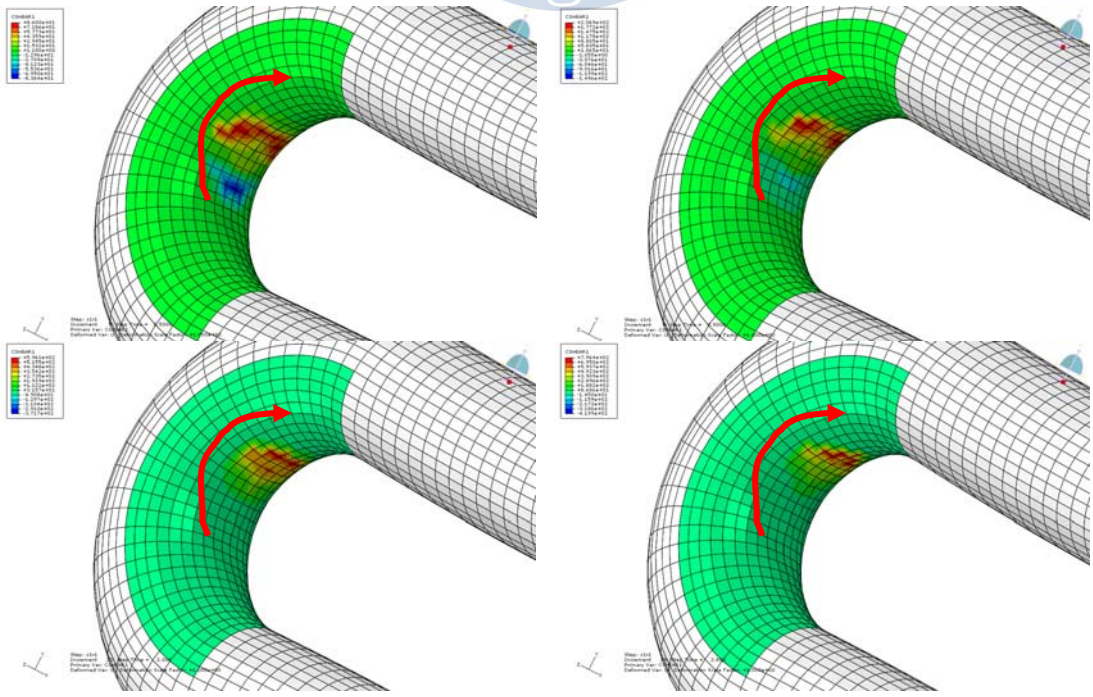

Fig.6-16 Contact shear stress generating surface tractions to chain link for IPB

6.6.1 Residual Strain and Stress

As mentioned, the contact surface between chain links was plastically deformed at the proof loading step. With the deformed surface, two chain links might be stuck each other not to easily rotate.

Based on the proof loads of 10875kN applied, the residual plastic strain was found abt. 16.4% at the adjacent part of links' contact, which is in Fig.6-17.

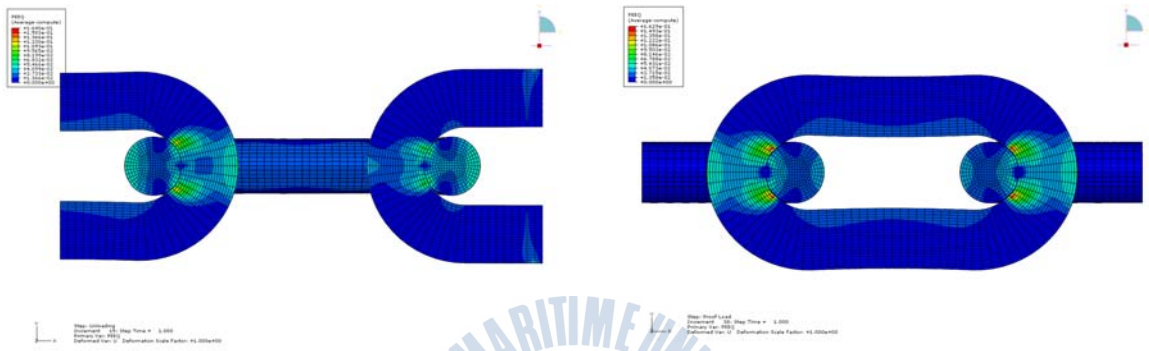

Fig.6-17 Residual plastic strain at unloading stage for OPB and IPB FE models

6.6.2 Interlink Equivalent Stiffness

In order to input the relevant bending stiffness between chain links to the fully dynamic analysis, interlink equivalent stiffness was defined and obtained on the basis of the descriptions of Section 6.4.

Fig.6-18 gives the relations between the OPB moment and interlink angle and the equivalent bending stiffness according to the applied nominal tensions, which was calculated from FE analysis. The bending stiffness calculated from OPB chain link model was around 150kN-m/deg.

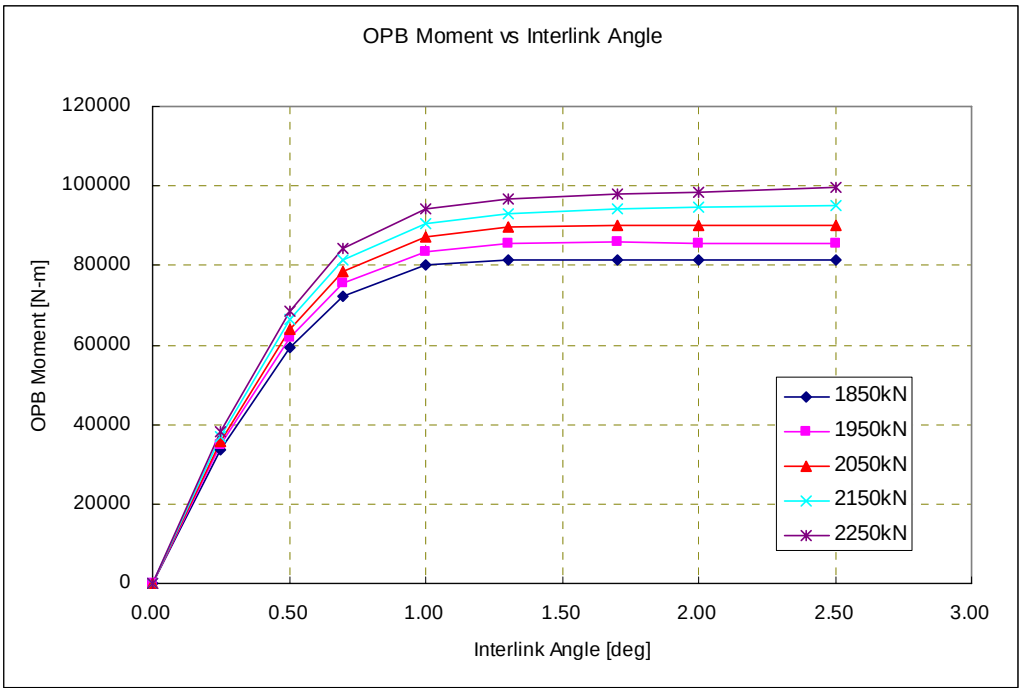

Nominal Tension	1850kN	1950kN	2050kN	2150kN	2250kN
Stiffness [kN-m/deg]	141.7	146.7	151.4	155.8	160.3

Fig.6-18 OPB moment vs interlink angles for different nominal tensions

The validation of the OPB moment vs interlink angles was undertaken referring to Jean et al. (2005). As shown in Fig.6-19 (NT = 2250kN), the OPB moments calculated by FE analysis were validated at the lower interlink angles; e.g. ≤ abt 0.5deg but, others are highly deviated.

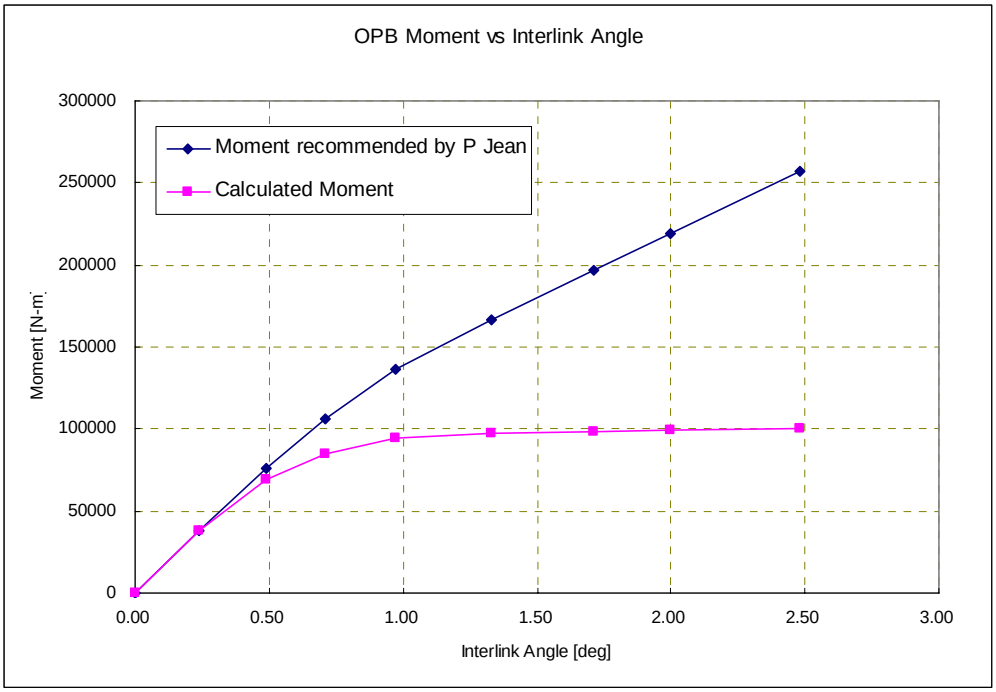

Fig.6-19 Comparison of OPB moments with equation by Jean et al. (2005)

Also, for IPB FE model, the equivalent bending stiffness between chain links was achieved as shown in Fig.6-20. The bending stiffness calculated from IPB chain link model was around 100kN-m/deg.

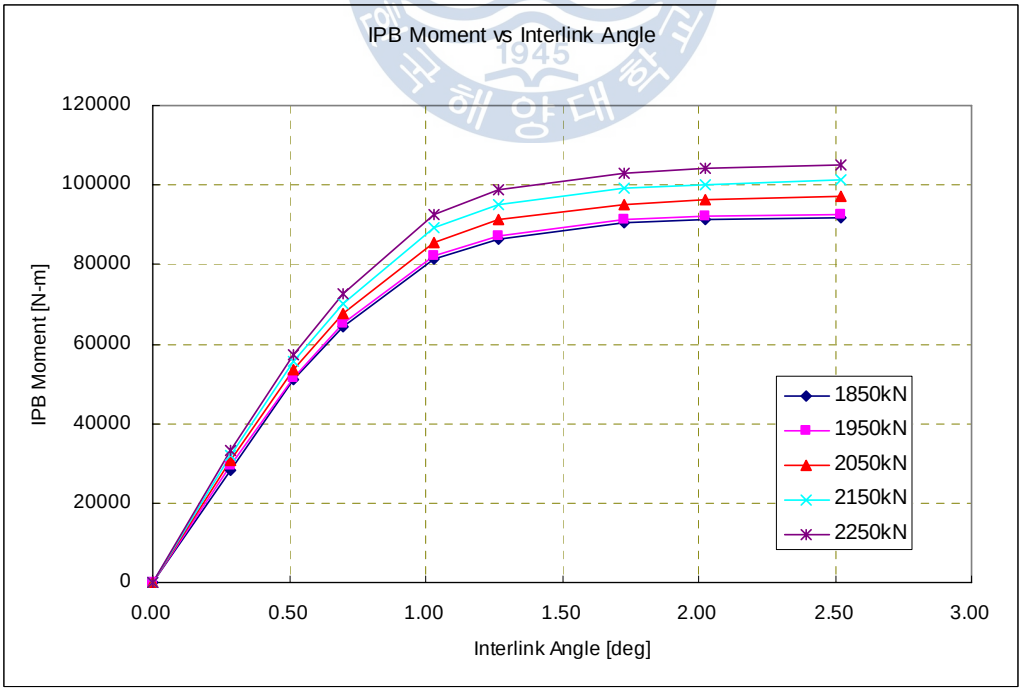

Nominal Tension	1850kN	1950kN	2050kN	2150kN	2250kN
Stiffness [kN-m/deg]	99.6	104.0	108.5	113.1	117.5

Fig.6-20 IPB moment vs interlink angles for different nominal tensions

6.6.3 Stress Results and SCFs

Post-processing of hotspot stresses from the non-linear FE analysis was performed based on the following notations; the nodes were classified with circumferential (i.e. Node index) and radial (i.e. Radial index) numbering system.

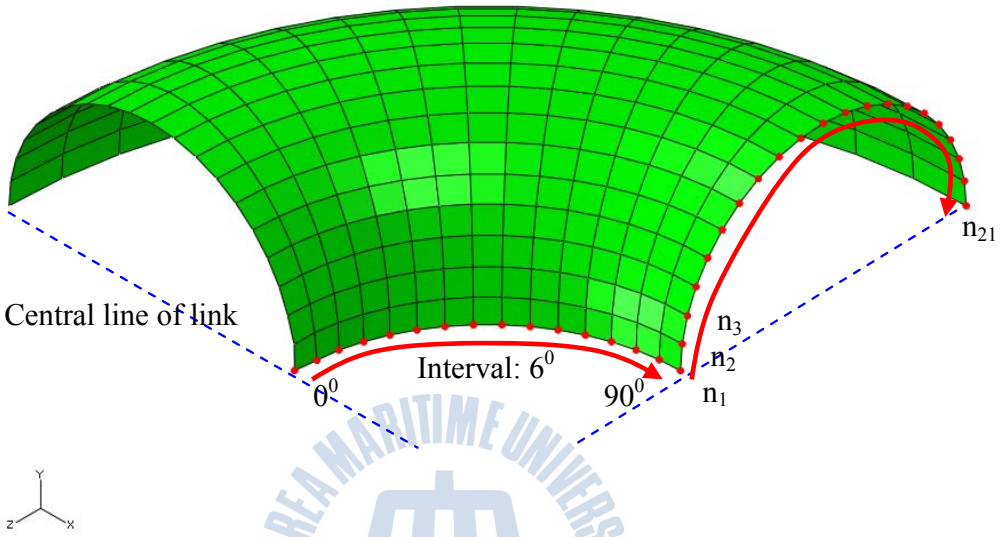

Fig.6-21 Notation of nodes for post-processing from FE analysis

1) SCF for Tension Loading

From the FE analysis the max hotspot stresses for the nominal tensions were found at the location presented in Fig.6-22 for OPB and IPB models. Both models had the max values at the same location, i.e. radial 78deg and n_1.

In particular, considering the nominal stress for each tension load, the stress concentration factors (SCF) were calculated with same value.

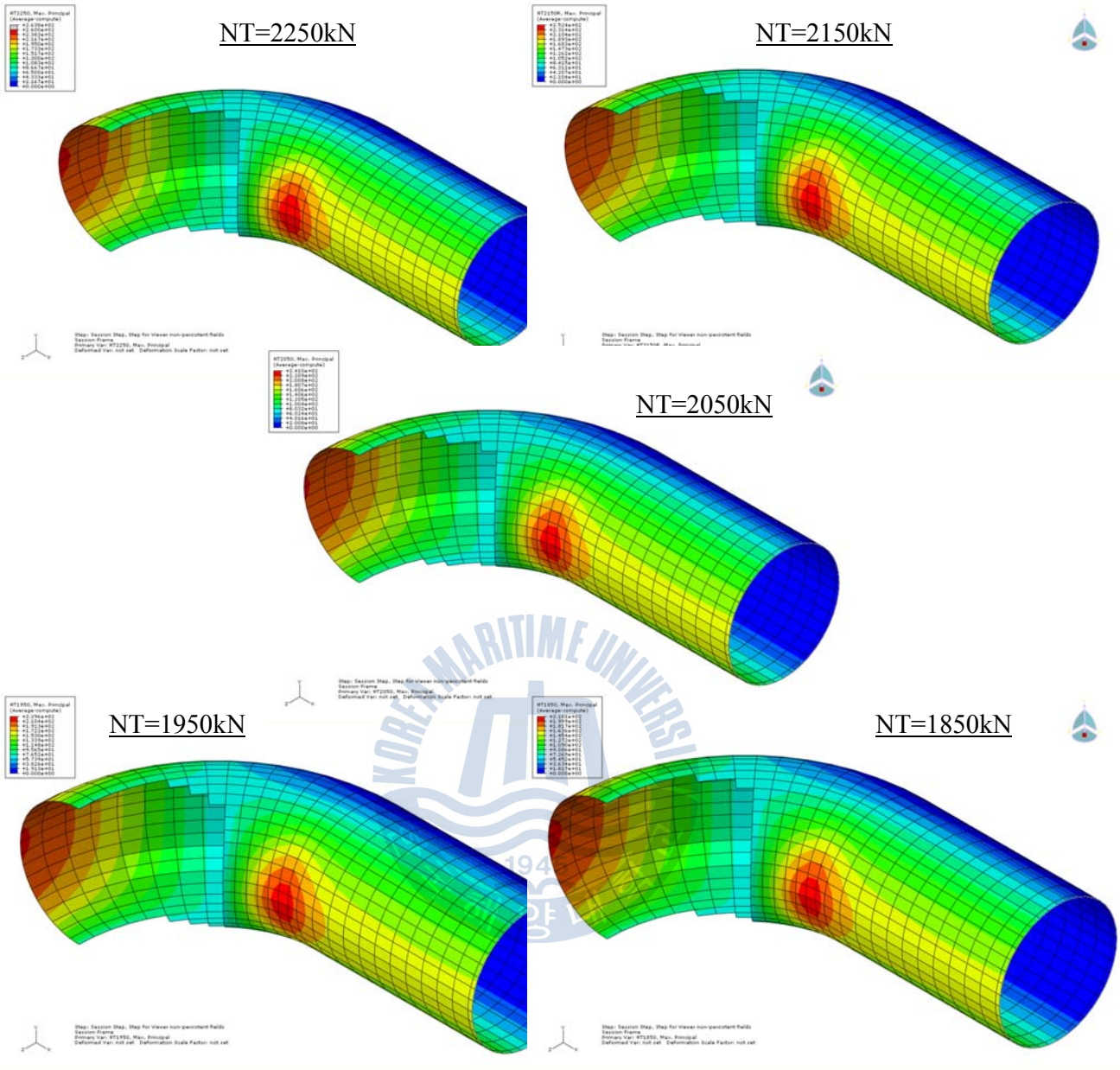

Fig.6-22 Contour of max principal stresses according to different tensions

The SCFs calculated from FE analysis were summarized as given in Table 6-2.

Table 6-2 Summary of SCF_{TT} for different nominal tensions

Tension	1850kN	1950kN	2050kN	2150kN	2250kN
σ_n	54.5	57.4	60.4	63.3	66.3
SCF_{TT}	3.9	3.9	3.9	3.9	3.8

These values were utilized to calculate hotspot stresses at every concerned location on chain surface in simulating the mooring dynamic behaviors based on the equations presented in Section 6.5. In Fig.6-23, the tension SCF values at the concerned nodes of a chain link are given.

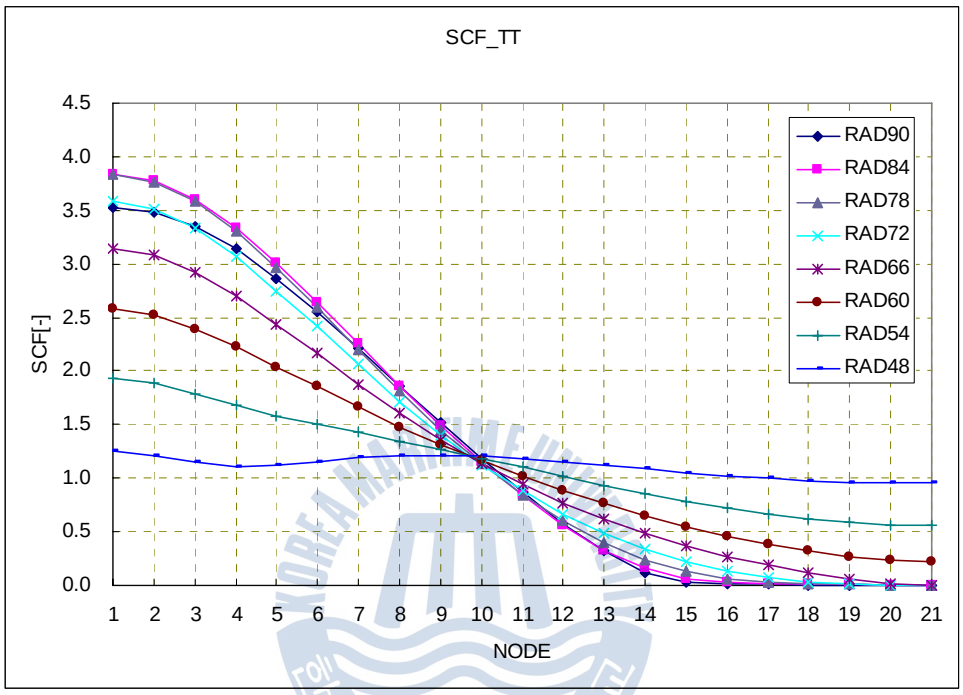

Fig.6-23 Tension SCF values for concerned nodes of chain link

2) SCF for OPB Model

Prior to the calculation of the SCFs from the OPB model, it is necessary to calculate the pure OPB stress induced from only the chain links' bending effects. The OPB stress can be derived from the following Eq.(6-10).

$$\sigma_{OPB} = \sigma_{Total} - (\sigma_{Proof} - \sigma_{NT}) \tag{6-10}$$

where, σ_{OPB} = OPB stress purely generated from OPB mechanism

σ_{Total} = Total stress at a stage from FE analysis

σ_{Proof} = Stress generated due to proof load

σ_{NT} = Stress generated due to nominal tension

Depending upon the value of OPB angles, the location of max principal stress was moved upward of a chain link. It is understood that due to the torsional effect of chain link's bar the torsional stresses also were generated additionally. Besides, with increasing the OPB angles, the hotspot areas were extended around the upper surface of the chain link. Fig.6-24 shows the stress contours for each step of OPB model, from which the stress patterns were found. And finally the constant stress patterns were kept. It is meant that increasing the OPB angle, the locking mode was initially generated and at a certain time the chain links slid along each contact surface as the sliding mode as shown in Fig.6-25, in which they have same stress contours.

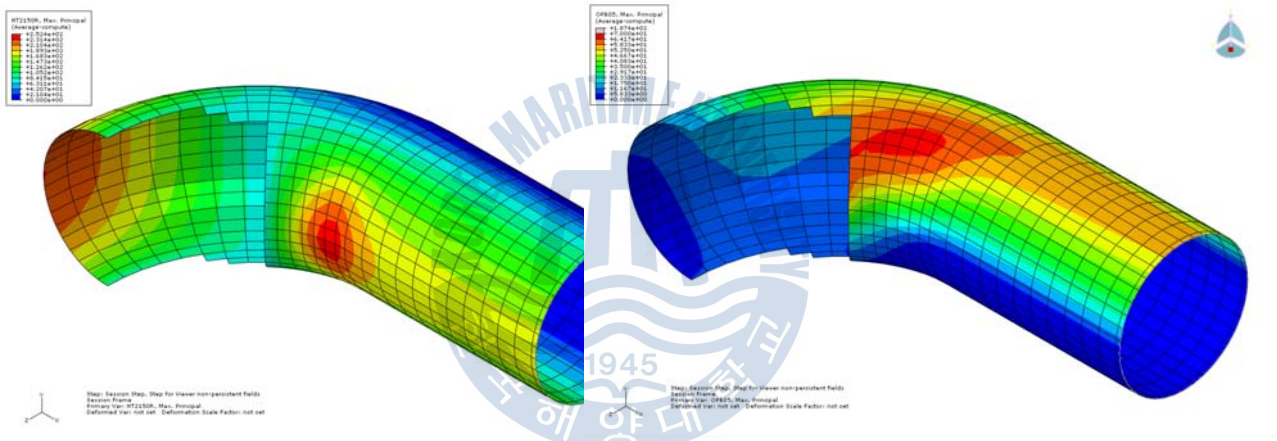

Fig.6-24 Stress contours of before- and after- OPB angles

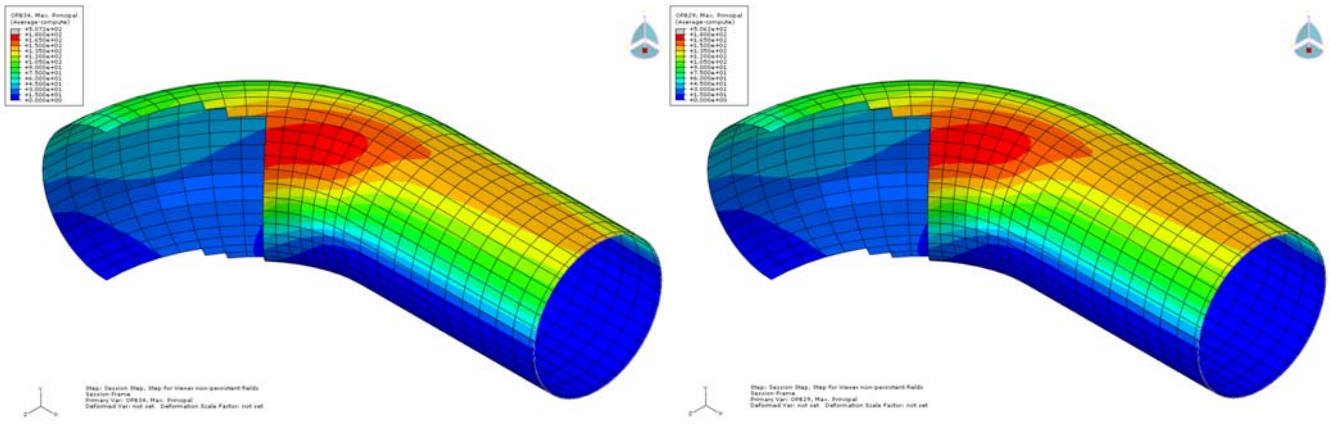

Fig.6-25 Stress contours showing sliding mode at the different steps for OPB model

Consequently, the max SCFs of all the reading nodes for OPB models was presented in Fig.6-26. These values were also utilized to calculate hotspot stresses at every concerned location on chain surface in simulating the mooring dynamic behaviors based on the equations presented in Section 6.5. The SCF increases with the OPB angle.

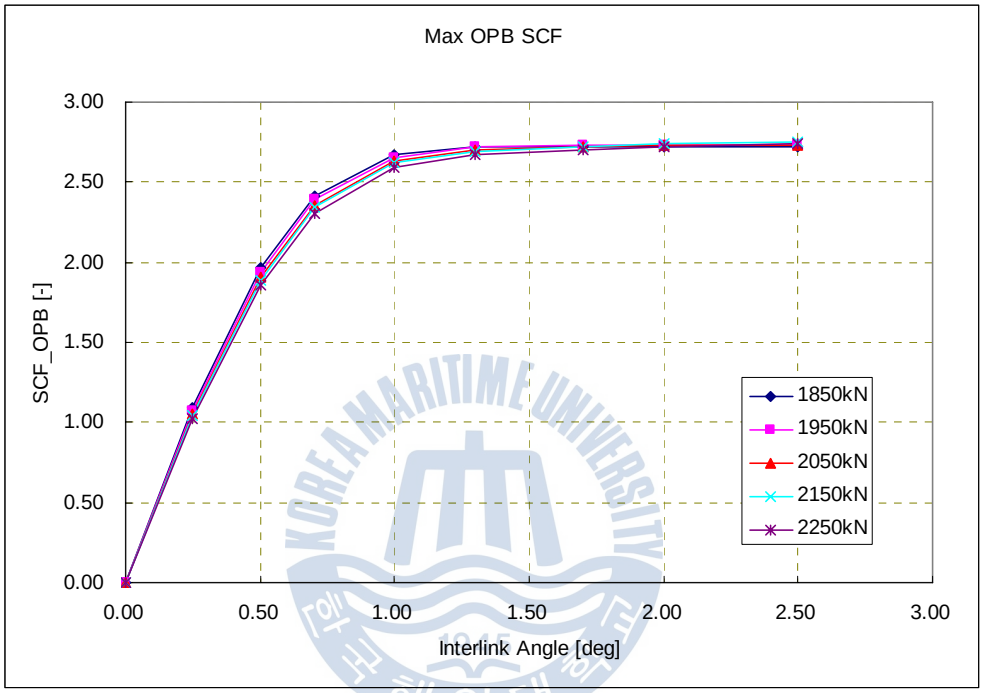

Fig.6-26 OPB SCFs according to chain interlink angle

For all the concerned nodes of a chain link, the OPB SCF values are indicated in Fig.6-27 and Fig.6-28 for interlink angles 0.25deg and 0.5deg respectively.

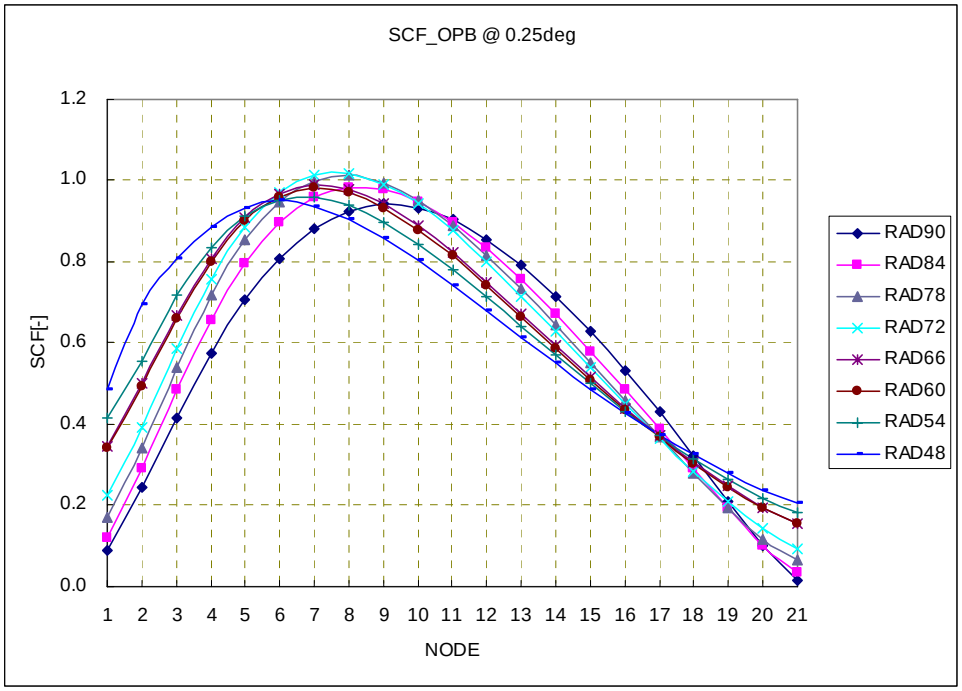

Fig.6-27 OPB SCF values for concerned nodes of chain link (α=0.25deg)

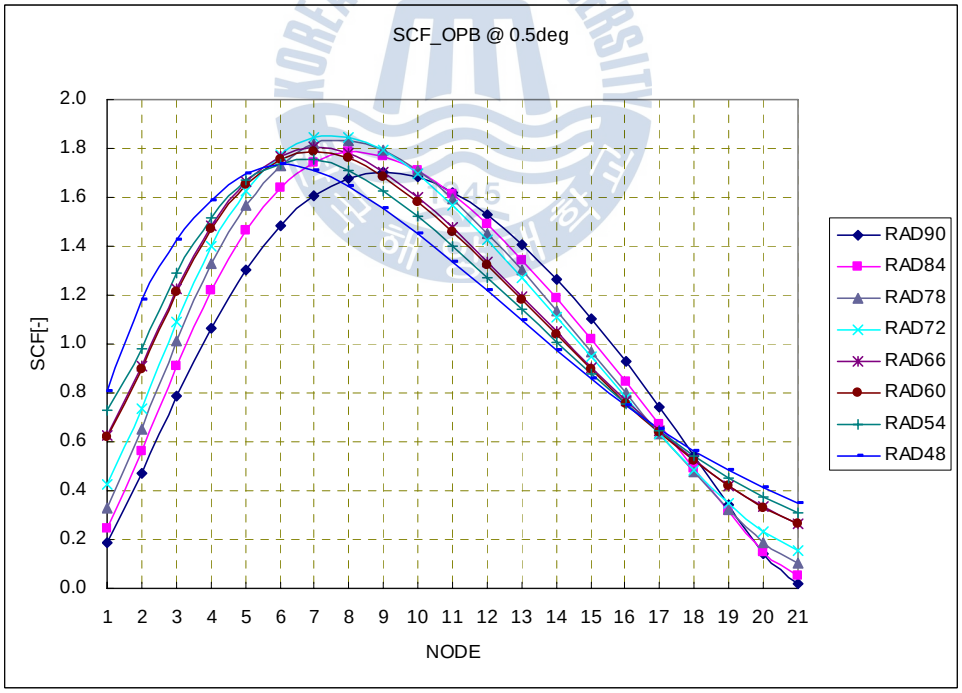

Fig.6-28 OPB SCF values for concerned nodes of chain link (α=0.5deg)

Introducing the equations, i.e. Eqs. (4-4) and (4-5), regarding OPB stress in sliding and locking modes mentioned in Section 4.1, the stresses calculated from the non-linear FE analysis were well matched as presented in Fig.6-29, in which the empirical constant k = 0.68 in the equation of the locking mode was used.

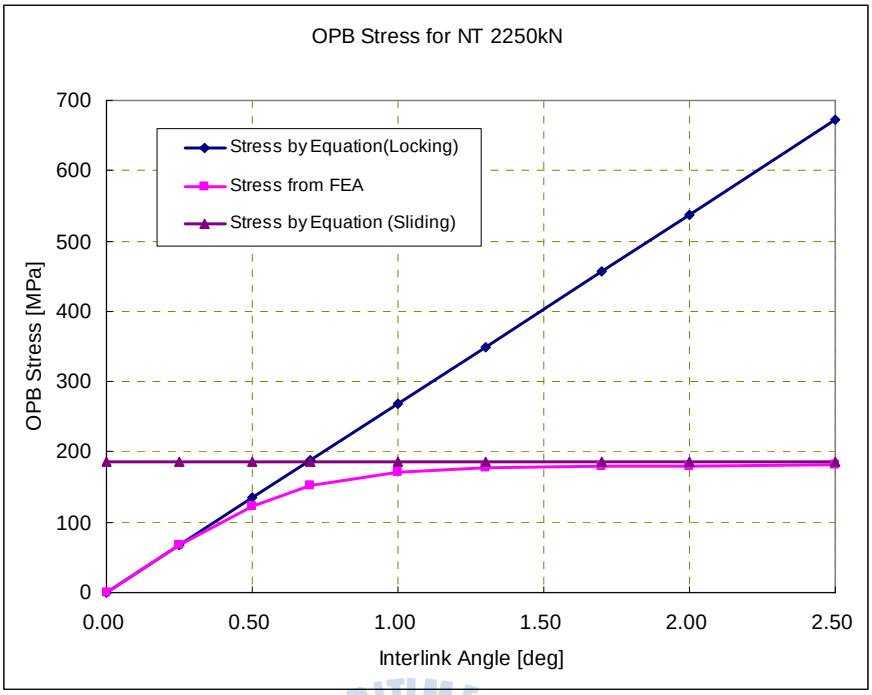

Fig.6-29 Comparison of OPB stresses calculated with the empirical equations

Accordingly, the OPB stresses from the FE analyses can be compared to those from the empirical equations for each nominal tension applied as shown in Fig.6-30 below.

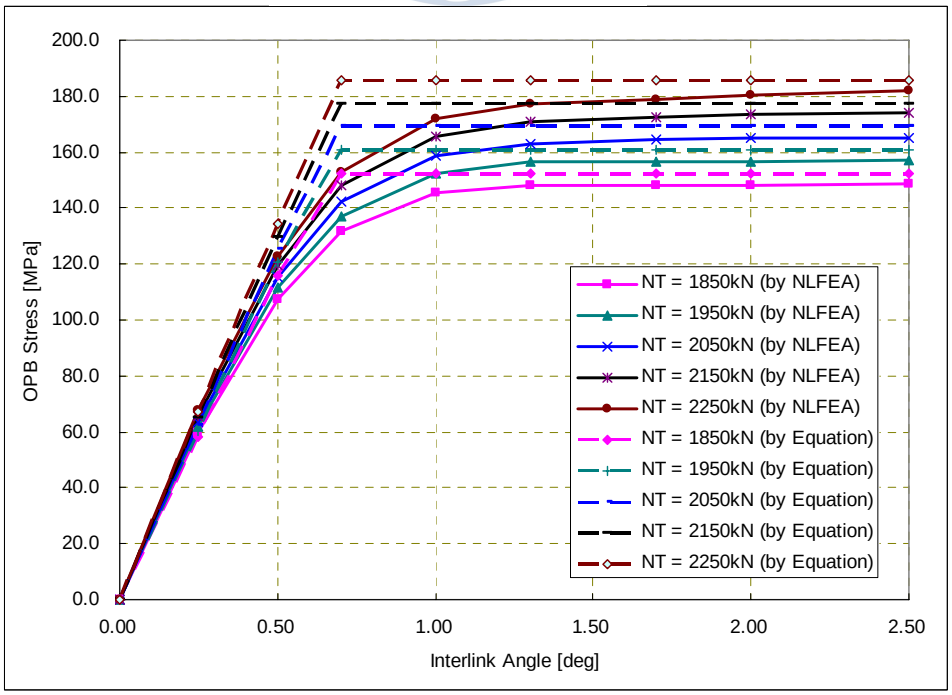

Fig.6-30 Results from NLFEA and empirical equations according to tensions

3) SCF for IPB Model

From the FE analysis for IPB model, it was found that IPB mechanism has similar conclusions with OPB model. For IPB model, it is necessary to calculate the pure IPB stress induced from only the chain links' bending effects as well. The IPB stress can be derived from the following Eq.(6-11).

$$\sigma_{IPB} = \sigma_{Total} - (\sigma_{Proof} - \sigma_{NT}) \tag{6-11}$$

where, σ_{IPB} = IPB stress purely generated from IPB mechanism

σ_{Total} = Total stress at a stage from FE analysis

σ_{Proof} = Stress generated due to proof load

σ_{NT} = Stress generated due to nominal tension

As presented in Fig.6-31, the max hotspot stresses due to IPB angle were found at the outer surface of a chain link. With increasing the IPB angle, the hotspot locations were moved toward the upper surface and, at the certain time the stress plot patterns were kept constantly. This means the chain links was moved from the locking mode to the sliding mode depending on the tensile force and friction coefficient.

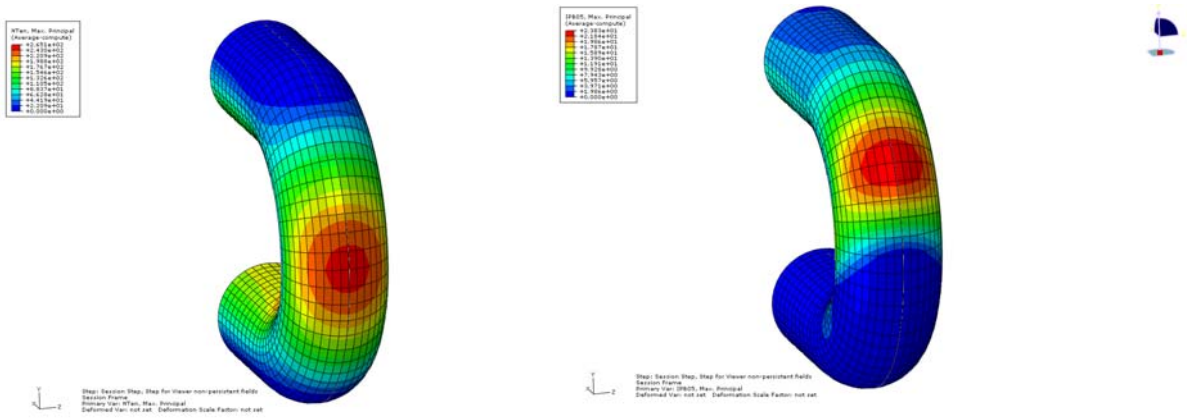

Fig.6-31 Stress contours of before- and after- IPB angles

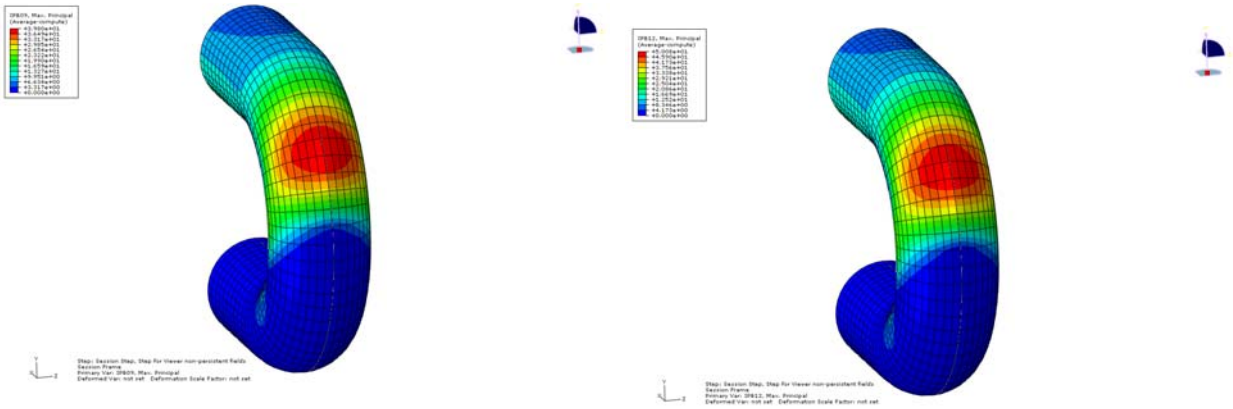

Fig.6-32 Stress contours showing the sliding mode at the different steps for IPB Model

The max SCFs of all the reading nodes for IPB models was presented in Fig.6-33. These values were also utilized to calculate hotspot stresses at every concerned location on chain surface in simulating the mooring dynamic behaviors based on the equations presented in Section 6.5. The SCF increases with the IPB angle as well.

For all the concerned nodes of a chain link, the IPB SCF values are indicated in Fig.6-34 and Fig.6-35 for interlink angles 0.25deg and 0.5deg respectively.

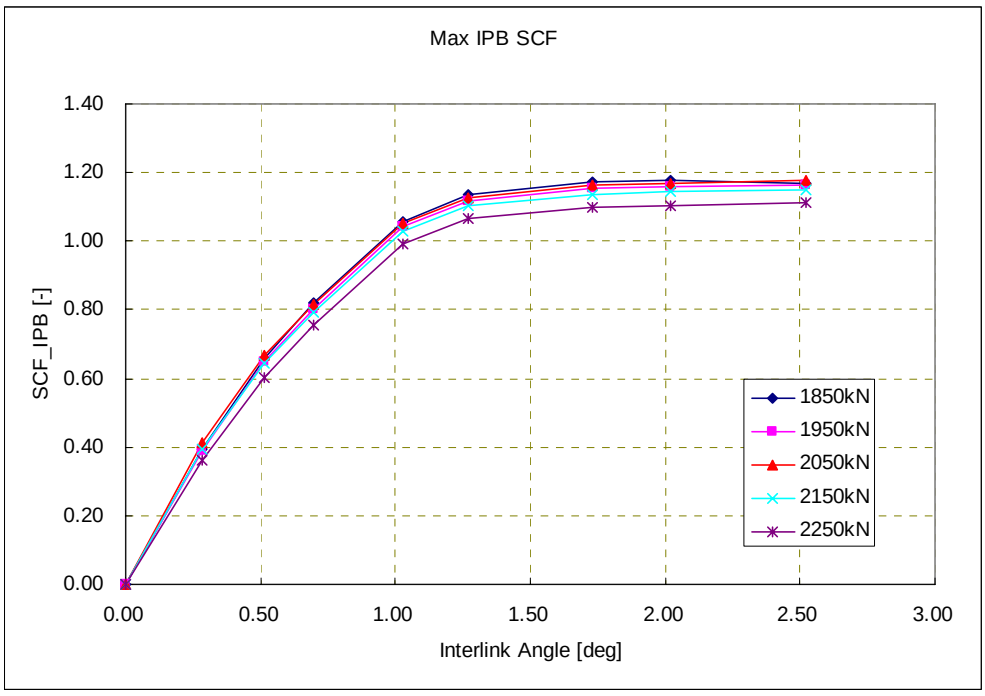

Fig.6-33 IPB SCFs according to chain interlink angle

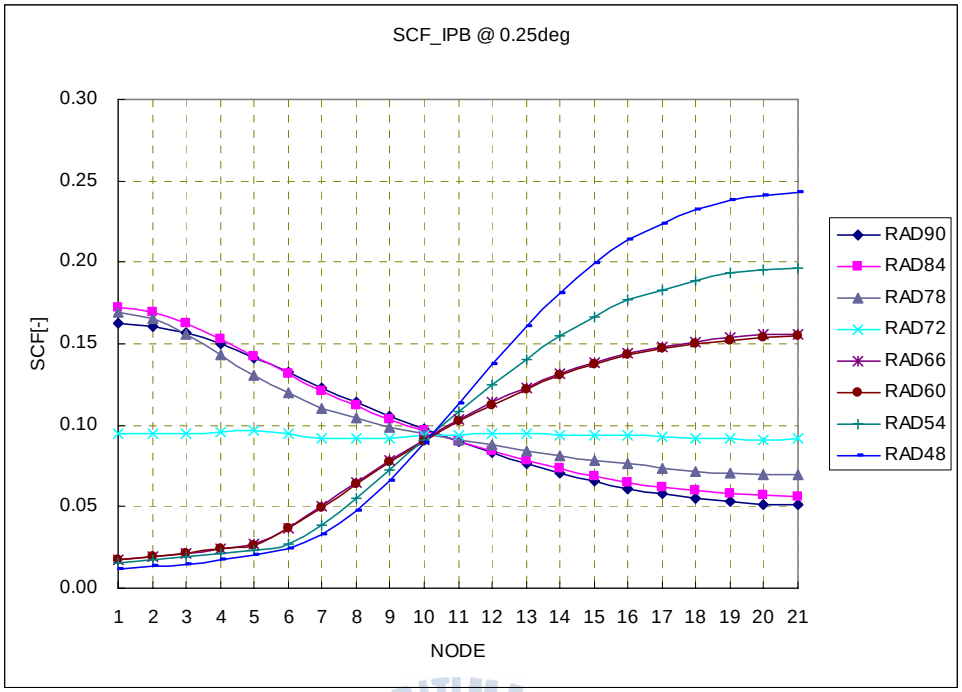

Fig.6-34 IPB SCF values for concerned nodes of chain link (β=0.25deg)

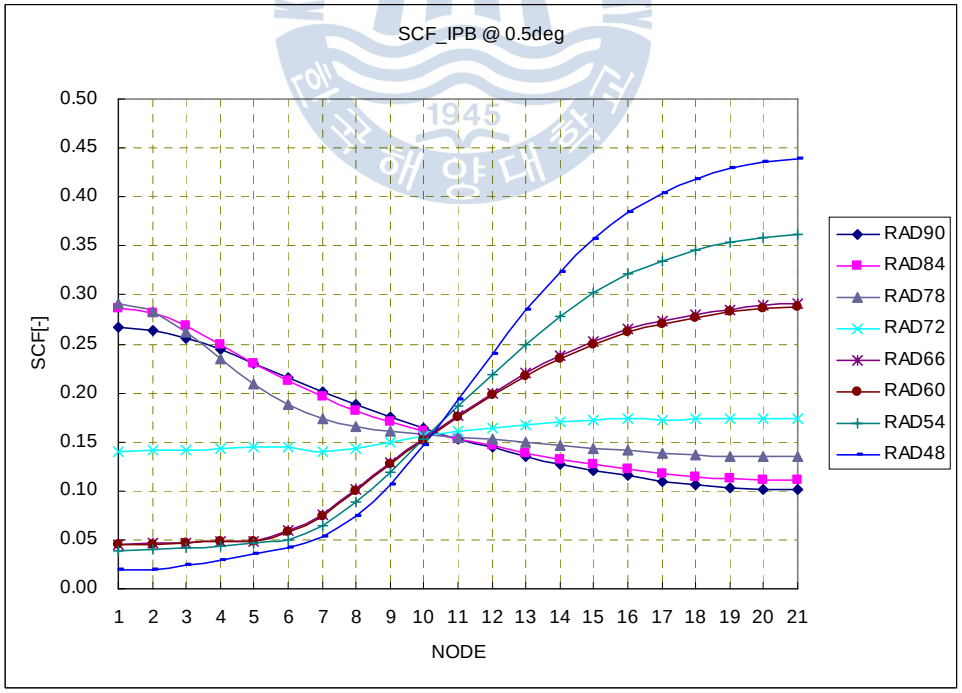

Fig.6-35 IPB SCF values for concerned nodes of chain link (β=0.5deg)

From the results of FE analyses, it is concluded that SCFs for IPB mode are relatively small comparing to OPB mode.

Fig.6-36 presents the contour of SCF values for tension load of each node and radial angle only for failure tentative area of the chain. And, the figures from Fig.6-37 to Fig.6-41 present the contours of SCF values for OPB interlink angle 0.25deg of each node and radial angle considering each nominal tension. For IPB interlink angle 0.25deg, the figures from Fig.6-42 to Fig.6-45 give the contours of SCF values.

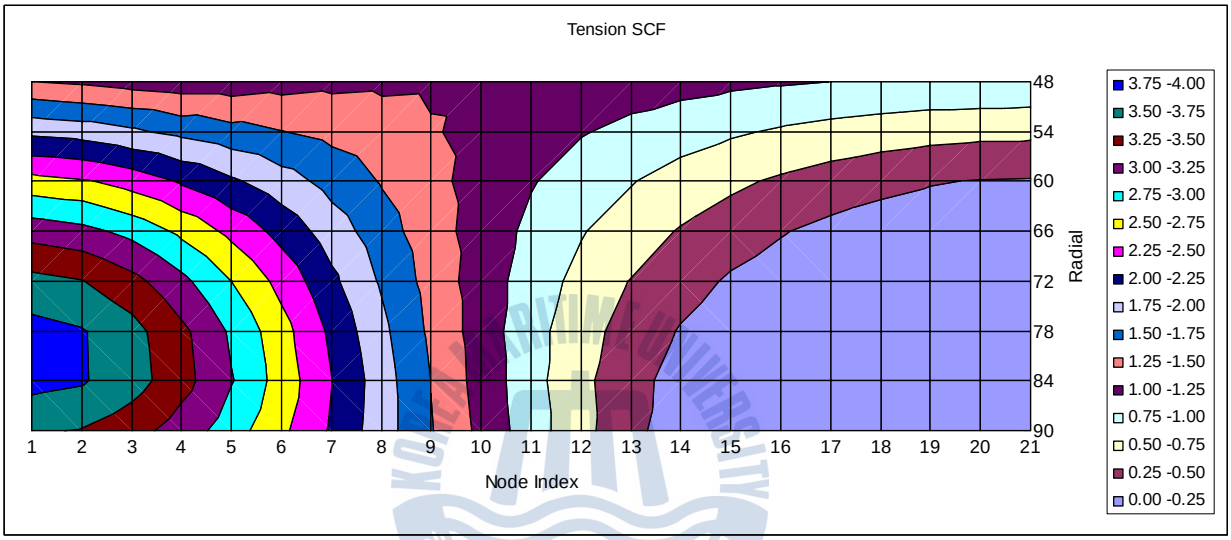

Fig.6-36 Tension SCF values calculated for FE model of chain link

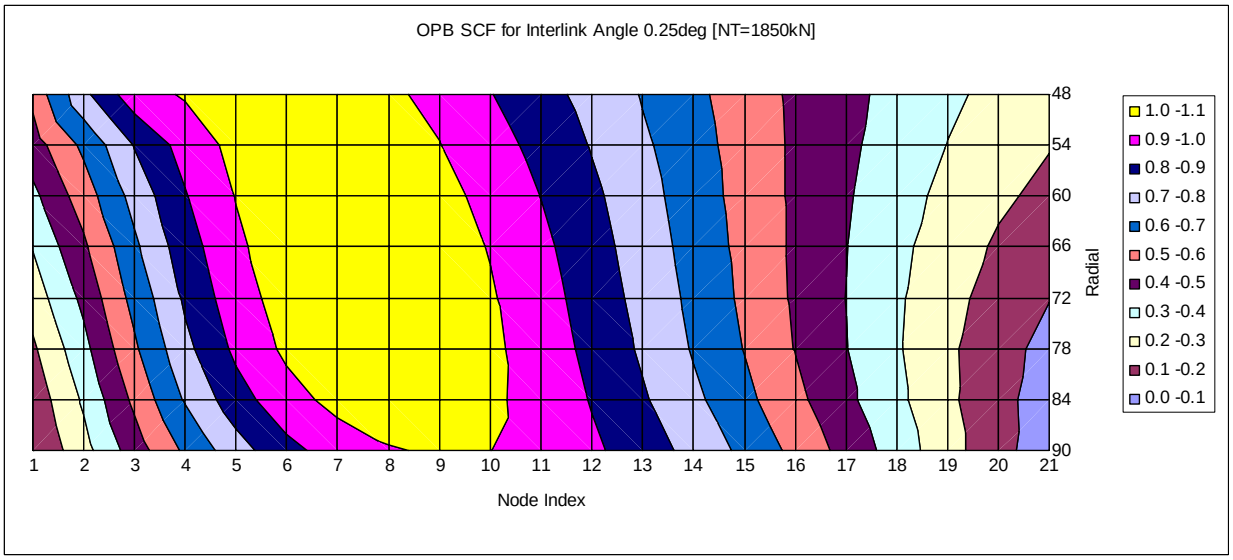

Fig.6-37 OPB SCF values calculated for FE model of chain (α=0.25deg and T=1850kN)

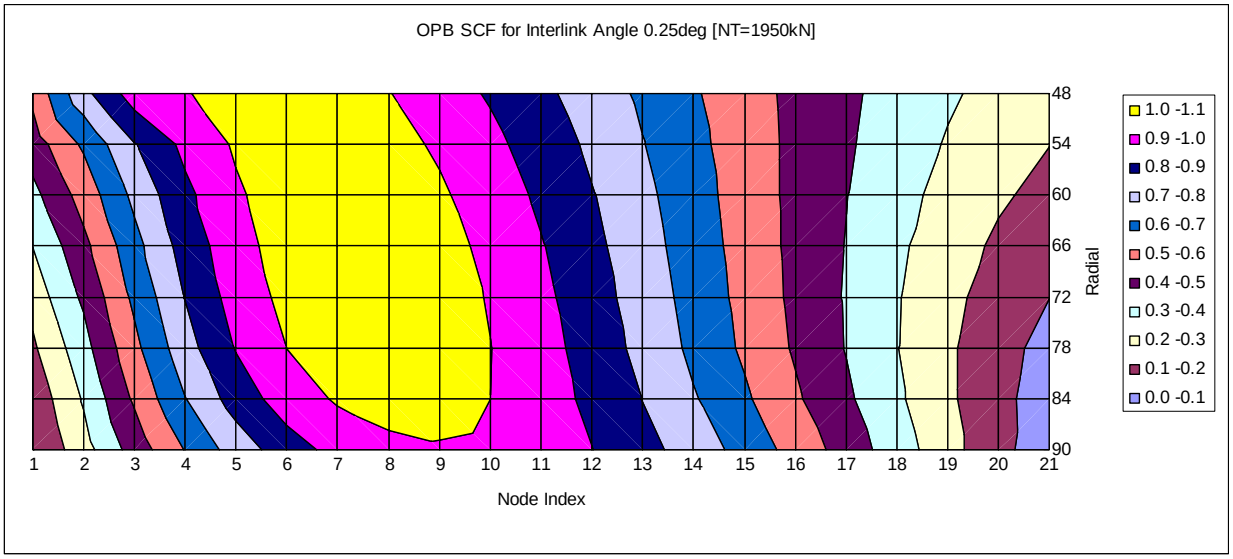

Fig.6-38 OPB SCF values calculated for FE model of chain (α=0.25deg and T=1950kN)

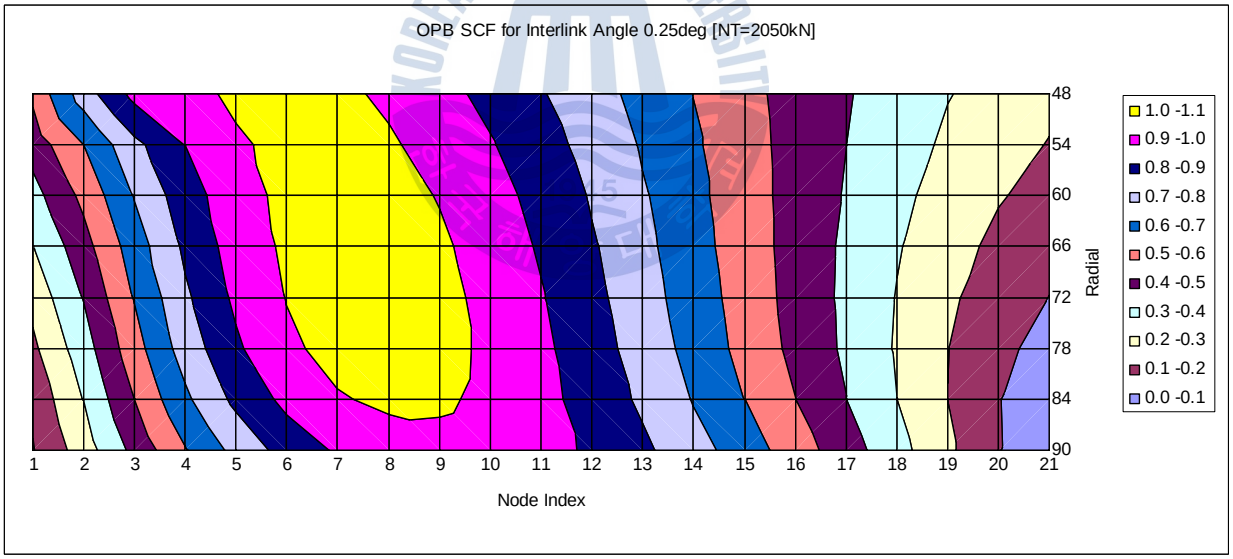

Fig.6-39 OPB SCF values calculated for FE model of chain (α=0.25deg and T=2050kN)

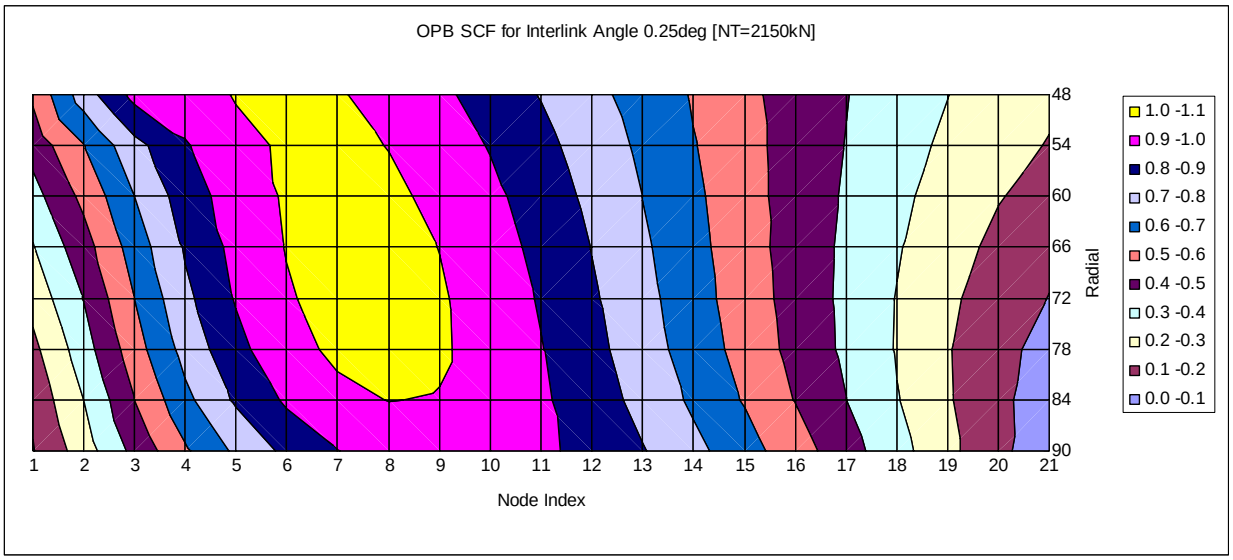

Fig.6-40 OPB SCF values calculated for FE model of chain (α=0.25deg and T=2150kN)

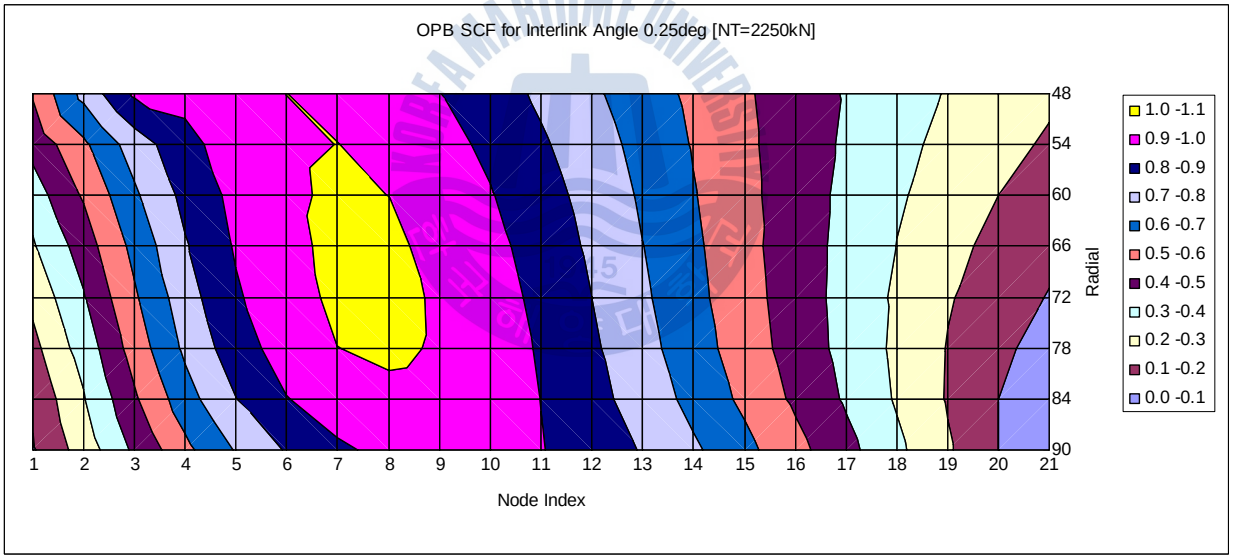

Fig.6-41 OPB SCF values calculated for FE model of chain (α=0.25deg and T=2250kN)

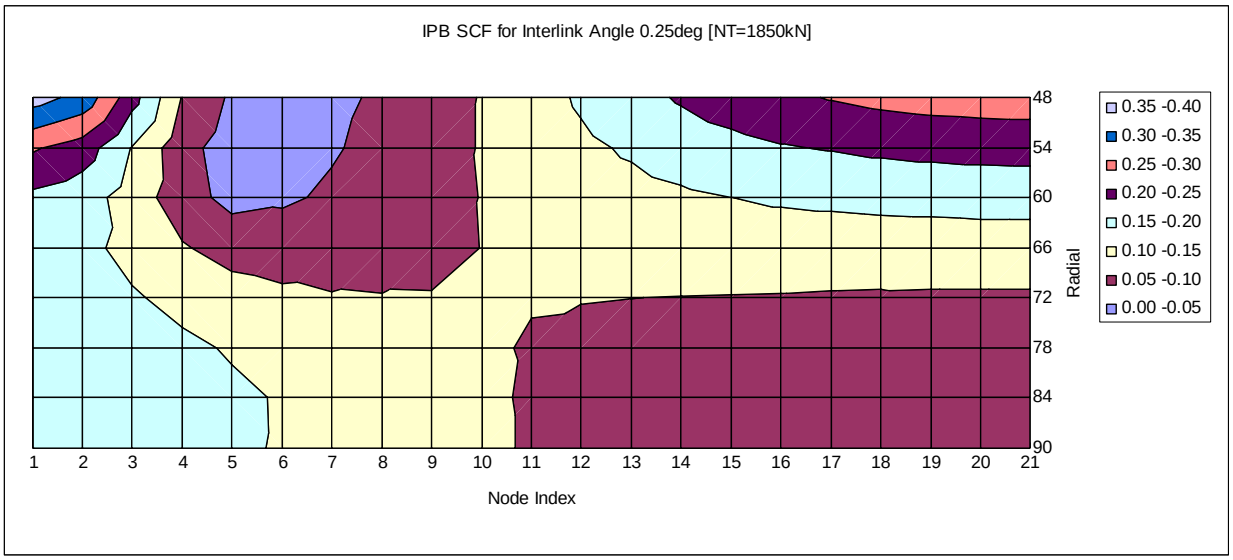

Fig.6-42 IPB SCF values calculated for FE model of chain (β=0.25deg and T=1850kN)

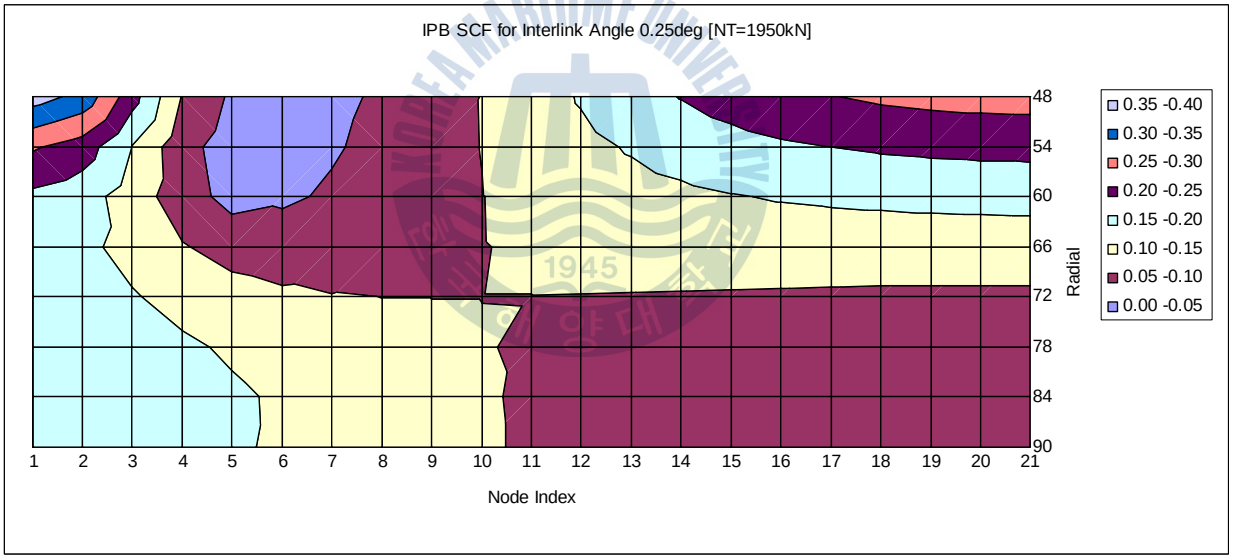

Fig.6-43 IPB SCF values calculated for FE model of chain (β=0.25deg and T=1950kN)

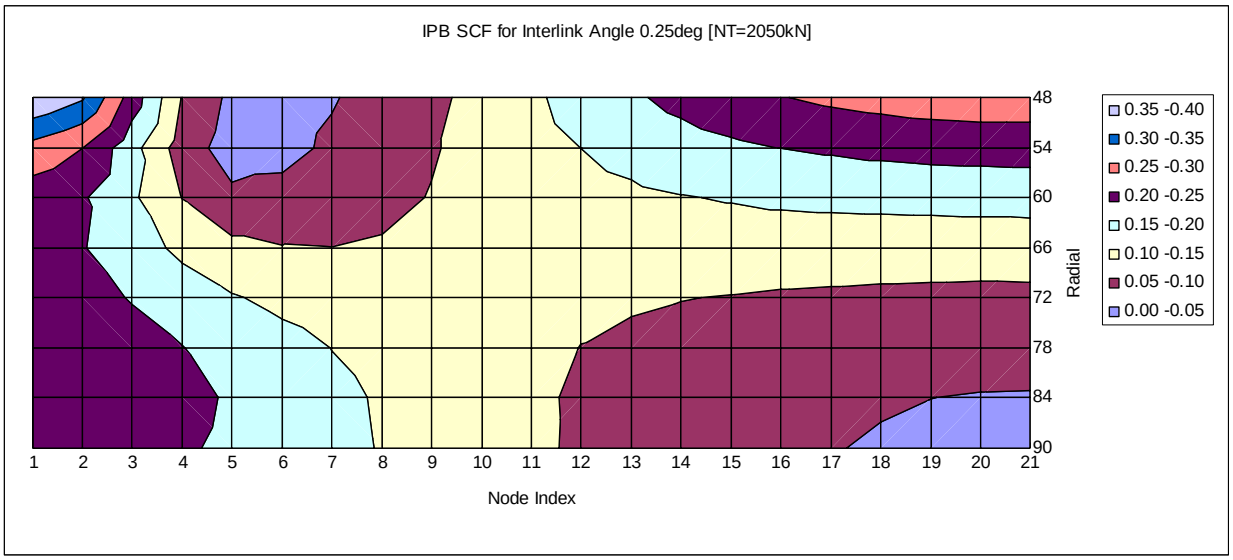

Fig.6-44 IPB SCF values calculated for FE model of chain (β=0.25deg and T=2050kN)

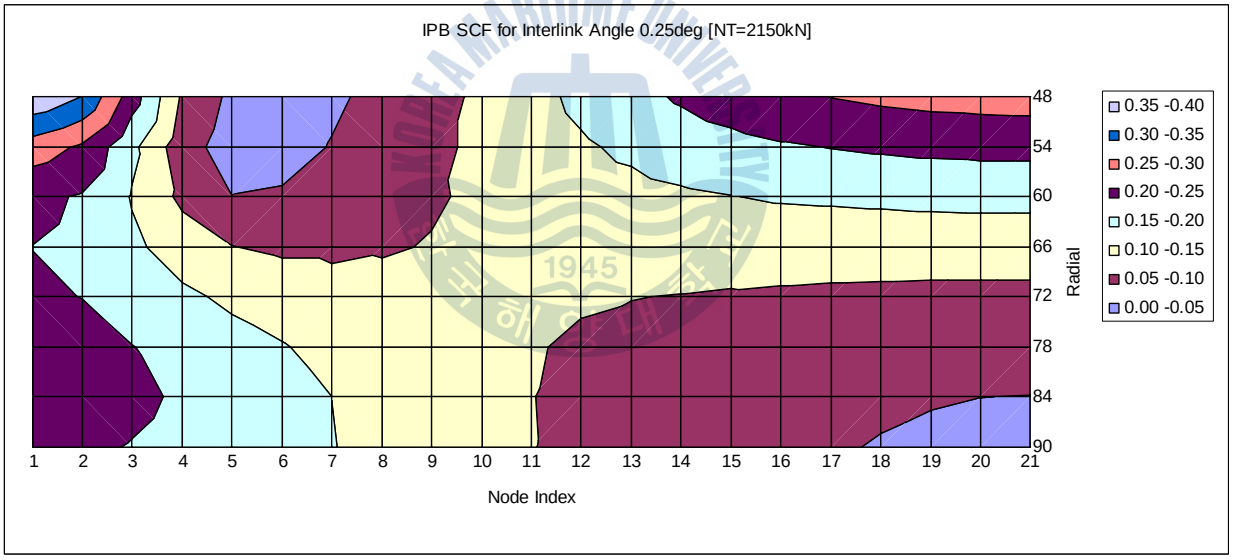

Fig.6-45 IPB SCF values calculated for FE model of chain (β=0.25deg and T=2150kN)

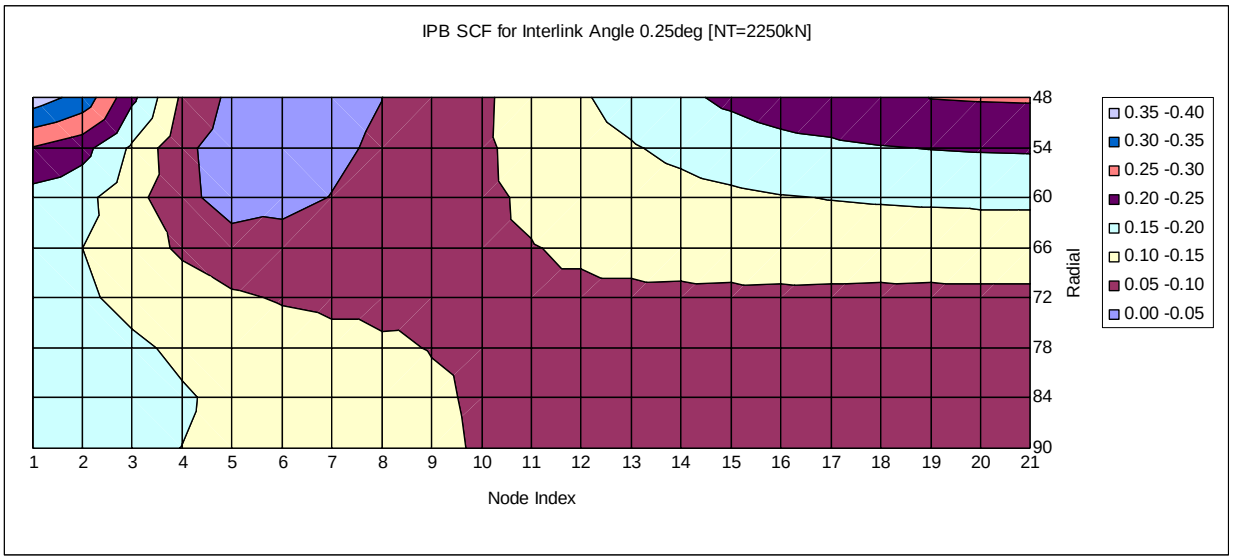

Fig.6-46 IPB SCF values calculated for FE model of chain (β=0.25deg and T=2250kN)

6.7 Effects on Friction Coefficient

As a parametric study, the effects on the friction coefficient were investigated with respect to the FE model of the OPB chain link. In this research, the studless chain of OD147 with R3 grade was taken into account as well. The frictionless between chain links along with the friction coefficient 0.3, 0.5 and 0.7 was also included in the study. And, the nominal tension of 2250kN was applied for all the models.

For the friction coefficient of 0.5, Fig.6-47 shows the contours of the max principal stresses due to OPB for each interlink angle.

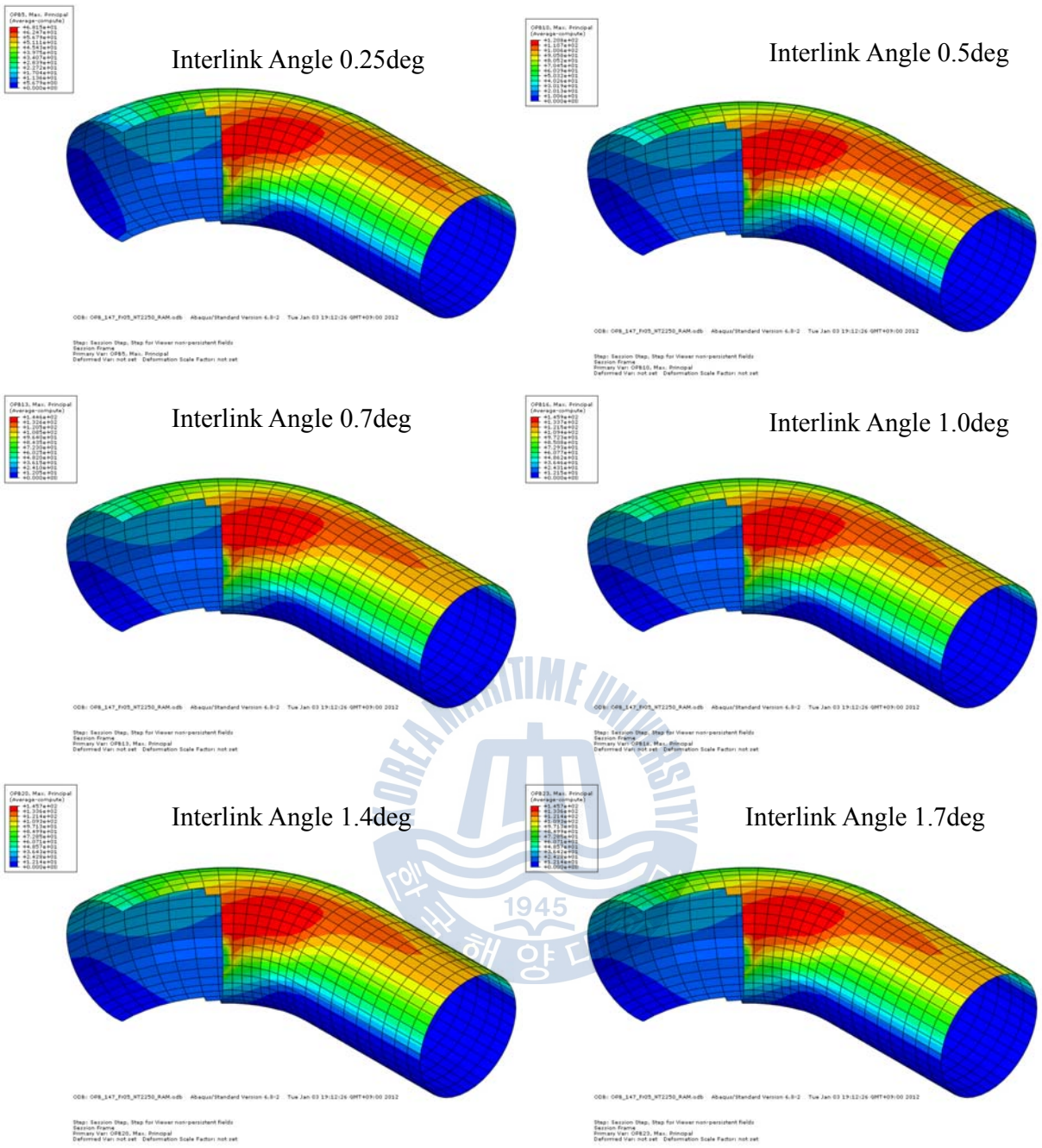

Fig.6-47 Contours of max principal stress for each interlink angle (friction 0.5)

For the friction coefficient of 0.3, Fig.6-48 shows the contours of the max principal stresses due to OPB for each interlink angle.

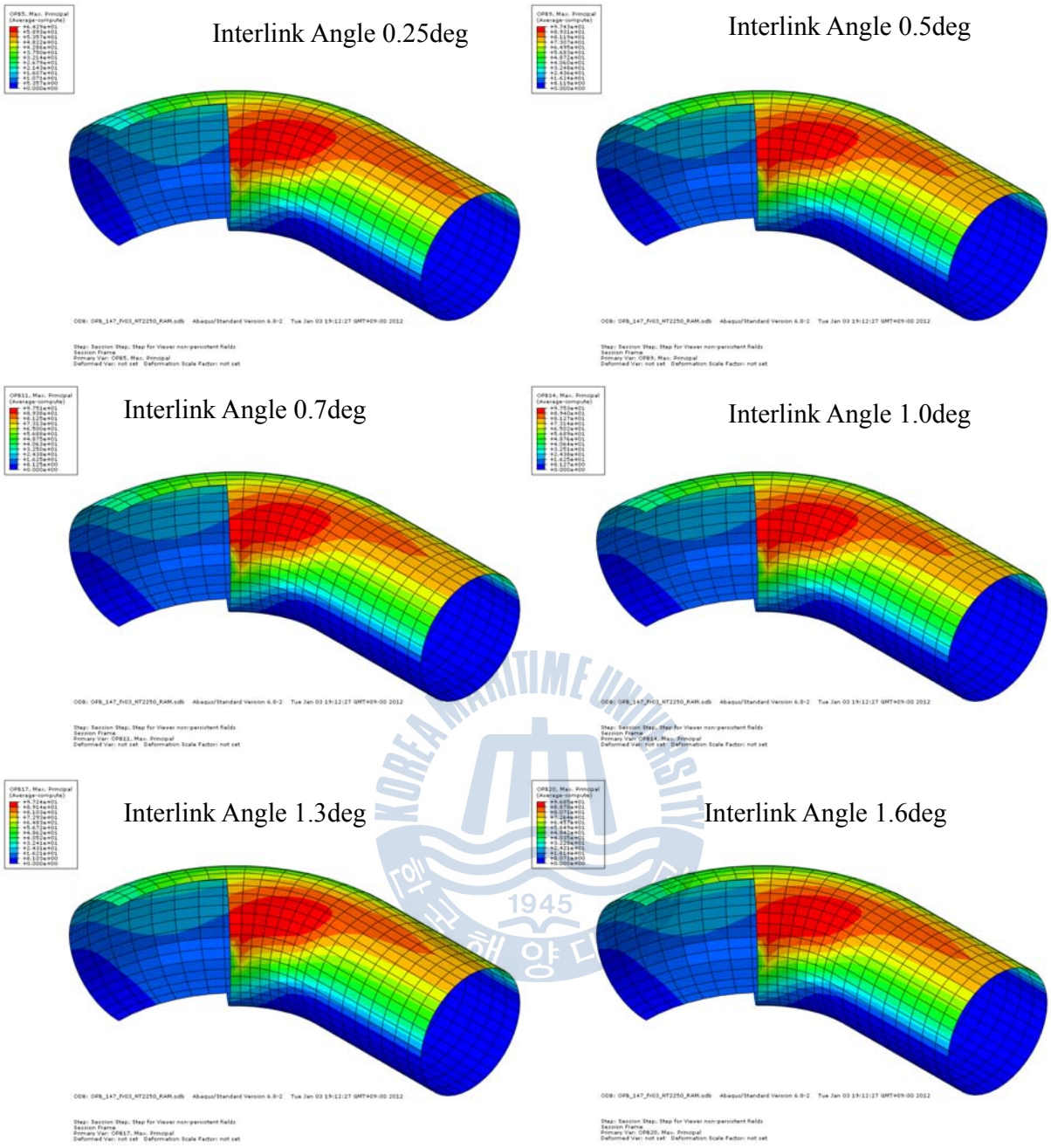

Fig.6-48 Contours of max principal stress for each interlink angle (friction 0.3)

However, excluding the friction coefficient in the analysis, the stresses due to the bending effects almost disappeared as shown in Fig.6-49.

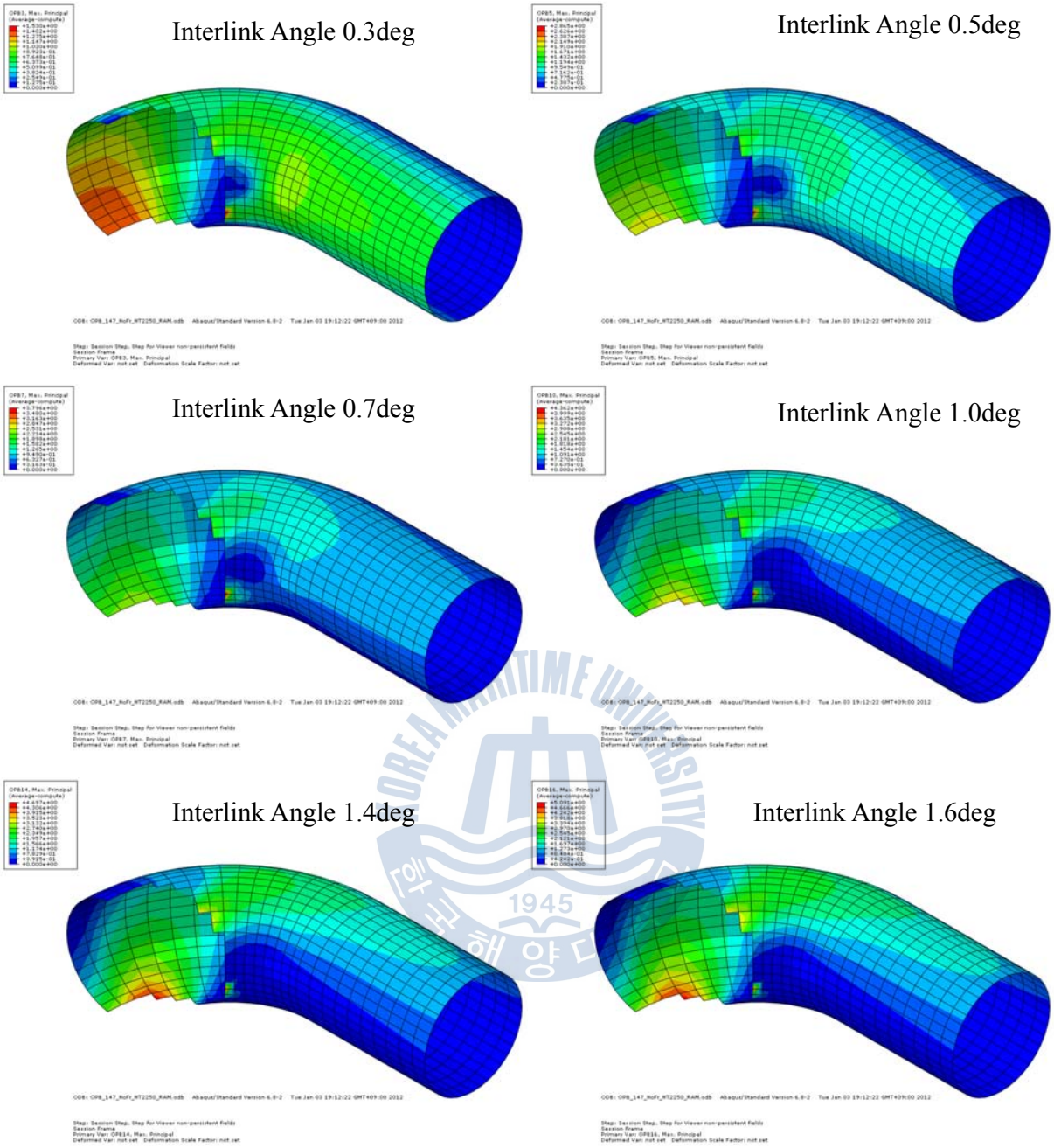

Fig.6-49 Contours of max principal stress for each interlink angle (frictionless)

Max stress concentration factors corresponding to the interlink angles calculated by the non-linear FE analysis were indicated in Fig.6-50. And, OPB moments and stresses versus interlink angles calculated were given in Fig.6-51 and Fig.6-52 respectively. From these graphs, it was well found that the friction coefficient is very important factor in calculating the fatigue assessment regarding the bending induced stress. Especially, for the frictionless situation, the chain links do not have the locking mode only but the sliding and rolling mode. Consequently, the higher

friction coefficient is taken into consideration; the higher stress due to OPB is generated. With the increase of friction coefficient, the sliding mode after locking mode of chain links was observed at the higher described angle as shown in Fig.6-53.

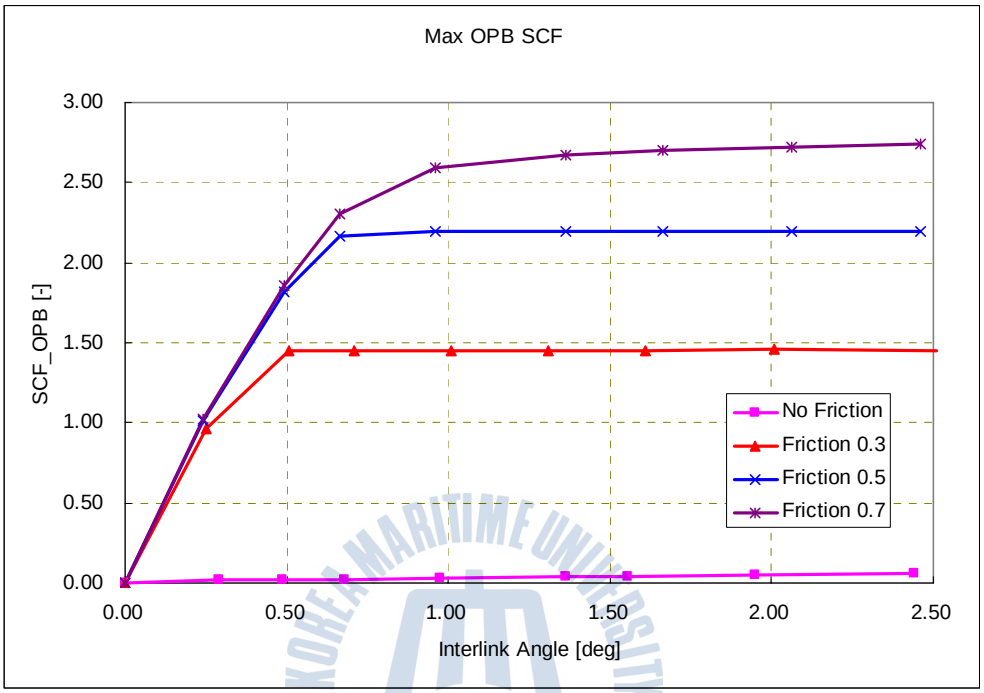

Fig.6-50 Max OPB SCFs according to interlink angles of chain

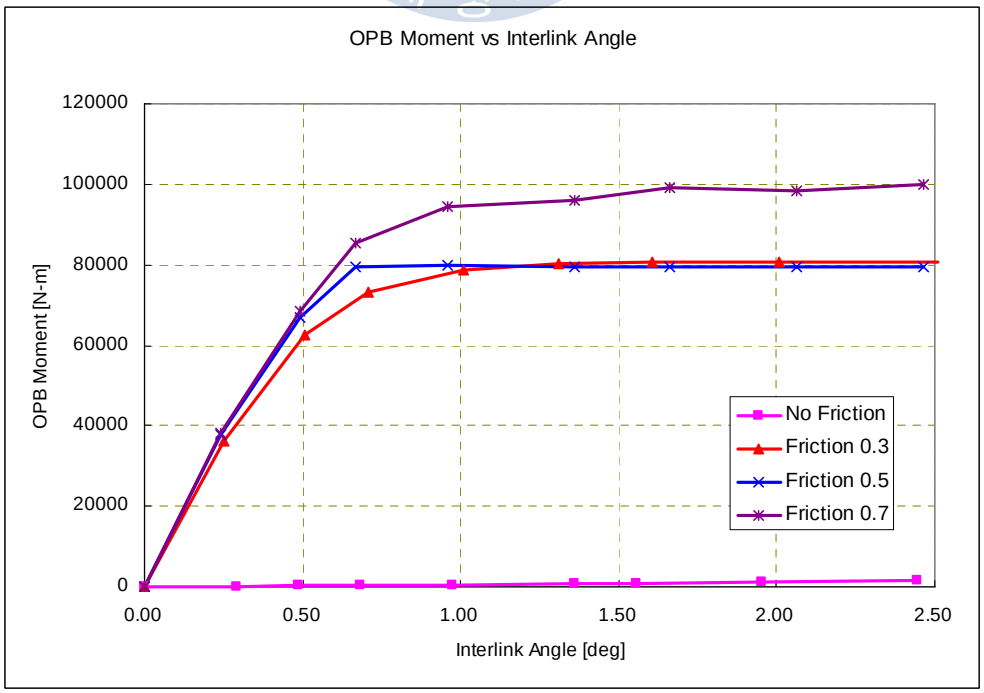

Fig.6-51 Max OPB moments according to interlink angles of chain

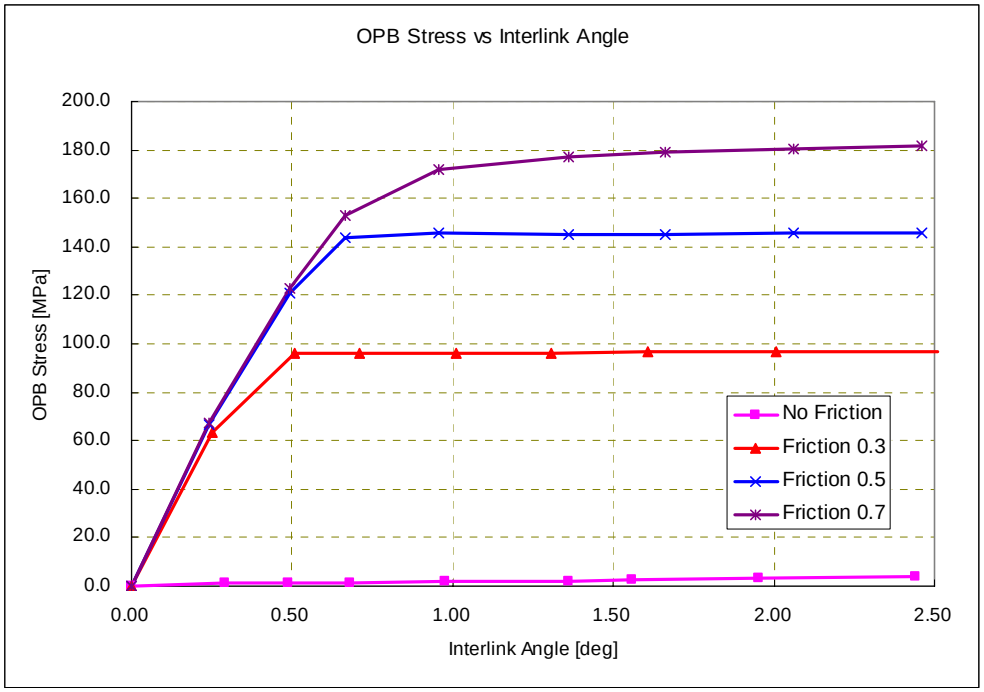

Fig.6-52 Max OPB stresses according to interlink angles of chain

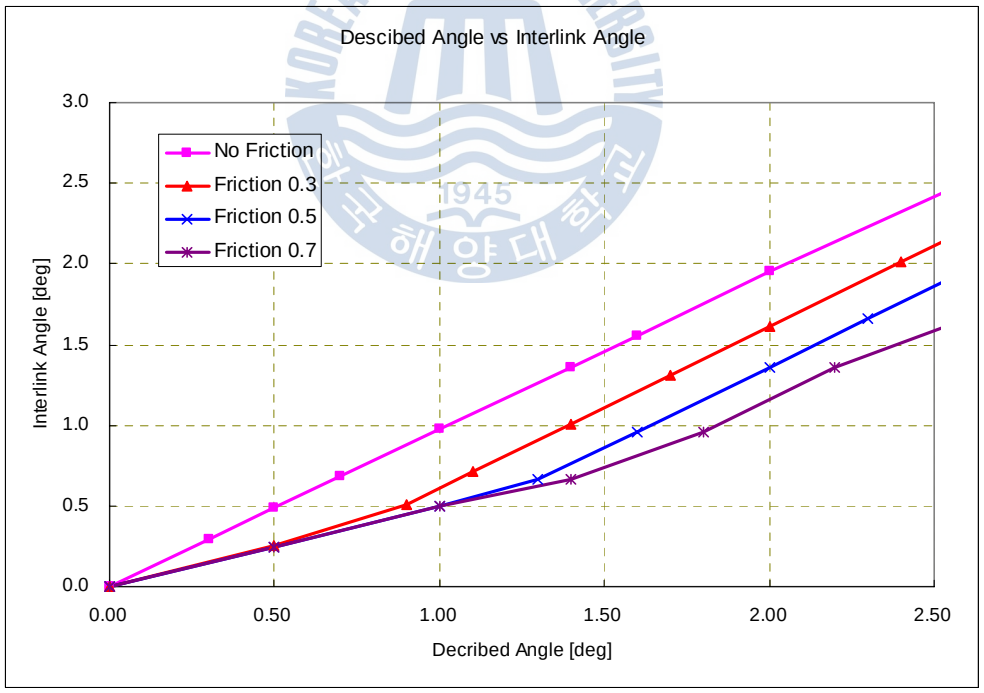

Fig.6-53 Interlink angles vs described angles according to interlink angles

7. Application to Spread-moored FPSO

7.1 Descriptions of FPSO

In this research, the FPSO for developing the eastern part of Block 17 of the offshore Angola was considered. The field has approx. 1291m water depth and sea bed conditions with a regular downward slope in south-west direction of 2%.

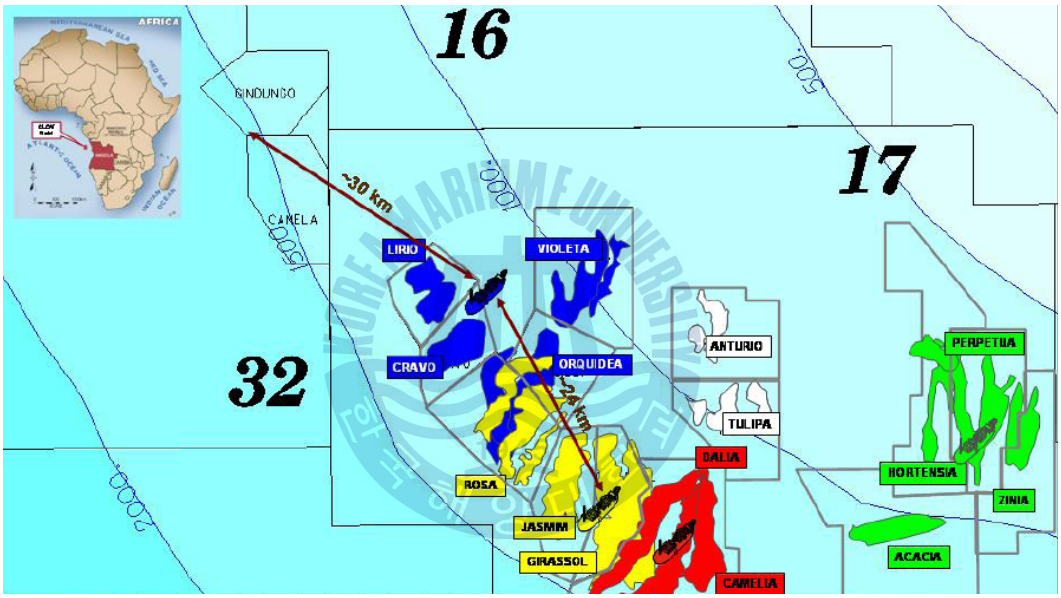

Fig.7-1 Location of Block 17 for the applied FPSO

The FPSO is station-kept by spread-mooring system along with taut configurations. The on-site heading of the FPSO was set by 22.5deg from the true North in East direction. The heading of FPSO was determined by taking into account the site environmental conditions. Long swells from South West are frequently recorded because of storms from Atlantic Ocean (ChevronTexaco, 2003; ISO, 2005a). The characteristics of the site obtained from many records on-site are followings;

- Mainly South West directional waves
- Swell governing sea states

- Multi-peaked spectral feature

The main particulars and characteristics of the FPSO are given in Table 7-1. The values were used as an example for the fatigue analysis to consider the chain OPB and IPB effects.

Table 7-1 Main particulars and characteristics of FPSO

Particulars	Value
Overall length	305m
Breadth molded	61m
Depth molded	32m
Equivalent draft	17.46m
Displacement	312,441ton
Radius of roll gyration (Kxx)	21.81m
Radius of pitch gyration (Kyy)	80.46m
Radius of yaw gyration (Kzz)	80.47m
Radius of gyration (Kxy)	45.34m
Longi. Center of Gravity from APP (LCG)	161.85m
Trans. Center of Gravity from keel (VCG)	20.59m
Natural roll period	19.5

7.2 Hydrodynamic Characteristics of FPSO

Based on the loading conditions presented in Section 7.1, the hydrodynamic analysis was performed. The added masses of FPSO considered were tabulated in Table 7-2 below. These values were obtained by calibrating the actual model test for the FPSO (Messager, 2011).

Table 7-2 Added masses of FPSO considered

Added Mass	Value
Ma_{xx} for Surge	2.64E+04ton
Ma_{yy} for Sway	2.26E+05ton
$Ma_{y\psi}$ for Sway/Yaw	1.37E+06ton-m^2
$Ma_{\psi\psi}$ for Yaw	1.2E+09ton-m

In hydrodynamic analysis of FPSO for the mooring analysis, the damping coefficient of the low frequency motions is a critical parameter, but it may be difficult to quantify (Lie, et al., 2007; Nielsen, et al., 2000; Waals, 2009; Yang, 2007). Therefore, in this research the damping coefficients were calibrated from the

results of model tests. From the calibrations, the following damping coefficients of the low frequency were determined.

- Surge motion : 2.0% of critical damping
- Sway motion : 3.1% of critical damping
- Yaw motion : 1.7% of critical damping

Note that BV (1998) recommended the damping values are 3% of critical damping for surge motion and for sway motion 5% for a spread-moored barge shaped vessel. The critical damping coefficients of a floating structure are calculated as Table 7-3 below.

Table 7-3 Calculation of critical damping coefficients

Motion	Equations	Damping Coefficient (non-dimensional)
Surge	$2\sqrt{K_{0xx}(M+m_{xx})}$	1.05E+04
Sway	$2\sqrt{K_{0yy}(M+m_{yy})}$	1.30E+4
Yaw	$2\sqrt{K_{0\varphi\varphi}(I_{zz}+I_{\varphi\varphi}+(M+m_{yy})X_G^2)}$	1.76E+08

where, M = Mass of FPSO

m_{ii} = Diagonal terms of the asymptotic added mass

$K_{o,ii}$ = Diagonal terms of the mooring stiffness

I_{zz} = Moment of inertia in yaw calculated at the center of gravity

$I_{\psi\psi}$ = Moment of inertia in yaw due to added mass

X_G = Distance of COG from FPSO coordinate system

The response amplitude operator (RAO) of 6 DOF motions and the quadratic transfer function (QTF) of low frequency wave loading in regular waves, e.g. surge, sway and yaw were calculated by WADAM, conventional software of DNV. From Fig.7-2 to Fig.7-7, the RAOs for 6 DOF motions of the FPSO are presented.

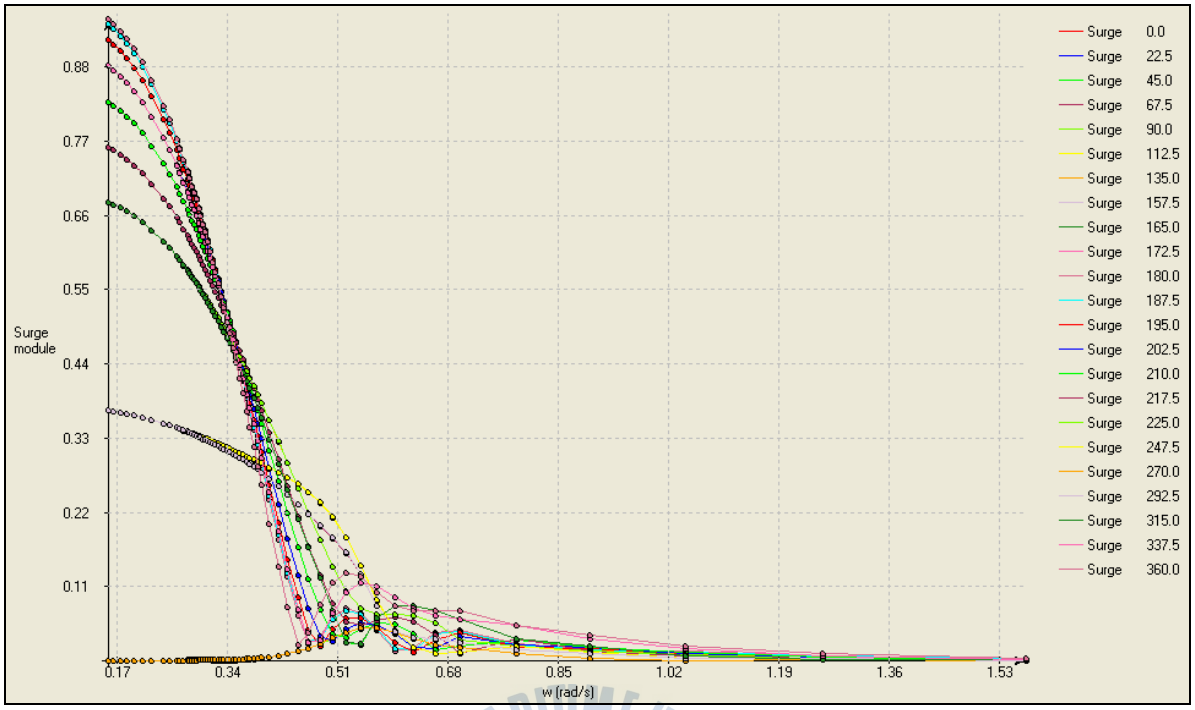

Fig.7-2 Surge RAO of FPSO for each wave heading

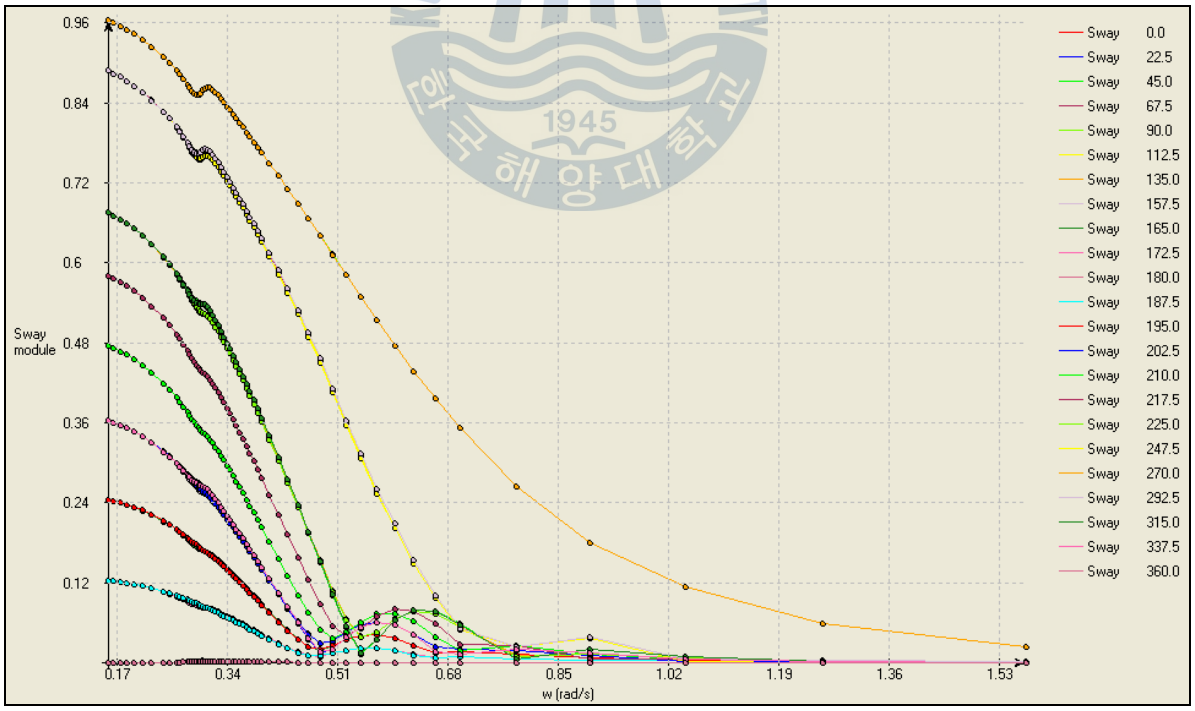

Fig.7-3 Sway RAO of FPSO for each wave heading

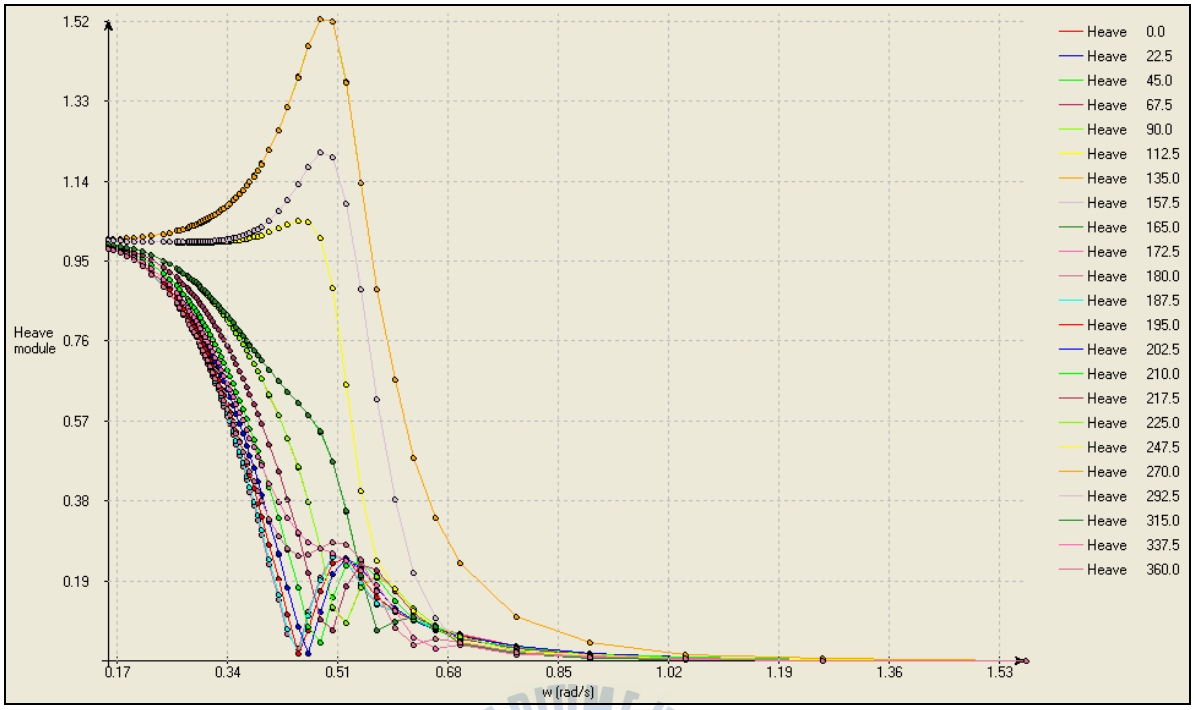

Fig.7-4 Heave RAO of FPSO for each wave heading

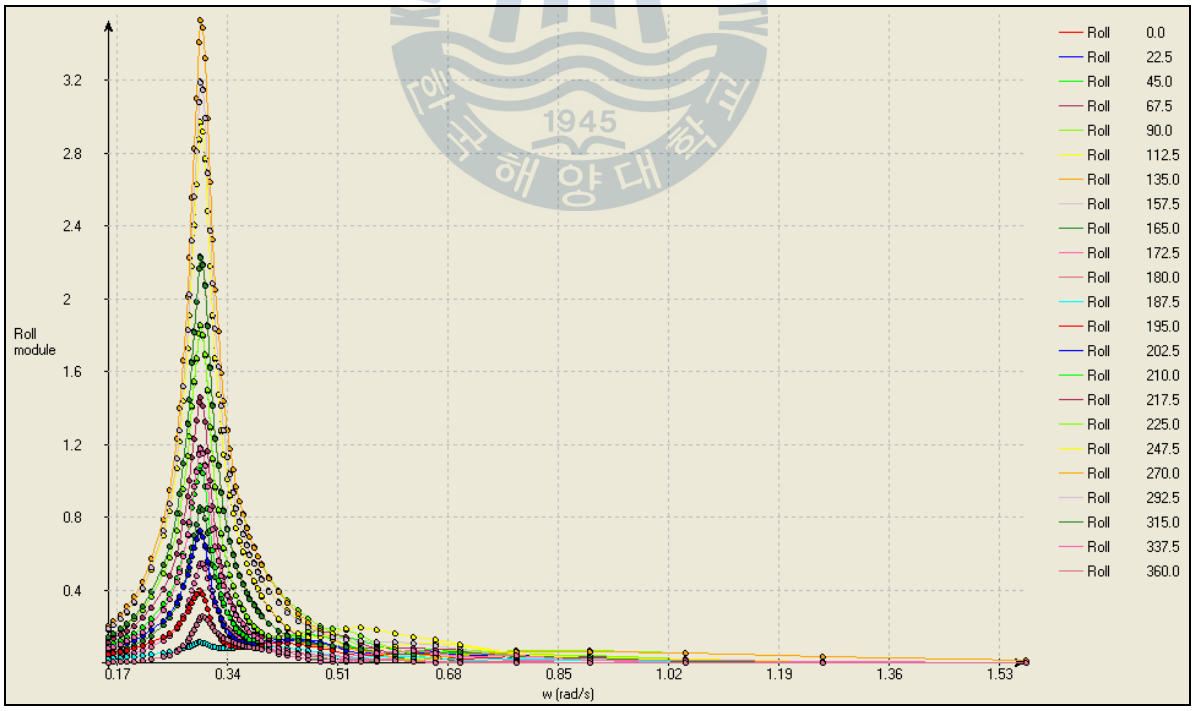

Fig.7-5 Roll RAO of FPSO for each wave heading

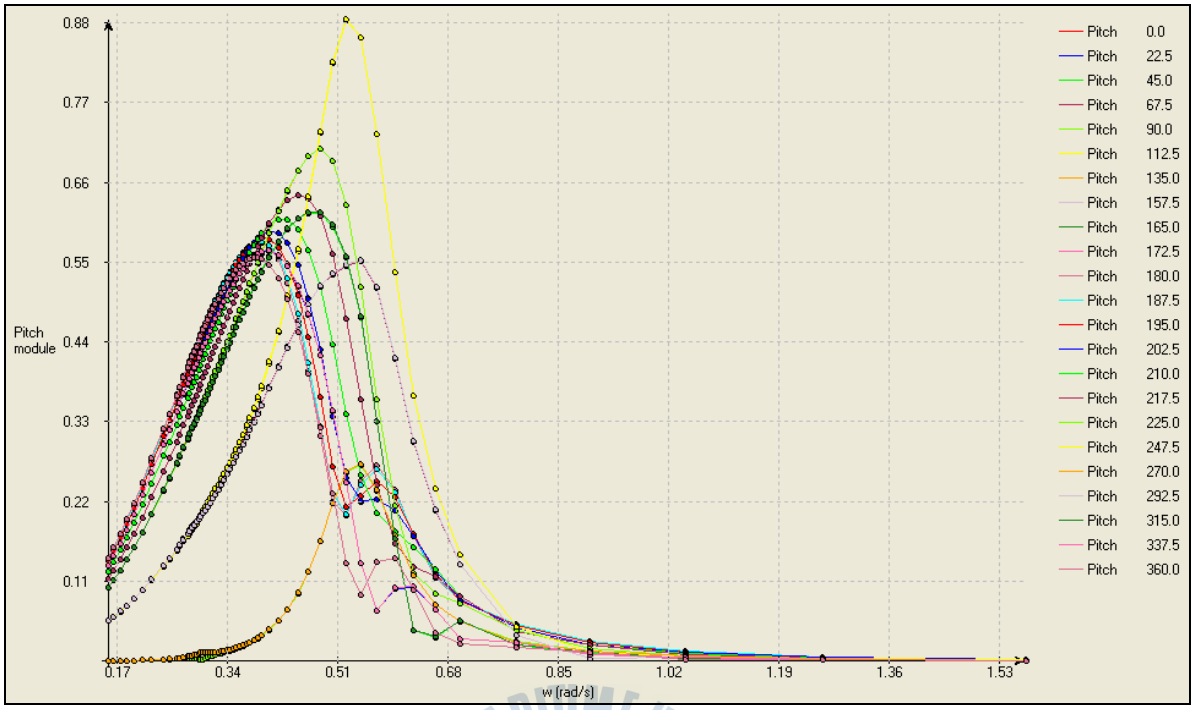

Fig.7-6 Pitch RAO of FPSO for each wave heading

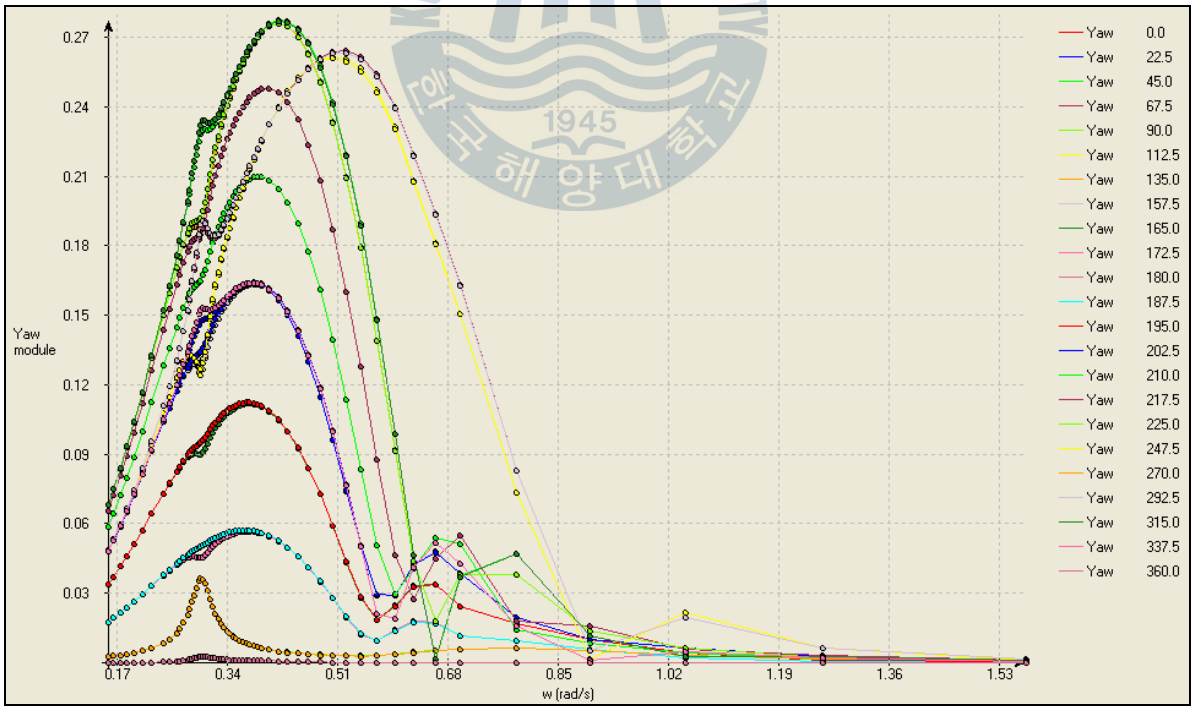

Fig.7-7 Yaw RAO of FPSO for each wave heading

The plots of the 2nd order mean wave loads QTF are presented in Fig.7-8 to Fig.7-10 below.

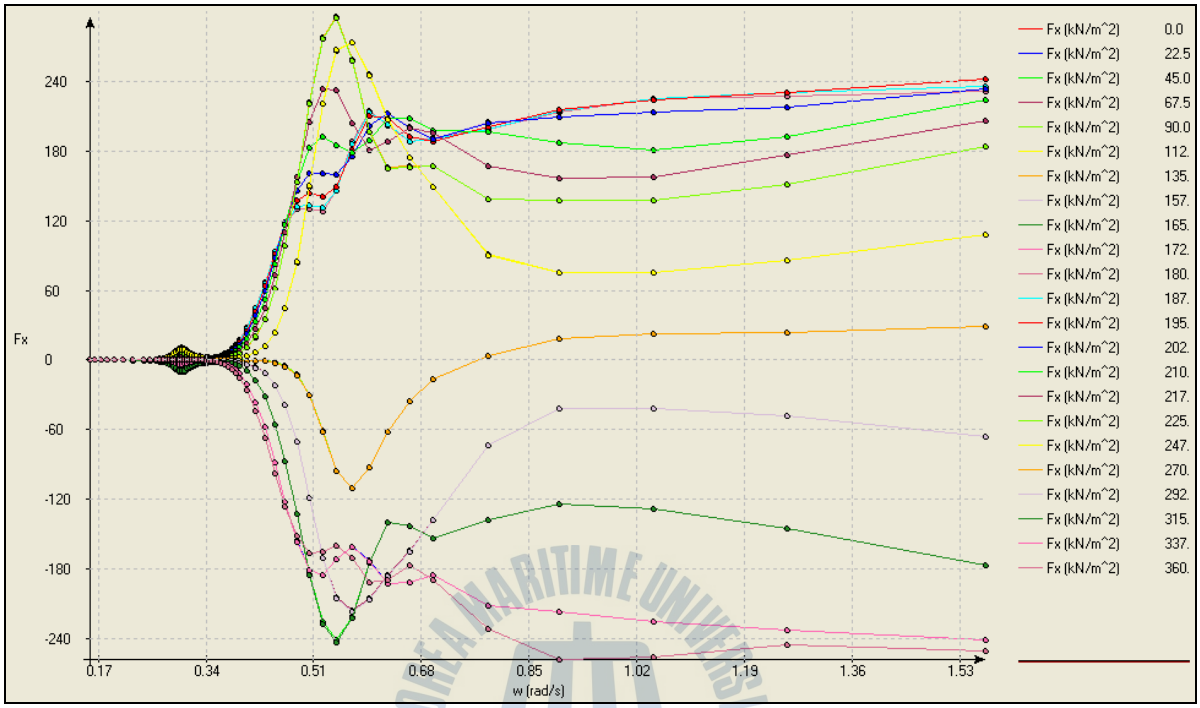

Fig.7-8 QTF of low frequency wave loading in longitudinal direction (Fx) of FPSO

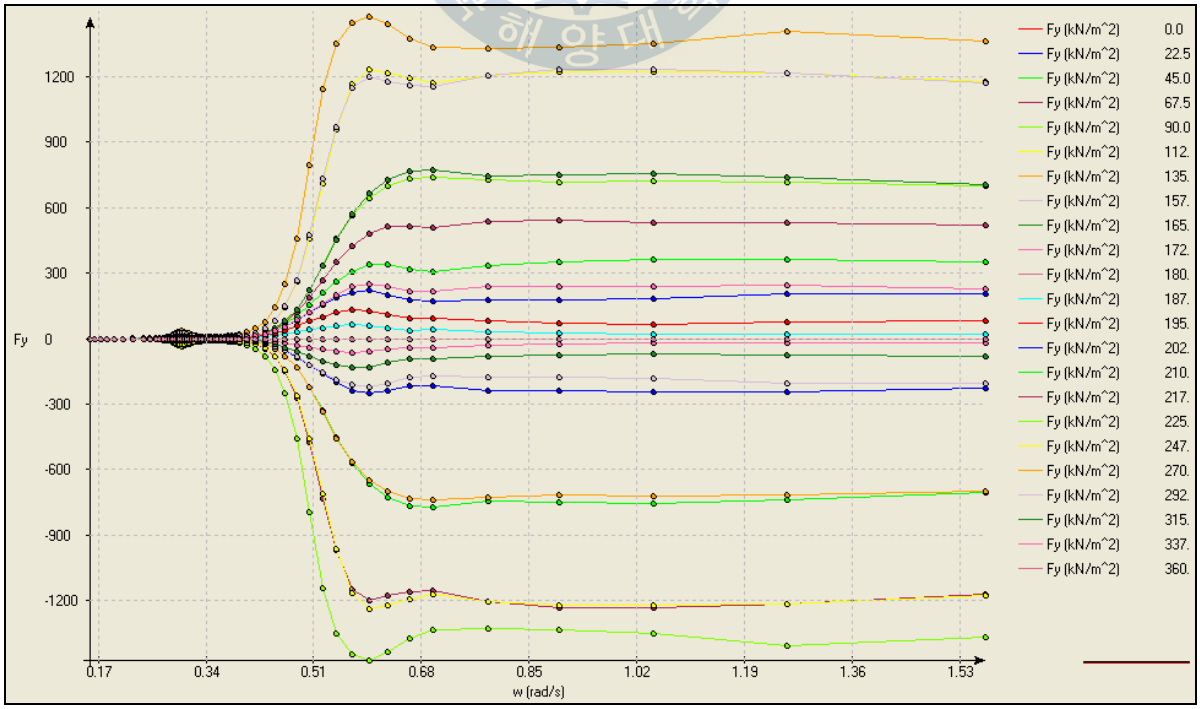

Fig.7-9 QTF of low frequency wave loading in transversal direction (Fy) of FPSO

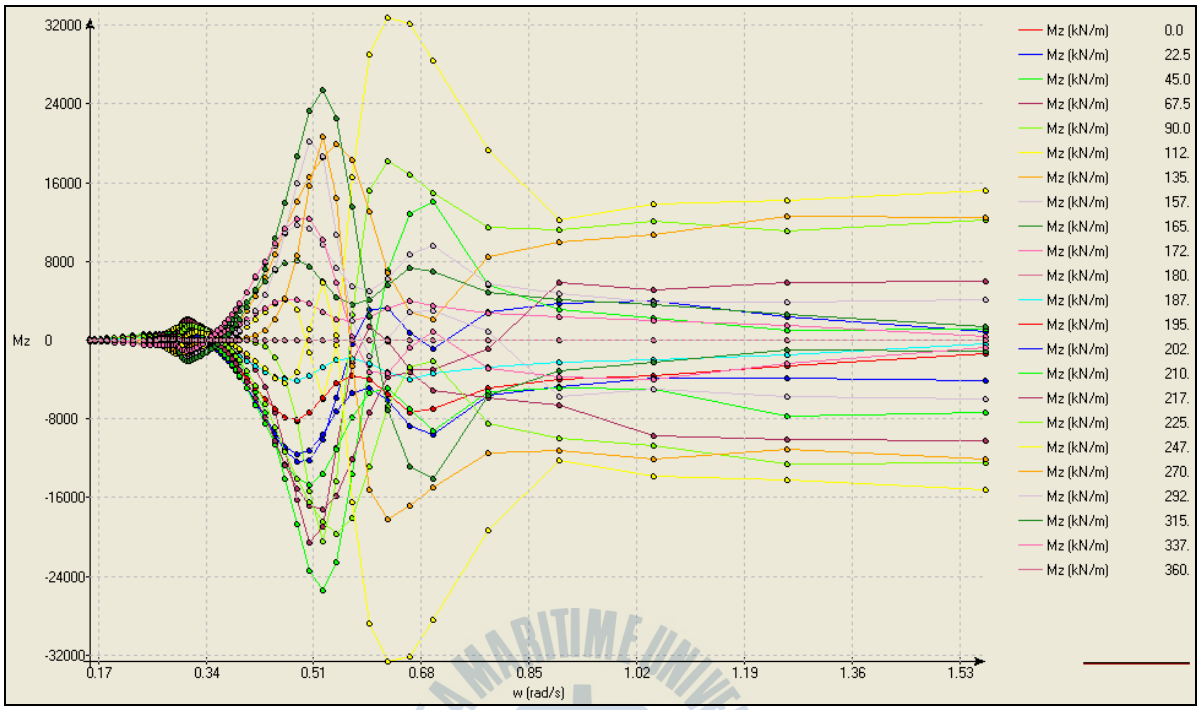

Fig.7-10 QTF of low frequency wave loading for moment in vertical axis (Mz) of FPSO

7.3 Mooring Arrangement

The heading of the FPSO is 22.5deg from the True North in East direction as shown in Fig.7-11. The FPSO is installed by the spread mooring system and there are 16 mooring lines around FPSO. The 4 mooring lines were composed as a cluster; i.e. 4 x 4 lines. The mooring lines are arranged with 1600m pattern radius.

The location of the FPSO was modeled with water depth of 1291m and the bottom slop of sea bed, 2% in South-West direction. Fig.7-12 illustrates the simulating model for mooring analysis for the FPSO in ARIANE7.

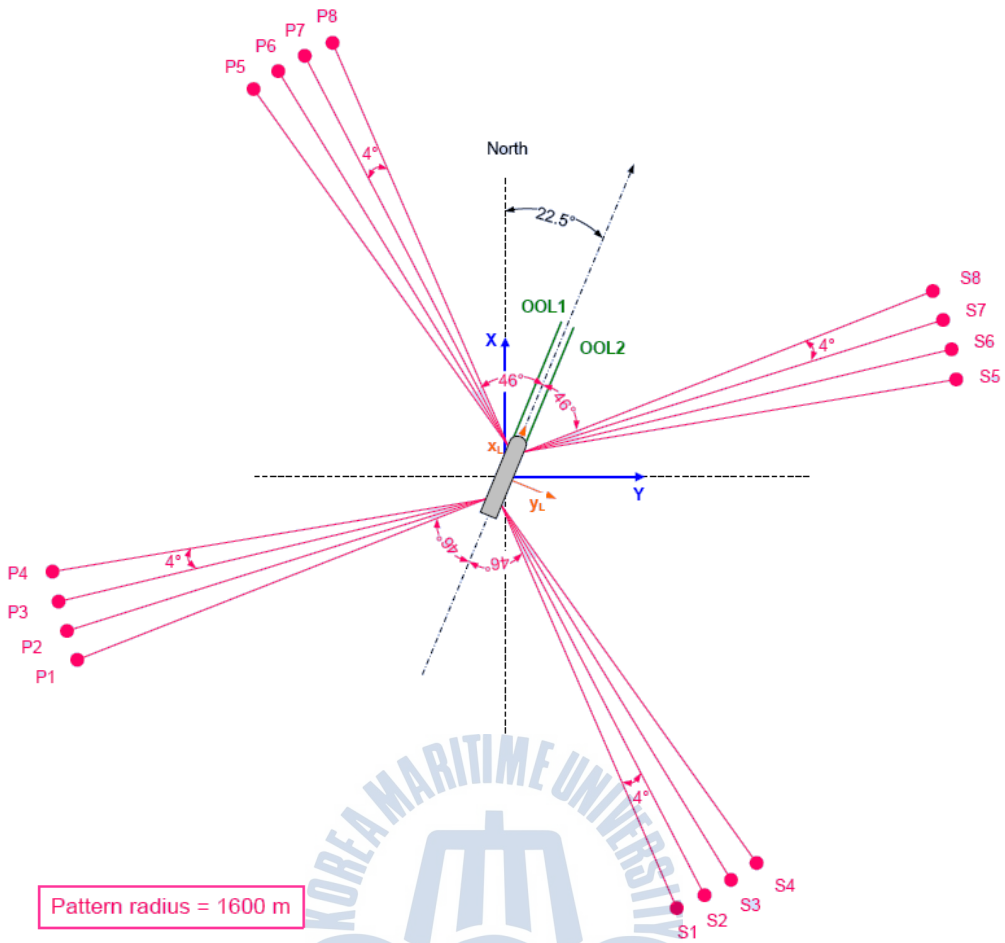

Fig.7-11 Arrangement of mooring lines of FPSO

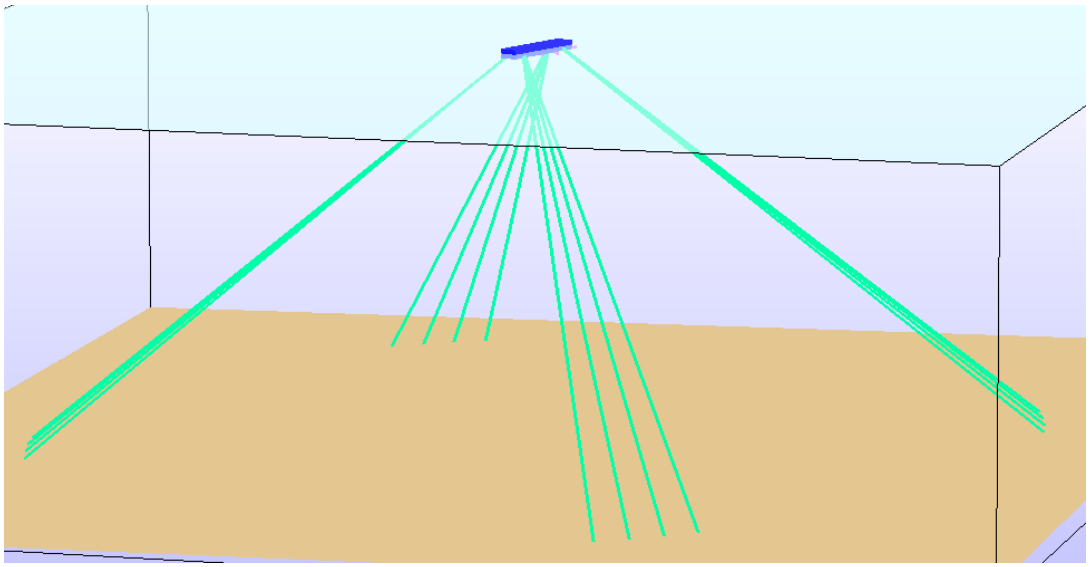

Fig.7-12 Model for mooring analysis with mooring arrangements from ARIANE7

The local FPSO coordinate system presented in Fig.7-13 was basically used to define most of coordinates. The coordinates of the fairleads connected with top-chains of mooring lines were defined in Table 7-4.

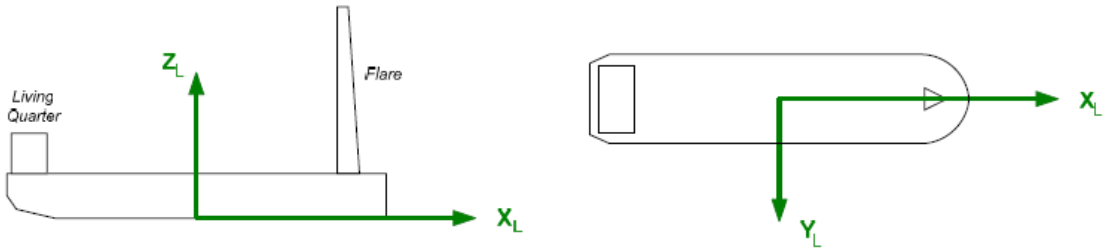

Fig.7-13 Local coordinate system of FPSO

Table 7-4 Coordinates of fairlead locations of FPSO

Mooring Line	X-Coord [m]	Y-Coord [m]	Z-Coord [m]
S8	107.05	31.26	7.76
S7	104.33	31.26	7.76
S6	101.45	31.26	7.76
S5	98.64	31.26	7.76
S4	-103.74	31.26	7.76
S3	-106.51	31.26	7.76
S2	-109.22	31.26	7.76
S1	-111.88	31.26	7.76
P1	-111.88	-31.26	7.76
P2	-109.22	-31.26	7.76
P3	-106.51	-31.26	7.76
P4	-103.74	-31.26	7.76
P5	98.64	-31.26	7.76
P6	101.45	-31.26	7.76
P7	104.33	-31.26	7.76
P8	107.05	-31.26	7.76

where, the coordinates of Y_L and Z_L were determined referring to the following Fig.7-14. And, the chain stoppers of the fairlead were selected with a pivot typed stopper supplied by Bardex.

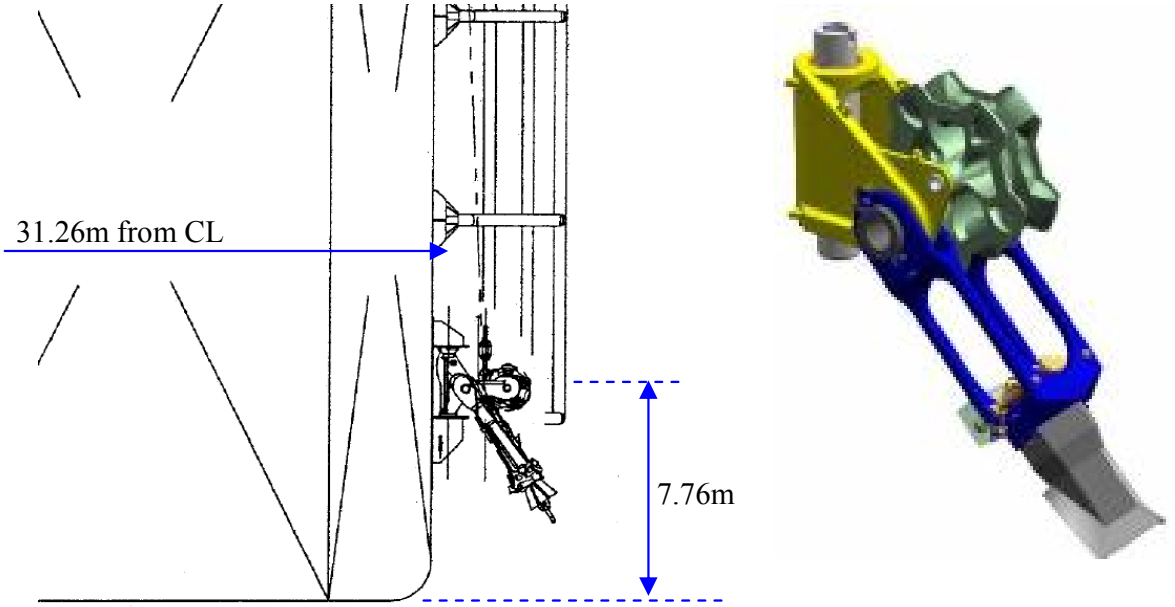

Fig.7-14 Coordinates of fairlead location and used pivot typed chain stopper

The mooring lines of the FPSO are made up of three components; top chain, wire and bottom chain. The top chains are connected at the fairleads of FPSO with chain stopper and while, the bottom chains are linked to the suction anchor on sea bed. Fig.7-15 gives brief configuration of the mooring line.

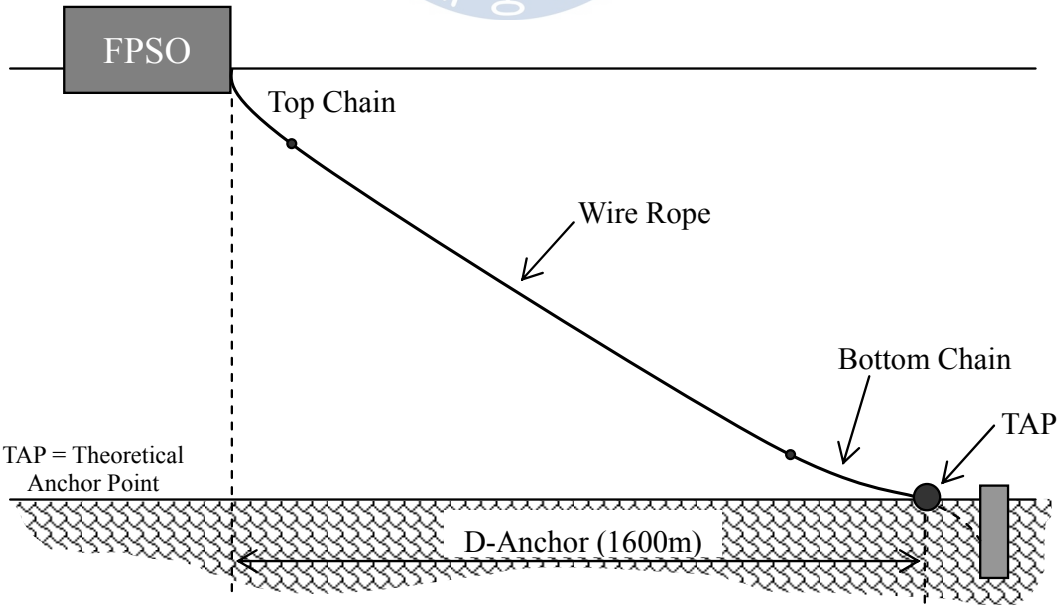

Fig.7-15 Components of mooring lines of the FPSO

In the analysis, the buried parts of bottom chains to suction anchoring point were not considered.

7.4 Characteristics of Mooring Lines

The mooring lines under consideration are composed of three components; top chain, wire rope and bottom chain. Their characteristics applied are presented in Table 7-5.

Table 7-5 Characteristics of mooring lines applied

Component	Characteristics	Value
Top Chain	Type	OD147 R3 Studless
	Length	27~62m
	MBL	15536kN
	Weight in air	437kg/m
	Weight in water	380kg/m
Wire Rope	Type	OD105.5 Spiral Strand
	Length	1850m
	MBL	12071kN
	Weight in air	58.16kg/m
	Weight in water	46.29kg/m
Bottom Chain	Type	OD132 R3 Studless
	Length	190m
	MBL	12993kN
	Weight in air	352kg/m
	Weight in water	306kg/m

And, the hydrodynamic characteristics considered for mooring lines are presented in Table 7-6 below.

Table 7-6 Hydrodynamic characteristics of mooring lines applied

Component	Characteristics	Value
Top Chain	Normal drag coef.	0.8
	Tangential drag coef.	0.0
	Normal inertia coef.	1.0
	Tangential added mass coef.	0.5
Wire Rope	Normal drag coef.	0.7
	Tangential drag coef.	0.0
	Normal inertia coef.	1.0
	Tangential added mass coef.	0.0
Bottom Chain	Normal drag coef.	0.8
	Tangential drag coef.	0.0
	Normal inertia coef.	1.0
	Tangential added mass coef.	0.5

7.5 Loads from Subsea Facilities

FPSO has a lot of lines from SURF (Subsea Umbilical, Riser and Flowlines) and OOL (Oil Offloading Line), which is necessary to consider the mooring analysis. In this research, they were taken into account by applying the thrust loads in ARIANE7, a quasi-dynamic analysis program, as given in Fig.7-16 according to their design configurations.

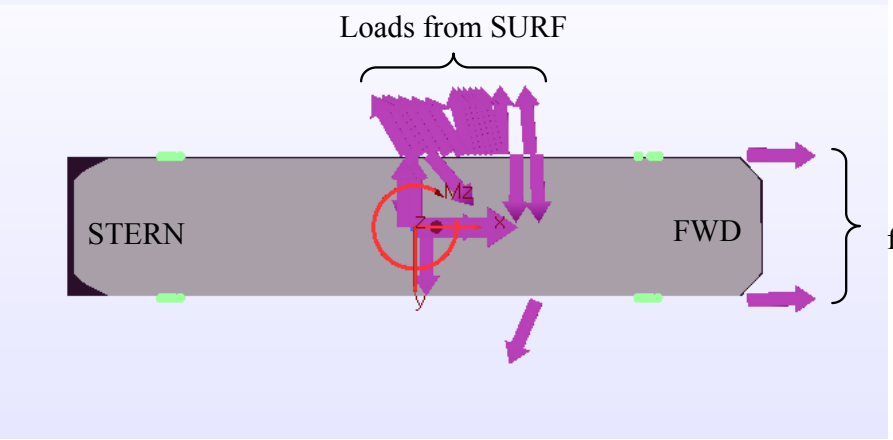

Fig.7-16 Application of loads from SURF and OOL in ARIANE7

The global static loads of SURF and OOL on the FPSO were divided into two phases; initial development and future development, but in this analysis both phases were all taken into consideration.

Table 7-7 Global loads on FPSO due to the loads from SURF and OOL

Load Component	Phase I Initial Development	Phase II Future Development
Fx [kN]	203	244
Fy [kN]	-296	-115
Mz [kN-m]	-7096	2828

7.6 Pretension Adjustment

Based on the mooring configurations described above, the static equilibrium analysis was performed to find out the equilibrium position of the FPSO and tensions of all the mooring lines. The analysis was carried out by ARIANE7. From the analysis, the static equilibrium position of the FPSO was calculated as Table 7-8 and, in Table 7-9 all the output from the static analysis were summarized for the mooring lines.

Table 7-8 Equilibrium position of the FPSO from static analysis

	East Position	North Position	Azimuth
FPSO global position	0.36m	0.37m	22.32deg

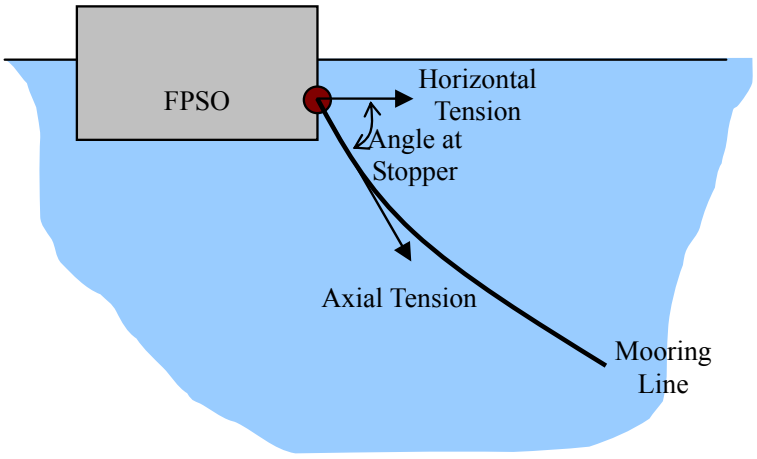

Fig.7-17 Illustration of tensions and angle at stopper for mooring lines

Table 7-9 Summary of mooring lines calculated from static analysis

Line	Paidout Length [m]	At Stopper of Fairlead			At TAP of Anchor	
		Th[kN]	T[kN]	Angle[deg]	Th[kN]	T[kN]
P1	2100	1254.98	2201.41	55.24	1254.98	1258.56
P2	2100	1243.07	2186.25	55.35	1243.07	1245.85
P3	2100	1229.52	2169.03	55.47	1229.52	1231.70
P4	2100	1214.42	2149.89	55.61	1214.42	1215.92
P5	2084	1122.07	1971.69	55.31	1122.07	1081.57
P6	2084	1101.68	1945.93	55.52	1101.68	1051.20
P7	2083.5	1090.84	1930.35	55.59	1090.84	1035.18
P8	2083.5	1073.65	1908.55	55.77	1073.65	1007.68
S1	2086.5	1285.37	2188.91	54.04	1285.37	1289.93
S2	2085	1287.57	2186.00	53.91	1287.57	1292.15
S3	2083.5	1289.28	2182.45	53.79	1289.28	1293.85
S4	2081.5	1300.06	2188.57	53.56	1300.06	1305.20
S5	2066.3	1188.84	1989.29	53.30	1188.84	1179.60
S6	2066.3	1177.65	1975.05	53.4.	1177.65	1163.85
S7	2066.3	1167.61	1962.30	53.49	1167.61	1149.67
S8	2066.3	1158.76	1951.08	53.57	1158.76	1137.12

7.7 Operational Sea States

The long term environment of the FPSO is characterized by main swell, secondary swell and local wind wave. For this research, the 84 sea states were considered, which is given in Appendix A. And, Ochi-Hubble wave spectrum for the mooring analysis was taken into account (Chakrabarti, 1994).

$$S(f) = \frac{1}{4}\sum_{1}^{3} \frac{\left(\frac{4\lambda_j + 1}{4} f_{pj}^4\right)^{\lambda_j}}{\Gamma(\lambda_j)} \frac{Hs^2}{f^{4\lambda_j + 1}} exp\left(-\frac{4\lambda_j + 1}{4}\left(\frac{f}{f_{p_j}}\right)^{-4}\right) \tag{7-1}$$

where, $S(f)$ = Spectral density of wave elevation (m^2/Hz)

λ_j = Peakness parameter of each wave component (j = 1; main swell, 2; secondary swell, 3; local wind wave), which can be obtain as below;

$$\lambda_j(T_{pj}) = 0.00205T_{pj}^3 - 0.0029T_{pj}^2 + 0.12665T_{pj} + 0.22932$$

Hs_j = Significant wave height of each wave component

f_{pj} = Peak frequency of each wave component

Wind spectrum is also necessary to perform the dynamic mooring analysis. In this research, Kaimal wind spectrum which is applicable to both low and high frequency spectrum (Jang, et al., 1998) was considered. The scatter diagram of the directional wind speed is presented in Appendix B.

$$\frac{f\,S_v(f)}{\sigma_{v(z)}^2} = \frac{A\,x}{(1+B\,x)^{\frac{5}{3}}} \tag{7-2}$$

where, $S_v(f)$ = Spectral density of wind speed fluctuations at elevation z (m^2/Hz)

$\sigma_{v(z)}$ = Standard deviation of fluctuating wind velocity

x = Non-dimensional frequency ($= \frac{f\,z}{V_{1hr}(z)}$)

A = 12 based on on-site records

B = 33 based on on-site records

z = Elevation from sea level

Current data was also derived from the site specific measurements. In Appendix C, the scatter diagram of the current speed is given.

7.8 Wind and Current Loads on FPSO

In the mooring analysis, the wind coefficients to calculate the wind loads were determined by calibrating the wind tunnel tests of the FPSO. Based on the wind screen area, the wind coefficients of the FPSO for the unitary wind velocity were calculated. Likewise, the current screen areas were determined in same way. In Table 7-10, the screen areas for wind and current were presented.

Table 7-10 Wind and current screen area of FPSO

	Wind Screen Area	Current Screen Area
Frontal Wind Direction	4175m^2	1148m^2
Transversal Wind Direction	14911m^2	5148m^2

The screen areas for wind and current are calculated based on contour of overall FPSO arrangement. In wind screen area, the areas above FPSO draft are included and, the areas below the draft are included in current screen area.

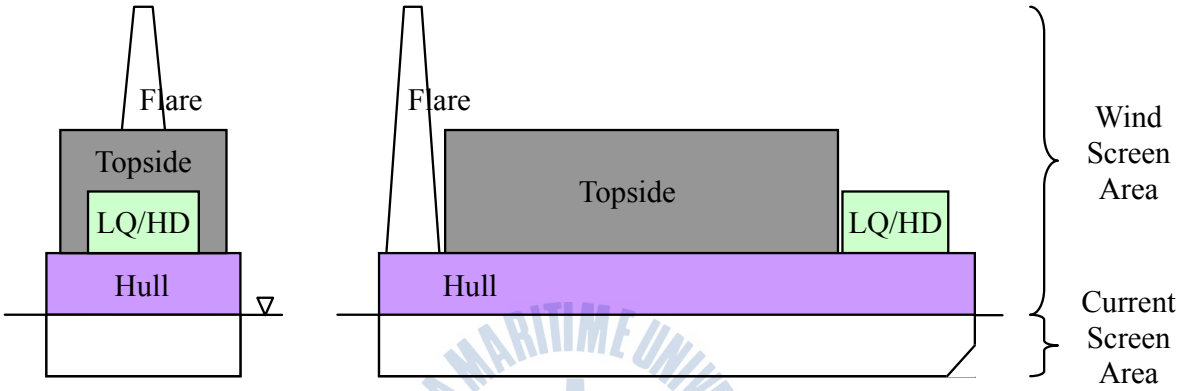

Fig.7-18 Wind and current screen areas of FPSO

The steady state force due to wind or current acting on the FPSO can be calculated using following equations; (7-3), (7-4) and (7-5), which are in general based on Morrison equation.

$$F_X = \frac{1}{2}\rho C_X A_X V^2 \tag{7-3}$$

$$F_Y = \frac{1}{2}\rho C_Y A_Y V^2 \tag{7-4}$$

$$M_Z = \frac{1}{2}\rho C_Z A_Y L_{pp} V^2 \tag{7-5}$$

where, F_X = Longitudinal force due to wind or current

F_Y = Transversal force due to wind or current

M_Z = Moment due to wind or current

ρ = Air density for wind force, and water density for current force

L_{pp} = Length of FPSO

C_X = Drag coefficient for longitudinal direction

C_Y = Drag coefficient for transversal direction

C_Z = Drag coefficient for moment

A_X, A_Y = Screen areas for wind or current in longi. and trans. direction

V = Wind velocity at 10m above sea level or equivalent current velocity

In Eqs.(7-3), (7-4) and (7-5) described above, the equivalent current velocity, as denoted in Eq.(7-6), for calculating current forces on the FPSO can be derived as below, in which $V_c(z)$ is a current velocity at each depth;

$$V_{eq} = \frac{1}{draft}\sqrt{\int_0^{draft} V_c(z)^2\, dz} \tag{7-6}$$

Through the model tests, the coefficients were determined (Messager, 2011). Fig.7-19 presents the coefficients for wind drag forces. And, the coefficients for current drag forces are given in Fig.7-20.

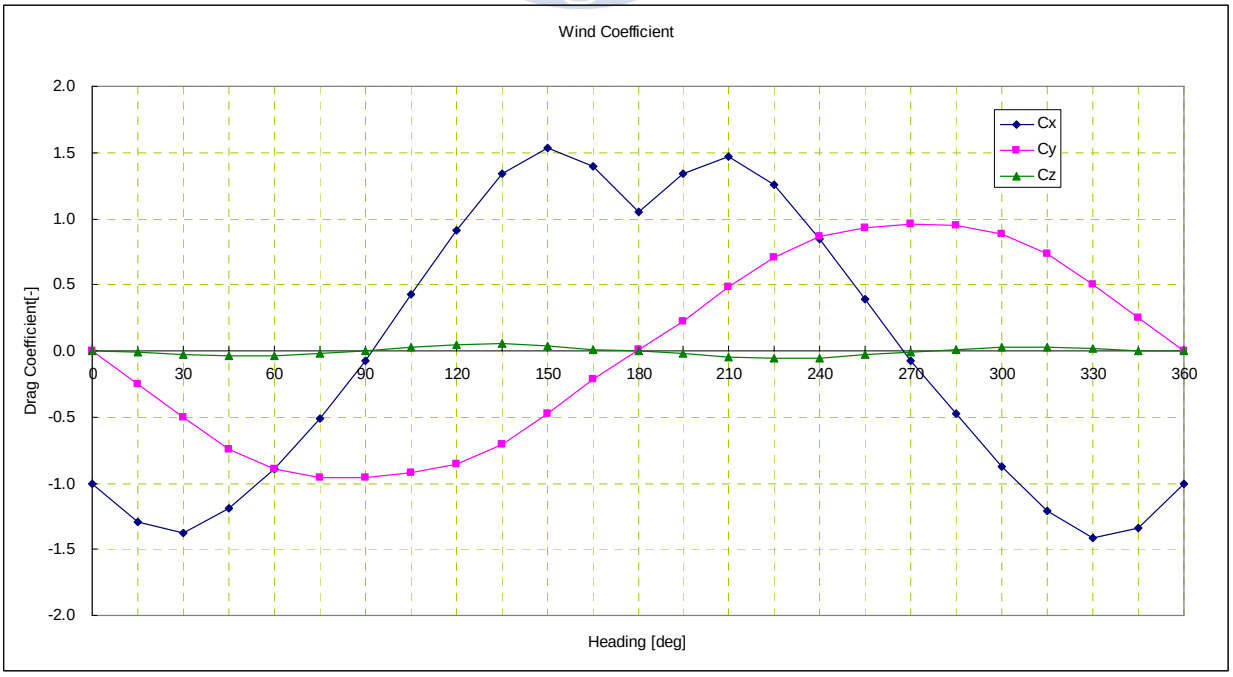

Fig.7-19 Wind drag coefficient of the FPSO

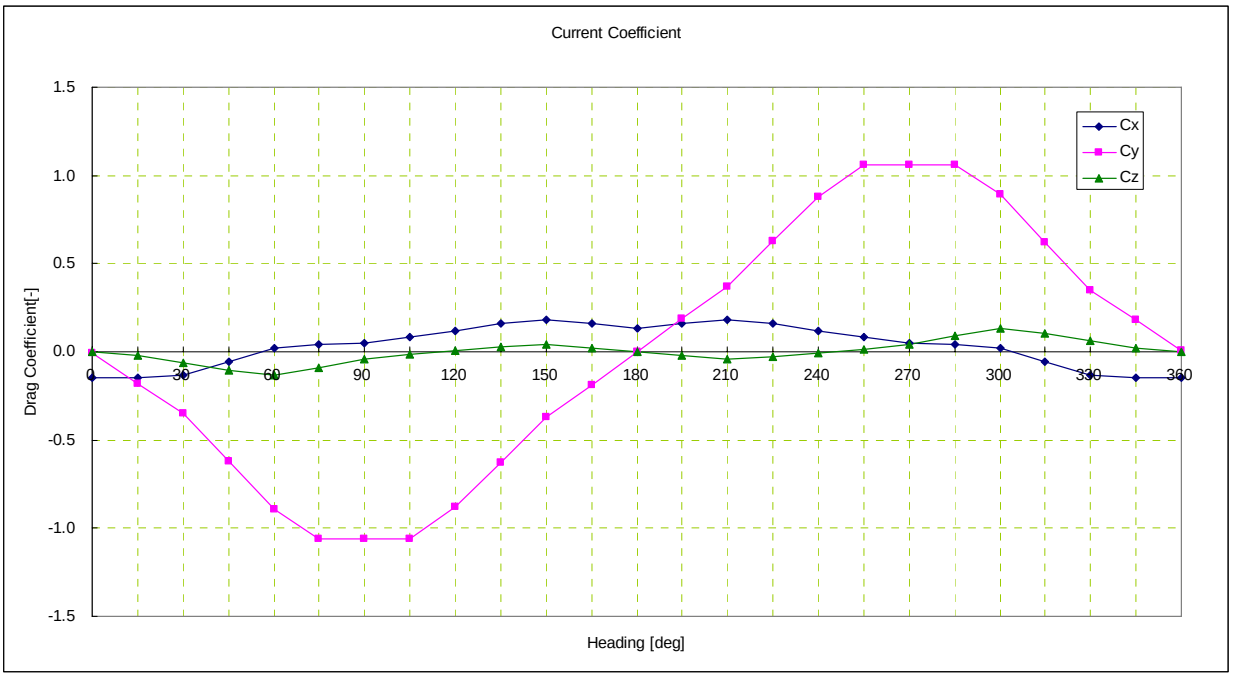

Fig.7-20 Current drag coefficient of the FPSO

7.9 Procedure of Chain Fatigue considering Bending Effects

The procedure for OPB fatigue of the top chain of the FPSO is proposed herein. As mentioned above, the quasi-dynamic analysis is much simpler approach than the fully dynamic analysis. In particular, since there are so many sea states to calculate fatigue damage, the quasi-dynamic analysis gives very advantageous solutions in this regard. Besides, using the quasi-dynamic approach for the mooring analysis, the motions of the FPSO considering the mooring legs' stiffness can be easily obtained. Thus, in this research the motions of the FPSO were calculated through the quasi-dynamic analysis by ARIANE7.

In general, the short term response is calculated based on 3 hours duration. However, to reduce the time consumption in the fatigue assessment, 30min duration was applied, which may be no influence on the exact results.

The overall methodology for the fatigue assessment of chain links of the spread-moored FPSO operating in deep water is presented in Fig.7-21.

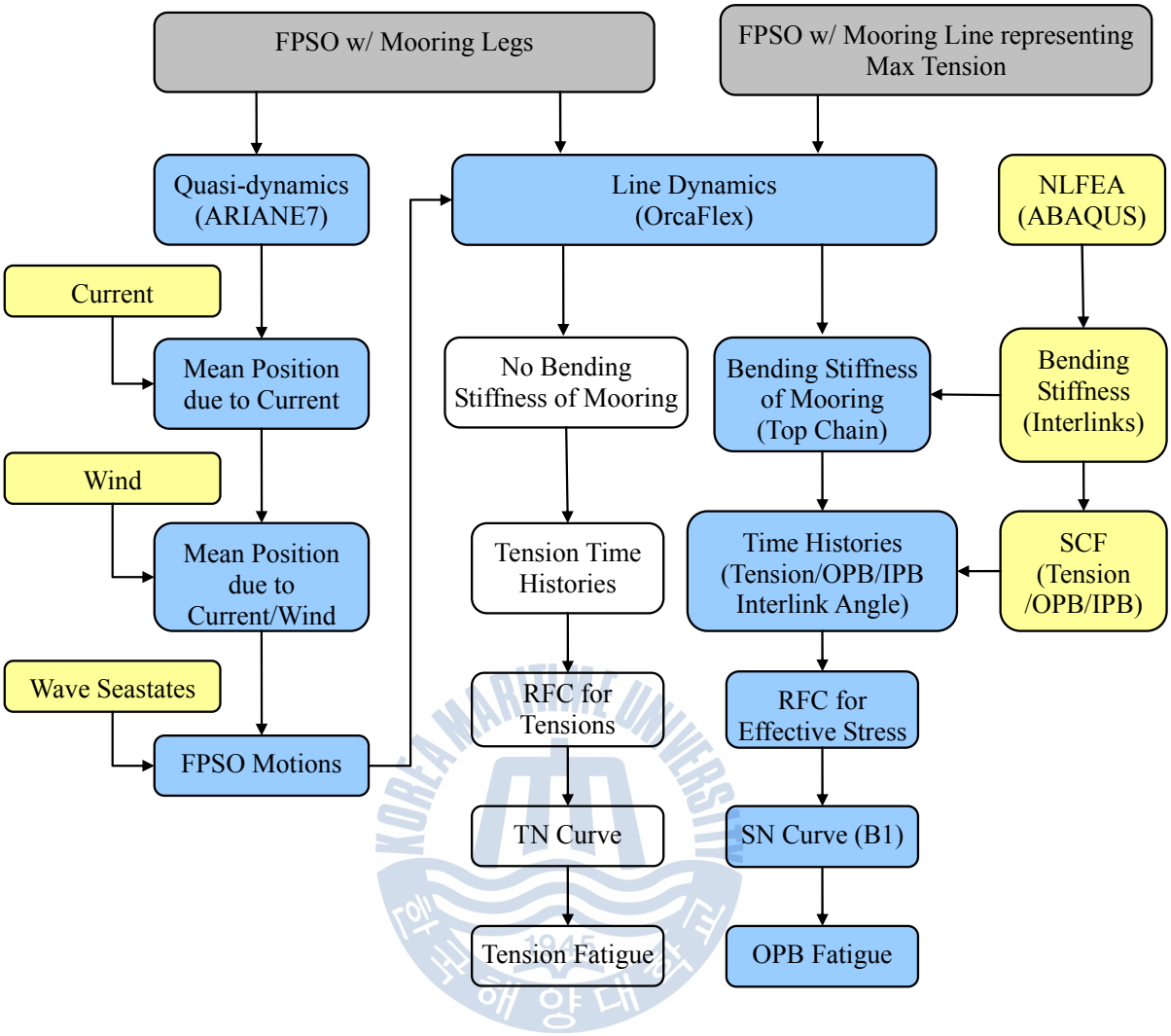

Fig.7-21 Procedure proposed for fatigue assessment of chain links including OPB

7.9.1 Mean Position

The mean positions due to current or wind sea states were calculated as per the following Eq.(7-7):

$$d_m = \frac{\sum_{i=1}^{seastates} R_i n_i}{N} \tag{7-7}$$

where, d_m = Mean position due to current or wind sea states

R_i = Position due to current or wind sea state i

n_i = Occurrence of current or wind sea state i

N = Total occurrence number ($= \sum n_i$)

Fig.7-22 presents the positions of the FPSO for all the current sea states and the mean position from the sea states. And, the positions of the FPSO from the current and wind sea states and the mean position are given in Fig.7-23.

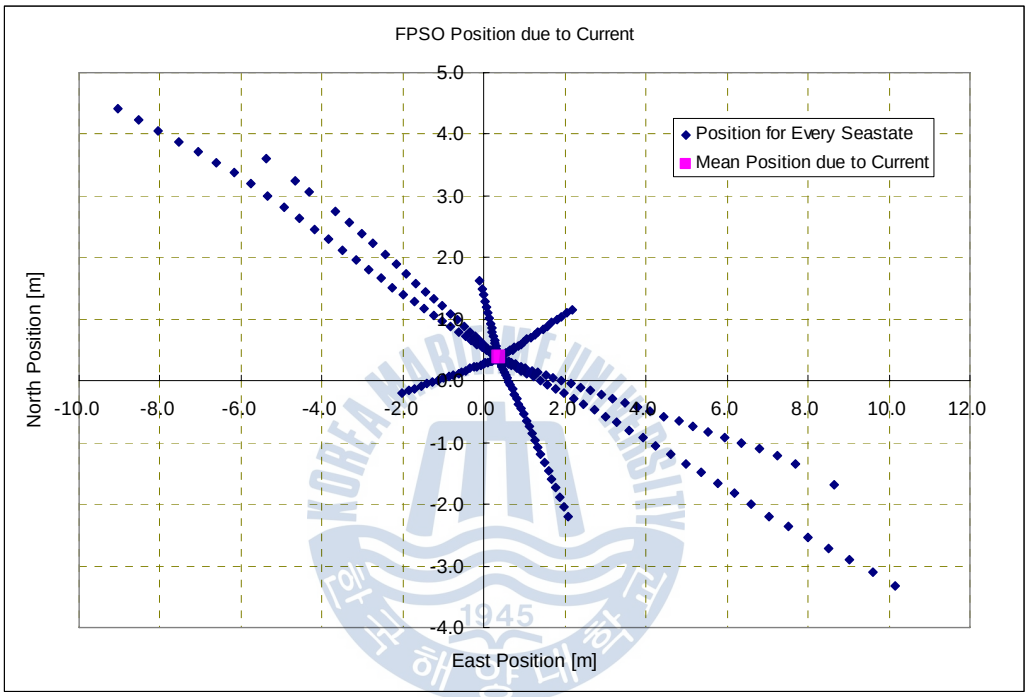

Fig.7-22 Positions of FPSO from current sea states and mean position

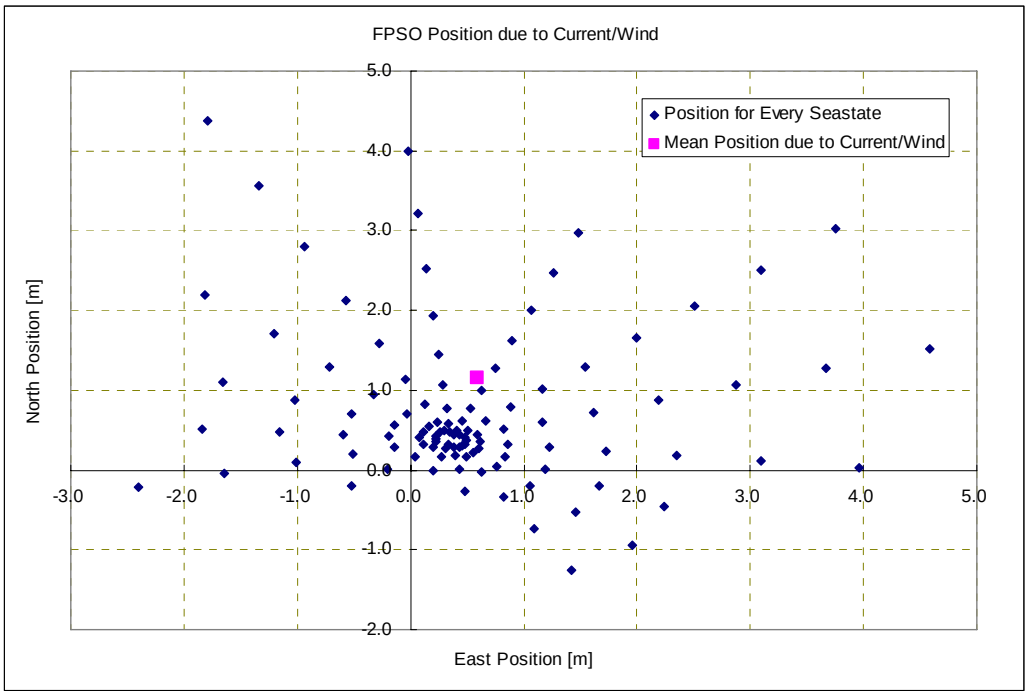

Fig.7-23 Positions of FPSO from current and wind sea states and mean position

7.9.2 Tension Fatigue

The tension fatigue of the mooring lines was performed by OrcaFlex, a fully coupled analysis tool. Fig.7-24 presents the modeling view of the FPSO along with the mooring legs.

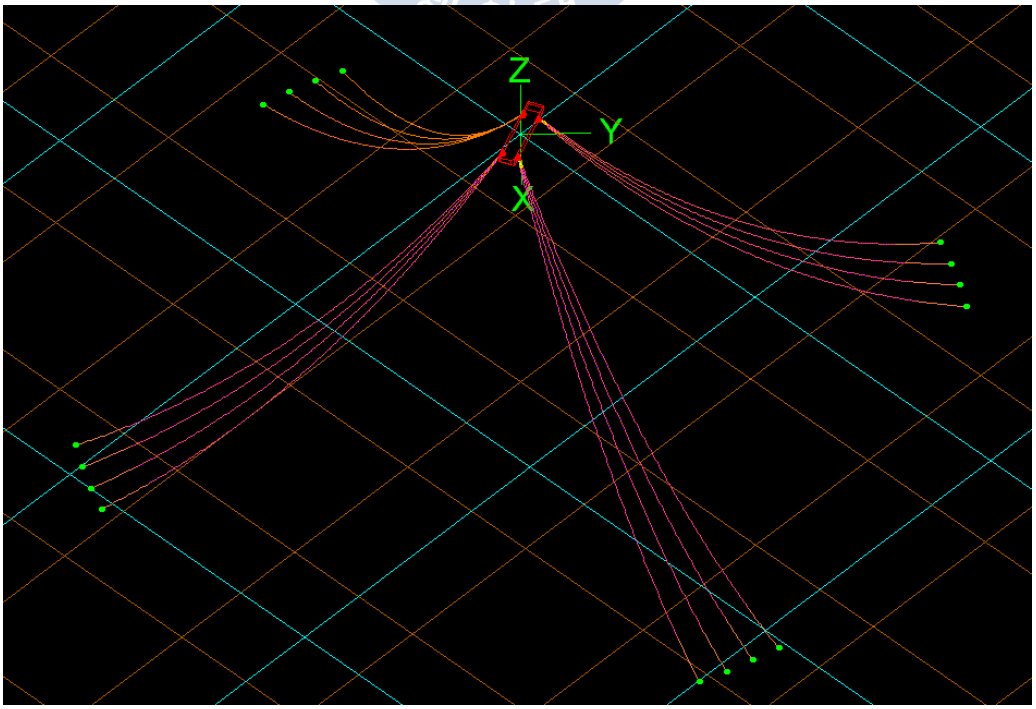

Fig.7-24 Modeling view of FPSO with mooring legs by OrcaFlex

The time histories of the dynamic tensions at the stopper position of the mooring lines are given in Fig.7-25 through Fig.7-40, which are examples for the sea state 0 among all the states. And, Fig.41 through Fig.46 shows the tensions computed by OrcaFlex, in which the mooring lines (P1,P8,S1 and S8) were chosen based on the min fatigue life in tension load and the mooring lines (P5 and S5) were additionally chosen considering the max tension per cluster.

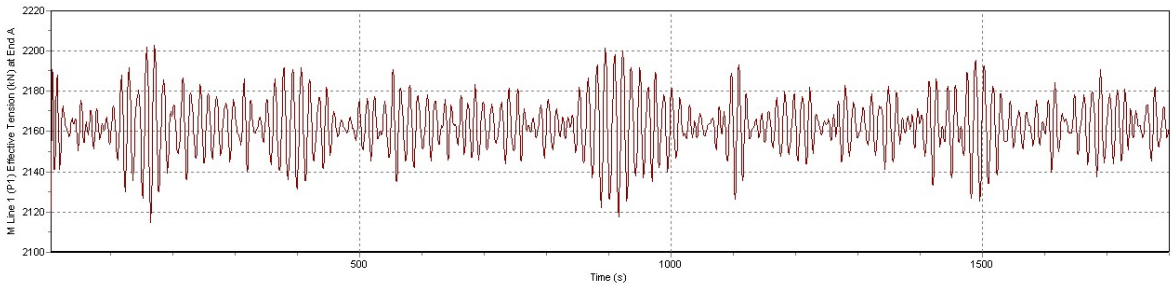

Fig.7-25 Time histories of dynamic tensions of mooring legs (P1) for sea state 1

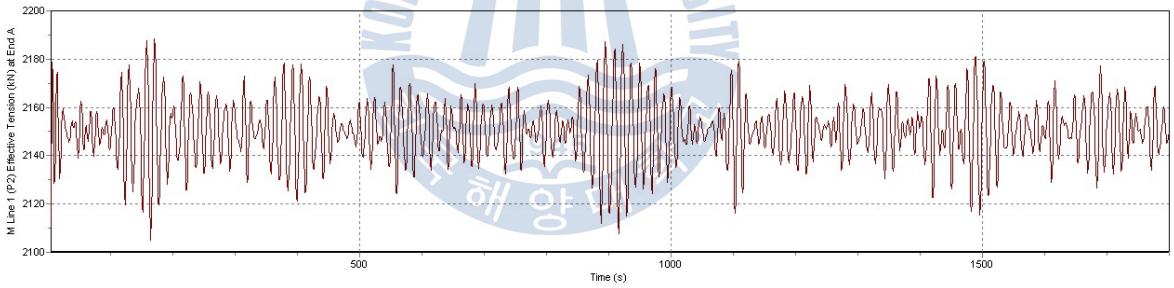

Fig.7-26 Time histories of dynamic tensions of mooring legs (P2) for sea state 1

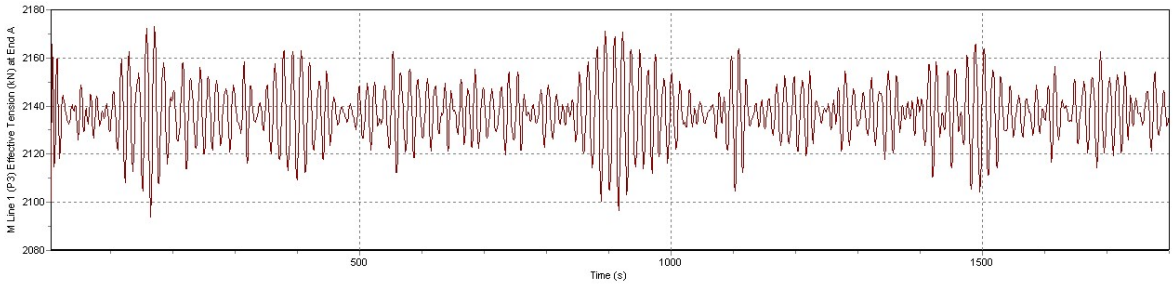

Fig.7-27 Time histories of dynamic tensions of mooring legs (P3) for sea state 1

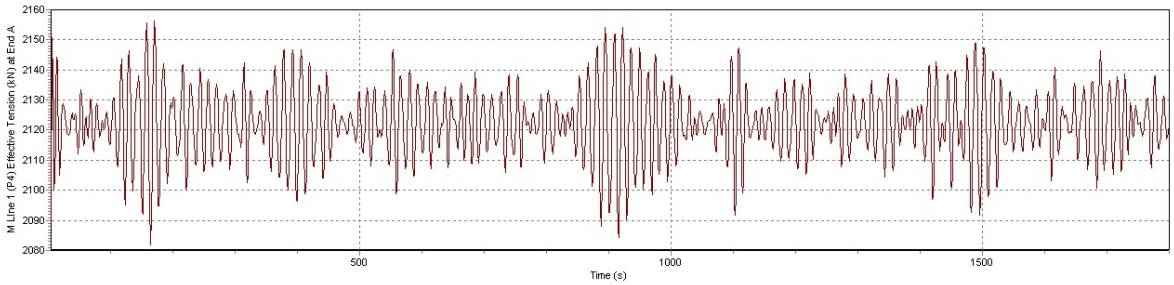

Fig.7-28 Time histories of dynamic tensions of mooring legs (P4) for sea state 1

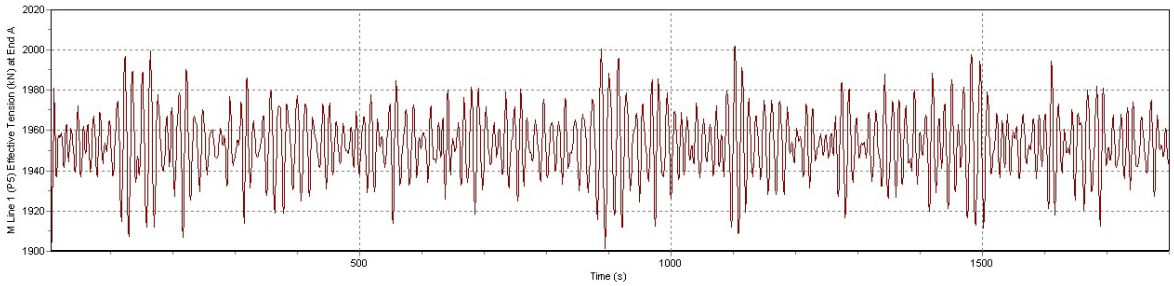

Fig.7-29 Time histories of dynamic tensions of mooring legs (P5) for sea state 1

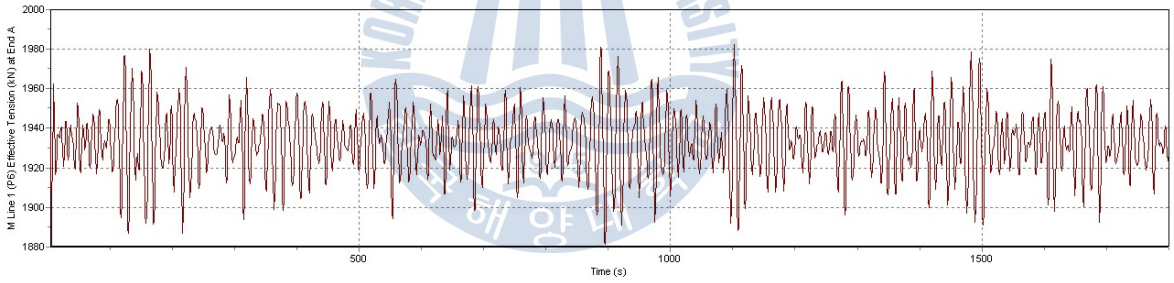

Fig.7-30 Time histories of dynamic tensions of mooring legs (P6) for sea state 1

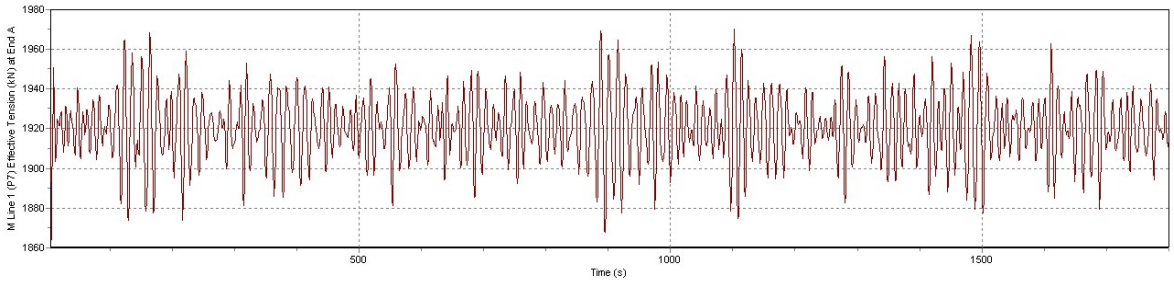

Fig.7-31 Time histories of dynamic tensions of mooring legs (P7) for sea state 1

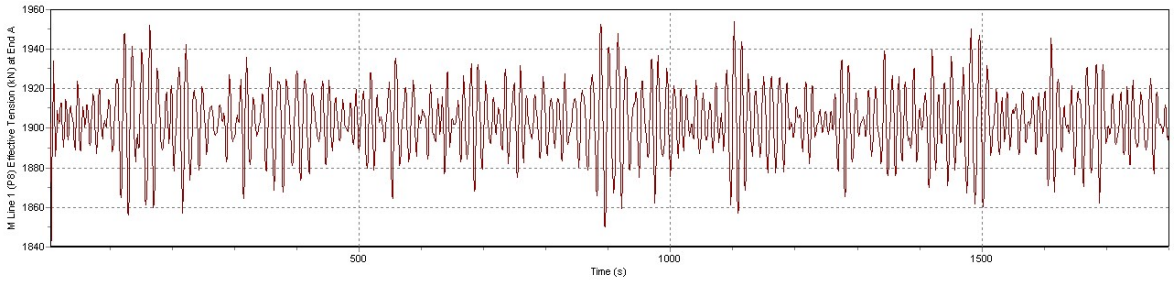

Fig.7-32 Time histories of dynamic tensions of mooring legs (P8) for sea state 1

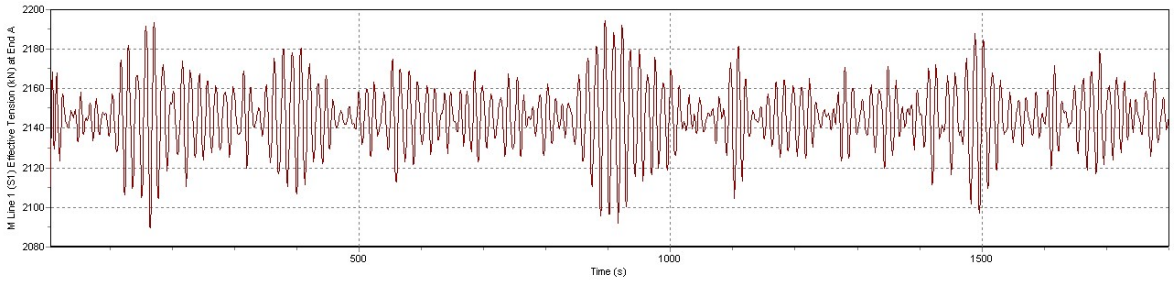

Fig.7-33 Time histories of dynamic tensions of mooring legs (S1) for sea state 1

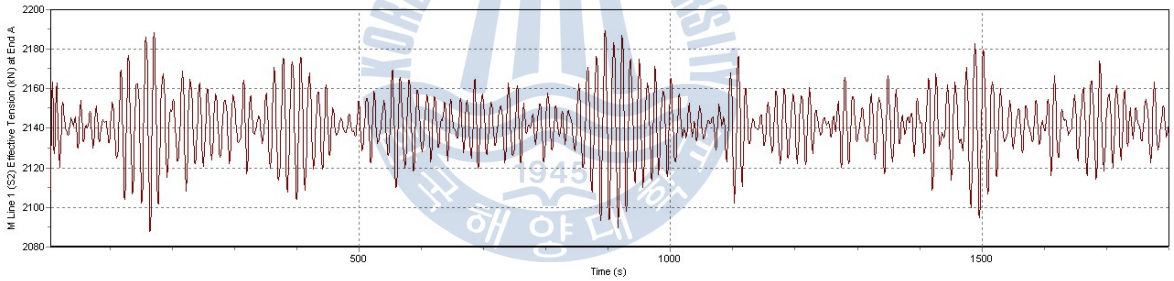

Fig.7-34 Time histories of dynamic tensions of mooring legs (S2) for sea state 1

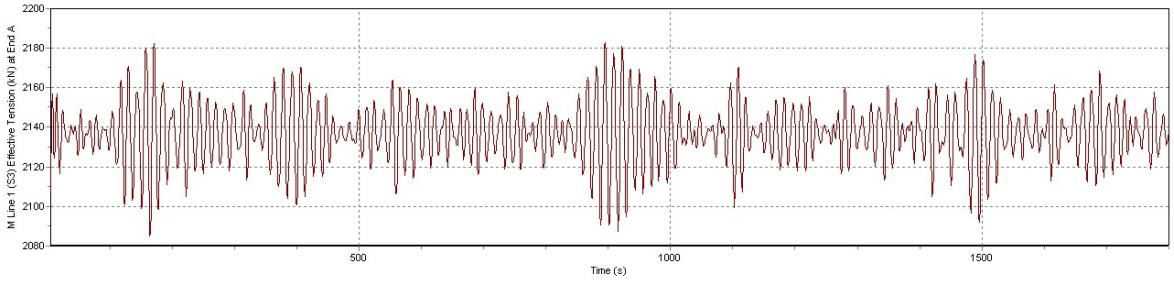

Fig.7-35 Time histories of dynamic tensions of mooring legs (S3) for sea state 1

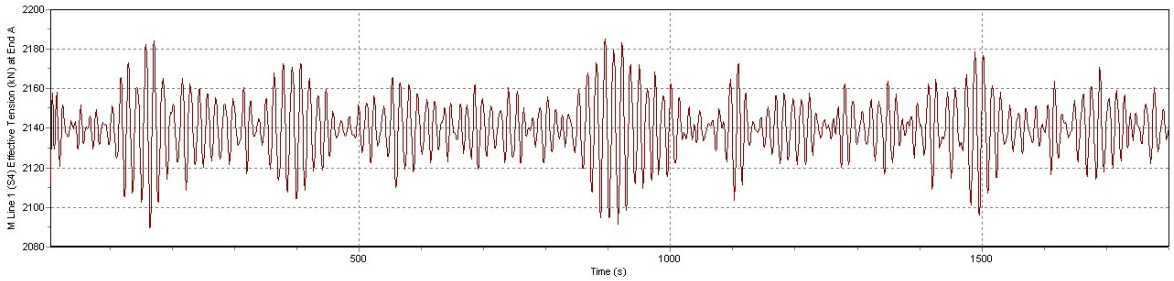

Fig.7-36 Time histories of dynamic tensions of mooring legs (S4) for sea state 1

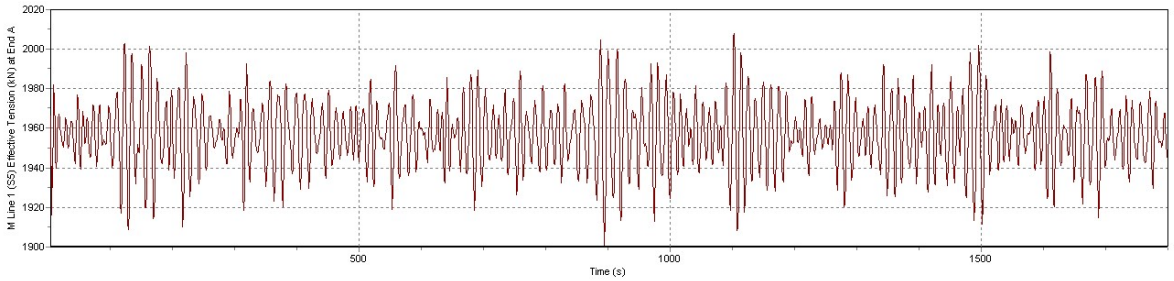

Fig.7-37 Time histories of dynamic tensions of mooring legs (S5) for sea state 1

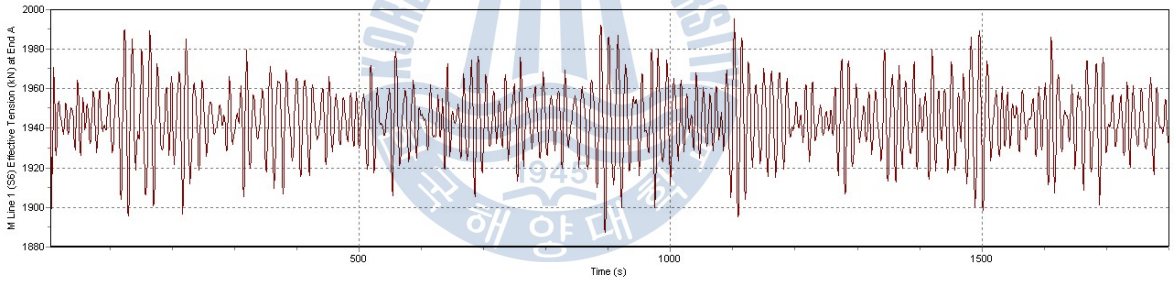

Fig.7-38 Time histories of dynamic tensions of mooring legs (S6) for sea state 1

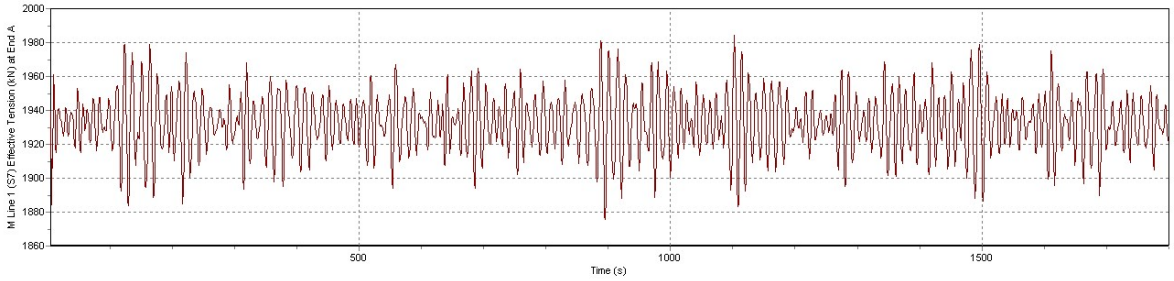

Fig.7-39 Time histories of dynamic tensions of mooring legs (S7) for sea state 1

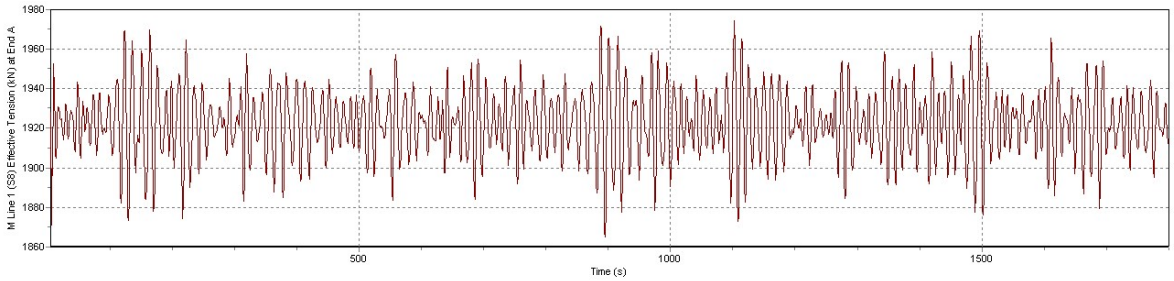

Fig.7-40 Time histories of dynamic tensions of mooring legs (S8) for sea state 1

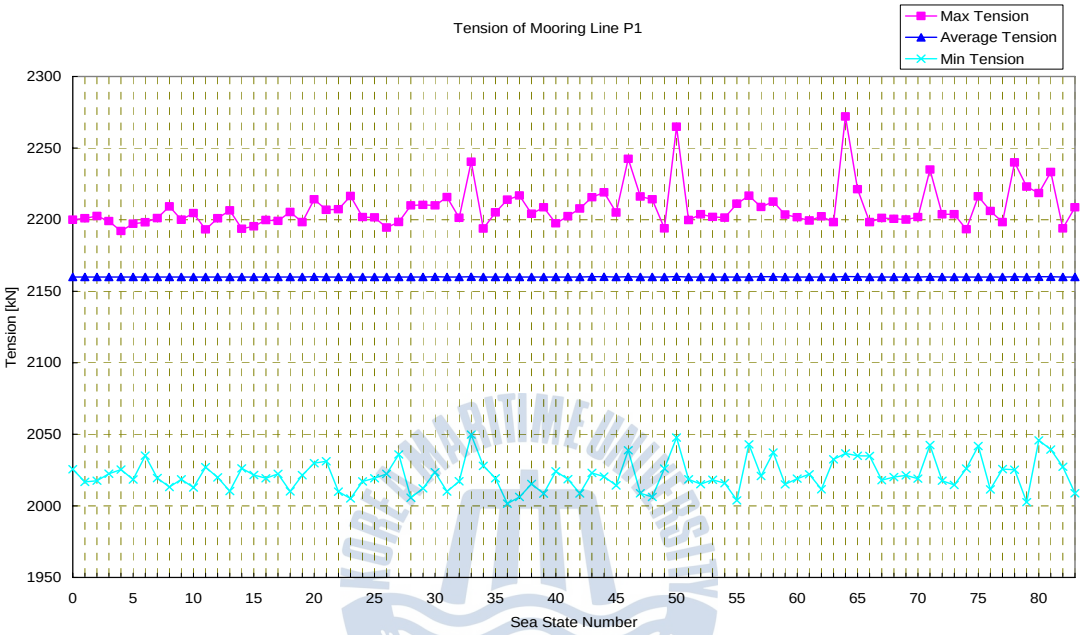

Fig.7-41 Tension of mooring line P1 for sea states considered

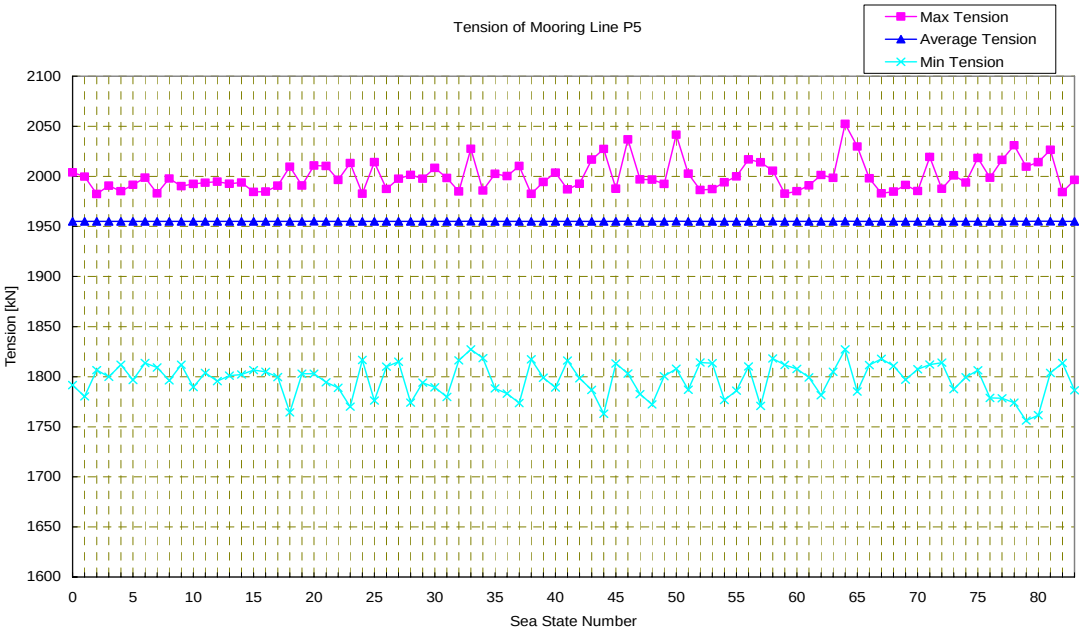

Fig.7-42 Tension of mooring line P5 for sea states considered

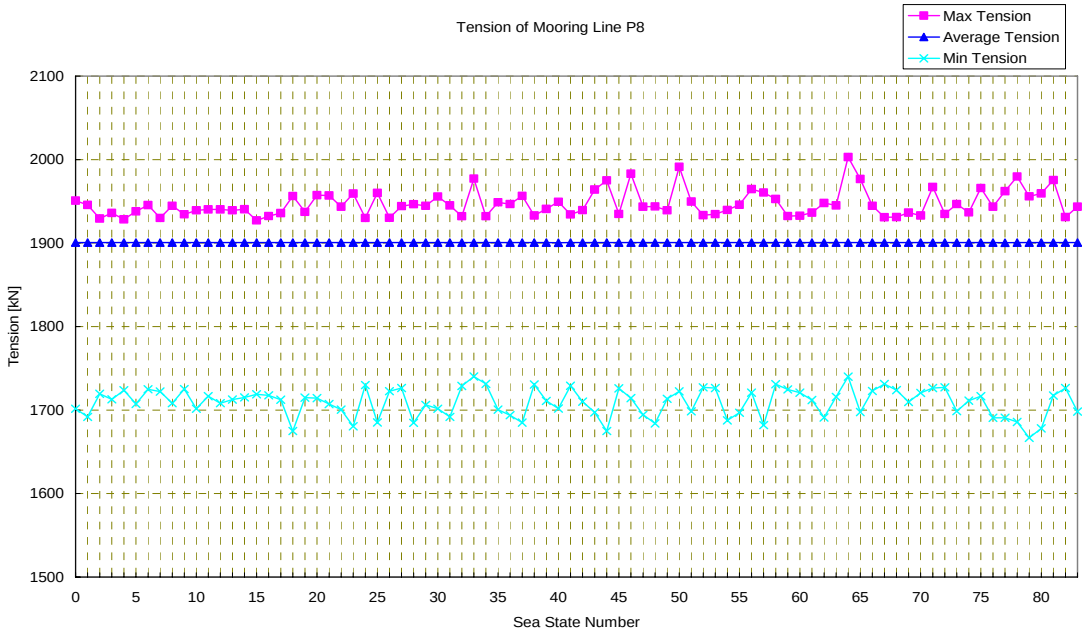

Fig.7-43 Tension of mooring line P8 for sea states considered

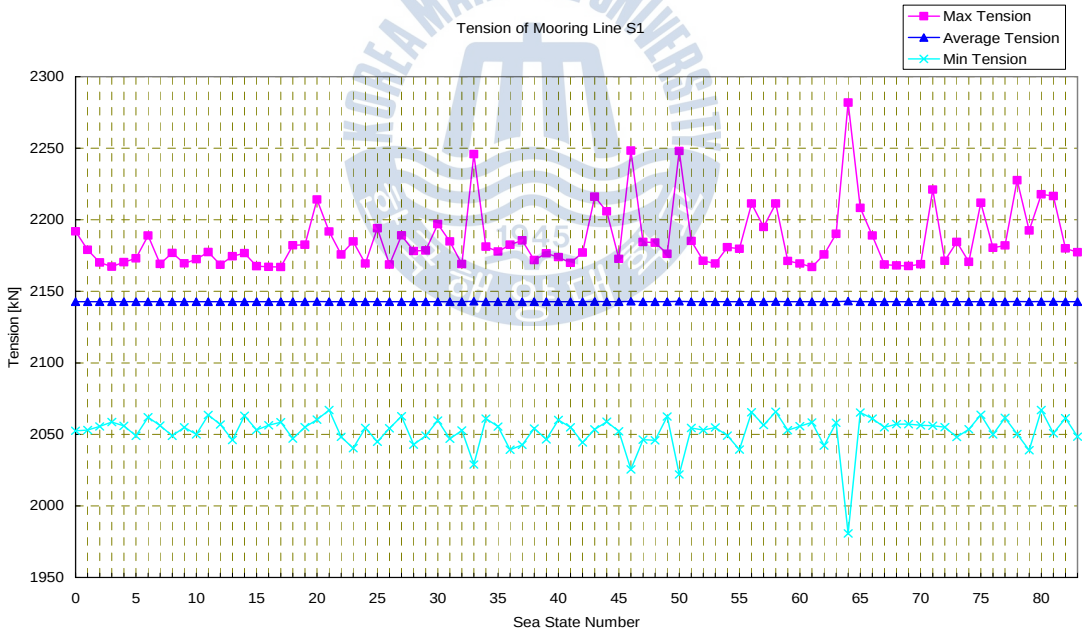

Fig.7-44 Tension of mooring line S1 for sea states considered

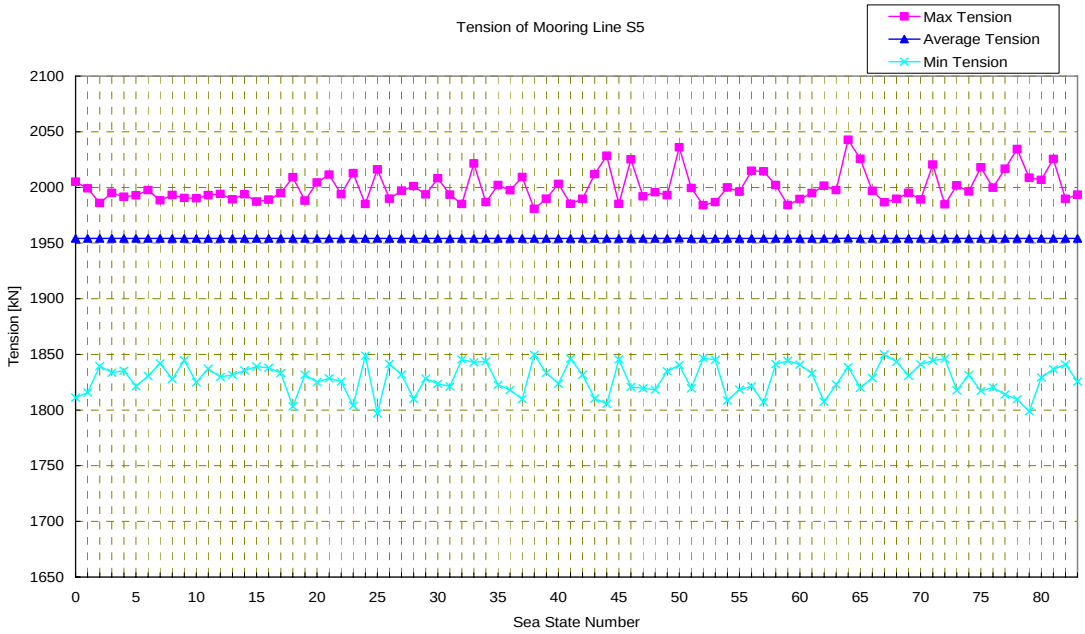

Fig.7-45 Tension of mooring line S5 for sea states considered

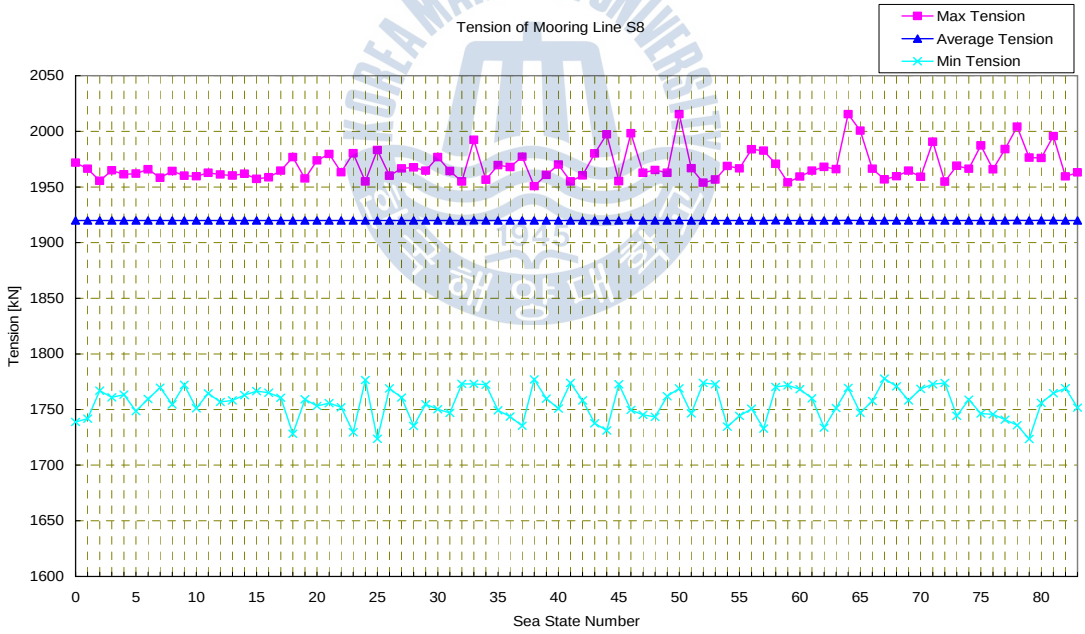

Fig.7-46 Tension of mooring line S8 for sea states considered

Through the rainflow counting method from the calculated tension time histories for each mooring line at the stopper location, the tension fatigue lives were calculated as shown in Table 7-11, which were obtained at the first link location of the top chain.

Table 7-11 Summary of tension fatigue lives of each mooring line

Mooring Leg	Fatigue Damage[-]	Fatigue Life[yr]	Min Fatigue Life in Cluster [yr]
P1	1.280154e-004	7.811562e+003	7.811562e+003 (at P1)
P2	1.089566e-004	9.177968e+003	
P3	9.196315e-005	1.087392e+004	
P4	7.702932e-005	1.298207e+004	
P5	1.940645e-004	5.152926e+003	4.833870e+003 (at P8)
P6	1.960229e-004	5.101445e+003	
P7	2.034299e-004	4.915697e+003	
P8	2.068736e-004	4.833870e+003	
S1	1.889638e-004	5.292020e+003	5.292020e+003 (at S1)
S2	1.691761e-004	5.911002e+003	
S3	1.508668e-004	6.628362e+003	
S4	1.383081e-004	7.230235e+003	
S5	2.043295e-004	4.894056e+003	4.477170e+003 (at S8)
S6	2.101091e-004	4.759431e+003	
S7	2.168707e-004	4.611042e+003	
S8	2.233554e-004	4.477170e+003	

7.9.3 Mooring Modeling for OPB fatigue

In order to calculate the time histories with respect to the OPB/IPB, the mooring lines were modeled considering the interlink stiffness based on the results from the non-linear FE analysis of ABAQUS and besides, the bending stiffness of the chain stopper assembly was reflected. Based on the information from the supplier of the chain stopper assembly, the break out angle 0.2deg in vertical direction and 0.5deg in horizontal direction were considered along with the bending stiffness of the assembly. Fig.7-47 indicates the bending moment of the latch housing in the stopper assembly according to the rotating angle.

For the rotation creating OPB in the first link, the stiffness 60316N-m/mm of the latch housing was supplied. And for the rotation creating IPB, 19818N-m/mm was supplied.

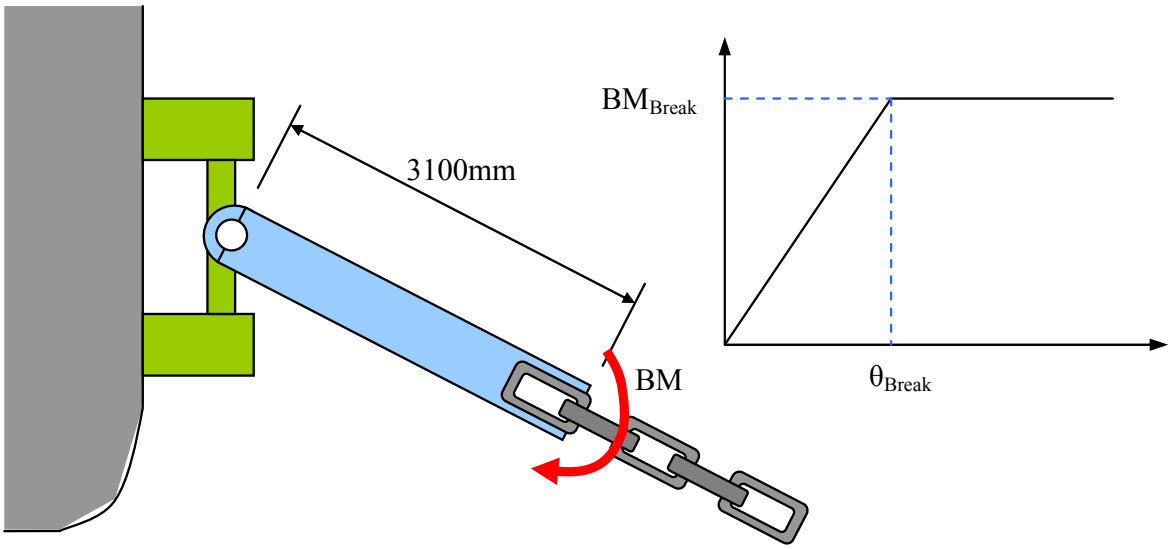

Fig.7-47 Bending moment and rotating angle of latch housing in chain stopper assembly

Based on the stiffness from the supplier, the bending stiffness for the rotation creating OPB in the first link before the break out angle 0.2deg can be calculated of 3260kN-m/deg. The values according to the rotating angle were applied in the mooring analysis by OrcaFlex. Besides, it is certain that the fairlead will slide vertically in the plane of the mooring line above the break out angle of 0.2deg for OPB and 0.5deg for IPB. Therefore, in order to take into account this phenomenon, a treatment of the time series of the OPB/IPB angles was performed. Once the angle exceeds the break out angle, the angle analyzed by OrcaFlex was taken constant at the angle and, the following angle was recalculated by considering the sliding effects. Fig.7-48 shows the example of the treatment for the fairlead sliding.

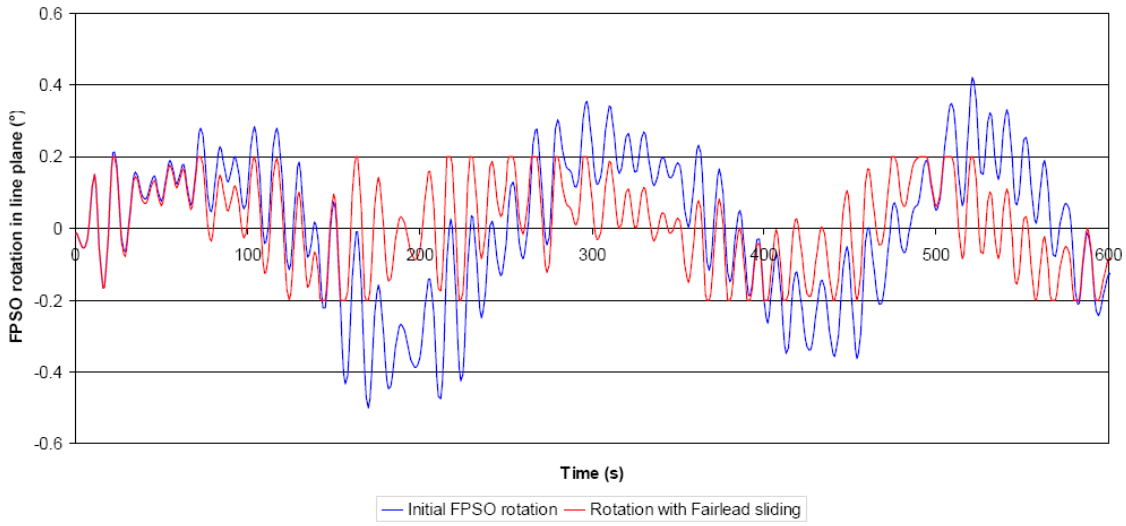

Fig.7-48 Example of treatment for fairlead sliding

The top chain links were modeled with the connection stiffness obtained from the non-linear FE analysis by ABAQUS. But, the bending stiffness of the wire rope and the bottom chains was not considered. Fig.7-49 shows the modeling idea used for the mooring analysis including the effects on the OPB/IPB.

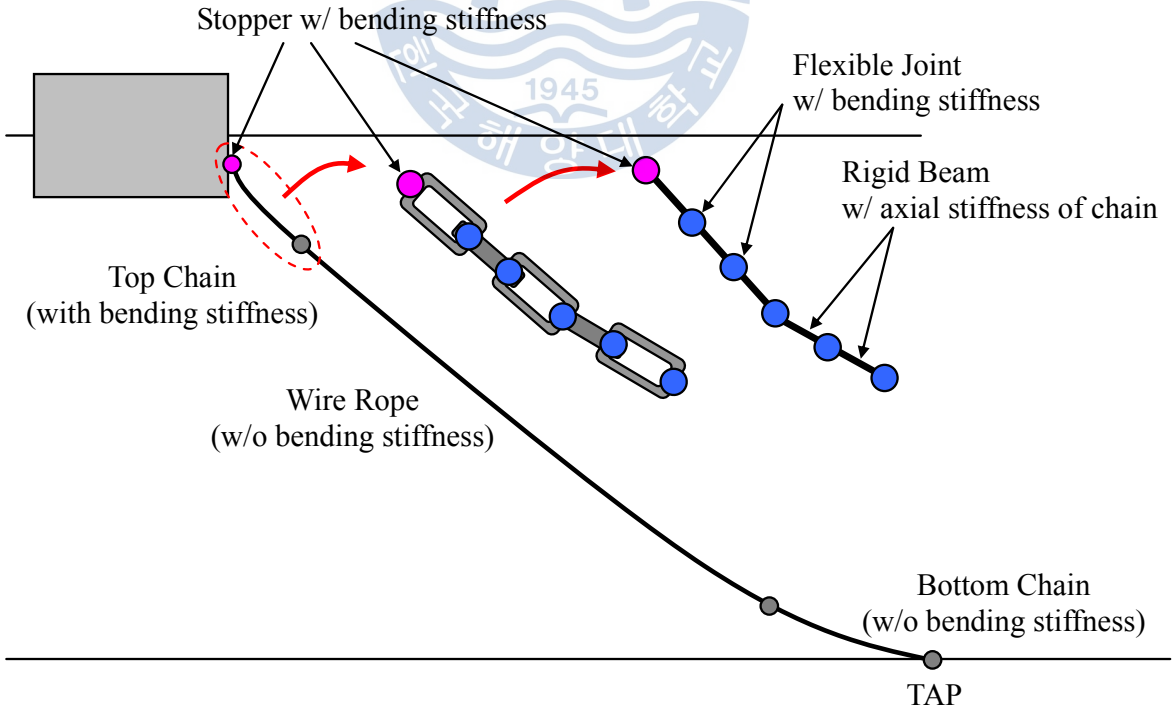

Fig.7-49 Modeling scheme of mooring lines for OPB fatigue

The bending moments at the flexible joints modeled in OrcaFlex were investigated to figure out the validity of the model of the mooring lines. As shown

in Fig.7-50 below, the bending moment in case of roll angle 0.2deg of the FPSO is rapidly decayed along line. Therefore, in the mooring analysis the top chain links were modeled with about 10 flexible joints from the stopper.

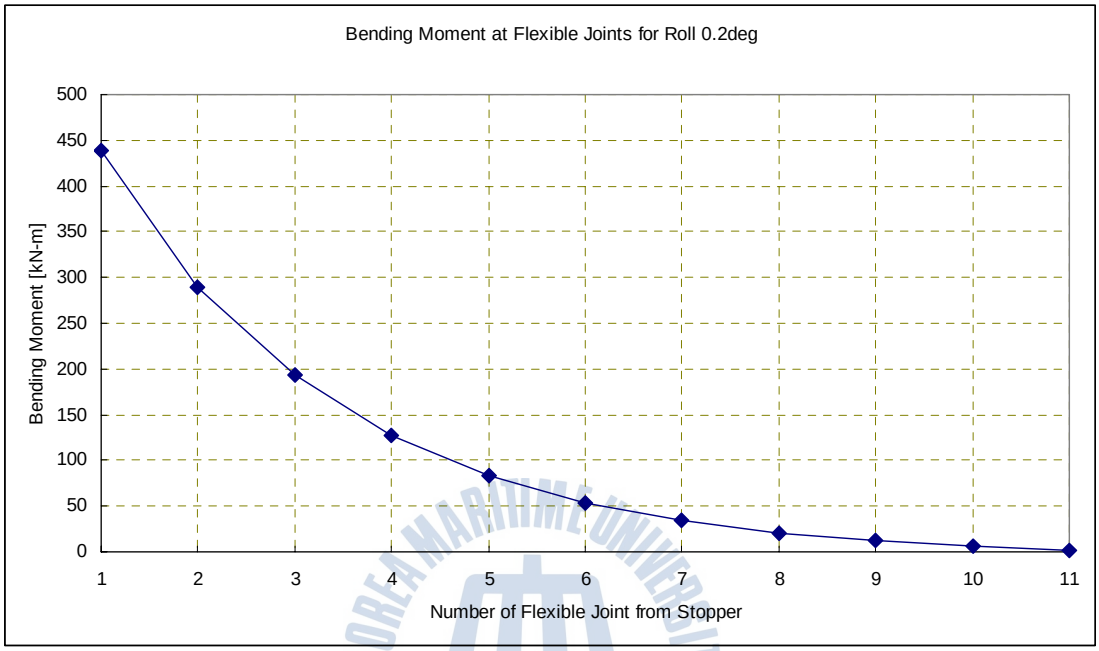

Fig.7-50 Bending moment at the flexible joints modeled in case of roll angle 0.2deg

7.9.4 Calculation of Resultant Stress

From the motions of the FPSO analyzed based on the quasi-dynamic approach, the dynamic behaviors of the mooring lines were computed by OrcaFlex. The tension and interlink angles for OPB/IPB were also obtained along the mooring line. In particular, the values at the concerned chain link, e.g. the first chain link, were selected to compute the resultant stress at the chain. The stress concentration factors were also taken into account in calculating the stress. The resultant stress can be derived as Eq.(7-8);

$$\sigma_{ijk} = \sigma_{TT_{ijk}} \pm \sigma_{OPB_{ijk}} \pm \sigma_{IPB_{ijk}}$$

$$= \sigma_{n_k}\left(\frac{\sigma_{TT_{ijk}}}{\sigma_{n_k}} \pm \frac{\sigma_{OPB_{ijk}}}{\sigma_{n_k}} \pm \frac{\sigma_{IPB_{ijk}}}{\sigma_{n_k}}\right)$$

$$= \sigma_{n_k}\left(SCF_{TT_{ijk}} \pm SCF_{OPB_{ijk}} \pm SCF_{IPB_{ijk}}\right)$$

$$= \frac{T_k}{A_{chain}}\left(SCF_{TT_{ijk}} \pm SCF_{OPB_{ijk}} \pm SCF_{IPB_{ijk}}\right) \quad (7\text{-}8)$$

where, σ_{ijk} = Resultant stress at chain's node i and radial index j and time k

σ_{TTijk} = Tensile stress at chain's node i and radial index j and time k

σ_{OPBijk} = OPB stress at chain's node i and radial index j and time k

σ_{IPBijk} = IPB stress at chain's node i and radial index j and time k

σ_{nk} = Nominal stress at time k

SCF_{TTijk} = SCF for tension at chain's node i and radial index j and time k

SCF_{OPBijk} = SCF for OPB at chain's node i and radial index j and time k

SCF_{IPBijk} = SCF for IPB at chain's node i and radial index j and time k

T_k = Tension at time k

In the calculation of the sectional area of the chain, some codes recommended that the chain corrosion be taken into account. Normally protection against chain corrosion and wear is provided by increase of chain diameter. ISO 19901 recommended using the allowance of 0.2mm ~ 0.8mm per year of the design life for those parts of a mooring line in the splash zone or zone of hard-bottom sea floor contact and 0.1mm ~ 0.2mm per year for the remaining length. While, API RP 2K recommended 0.2mm ~ 0.4mm per year in the splash zone. In this research, the corrosion and wear allowance of 0.4mm per year was applied.

With the mechanism of chain links along with the chain stopper, it is necessary to consider the moment direction. For instance, the OPB interlink angle will make tractions on the upper surface whereas the lower surface will be in compression in

the plus OPB moment. And, the IPB interlink angle will be coupled depending upon the moment direction. In Fig.7-51, the illustration for the combinations of OPB/IPB interlink angles is presented.

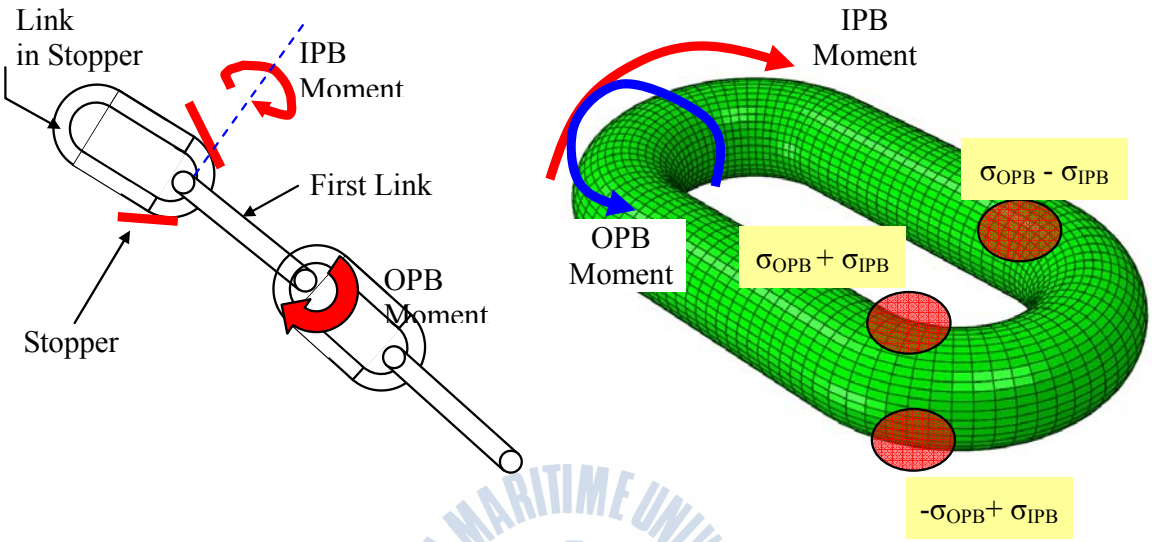

Fig.7-51 Example of combination of OPB and IPB interlink angles

7.10 Results from OPB and IPB Fatigue Analysis

Based on the procedure mentioned above, the fatigue lives corresponding to the fatigue damage were computed. Figures from Fig.7-52 to Fig.7-57 present the fatigue lives in year at the indicated nodes on the chain surface of the first chain link, for which the 4 mooring lines were chosen based on the max tension per cluster.

Node	Radius [deg]																
	0	6	12	18	24	30	36	42	48	54	60	66	72	78	84	90
1												16935	3296	958	1059	1335
2												9767	2119	687	759	976
3										3328	4395	4527	1223	525	591	665
4										2105	2412	2529	763	461	452	543
5										1499	1397	1454	543	393	381	447
6										1112	1008	1014	431	352	344	399
7									1202	907	776	762	418	341	326	379
8									929	691	648	632	386	346	331	360
9								1093	705	618	520	500	385	344	349	339
10								737	595	539	489	465	403	394	356	373
11								533	480	434	465	444	443	433	427	429
12								346	360	381	453	439	517	501	553	524
13								266	308	375	451	445	612	714	675	629
14								203	270	367	465	457	773	955	1475	3788
15								178	234	328	470	468	1033	2009	28023	16235
16								157	228	324	547	554	1883	7873	93812	19573
17								152	223	354	543	663	5453	36762	75480	24328
18								144	214	340	629	1088	27689	119207	102394	72253
19								139	205	377	717	2631	84527	166525	337682	128930
20								147	215	363	809	11826	122622	307985	131663	1095045
21								139	230	391	886	16069	84082	163298	87515	320619

Contact Zone

Fig.7-52 Fatigue lives (year) calculated for first link including effects on OPB and IPB (P1)

Node	Radius [deg]																
	0	6	12	18	24	30	36	42	48	54	60	66	72	78	84	90
1												17235	3679	1190	1313	1654
2												9930	2419	851	939	1205
3										3562	4760	4820	1400	658	738	823
4										2236	2602	2708	883	575	578	688
5										1613	1490	1548	626	483	476	565
6										1184	1084	1088	502	424	422	502
7									1284	974	840	837	483	403	398	468
8									1013	766	727	708	444	411	395	439
9								1199	806	713	601	577	449	404	415	406
10								872	716	644	580	550	477	466	417	438
11								677	604	539	574	538	522	507	496	498
12								467	472	486	568	544	615	583	651	606
13								372	419	494	576	568	750	862	796	738
14								293	380	502	603	606	978	1114	1617	4148
15								264	338	451	636	641	1254	2225	36533	16537
16								234	336	459	771	768	2179	8910	91762	19631
17								229	334	516	771	836	6321	48323	80591	23982
18								220	326	504	928	1325	37699	197059	110143	75192
19								215	311	569	1078	3213	143122	297568	542444	118908
20								234	333	544	1236	17488	250086	639168	179232	2809742
21								225	362	587	1378	27137	152474	285024	108999	537332

Contact Zone

Fig.7-53 Fatigue lives (year) calculated for first link including effects on OPB and IPB (P5)

Node	Radius [deg]															
	0	6	12	18	24	30	36	42	48	54	60	66	72	78	84	90
1												9288	5341	2690	3245	4309
2												5170	2878	1483	1762	2393
3										2074	2608	2532	1372	866	1042	1252
4										1316	1461	1465	781	609	657	845
5										971	907	919	525	457	479	601
6										764	706	692	410	373	391	485
7									852	665	591	573	385	343	351	425
8									745	577	539	519	360	344	345	389
9								895	650	564	492	469	371	345	355	363
10								752	638	566	505	478	408	398	369	388
11								670	588	521	536	504	469	455	444	446
12								541	525	523	573	550	571	540	570	526
13								483	511	572	628	623	713	765	693	638
14								422	511	629	716	708	940	1015	1107	1211
15								409	496	627	814	789	1285	1648	2888	4399
16								391	530	690	1047	1026	2107	3554	7923	8793
17								406	561	822	1145	1275	4737	9535	17834	23054
18								411	584	865	1449	2244	21164	36744	64985	47494
19								417	593	1032	1810	8142	172259	192203	182437	464374
20								461	662	1055	2227	64156	196458	442410	705062	1385391
21								456	741	1208	2640	29474	164652	333142	5510340	785005

Contact Zone

Fig.7-54 Fatigue lives (year) calculated for first link including effects on OPB and IPB (S1)

Node	Radius [deg]															
	0	6	12	18	24	30	36	42	48	54	60	66	72	78	84	90
1												8845	3520	1298	1417	1791
2												6643	2535	976	1067	1373
3											5121	4409	1659	782	861	973
4										3254	3302	3073	1150	720	707	840
5										2453	2142	2084	869	636	616	723
6										1902	1648	1588	717	587	572	663
7									2130	1591	1346	1282	724	589	557	644
8									1673	1243	1155	1115	690	618	588	638
9								1968	1280	1123	945	907	701	627	634	613
10								1332	1082	984	897	857	740	725	656	685
11								959	871	792	854	809	814	796	788	790
12								622	651	692	824	800	949	927	1012	963
13								476	553	673	815	816	1116	1268	1197	1119
14								359	481	658	846	829	1366	1598	1775	1663
15								313	416	587	856	844	1736	2089	2774	3338
16								273	403	580	991	962	2239	3117	5008	5902
17								263	390	637	976	995	3288	5939	9321	10380
18								250	374	605	1126	1218	6017	11092	17953	19495
19								238	359	668	1277	1820	11776	19972	27752	49914
20								250	375	631	1386	3446	20544	41456	42170	98382
21								236	396	675	1510	4543	24984	55101	58162	168454

Contact Zone

Fig.7-55 Fatigue lives (year) calculated for first link including effects on OPB and IPB (S5)

From the results, it was found that the mooring line with higher tension is much critical in terms of OPB fatigue.

On the effects of OPB and/or IPB, the studies for the mooring line P1 and S1 were performed. In Fig.7-56 and Fig.7-57, the fatigue lives of the first link only for the tension load were summarized, from which the min fatigue life was found as expected at the curved surface located at the central surface inside the chain link, i.e. node index 1 and radial index 78. However, only taking the effects of OPB; i.e. excluding the IPB effects, the critical points were moved to the radius 72deg as indicated in Fig.7-58 and Fig.7-59.

Node	Radius [deg]															
	0	6	12	18	24	30	36	42	48	54	60	66	72	78	84	90
1												11785	8028	6505	6557	8374
2												12607	8518	6875	6875	8740
3										64227	26646	14795	9976	8028	7895	9798
4										77687	33668	18924	12731	10158	9886	11898
5										93390	43389	25672	17712	14204	13507	15582
6										106990	58178	36552	25991	21202	19794	22215
7									218591	125970	80528	55437	42138	34594	31912	34127
8									207930	149717	113629	88267	72392	62121	56331	57245
9								242203	202859	179830	160159	146439	131406	120829	111356	104892
10				Contact Zone				202859	207930	218591	235993	248633	255293	255293	242203	224196
11								179830	218591	276755	347115	443496	540537	621492	621492	559392
12								167665	235993	347115	522521	806866	1224755	1705375	2097536	1887946
13								156574	262192	457957	839137	1622871	3131017	6209832	10250190	11241490
14								149717	284442	599814	1341324	3330810	9372100	30275410	89931950	276755100
15								146439	318204	776229	2214040	7895254	34594390	167665200	1705371000	1.3643E+10
16								143256	347115	986907	3784427	18714680	167665200	1073942000	1.3643E+10	4.6045E+10
17								140164	368361	1224755	6209832	53704790	1073942000	5755625000	4.6045E+10	3.6836E+11
18								140164	391377	1545605	11241490	213172100	1.3643E+10	4.6045E+10	3.6836E+11	3.6836E+11
19								137161	416351	1793567	18714680	1705371000	3.6836E+11	3.6836E+11	3.6836E+11	3.6877E+14
20								137161	429638	1989065	26646480	3.6836E+11	3.6877E+14	3.6877E+14	3.6836E+11	3.6877E+14
21								137161	429638	2097536	30275410	3.6877E+14	3.6877E+14	3.6877E+14	3.6836E+11	3.6877E+14

Fig.7-56 Fatigue lives (year) calculated for first link excluding effects on OPB and IPB (P1)

Node	Radius [deg]															
	0	6	12	18	24	30	36	42	48	54	60	66	72	78	84	90
1												7308	4978	4034	4066	5193
2												7818	5282	4263	4263	5420
3										39827	16524	9175	6186	4978	4896	6076
4										48174	20877	11735	7894	6299	6131	7378
5										57912	26906	15919	10983	8808	8376	9663
6										66345	36076	22666	16117	13147	12274	13776
7									135549	78114	49936	34377	26130	21452	19788	21162
8									128938	92840	70461	54734	44890	38521	34931	35497
9								150191	125793	111513	99315	90807	81485	74926	69052	65044
10				Contact Zone				125793	128938	135549	146340	154178	158307	158307	150191	139024
11								111513	135549	171616	215246	275013	335188	385388	385388	346879
12								103970	146340	215246	324016	500339	759472	1057505	1300685	1170718
13								97092	162586	283980	520350	1006345	1941548	3850724	6356154	6970859
14								92840	176383	371946	831757	2065440	5811651	18773820	55766930	171616200
15								90807	197319	481341	1372929	4895857	21452010	103969700	1057502000	8460040000
16								88833	215246	611982	2346728	11605000	103969700	665950200	8460040000	2.8553E+10
17								86916	228421	759472	3850724	33302380	665950200	3569125000	2.8553E+10	2.2844E+11
18								86916	242693	958432	6970859	132187900	8460040000	2.8553E+10	2.2844E+11	2.2844E+11
19								85053	258180	1112193	11605000	1057502000	2.2844E+11	2.2844E+11	2.2844E+11	2.2858E+14
20								85053	266419	1233422	16523520	2.2844E+11	2.2858E+14	2.2858E+14	2.2844E+11	2.2858E+14
21								85053	266419	1300685	18773820	2.2858E+14	2.2858E+14	2.2858E+14	2.2844E+11	2.2858E+14

Fig.7-57 Fatigue lives (year) calculated for first link excluding effects on OPB and IPB (S1)

Node	Radius [deg]															
	0	6	12	18	24	30	36	42	48	54	60	66	72	78	84	90
1	Contact Zone											22682	14866	10499	9378	11274
2												15604	16394	13708	13396	16551
3										5515	7567	7481	10215	11388	13255	17459
4										3253	3828	3968	5082	6027	7766	11501
5										2280	2463	2558	2909	3494	4290	6234
6										1906	2036	2023	2050	2268	2757	3887
7									2102	1800	1788	1778	1666	1772	2063	2754
8									2284	1894	1759	1697	1470	1572	1773	2116
9								2859	2479	2071	1949	1831	1504	1519	1588	1843
10								3477	3173	2664	2250	2072	1659	1602	1611	1743
11								4755	3769	3064	2743	2462	1915	1823	1758	1774
12								6537	4993	4090	3401	3116	2437	2206	2103	1891
13								9247	6826	5607	4499	4233	3228	3057	2757	2501
14								12683	10193	8012	6532	6052	4744	4724	4469	10801
15								19218	14897	12073	10049	8586	7822	8144	1189117	12933
16								28274	23027	19550	16727	13944	13690	43735	52721	16124
17								43262	38251	32172	26145	23533	36346	1559447	62049	21986
18								62392	62349	51260	49216	41634	9512936	417790	91024	62820
19								92593	97188	102188	97645	85818	350387	564719	564719	149560
20								135566	160764	178653	204110	442878	516075	829605	216851300	1462953
21								178323	280278	352561	444239	342572	2031921	7421257	20464900	466936700

Fig.7-58 Fatigue lives (year) calculated for first link including effects on IPB (P1)

Node	Radius [deg]															
	0	6	12	18	24	30	36	42	48	54	60	66	72	78	84	90
1	Contact Zone											10541	8166	6092	5593	6792
2												6500	7619	6921	7115	8961
3										2733	3434	3239	4271	4773	5742	7720
4										1676	1864	1845	2241	2581	3246	4812
5										1216	1250	1256	1377	1604	1929	2749
6										1043	1059	1028	1021	1108	1322	1832
7									1182	995	963	928	861	905	1039	1370
8									1277	1053	969	924	798	834	927	1098
9								1594	1380	1156	1085	1018	839	845	878	1009
10								1906	1750	1483	1265	1171	946	915	918	988
11								2514	2066	1712	1554	1412	1114	1077	1039	1043
12								3381	2701	2280	1940	1808	1463	1349	1299	1168
13								4682	3613	3120	2583	2509	1989	1885	1650	1476
14								6290	5294	4443	3764	3630	2937	2756	2411	2133
15								9253	7639	6651	5804	5287	4622	4371	4444	4962
16								13209	11586	10633	9668	8618	7878	7856	9913	9293
17								19501	18729	17013	15134	14425	14548	16923	20297	21028
18								27286	29594	26729	28455	24371	35550	46264	58954	45958
19								39048	44813	51867	56101	46411	133987	173732	173732	249818
20								56706	71360	88298	115740	153220	800737	1242728	879064	2070514
21								74449	119310	166681	245357	544473	2785707	8559142	11253970	154613300

Fig.7-59 Fatigue lives (year) calculated for first link including effects on IPB (S1)

As a result, the min fatigue lives considering each effect on tension, OPB and IPB can be located on the chain link as shown in Fig.7-60.

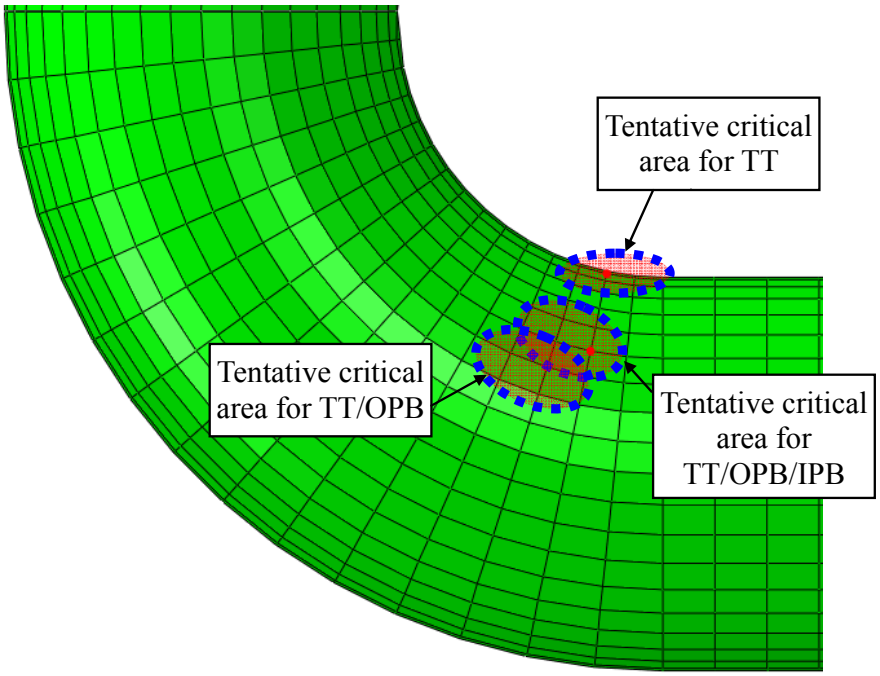

Fig.7-60 Tentative critical areas considering each effect on TT, OPB and IPB

The results of the considered mooring lines calculated based on the proposed procedures are presented in Fig.7-61. As shown in Fig.7-61, the least fatigue life at the highest tensioned mooring leg, i.e. P1, was calculated. And, the comparison of fatigue lives for each calculation method is given in Fig.7-62, from which, considering the effects on OPB and IPB, the fatigue life at the first chain link dramatically decreased. Besides, it was found that the effect on IPB is significant in terms of fatigue strength.

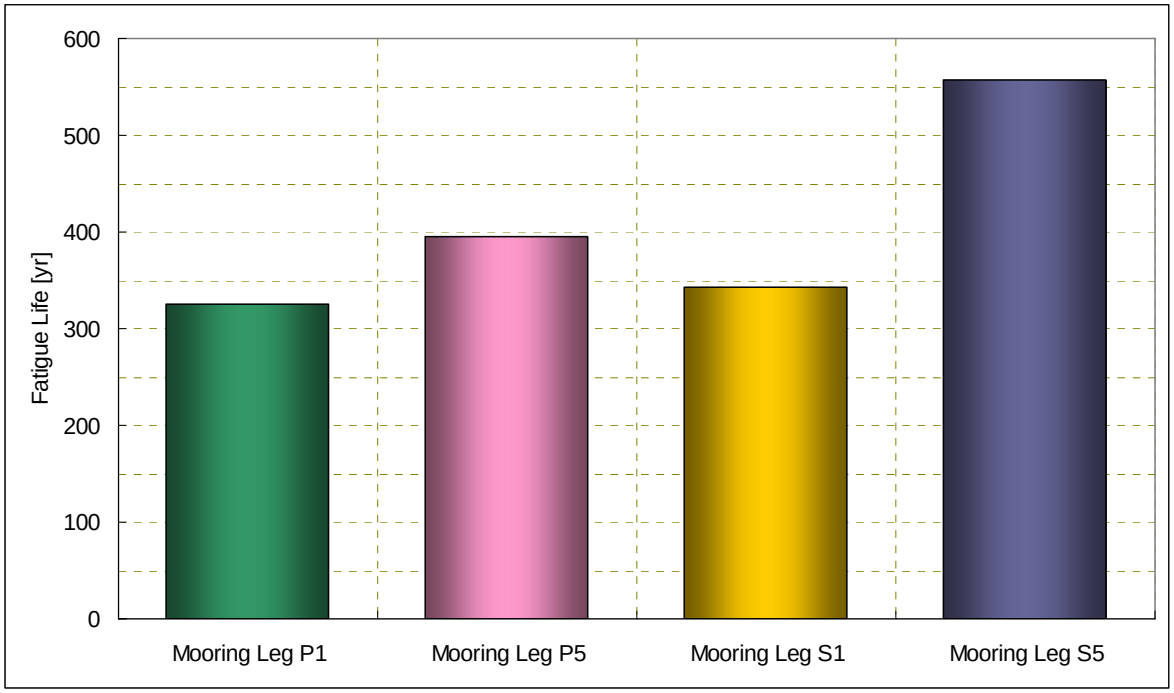

Fig.7-61 Results for considered mooring legs as per proposed procedures

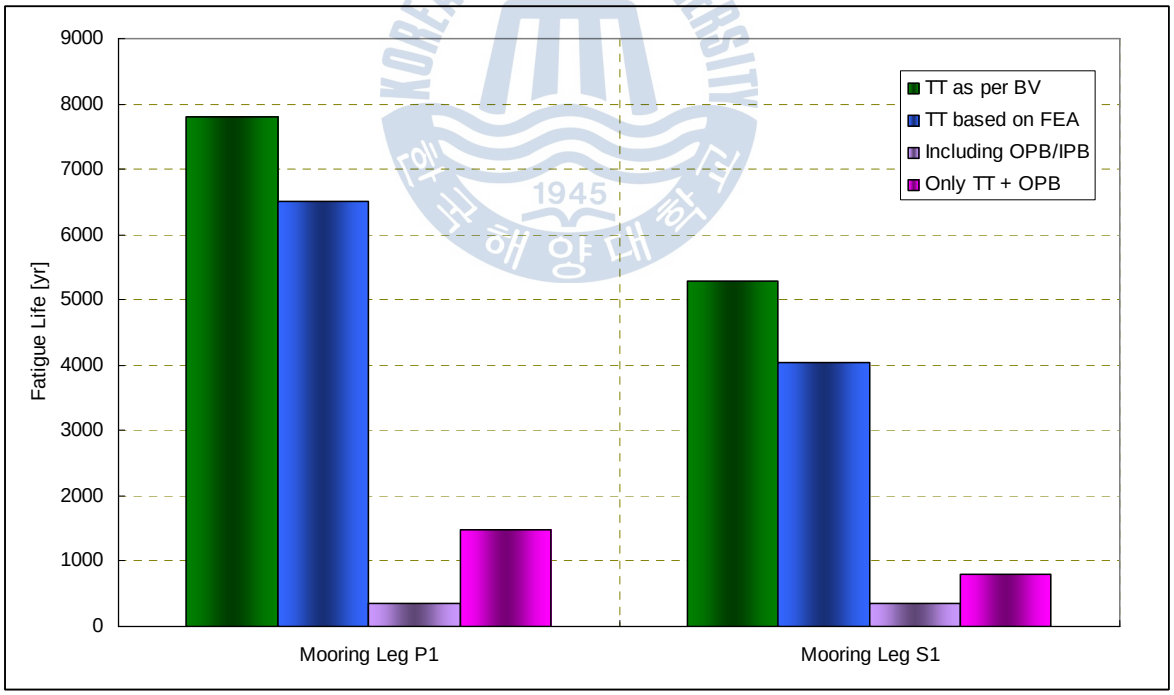

Fig.7-62 Comparisons of fatigue lives (year) according to used procedures

For the post-processing works with many values from the line dynamics, a useful program named as 'ChainFOS' was generated and utilized. In Appendix D, the manual on how to use the tool is briefly described.

8. Conclusion

In general, fatigue assessment for mooring lines has been carried out by focusing primarily on the tension load. This is due to the fact that it is occasionally not considered in the case of conventional ships as most of the procedures regarding classifications and certifications are prescribed in multiple class codes. However, because offshore floating structures like FPSOs and FPUs must remain in a fixed position for their entire lives, it would be too difficult to maintain all of the mooring systems on-site during operation. Therefore, mooring systems for offshore floating structures require more stringent requirements.

In particular, offshore floating facilities operating in deep water or ultra-deep water (depths of more than 1500m) should be strictly designed with both strength and fatigue endurance limits in mind. However, the taut and semi-taut mooring configurations normally utilized in deep waters generate additional fatigue damage on the first chain link of the chain stopper as well as fatigue damage from tension.

Research with regards to the friction-induced bending stress of mooring chains was initiated as a result of failures of the mooring chain links of the Girrasol offloading buoy. From the many investigations of the incident, it was determined that bending-induced fatigue on the chain contributed to such failures. In addition, interlink friction, tension, and proof load were identified as significant factors in instances where the phenomenon occurred. It should be noted that the proof load is generally undertaken in the manufacturing yard to confirm structural strength, which is known to sometimes cause a permanent deformation of the contact surfaces and also affect the rotation of the chain links. However, this study dealt with the mooring chains of a deep-water, spread-moored FPSO with a semi-taut mooring configuration.

In order to determine the stress concentration factors (SCF) of the chain link, a non-linear FE analysis was performed using ABAQUS. In this research, a grade R3,

OD147 studless chain (a type of offshore mooring chain) was utilized. The friction coefficient of 0.7, a slightly conservative value, was taken into consideration as per the recommendations of OPB JIP.

Two models were considered: OPB and IPB. For each model, the boundary and loading conditions were appropriately modeled to accurately simulate the symmetric behaviors and elastoplastic deformation of the contact surface between chain links. For instance, the proof load was first applied and subsequently released, after which the normal steps were applied. Through the FE analyses, the stress patterns along the link were found, and the stress concentration factors at every concerned node on the chain were calculated. Through this process, it was found that the stresses due to tension were concentrated around the neutral line inside the chains, whereas bending from OPB or IPB moved upward or downward along the surface. It was also observed that at an interlink angle the chain link's mode changed from locking mode to sliding mode.

As indicated in Chapter 7, a fatigue assessment procedure for the mooring chain including the effects of friction-induced bending stress was proposed. Also, a study of the application of OPB/IPB phenomena was carried out with the practical spread-moored FPSO for oil production in water deeper than 1000m. The FPSO was positioned with 16 mooring legs (4 mooring legs per cluster), and its mooring lines were connected to the suction anchor on the seabed using a semi-taut mooring configuration.

The 6 DOF motions of the FPSO were computed in time domain using the quasi-dynamic approach, for which ARIANE7, software made by BV, was utilized with full mooring configurations. Also, the dynamic behaviors of the mooring lines were analyzed using Orcina's OrcaFlex. In the modeling of the mooring lines, the bending stiffness calculated from non-linear FE analyses was considered as input data. To count the cycle numbers and compute the range of chain interlink angles for OPB and IPB, the rainflow counting method was used.

In order to calculate the fatigue life due to the bending effects on chain links, mooring lines with a maximum tension per cluster were chosen and investigated. Without question, it was necessary to take into consideration the effects on OPB/IPB in computing the fatigue life of the mooring lines, especially for offshore floating structures operating in deep water. From these calculations, it was found that the fatigue life decreased dramatically as a result of these factors. As a result, the fatigue life as per the procedure recommended in this research was much lower than that obtained from the code guidelines. In addition, it was concluded that the IPB cannot be ignored when calculating the fatigue life in terms of the bending-induced fatigue damage of the chain links. Considering the design fatigue factor (DFF) of 10 for forged nodes, which represents a required fatigue life of 200 years in case of a service life 20 years, the calculated fatigue life of around 300 years in this study may provide an insufficient fatigue margin from a practical design point of view.

However, this paper covers results only for the FE-based mechanism between chain links to determine the friction-induced bending effects in which the basis was theoretical and analytical. Therefore, in a future project, to reach more definitive conclusions, it will be necessary to a) look into other effects on the chain's OPB/IPB fatigue, such as corrosion and marine growth on mooring chains, and b) to collect various experimental data. Otherwise, special answers to completely overcome this issue should be established (Blanc, et al., 2006).

References

Almar-Naess, A. 1985. *Fatigue Handbook Offshore Steel Structures.* TAPIR

American Bureau of Shipping (ABS), 1999. *Guide for Certification of Offshore Mooring Chain,* ABS

American Bureau of Shipping (ABS), 2004. *Guide for Building and Classing Floating Production Installations,* ABS

American Petroleum Institute (API), 2001. *Design, Manufacture, Installation and Maintenance of Synthetic Fiber Ropes for Offshore Mooring.* API RP-2SM

American Petroleum Institute (API), 2005. *Design and Analysis of Stationkeeping Systems for Floating Structures.* API RP-2SK

American Standard of Testing and Materials (ASTM), 2005. *Standard Practices for Cycle Counting in Fatigue Analysis,* ASTM

Bang, P., 2002. Girassol: The FPSO Presentation and Challenges, *Offshore Technology Conference* 14172

Blanc, C. Isnard, J.L. Smith, R., 2006. Deepwater Oil Export Systems: Past, Present, and Future, *Offshore Technology Conference* 18085

Boom, H.J.J., 1985. Dynamic Behaviour of Mooring Lines. *Elsevier Science Publishes B.V.*

Boresi, A.P. Schmidt, R.J. Sidebottom, O.M., 1993. *Advanced Mechanics of Materials.* 5th Ed. John Wiley & Sons

Brake, E.T. Cammen, J.D. Uittenbogaard, R., 2007. Calculation Methodology of Out of Plane Bending of Mooring Chains, *International Conference on Offshore Mechanics and Arctic Engineering*

Brown, D.T. Mavrakos, S., 1999. Comprative Study on Mooring Line Dynamic Loading. *Marine Structures*

Brown, M.G. Hall, T.D. Marr, D.G. et al., 2005. Floating Production Mooring Integrity JIP – Key Findings, *Offshore Technology Conference* 17499

Brown, D.T. Chatjigeorgion, I.K. Boom, W.C. et al, 2006. *Floating Production Systems,* International Ship and Offshore Structures Congress (ISSC) Vol.2

Bureau Veritas (BV), 1998. *Quasi-Dynamic Analysis of Mooring Systems using ARIANE Software,* BV NI 461

Bureau Veritas (BV), 2004. *Classification of Mooring Systems for Permanent Offshore Units,* BV NI 493

Bureau Veritas (BV), 2009. *ARIANE7 Theoretical Manual,* BV

Chakrabarti, S.K., 1994. *Hydrodynamics of Offshore Structures.* Computational Mechanics Publications Southampton Boston

Chakrabarti, S.K., 2008. Challenges for a Total System Analysis on Deepwater Floating Systems, *Open Mechanical Journal*

Chen, X. Zhang, J. Johnson, P. Irani, M., 2001. *Dynamic Analysis of Mooring Lines with Inserted Springs.* Applied Ocean Research

ChevronTexaco, 2003. *Metocean Design Basis Deepwater Nigeria,* Report of Agbami FPSO

Connaire, A. Kavanagh, K. Ahilan, R.V. Goodwin, N.P., 1999. Integrated Mooring and Riser Design: Analysis Methodology, *Offshore Technology Conference* 10810

Dahlberg, R. Ronold, K.O. Strom, P.J. Mathisen, J., 2006. Calibrated Geotechnical Design Code for Suction Anchors in Clay, *Offshore Technology Conference* 18036

Denayrolles, A., 2011. *OPB/IPB in Top Chains Finite Element Analysis,* Report of DORIS for Clov FPSO

Det Norske Veritas (DNV), 1999. *FPSO Fatigue Methodology Specification,* ExxonMobil Report No.99-3503

Det Norske Veritas (DNV), 2004. *Global Performance Analysis of Deepwater Floating Structures,* DNV RP-F205

Det Norske Veritas (DNV), 2005a. *Geotechnical Design and Installation of Suction Anchors in Clay,* DNV RP-E303

Det Norske Veritas (DNV), 2005b. *Damage Assessment of Fiber Ropes for Offshore Mooring,* DNV RP-E304

Det Norske Veritas (DNV), 2009a. *Offshore Mooring Chain,* DNV OS-E302

Det Norske Veritas (DNV), 2009b. *Offshore Mooring Steel Wire Ropes,* DNV OS-E304

Det Norske Veritas (DNV), 2010a. *Postition Mooring,* DNV OS-E301

Det Norske Veritas (DNV), 2010b. *Offshore Mooring Fibre Ropes,* DNV OS-E303

Det Norske Verita (DNV), 2011. *Fatigue Design of Offshore Steel Structures,* DNV RP-C203

Eltaher, A. Chang, K.T., 2003. Industry Trends for Design of Anchoring Systems for Deepwater Offshore Structures, *Offshore Technology Conference* 15265

Fernandez, J., 2008. Reliability of Mooring Chains, *TEKNA Conference on DP and Mooring of Floating Offshore Units*

Gao, Z., 2008. Stochastic Response Analysis of Mooring Systems with Emphasis on Frequency-domain Analysis of Fatigue due to Wide-band Response Process, Ph.D. Norwegian University of Science and Technology

Gao, Z. Moan, T., 2005. Time Variant Reliability of Mooring System considering Corrosion Deterioration, *International Conference on Offshore Mechanics and Arctic Engineering*

Gao, Z. Moan, T., 2007a. *Fatigue Damage induced by non Gaussian Bimodal Wave Loading in Mooring Lines,* Applied Ocean Research

Gao, Z. Moan, T., 2007b. *Fatigue Damage under Combined High and Low Frequency Gaussian Load Processes considering a Two-slope SN curve,* Applications of Statistics and Probability in Civil Engineering

Gao, Z. Moan, T., 2008. Frequency-Domain Fatigue Analysis of Wide-band Stationary Gaussian Processes using a Trimodal Spectral Formulation. *International Journal of Fatigue*

Hall, A.D., 2005. Cost Effective Mooring Integrity Management, *Offshore Technology Conference* 17498

Hassan, A.M.A. Downie, M.J. Incecik, A., 2009. Contribution of the Mooring System to the Low-frequency Motions of a Semisubmersible in Combined Wav and Current, *International Conference on Offshore Mechanics and Arctic Engineering*

Health & Safety Executive (HSE), 2006. *Floating Production System JIP FPS Mooring Integrity,* HSE Report 444

Heurtier, J.M. Le-Buhan, P. Fontaine, E. et al., 2001. Coupled Dynamic Response of Moored FPSO with Risers, *Preceedings of the International Offshore and Polar Engineering Conference*

Huang, K., 2002. Mooring System Design Considerations for FPSOs, *International Conference on Offshore Mechanics and Arctic Engineering*

Huang, K. Bai, Y., 2001. Reliability Methods for Deepwater Position-Mooring Design and Analysis, *Offshore Technology Conference* 13269

Hwang, O.J. Jun, S.H. Kang, J.K., 2008. A Study on Spectral Fatigue Assessment of FPSO operating in Wave and Swell Sea-state; West Offshore of Africa, *Asian-Pacific Technical Exchange and Advisory Meeting on Marine Structures*

International Standard Organization (ISO), 2005a. *Petroleum and Natural Gas Industries – Specific Requirements for Offshore Structures – Part 7: Stationkeeping Systems for Floating Offshore Structures and Mobile Offshore Units,* ISO 19901-7

International Standard Organization (ISO), 2005b. *Petroleum and Natural Gas Industries – Specific Requirements for Offshore Structures – Part 1: Metocean Design and Operating Considerations,* ISO 19901-1

Jang, J.J. Lee, Y.L., 1988. A Study of Along Wind Speed Power Spectrum for Taiwan Area. *Journal of Marine Science and Technology* Vol.6

Jean, P. Goessens, K. L'Hostis, D., 2005. Failure of Chains by Bending on Deepwater Mooring Systems, *Offshore Technology Conference* 17238

Jiao, G. Moan, T., 1990. Probabilistic Analysis of Fatigue due to Gaussian Load Processes. *Probabilistic Engineering Mechanics* Vol.5

Journee, J.M.J. Massie, W.W., 2001. *Offshore Hydrodynamics,* 1st Ed. Delft University of Technology

Kang, C.H., 2011. A Study on Frequency Domain Methodologies for Fatigue Damage Assessment under Wide-band Random Wave Loading. MSc. Inha University

Kang, C.H. Lim, Y.C. Kim, K.S. Choung, J.M., 2010. A Study on Out-of-Plane Bending Mechanism of Mooring Chains for Floating Offshore Plants, *Asian-Pacific Technical Exchange and Advisory Meeting on Marine Structures*

Lanquetin, B., 2006. Experience Gained from Floating-Units Integrity Management, *Offshore Technology Conference* 18146

Lie, H. Gao, Z. Moan, T., 2007. Mooring Line Damping Estimation by a Simplified Dynamic Model, *International Conference on Offshore Mechanics and Arctic Engineering*

Lim, Y.C. Kim, K.S. Choung, J.M. Kang, C.H., 2010. A Study on Out-of-Plane Bending Mechanism of Mooring Chains for Floating Offshore Plants. *Journal of the Society of Naval Architects of Korea* Vol.47 No.4

Messager, J.C., 2011. *FPSO Model Tests Load Coefficients & Mooring Analysis Calibration*, Report for Clov FPSO

Melis, C. Jean, P. Vargas, P.M., 2005. Out-of-Plane Bending Tests of Chain Links, *International Conference on Offshore Mechanics and Arctic Engineering*

Nielsen, F.G. Bindingbo, A.U., 2000. Extreme Load in Taut Mooring Lines and Mooring Line induced Damping: an Asymptotic Approach. *Applied Ocean research*

Noble Denton Europe (NDE), 2005. *Floating Production System JIP FPS Mooring Integrity,* NDE Report No:A4163/MGB

Noble Denton Europe (NDE), 2001. *FPSO Mooring System Integrity Study,* United Kingdom Offshore Operators Association

Norwegian Standards (NORSOK), 2004a. *Design of Steel Structures,* NORSOK N-004 Rev.4

Norwegian Standards (NORSOK), 2004b. *Structural Design,* NORSOK N-001 Rev.4

Ong, P.P.A. Pellegrino, S., 2003. Modeling of Seabed Interaction in Frequency Domain Analysis of Mooring Cables, *International Conference on Offshore Mechanics and Arctic Engineering*

Orcina, 1987. *OrcaFlex Manual*

Ormberg, H. Sodahl, N. Stinkjer, O., 1998. Efficient Analysis of Mooring Systems Using Decoupled and Coupled Analysis, *International Conference on Offshore Mechanics and Arctic Engineering*

Petruska, D.J. Castille, C. Colby, C.A. et al., 2008. API RP 2SK: Stationkeeping – An Emerging Practice, *Offshore Technology Conference* 19607

Ramberg, W., Osgood, W., 1943. *Description of Stress-Strain Curves by Three Parameters,* National Advisory Committee for Aeronautics, Technical Note No. 902

Rampi, L. Vargas, P., 2006. Fatigue Testing of Out-of-Plane Bending Mechanism of Chain Links, *International Conference on Offshore Mechanics and Arctic Engineering*

Ridge, I.M.L. Hobbs, R.E. Fernandez, J., 2006. Predicting the Torsional Response of Large Mooring Chains, *Offshore Technology Conference* 17789

Single Buoy Moorings (SBM), 2006. Chain Out of Plane Bending Fatigue, *FPSO Research Forum* (Initiative Presentation Material of OPB JIP)

SIMULIA, 2008. *ABAQUS Analysis User's Manual*

Shu, H. Loeb, D.A., 2006. Extending the Mooring Capability of a Mobile Offshore Drilling Unit, *Offshore Technology Conference* 17995

Sparrevik, P., 2002. Suction Pile Technology and Installation in Deep Waters, *Offshore Technology Conference* 14241

Thomas, C., 2011. *Top Chain Fatigue Analysis including OPB and IPB Phenomena,* Report for Clov FPSO

TOTAL, 2004. Girassol Buoy & FPSO Tandem Offshore Operation Feedback, *FPSO Research Forum*, Paris

Vargas, P.M. Hsu, T.M. Lee, W.K., 2004. Stress Concentration Factors for Stud-less Mooring Chain Links in Fairleads, *International Conference on Offshore Mechanics and Arctic Engineering*

Waals, O.J., 2009. The Effect of Wave Directionality on Low Frequency Motions and Mooring Forces, *International Conference on Offshore Mechanics and Arctic Engineering*

Wyllie, M.W.J. Joynson, J., 2006. Recent Trends in FPSO Design and Project Execution Applied to Leased Vessels, *Offshore Technology Conference* 18061

Yang, W. S., 2007. *Hydrodynamic Analysis of Mooring Lines based on Optical Tracking Experiments,* Ph.D. Texas A&M

Appendix A. Wave Scatter Diagram in Operational Sea States

Sea state	Inc1 (deg)	Hs1 (m)	Tp1 (sec)	Inc2 (deg)	Hs2 (m)	Tp2 (sec)	Inc3 (deg)	Hs3 (m)	Tp3 (sec)	Nbr (-)
1	225	1.25	13	202.5	0.75	9	180	0.25	7	230
2	202.5	1.25	13	202.5	0.75	9	202.5	0.25	5	228
3	202.5	0.75	11	202.5	0.75	7	180	0.25	5	218
4	202.5	1.25	11	0	0	0	0	0	0	198
5	225	0.75	13	202.5	0.25	9	180	0.25	5	184
6	225	0.75	13	202.5	0.75	9	180	0.25	5	184
7	225	1.25	13	202.5	0.25	7	157.5	0.75	5	179
8	202.5	0.75	11	202.5	0.25	7	337.5	0.75	5	146
9	225	0.25	15	202.5	0.75	11	202.5	0.25	5	146
10	202.5	1.25	9	0	0	0	0	0	0	141
11	202.5	0.75	13	202.5	0.75	9	180	0.25	7	131
12	202.5	1.25	13	0	0	0	0	0	0	126
13	202.5	1.25	11	202.5	0.75	7	180	0.25	5	102
14	225	0.25	13	202.5	0.75	9	202.5	0.25	5	102
15	202.5	1.25	13	202.5	0.25	7	180	0.25	5	91
16	225	0.75	11	202.5	0.75	7	135	0.75	5	90
17	202.5	0.75	13	202.5	0.25	9	202.5	0.25	5	88
18	202.5	1.25	11	202.5	0.25	5	225	0.25	5	88
19	202.5	1.25	13	202.5	1.25	9	180	0.25	9	85
20	225	0.75	15	202.5	0.75	9	180	0.25	9	85
21	225	1.25	15	202.5	0.75	9	202.5	0.25	9	85
22	202.5	1.75	13	0	0	0	0	0	0	84
23	225	0.25	15	225	0.75	11	202.5	0.25	5	83
24	225	0.25	15	202.5	1.25	11	202.5	1.25	9	79
25	202.5	0.75	9	202.5	0.25	7	202.5	0.25	3	77
26	225	1.25	13	202.5	1.25	9	90	0.75	5	75
27	225	0.75	11	202.5	0.25	7	180	0.25	5	74
28	225	1.25	13	0	0	0	0	0	0	73
29	202.5	0.75	13	202.5	1.25	9	202.5	0.25	7	70
30	202.5	0.25	15	202.5	0.75	11	202.5	0.25	7	67
31	202.5	1.25	15	202.5	0.75	9	202.5	0.75	9	58
32	225	0.25	17	202.5	0.75	11	180	0.25	7	58
33	225	0.25	13	202.5	0.25	9	202.5	0.25	5	56
34	225	1.75	15	0	0	0	0	0	0	56
35	225	0.75	15	202.5	0.25	9	202.5	0.25	7	53
36	202.5	0.75	15	202.5	0.75	11	202.5	0.75	7	51
37	202.5	0.25	13	202.5	1.25	9	202.5	0.25	7	48

Sea state	Inc1 (deg)	Hs1 (m)	Tp1 (sec)	Inc2 (deg)	Hs2 (m)	Tp2 (sec)	Inc3 (deg)	Hs3 (m)	Tp3 (sec)	Nbr (-)
38	202.5	0.25	15	202.5	1.25	11	202.5	0.25	9	48
39	202.5	0.25	11	202.5	0.75	7	180	0.25	5	47
40	202.5	0.25	13	202.5	0.75	9	180	0.25	7	47
41	202.5	1.75	11	0	0	0	0	0	0	47
42	225	0.25	15	202.5	0.25	11	202.5	0.25	7	47
43	225	0.25	11	202.5	0.75	9	202.5	0.25	5	46
44	225	1.25	15	202.5	1.25	9	202.5	0.75	7	46
45	202.5	1.25	15	202.5	1.25	11	180	0.75	9	44
46	202.5	0.75	9	202.5	0.75	7	202.5	0.75	5	43
47	202.5	0.25	11	202.5	0.25	9	180	0.25	5	42
48	225	1.75	15	202.5	0.75	9	202.5	0.25	9	42
49	202.5	0.25	17	202.5	0.75	11	180	0.25	9	40
50	225	0.25	17	225	0.75	11	180	0.25	5	40
51	202.5	1.25	13	180	0.25	7	180	0.25	7	39
52	202.5	2.25	15	0	0	0	0	0	0	39
53	225	0.75	15	225	0.75	11	202.5	0.75	7	39
54	202.5	0.25	13	202.5	0.25	9	202.5	0.25	5	38
55	225	0.25	15	225	0.25	11	202.5	0.25	7	38
56	202.5	1.25	13	180	0.75	9	180	0.25	5	36
57	225	0.25	13	202.5	1.25	9	180	0.25	7	36
58	225	1.75	13	0	0	0	0	0	0	36
59	202.5	1.75	13	202.5	0.75	9	202.5	0.25	7	35
60	225	1.25	15	202.5	0.25	9	180	0.25	9	35
61	202.5	0.75	11	180	0.25	7	180	0.25	5	34
62	202.5	1.25	11	225	0.25	5	202.5	0.25	5	34
63	225	0.75	13	202.5	1.25	9	225	0.25	5	34
64	225	1.25	13	180	0.75	7	202.5	0.75	5	34
65	225	2.25	15	0	0	0	0	0	0	34
66	202.5	2.25	13	0	0	0	0	0	0	33
67	225	1.25	13	180	0.25	7	202.5	0.25	5	33
68	202.5	0.75	9	0	0	0	0	0	0	31
69	202.5	0.75	11	0	0	0	0	0	0	31
70	202.5	1.25	11	180	0.25	7	225	0.25	5	30
71	202.5	0.75	11	225	0.25	7	180	0.25	7	29
72	202.5	1.75	15	0	0	0	0	0	0	29
73	202.5	0.25	15	202.5	0.25	11	202.5	0.25	7	28
74	225	0.75	15	202.5	1.25	9	180	0.75	7	27
75	225	1.25	11	202.5	0.25	7	90	0.75	5	27
76	225	1.75	13	202.5	0.75	7	225	0.25	7	27
77	202.5	0.75	15	202.5	1.25	9	180	0.75	9	26

Sea state	Inc1 (deg)	Hs1 (m)	Tp1 (sec)	Inc2 (deg)	Hs2 (m)	Tp2 (sec)	Inc3 (deg)	Hs3 (m)	Tp3 (sec)	Nbr (-)
78	202.5	2.25	11	0	0	0	0	0	0	26
79	202.5	1.75	15	202.5	1.25	9	0	0	0	25
80	225	0.25	17	202.5	1.25	11	202.5	0.75	9	25
81	225	1.25	17	225	0.75	13	180	0.75	9	24
82	202.5	1.75	15	202.5	0.75	7	202.5	0.75	9	23
83	225	0.75	15	225	0.25	11	202.5	0.25	7	23
84	202.5	0.25	15	225	0.75	11	202.5	0.25	7	22
Total										5628

Appendix B. Wind Scatter Diagram in Operational Sea States

Vw [m/s]	N	NNE	NE	ENE	E	ESE	SE	SSE	S	SSW	SW	WSW	W	WNW	NW	NNW	Total
	0	22.5	45	67.5	90	112.5	135	157.5	180	202.5	225	247.5	270	292.5	315	337.5	
0.5	0.01	0.01	0.00	0.01	0.01	0.00	0.02	0.02	0.03	0.03	0.01	0.02	0.01	0.01	0.01	0.00	0.204
1.5	0.05	0.03	0.06	0.05	0.09	0.15	0.23	0.38	0.49	0.49	0.47	0.34	0.17	0.09	0.05	0.06	3.199
2.5	0.04	0.03	0.06	0.07	0.14	0.35	0.70	1.62	2.54	2.86	2.03	1.08	0.50	0.25	0.11	0.07	12.44
3.5	0.02	0.01	0.01	0.01	0.06	0.20	0.81	2.93	6.65	7.07	3.96	1.43	0.45	0.12	0.06	0.01	23.81
4.5			0.01	0.01	0.01	0.06	0.39	2.90	9.42	10.35	4.88	1.28	0.27	0.06	0.01	0.01	29.64
5.5				0.00	0.00	0.01	0.12	1.27	6.09	8.45	3.97	0.86	0.10	0.01	0.01	0.01	20.88
6.5				0.00			0.01	0.26	1.83	3.77	2.08	0.28	0.01				8.239
7.5								0.02	0.24	0.69	0.42	0.07	0.01				1.445
8.5								0.01	0.01	0.07	0.04	0.01					0.140
9.5										0.00	0.00						0.004
Total	0.12	0.07	0.13	0.15	0.32	0.76	2.28	9.40	27.3	33.8	17.9	5.36	1.51	0.55	0.26	0.16	100.0

Appendix C. Current Scatter Diagram in Operational Sea States

Vcr	N	NE	E	SE	S	SW	W	NW	Total
[m/sec]	0	45	90	135	180	225	270	315	
0.01	0.109	0.124	0.094	0.101	0.096	0.079	0.092	0.067	0.762
0.03	0.329	0.294	0.324	0.294	0.265	0.28	0.282	0.322	2.39
0.05	0.502	0.579	0.567	0.49	0.396	0.381	0.458	0.473	3.846
0.07	0.69	0.839	0.779	0.641	0.571	0.562	0.579	0.567	5.228
0.09	0.836	1.108	1.007	0.779	0.737	0.633	0.71	0.601	6.411
0.11	0.881	1.175	1.212	0.836	0.73	0.735	0.73	0.705	7.004
0.13	0.96	1.311	1.331	0.883	0.802	0.69	0.752	0.814	7.543
0.15	0.994	1.541	1.274	1.014	0.93	0.623	0.715	0.799	7.89
0.17	0.972	1.405	1.388	0.98	0.853	0.67	0.737	0.752	7.757
0.19	0.98	1.277	1.366	0.9	0.745	0.544	0.658	0.809	7.279
0.21	0.836	1.321	1.22	0.94	0.596	0.423	0.564	0.777	6.677
0.23	0.727	1.004	1.158	0.928	0.581	0.393	0.48	0.668	5.939
0.25	0.614	0.97	1.098	0.712	0.47	0.317	0.443	0.611	5.235
0.27	0.537	0.811	0.987	0.673	0.388	0.26	0.391	0.643	4.69
0.29	0.51	0.772	0.97	0.552	0.28	0.215	0.421	0.576	4.296
0.31	0.46	0.562	0.762	0.5	0.186	0.146	0.346	0.567	3.529
0.33	0.416	0.502	0.547	0.411	0.129	0.121	0.25	0.552	2.928
0.35	0.346	0.349	0.413	0.331	0.072	0.119	0.203	0.534	2.367
0.37	0.247	0.297	0.304	0.19	0.054	0.059	0.203	0.44	1.794
0.39	0.257	0.21	0.324	0.166	0.017	0.047	0.176	0.366	1.563
0.41	0.237	0.131	0.181	0.099	0.007	0.032	0.114	0.329	1.13
0.43	0.148	0.077	0.111	0.03	0.005	0.017	0.106	0.247	0.741
0.45	0.163	0.077	0.101	0.037		0.007	0.094	0.183	0.662
0.47	0.111	0.049	0.072	0.02		0.005	0.067	0.161	0.485
0.49	0.111	0.042	0.047	0.01		0.002	0.074	0.151	0.437
0.51	0.099	0.037	0.027			0.005	0.062	0.129	0.359
0.53	0.082	0.012	0.027	0.005		0.005	0.035	0.079	0.245
0.55	0.069	0.007	0.035	0.002			0.027	0.067	0.207
0.57	0.03	0.005	0.032				0.02	0.054	0.141
0.59	0.025		0.049	0.002			0.017	0.047	0.14
0.61	0.01		0.049				0.01	0.04	0.109
0.63	0.005		0.022				0.005	0.059	0.091
0.65	0.002		0.022					0.049	0.073
0.67			0.01				0.002	0.01	0.022
0.69			0.007					0.012	0.019
0.71			0.002					0.002	0.004
Total	13.30	16.89	17.92	12.53	8.91	7.37	9.82	13.26	100.0

Appendix D. Manual of ChainFOS

ChainFOS was made to simplify all the post processes with respect to the computation of the fatigue life considering the effects on OPB/IPB phenomenon of chain links. ChainFOS is 'Chain Fatigue including OPB Strength'.

The processes are divided by five steps; 1) generating time series, 2) reading OPB/IPB SCFs, 3) calculating stress series, 4) performing rainflow counting and finally 5) calculating fatigue damages. In Fig.D-1, the view of ChainFOS along with the functions of buttons is given.

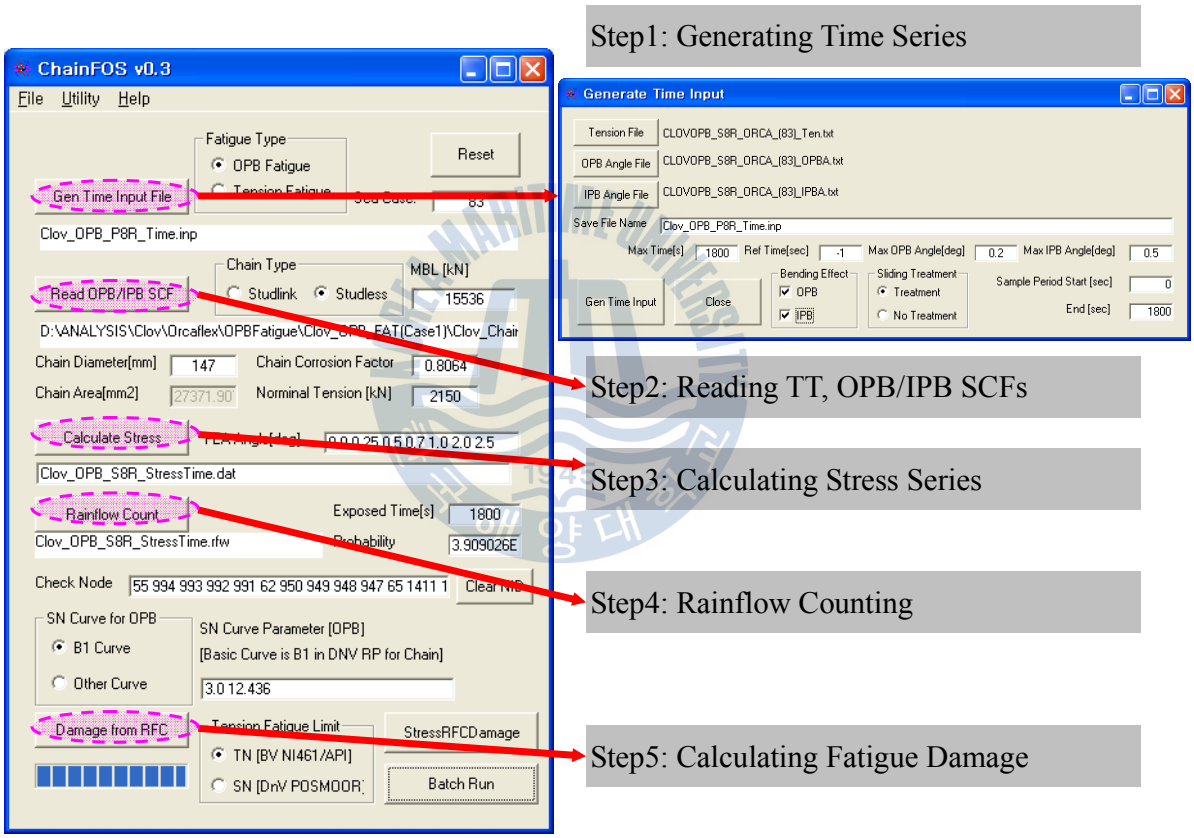

Fig.D-1 View of ChainFOS along with the function of buttons

1) Generating time series: this step is to read values of tension, OPB interlink angle and IPB interlink angle corresponding to the time history from OrcaFlex output.

2) Reading OPB/IPB SCFs: this step is to read the SCFs at every possible node on chain surface, which is from the results of non-linear FE analysis by ABAQUS.

3) Calculating stress series: this step is to calculate the resultant stress by combining TT, OPB and IPB along with the calculated SCF values at every possible node.

4) Rainflow counting: this step is to perform the rainflow counting method to count the number of cycles and stress ranges.

5) Calculating fatigue damage: this step is to calculate the fatigue damages at every possible node utilizing SN curve and Miner's Rule.

Note that the TT fatigue damage can be calculated as well by checking the button of the fatigue type, in which the codes of DNV POSMOOR or BV NI 493 are applicable. Furthermore, the batch button makes users quickly review all the sea states for every node by just one click.

감사의 글

인생 40을 공자는 사물의 이치를 터득하고 세상에 흔들리지 않는 나이라 하여 '불혹'이라 하였다. 미국의 16대 대통령인 링컨 또한 절친한 사이로부터 비서로 추천된 사람을 되돌려 보내며 '사람의 나이 40이 되면 자기 얼굴에 책임을 져야 한다' 라고 말하였다. 이런 말들 속에 나의 모습은 어떨까 반문하여 보며 40여 년의 세월 동안 나를 있게 하고, 특별히 본 논문이 나오기까지 여러모로 도와주신 모든 분들께 감사의 인사를 드리고 싶다.

우선, 박사과정을 수료한 후 10년이 흐른 시점까지도 항상 학문적으로나 생활 면에서 귀감이 되어준 최경식 교수님께 감사 드리고 싶다. 그리고, 본 논문이 나오기까지 학문적 조언과 학자로써의 품의를 보여 주시며 심사해주신 이주성 교수님, 서영교 교수님, 정준모 교수님, 이승재 교수님께 심심한 감사의 인사를 드리고 싶다. 특별히, 울산과 인천에서 먼 거리를 마다하지 않으시고 논문 심사를 사회를 위한 또 하나의 봉사라고 말씀하시는 이주성 교수님과 정준모 교수님께 재차 감사를 드리고 싶다.

시간이 흐르면서 '사람이 홀로 선다는 게 얼마나 교만일까' 하는 생각이 자주 든다. 사람은 원래 홀로 설 수 없는 존재인걸 이제야 깨닫는 게 우습기도 하다. 성경에도 두 사람이 한 사람보다 낫고 삼겹 줄이면 쉽게 끊어지지 않는다고 했듯이, 일상 속에서 함께해온 동료들에게 감사 드리고 싶다. 첫 사회에 발을 디딘 애띤 사회 초년생을 훌륭하게 자랄 수 있도록 배려와 격려로 실력을 쌓도록 도와주신 윤기영 부장님을 포함한 현대중공업의 모든 선후배님들과, 대우조선해양 선박해양연구팀 팀장님 이하의 모든 연구원들께 감사 드린다. 특별히 본 논문을 통해 늦깎이 박사과정을 마치도록 허락해 주신 이성근 전무님을 비롯한 조태익 전무님, 이정한 전무님, 오영태 위원님, 김용수 이사님, 강중규 부장님, 전석희 차장님께 심심한 감사를 표하고 싶다. 아울러, 대우조선해양의 선박과 해양할 것 없이 최고의 구조분야 전문가 그룹인 구조R&D 형님, 아우들 그리고, 구조연구개발3파트의 후배들과, 본 논문의 일부인 계류삭 모델링 작

업, FPSO 운동해석, 모델시험 자료를 제공하고 도와준 강찬회 사원, 정성준 대리께 감사 드린다.

나이 마흔이 넘으면 철이 든다고 한다. 이제서야 부모님들의 마음을 헤아릴 수 있다는 게 다소 서글프기도 하지만 살아갈수록 그 깊이와 헤아림에 절로 고개가 숙여진다. 이 논문이 얼마나 그분들의 사랑에 보답이 될지 모르지만, 진정 존경하고 사랑하는 어머님과 장인, 장모님께 진심 어린 감사를 드리고 싶다. 그리고 끝까지 믿음의 눈으로 지켜봐 주신 친가와 처가댁 형제들 그리고 주안에서 형제 된 모든 교우들께 감사 드린다.

내 삶의 기업인 '가은'이와 '예종'이... 이 자녀들을 생각하면 가슴이 벅차 오른다. 여러 모양의 세상 어려움 속에서도 이 아이들이 복된 모습으로 자라나길 소망한다. 자녀들은 전통에 가득 찬 화살이라고 했듯이 앞으로 이들이 세상의 어려움을 뚫고 날아갈 것을 소망하며 '너희들이 있어줘서 힘이 되었다'고 전하고 싶다.

글을 적으며 벌써 만 20년이 되었다는 걸 깨닫는다. 1992년 11월말 오래된 작은 교회당에서의 첫 만남에서 지금은 내 옆의 반려자로 애인으로 때로는 꿈을 나누는 친구로 살아가고 있는 아내 '경림'에게 진심 어린 사랑과 존경을 전하고 싶다. 마지막으로 '나의 나 된 것은 그분의 은혜로다'라고 고백하고 싶다. Sole Deo Gloria~